2016

PROPERTY ANALYSIS OF THE ASPHALT MATERIALS USING MOLECULAR DYNAMICS (MD) METHOD

Hui Yao
Michigan Technological University, huiyao@mtu.edu

PROPERTY ANALYSIS OF THE ASPHALT MATERIALS USING MOLECULAR DYNAMICS (MD) METHOD

By

Hui Yao

A DISSERTATION

Submitted in partial fulfillment of the requirements for the degree of

DOCTOR OF PHILOSOPHY

In Civil Engineering

MICHIGAN TECHNOLOGICAL UNIVERSITY

2016

This dissertation has been approved in partial fulfillment of the requirements for the Degree of DOCTOR OF PHILOSOPHY in Civil Engineering.

Department of Civil and Environmental Engineering

Dissertation Co-Advisor: *Zhanping You*

Dissertation Co-Advisor: *Qingli Dai*

Committee Member: *Patricia Heiden*

Committee Member: *Jianping Dong*

Department Chair: *David Hand*

Table of Contents

List of Figures

List of Tables

Preface

This dissertation uses the Molecular Dynamics (MD) method to simulate the asphalt material with different components: asphaltenes, aromatics and saturates. The multi-layer graphite nanoplatelets (xGNP) modified asphalt model is also generated to evaluate the effect of xGNP particles on asphalt. Different properties of these asphalt models are computed and analyzed. The relationships between asphalt-aggregate and asphalt-modifier are explored and discussed, as well as the self-diffusion of the asphalt binder. The contents in this dissertation are published or submitted to different journals. The details are shown as follows.

Chapter 1 of this dissertation introduces my dissertation, which includes these sections: Background, Problem Statement and Challenges, Objectives and Scopes, Hypotheses, and organization of chapters. The results were collected and analyzed by me. I completed these chapters with my advisors, Prof. Zhanping You and Prof. Qingli Dai.

Chapter 2 of this dissertation highlights the literatures on asphalt and the application of MD in the asphalt material at the atomistic scale. We plan to submit this chapter to the journal of "*Construction and Building Materials*". The simulation codes and test methods were developed, and the results were collected and analyzed by me. I completed these chapters with my advisors, Prof. Zhanping You and Prof. Qingli Dai.

Chapter 3 of this dissertation simulates the asphalt model using common components from the references and predicts the physical properties of asphalt material. This chapter has been published in the journal of "*Fuel*", and the copyright permission is

attached in Appendix A. The simulation codes and test methods were developed, and the results were collected and analyzed by me. I completed these chapters with my advisors, Prof. Zhanping You and Prof. Qingli Dai.

Chapter 4 of this dissertation investigates the moisture susceptibility of nano hydrated lime (NHL) modified asphalt mixtures and it determines the fundamental factors of moisture damage in asphalt mixtures using the MD method. This chapter has been published in the journal of "*Construction and Building Materials*", and the copyright permission is attached in Appendix A. The simulation codes and test methods were developed, and the results were collected and analyzed by me. I completed these chapters with my advisors, Prof. Zhanping You and Prof. Qingli Dai.

Chapter 5 of this dissertation explains the generation of the xGNP modified asphalt model and calculates the properties of the asphalt binders using the MD method. We plan to submit this chapter to the journal of "*Construction and Building Materials*". The simulation codes and test methods were developed, and the results were collected and analyzed by me. I completed these chapters with my advisors, Prof. Zhanping You and Prof. Qingli Dai.

Chapter 6 of this dissertation analyzes different modulus properties of these asphalt models compared with those of the control asphalt model. We plan to submit this chapter to the "*ASCE journal of Materials in Civil Engineering*". The simulation codes and test methods were developed, and the results were collected and analyzed by me. I completed these chapters with my advisors, Prof. Zhanping You and Prof. Qingli Dai.

Chapter 7 of this dissertation provides an understanding of the mechanism of self-healing and diffusion of the asphalt on aggregates. We plan to submit this chapter to the journal of "*Fuel*". The simulation codes and test methods were developed, and the results were collected and analyzed by me. I completed these chapters with my advisors, Prof. Zhanping You and Prof. Qingli Dai.

Chapter 8 of this dissertation provides the summary, conclusions and recommendations for future studies. The simulation codes and test methods were developed, and the results were collected and analyzed by me. I completed these chapters with my advisors, Prof. Zhanping You and Prof. Qingli Dai.

Acknowledgements

I would like to express my deepest gratitude to my advisors, Prof. Zhanping You and Prof. Qingli Dai for their support and guidance in my dissertation. They give me an opportunity to learn from them and conduct research on materials, and it is my honor to be their student. They encourage me to keep my enthusiasm for research and also provide me with inspiration and financial support to complete this study. I also extend my great appreciation to my committee members, Prof. Patricia Heiden and Prof. Jianping Dong for reviewing my work.

I would like to acknowledge suggestions and help from the faculty, staff, and students in the Department of Civil and Environmental Engineering, especially thanks to Prof. Jacob Hiller, and Dr. Min Wang from the Department of Mathematical Sciences.

Thanks to all my friends, Rong Liu, Rui Yan, Wei Chen, Mingxiao Ye, Yongliang Jin, Yinghong Qin, Huanxin Zhang, Yaoxian Huang, Shichang Ma, Kay Mi Liu, Shuaicheng Wang, Xiao Sun, Shuaicheng Guo, Zigeng Wang, Chao Lu, Ruizhe Si, Wanbing Bai, Aaron Dayton, Keith Anderson, and Kelsey Bird, especially thanks to Paul Pebler and Pei Tang for their encouragement and help.

Thanks to my colleagues and group members, Christopher DeDene, Shu Wei Goh, Yu Liu, Baron Colbert, Julian Mills-Beale, Xu Yang, Mohd Rosli Mohd Hasan, David Porter, Dongdong Ge, Siyu Chen, Huijun Shao and Tristan Kolb.

Finally, I sincerely appreciate my parents and wife, and all they have done for me, endless love, strong support and encouragement.

Abstract

The main objectives of this dissertation are to build the Molecular Dynamics (MD) model for the asphalt binders with three components, asphaltenes, aromatics and saturates, and analyze the properties of the asphalt models to discover the interactions and mechanisms of asphalt-aggregate and asphalt-modifier. The contributions of this dissertation are summarized as follows: (1) the Amber Cornell Extension Force Field (ACEFF) was assigned to each component, and most of the parameters of the force field were obtained from the General Amber Force Field (GAFF). Electrostatic Potential (ESP) charges were assigned to each atom with the NWChem calculation; (2) the modified asphalt model with the multi-layer graphite nanoplatelets (xGNP) was generated by the MD method to analyze the effect of the modifier on the asphalt binder model; (3) the aged components of the asphalt model were proposed, and the analysis of moisture susceptibility of asphalt-aggregate by the MD method; (4) the interaction or diffusion of the asphalt binder on aggregates was also realized by the MD method.

The MD simulations and laboratory test evaluations show that (1) the MD asphalt model with ACEFF and ESP charges has a better prediction for the different properties than the reference model; (2) The primary aging products in the asphalt binder contain ketones, carboxylic acids and anhydrides. The difference in adhesion was observed between aggregate-asphalt and aggregate-water interfaces; (3) the addition of xGNP nanoplatelets in the asphalt model increased the density, viscosity and thermal conductivity. The same trend was observed in the experimental data. A better observation of these

properties was found in the xGNP modified asphalt model compared to the base asphalt model; (4) Different moduli of the asphalt binder models had a trend similar to that of the laboratory test results; (5) The asphalt started to diffuse when the activation energy was reached, and the contact angle and area of the asphalt-aggregate interface changed. Therefore, the findings or conclusions in this dissertation have a good guidance for improving the performance of asphalt binders. Most importantly, this dissertation provides a promising way to analyze and develop the material and its properties.

Chapter 1 Introduction

The purpose of this chapter is to provide an introduction of my dissertation, and the dissertation includes these sections: Background, Problem Statement and Challenges, Objectives and Scopes, Hypotheses, and Organizations of Chapters.

1.1 Background

Asphalt has been widely applied for pavement throughout the world, and the usage and demand of asphalt binders increases significantly. Ninety percent of the pavement in the United States has been paved with asphalt mixtures, and the loose asphalt mixtures are formed using the aggregates mixed with asphalt binder at a certain ratio. The asphalt mixtures are placed on the surface of pavements by apparatuses. Another important application for asphalt is the waterproofing product. The rheological properties of different asphalt binders are tested and evaluated by many researchers, and the macro performance improvement of the asphalt binders links to the microstructural changes [1-4]. Modified asphalt binders have been used tremendously in pavement engineering due to the improvements in quality. The microstructural changes and movements of atoms or molecules of the asphalt binder still need to be determined and discussed under different conditions. The relationships of asphalt-aggregate and asphalt-modifier also need to be explored. Researchers from different research areas try to figure out the mechanisms and interactions of the movement of asphalt binders, and the molecular dynamics (MD) simulation could be an efficient way to explore the mechanism [5].

Asphalt is a brown to black cementitious material and a byproduct of petroleum engineering. It is strong, readily adhesive, highly waterproof and durable. The adhesive properties of the asphalt binder are utilized to coat aggregates [6]. The characteristics of the asphalt binder contribute to the quality of the asphalt pavement. Asphalt material is also stable and highly resistant to acids and alkalis. However, the asphalt material can be dissolved in petroleum solvents and emulsified by water [6]. The states or properties of the asphalt binder can be changed by heat and temperature. The asphalt binder presents an elastic property under cold environments, but in a hot condition, the asphalt binder shows a viscous performance or reaches a fluid state [7, 8]. The characteristics of the asphalt binders are different depending on location, and the components of the asphalt binder are slightly different [6]. Natural asphalt was found and utilized as the road materials or waterproof products by ancient Babylonians, Egyptians, Greeks and Romans [9]. The first asphalt pavement was built in 1870 in Newark, New Jersey. In 1876, the first sheet asphalt pavement (lake asphalt, fine sand mix) was constructed in Washington, D.C. [10]. The use of asphalt binder has rapidly grown after the 1940s throughout the world [11]. The demand of the asphalt material stimulates technological development. As the refining technology for crude oil has been developing, it boosts the production and application of asphalt binder. The chemical and physical properties of the asphalt binders improve to meet the requirements for local standards [1, 3, 4, 6]. In addition, the properties of the asphalt binders were simulated by many simulation methods at different scales, such as Discrete Element Method (DEM) or Finite Element Method (FEM). Few researchers demonstrated and analyzed the characteristics of the asphalt binder and its components on the atomic scale.

1.2 Problem Statement and Challenges

Asphalt from different sources, and modified asphalt binders are widely used for pavement, and the modifiers may or may not improve the performance of asphalt pavement. The performance tests are normally employed to evaluate the modified asphalt binder. Researchers usually make samples to test the performance after the asphalt binder has been modified, and it takes time to mix/compact and test samples. The procedures discuss the cost of the materials and labor, and most importantly, the time wasted if the new modifier does not work. Considering the traditional simulation methods, like the Discrete Element Method (DEM) or Finite Element Method (FEM), the test simulations restore the test process and obtain the simulation data. However, few researchers study the components of the asphalt binder on the atomic scale and understand the fundamental principles and mechanisms during the mixing and modification of the asphalt and modified systems under different conditions. In addition, the interaction between asphalt and aggregates still needs to be explored with or without water to access the moisture damage in the asphalt mixtures, especially from an energy viewpoint. The self-healing or self-diffusion of the asphalt binder on aggregates also needs to be discovered in the process of healing or movement of the asphalt binder. Furthermore, the study of the molecular structure of the asphalt binder is still a leading edge research topic in the field of civil engineering materials, and more problems or challenges will be faced in material developments. The statements are discussed as follows.

(1) The development timelines for new materials due to economic competition and development are needed to be discussed and developed, as well as the increasing cost of materials and labor during the development and manufacturing;

(2) The discussion of the molecular structure of the asphalt binder helps understand the asphalt material and its components, and it can bring new ways and thoughts to improve the performance of asphalt binders and mixtures;

(3) The interactions between asphalt and aggregates are determined from the atomic scale or molecular structures, especially from the perspective of energy. The influential factors of water susceptibility of asphalt mixtures are discovered, especially the effect of aging of the asphalt binder;

(4) The new parameters of force fields or optimization methods are needed and discussed during the generation of the asphalt model or other models. It is necessary that the property change and its molecular mechanism of the asphalt binder is explained under different conditions;

(5) The interactions between modifiers and asphalt need to be explained on the atomic scale, as well as the improvement mechanisms of modified asphalt binders;

(6) The self-diffusion of the asphalt binder is also an essential part of the self-healing properties. It is necessary to discuss and explore the diffusion or movement mechanisms of the asphalt binder on aggregates on the atomic scale under different conditions, as well as the interface interactions between asphalt and aggregates.

1.3 Objectives and Scopes

The objectives of this dissertation are to utilize the Molecular Dynamics (MD) method to simulate the control and modified asphalt binders, and to predict physical or chemical properties of the asphalt binder models or mixture models. The fundamental behaviors or mechanisms of asphalt materials during heating and modifications are discussed and explained. The results of the studies in this dissertation can be guided and generalized for future research or applications. The research objectives are concluded as follows.

(1) Collect literatures on asphalt and the application of MD in asphalt material on the atomic scale. The research experience and results of the MD application from other researchers were summarized and analyzed.

(2) Simulate the asphalt model using common components from the references, and predict the physical properties of the asphalt material. The Amber Cornell Extension Force Field was adopted and utilized in the asphalt model system, and the experimental parameters associated with this force field were obtained from the General Amber Force Field (GAFF). The density, glass transition temperature and viscosity of the base asphalt model were computed and analyzed.

(3) Investigate the moisture susceptibility of asphalt mixtures modified with nano hydrated lime (NHL) and determine the fundamental factors of moisture damage in asphalt mixtures using the MD method, as well as analyze the effect that the aging of asphalt binders has on the moisture damage in asphalt mixtures.

(4) Generate the MD model of the multi-layer graphite xGNP nanoplatelets for the modification of the asphalt model. The control asphalt model consists of three components: asphaltenes, aromatics, and saturates. This modified asphalt model was verified through density calculations and comparisons. The multi-layer graphite model was randomly added to the control asphalt model, and the xGNP modified asphalt model was built. After the verification of the model, the properties of the control and xGNP modified asphalt were computed and analyzed using the MD method, and the material properties include the glass transition temperature, viscosity and thermal conductivity.

(5) Simulate the asphalt modified with exfoliated multi-layered graphite nanoplatelets (xGNP) using the MD method, and analyze different modulus properties of these asphalt models compared with those of the control asphalt model.

(6) Understand the mechanism of the self-healing and diffusion of the asphalt on aggregates. The microscale asphalt mastic samples were prepared with asphalt and fine aggregates of a small size (less than 0.3 mm). Microscale dynamic X-ray computed tomography was conducted to capture the self-diffusion process of the asphalt in a microscale asphalt mastic sample at 80^{o}C using the Advanced Photon Source (APS) beamline 2-BM at Argonne National Laboratory. The contact angle, activation energy and Mean Squared Displacement (MSD) were analyzed to describe the self-healing behaviors of the asphalt materials.

1.4 Hypotheses

When the types of atoms and composition are determined in the model, the bonds of atoms are defined by the setting of force fields. The bond lengths with the force constants in all of the bonds of models are recorded [12]. Based on the literature review [12, 13], the asphalt models and their components are created using the following assumptions. The angle parameters, dihedral parameters and force constants are assumed due to the non-availability of the angle and dihedral types, or these parameters were still being found and developing. The models in this dissertation were built based on these assumptions before optimization and ensembles. (1) Length assumptions: the lengths of "CH_3-CH_2, CH_2-CH_2, CH_2-CH, CH_3-C and CH=C" in straight lines are assumed to be the same bond length (around 1.53 Angstrom); the lengths of "C=C, CH=CH and C=CH" in the aromatic ring are assumed to be the same bond length (around 1.43 Angstrom); the lengths of "CH_2-CH_2 and CH_2-C" in a six-membered ring are assumed to be the same bond length (around 1.43 Angstrom). (2) Angle assumptions: the angle parameters of "CH-CH_2-CH_3, CH=C-CH_3, CH=C=CH, CH=C-CH_2, C-CH_2-CH_3, C=C-CH_3, C=CH=C, C=C=C, C-CH_2-CH_2, CH_2-CH_2-CH_2, CH_2-CH_2-CH_3 and CH_2-C=C" are the same; the angle constants of "C-S-C and C-S-CH" are the same. (3) Dihedral assumptions: the parameters of "CH_3-CH_2-CH_2-CH_2, CH_3-CH_2-CH_2-C, CH_3-C=CH=C, CH_3-C=C=C, CH_3-CH_2-C=CH, CH_3-CH_2-CH_2=C, CH_2-CH_2-CH_2-C, CH_2-CH_2-C=C, CH_2-CH_2-C=CH, CH_2-CH=C=CH, CH=C=C=C, CH=CH=C=C, and CH=C=CH=CH" are the same as the parameters of "C-C-C-C" (aromatic carbon atoms); carbon atoms in "CH_3-CH_2-CH_2=C and CH_3=CH_2=CH_2=CH_2"

are assumed to be aliphatic carbon atoms in the plane; atoms in "CH_3=C=C-S and C-S-C=C" are assumed to be on the same plane (Carbon: C; Hydrogen: H; and Sulfur: S).

1.5 Organization of This Dissertation

This dissertation is composed of eight chapters, and each chapter in this dissertation is published or submitted for journal publications. The details of the chapters are discussed and described as follows.

(1) Chapter 1 provides an introduction of the dissertation, and the dissertation includes these sections: Background, Problem Statement and Challenges, Objectives and Scopes, Hypotheses, and Organizations of Chapters.

(2) Chapter 2 presents a literature review for the application of the MD method. The purpose of this chapter is to collect the literatures on asphalt and the application of MD in the asphalt material on the atomic scale. The research experience and results of the MD application from other researchers were summarized and analyzed. We learned from other researchers, and established background information on the MD method or its application in asphalt material. Several parts of the MD method were organized and reviewed, which include the sections: Modified asphalt, Multiscale analysis, Molecular dynamics, Force fields, Optimization methods, MD simulation on the asphalt model, MD simulation on asphalt-aggregate and asphalt-modifier models. The advantages of the MD method were explored and listed for material developments. In addition, additional topics and future research issues were also discussed.

(3) Chapter 3 introduces the MD method to simulate the asphalt model using common components from the references and to predict the physical properties of asphalt

material. The asphalt model consists of three components: asphaltene, aromatic, and saturate, at the ratio of 5:27:41. The docosane and 1, 7-Dimethylnaphthalene represents the saturate and naphthene aromatic, respectively. The Amber Cornell Extension Force Field was adopted and utilized in the asphalt model system, and the experimental parameters associated with this force field were obtained from the General Amber Force Field (GAFF). The geometry and energy optimizations of the molecular components were used to establish the stable asphalt model system. The density of the asphalt model system was calculated with the Amber Cornell Extension Force Field. The predicted densities were compared with the laboratory data to verify the model. Moreover, the glass transition temperature range of the molecular asphalt model was computed from the relationship between the specific volumes and temperatures after the molecular dynamics experimental simulation. The glass transition temperature range had a good correlation with the experimental data. The viscosity data of the molecular asphalt model was calculated using the Muller-Plathe algorithm. The predicted viscosities at specific temperatures were also compared and discussed with the laboratory data and other published results. In addition, the bulk modulus of the molecular asphalt model was determined and obtained by applying the small strain in the model boundaries. The results of the analysis of the bulk modulus in the asphalt model were compared with the reference data, and these predicted results were better than the reference values.

(4) Chapter 4 demonstrates the extraction and analysis of polar components in the asphalt binder and the adhesion between asphalt and aggregate models. The purpose of this study is to investigate the moisture susceptibility of nano hydrated lime (NHL)

modified asphalt mixtures and determine the fundamental factors of moisture damage in asphalt mixtures using the MD, as well as analyze the effect that the aging of the asphalt binders has on the moisture damage in asphalt mixtures. The NHL was added to the control asphalt to make NHL modified asphalt. The modified asphalt was mixed with aggregates to form NHL modified asphalt mixtures. The tensile strength ratio (TSR) test was used to evaluate the moisture susceptibility of asphalt mixtures. When the TSR test was done, different solutions were used to extract the polar groups from the tested asphalt mixtures, and the polar groups were analyzed using Fourier transform infrared spectroscopy (FTIR) attenuated total reflection (ATR). When asphalt oxidizes, the six functional groups (ketones, carboxylic acids, anhydrides, aldehydes, amides and esters) with the carbonyl group can be found in the polar part of asphalt based on FTIR ATR spectral data and references. The polar groups with the carbonyl group also indicate the extent of oxidation of asphalt binders. The FTIR test results indicate that carboxylic acids and ketones were the primary aging products in asphalt, and these two carbonyl groups relate to the rutting resistance and moisture susceptibility of asphalt mixtures. Furthermore, the MD interface systems of asphalt-aggregate and aggregate-water were created, as well as the separated systems (asphalt, water, and aggregates). The essential mechanisms for the moisture susceptibility of asphalt mixtures were explored with MD simulations. The potential energies of the interface systems and each separated system were computed to obtain the adhesion energies of the interface MD models. The differences in adhesion between the asphalt-aggregate and aggregate-water systems show that water tends to bind to the aggregate rather than the asphalt. This also explains the displacement of water that occurs in asphalt mixtures when there

is moisture damage. In addition, the effect of asphalt aging on the moisture susceptibility of the asphalt mixture was also analyzed using MD interface models. The MD results demonstrate that the aging group in asphalt is helpful in reducing the moisture damage in asphalt mixtures.

(5) Chapter 5 shows the generation of the modified asphalt model and calculation of different properties. The molecular model of the multi-layer graphite xGNP nanoplatelets was created for the modification of the asphalt model, and the control asphalt model consists of three components: asphaltenes, aromatics, and saturates, based on our group's previous study. The multi-layer graphite model was randomly added to the control asphalt model, and the xGNP modified asphalt model was generated. This modified asphalt model was verified through the density calculations and comparisons. After the verification of the model, the properties of the control and xGNP modified asphalt were computed and analyzed using the MD method, and the material properties include the glass transition temperature, viscosity and thermal conductivity. Meanwhile, laboratory tests were conducted to evaluate the viscosity and thermal conductivity of the control and xGNP modified asphalt. The test and MD simulation results show that: (1) the density of the xGNP modified asphalt model is higher than that of the control asphalt model; (2) the glass transition temperature (250 K) of the xGNP modified asphalt model is closer to the laboratory data of the asphalt binders from the Strategic Highway Research Program (SHRP) than that of the control asphalt model; (3) the viscosities of the xGNP modified asphalt model at different temperatures are higher than those of the control asphalt, and it coincides with the trend in the laboratory data. The viscosities of the xGNP modified asphalt model are also

closer to the laboratory data of the xGNP modified asphalt compared to those of the control asphalt; (4) the thermal conductivities of the xGNP modified asphalt model are higher than those of the control asphalt model at different temperatures, and it is consistent with the trend in the laboratory data. Therefore, xGNP particles improve the performance of the modified asphalt, and the same effect of xGNP model is found in the asphalt model using the MD method.

(6) Chapter 6 describes the method and procedure to generate the modified asphalt model and calculate different moduli. The objective of this chapter is to simulate the exfoliated multi-layered graphite nanoplatelets (xGNP) modified asphalt using the MD method, and to analyze different modulus properties of these asphalt models compared with those of the control asphalt model. The multi-layered graphene model was used to represent the xGNP particles, which was used to modify the control asphalt in the laboratory. The control asphalt model was used in the previous study by the authors. The xGNP model was randomly placed in the control asphalt model to prepare the xGNP modified asphalt model using the same conditions and procedures as those in the laboratory preparation. When the xGNP modified asphalt model was generated, the densities of the control and xGNP modified asphalt models were computed and verified. Different properties of these models were simulated and calculated in MD simulations using procedures similar to those in the experiments, which include the bulk modulus, Young's modulus, shear modulus and Poisson's ratio. The simulation results indicate that the modulus trends of these asphalt models are the same as those of laboratory data. The MD simulation data is larger than the laboratory results due to several reasons

discussed in this study. In addition, Poisson's ratios calculated from MD simulations coincide with the laboratory results.

(7) Chapter 7 displays the self-healing behaviors and MD simulations of the asphalt material. This chapter aims to understand the mechanism of the self-healing and diffusion of the asphalt on aggregates. The microscale asphalt mastic samples were prepared with asphalt and fine aggregates of a small size (less than 0.3 mm). The microscale dynamic X-ray computed tomography was conducted to capture the asphalt self-diffusion process on a microscale asphalt mastic sample controlled at 80^{o}C using the Advanced Photon Source (APS) beamline 2-BM at Argonne National Laboratory. The contact angle, activation energy and Mean Squared Displacement (MSD) were analyzed to describe the self-healing behaviors of the asphalt materials. The MD method was employed to simulate the asphalt molecular diffusion process at different temperatures and compute the contact angle between the asphalt and aggregate models. The contact angle goniometer was selected to measure the contact angle between the asphalt droplet and aggregates at different temperatures. The results of the tests and MD simulations show that (1) the asphalt diffused after heating from the x-ray images, and the stages and mechanism of the diffusion process of the asphalt on the aggregates were brought up; (2) a low contact angle was observed in the interface model of asphalt and aggregates at low temperatures using the MD method. The wetting condition changed from partial non-wetting to wetting after heating in the interface model. The molecules of the asphalt model at high temperatures moved faster than when under low temperatures; (3) the test results of the contact angle between the asphalt and aggregates verified the assumption of the diffusion process of the asphalt material, which is made

by the authors. The test data also validated the MD simulation results at different temperatures.

(8) Chapter 8 provides the summary, conclusions and recommendations for future studies.

Chapter 2 Review of the Molecular Dynamics (MD) application in the asphalt material

2.1 Overview

Molecular Dynamics (MD) is a new research tool to analyze the properties of the materials. The usage of the MD method can decrease the discovery time for new materials, and reduce the cost of materials and labor during material development. Asphalt material is widely used for pavement and waterproofing products. The MD application in the asphalt material have been studied by few scholars. The purpose of this study is to collect the literatures about the asphalt and the application of MD in the asphalt material on the atomic scale. The research experience and results of the MD application from other researchers were summarized and analyzed. We learned from other researchers, and established background information on the MD method or its application in asphalt material. Several parts of the MD method were organized and reviewed, which include the sections: Modified asphalt, Multiscale analysis, Molecular dynamics, Force fields, Optimization methods, MD simulation on the asphalt model, MD simulation on asphalt-aggregate and asphalt-modifier models. The advantages of the MD method were explored and listed for material developments. In addition, additional topics and future research issues were also discussed.

The full text of this chapter will be submitted for publication.

2.2 Introduction

There are two common types of pavement widely used in the world, concrete and asphalt pavement. The performance of asphalt pavement majorly depends on the properties of asphalt and aggregates, as well as modifiers, which are commonly used to improve the mechanical and pavement performance. The underlying chemical structure of asphalt determines its properties and adhesion/bonding forces with the aggregates and modifiers. Asphalt is relatively stable and highly resistant to acids and alkalis [6]. However, asphalt can be dissolved in petroleum solvents and emulsified by water. The state of asphalt can be changed by heat and weather, and ambient temperatures strongly affect the performance of asphalt. In a cold environment, the asphalt mainly presents the elastic property, but in a hot environment, the asphalt mostly shows the viscous property and even reaches the liquid state at higher temperatures [4, 14, 15].

Asphalt is a residue from the distillation process for crude oil under a boiler, and it is composed of many elements (carbon: 82.9% - 86.8%; hydrogen: 9.9% - 10.9%; nitrogen: 0.2% - 1.1%; sulfur: 1.0% to 5.4% and oxygen: 0.2% - 0.8% [6]). There are also trace amounts of some metal atoms in the asphalt. The locations of these atoms and connections affects the properties of asphalt. The oxidation of asphalt is the primary issue for the performance of asphalt and it causes the degradation of asphalt. In accordance with the Superpave report [6], asphalt has been separated by the Corbett and Rostler methods. Four components, asphaltenes, saturates, napthene aromatics and polar aromatics were separated by the Corbett method and five components, asphaltenes, paraffins, second acidiffins, first acidiffins and nitrogen bases, by the Rostler method. Asphalt is from different sources with

different compositions. In addition, asphalt can be used for waterproofing products, besides paving roads.

The performance of the asphalt binders and mixtures is tested and analyzed by different tests. The researchers have used many computational tools or methods to understand the asphalt and its behaviors under different loading and temperature conditions. The Discrete Element Method (DEM) and Finite Element Method (FEM) are commonly used to simulate the asphalt and explore the responses of asphalt binders or mixtures. The asphalt material and the analysis tool, Molecular Dynamics (MD), are mainly discussed in this study.

2.3 Modified Asphalt

The distress of asphalt pavement occurs after a few years of service. Different modifiers are applied to improve the overall performance of asphalt binders and mixtures, and extend the pavement life. Based on the literature review [16], the polymer materials were widely used for the modification of asphalt, and polymer modifiers include Styrene-Butadiene-Styrene (SBS) [17], Styrene-Butadiene-Rubber (SBR) [18], Ethylene Glycidyl Acrylate (EGA) [19], rubber [20, 21], different fibers [22-24], plastics [25, 26], etc. The SBS modified asphalt binder increased the flexibility and cracking resistance at low temperatures, and also increased the resistance to rutting and healing characteristics compared to unmodified asphalt binder [17, 27, 28]. The SBR can increase the ductility, elasticity, adhesion and cohesion between the asphalt and aggregates, as well as the reduction of oxidation in the asphalt mixtures [18, 29]. The EGA largely decreased the moisture susceptibility of the asphalt pavement, and also reduced the permanent

deformation by increasing the amounts of EGA in asphalt pavement [19]. The original rubber results in the improvement of ductility and resistance to rutting in asphalt pavement. The effect of the rubber or crumb rubber contents, particle size and temperature on the performance of rubber modified asphalt binder was analyzed. The crumb rubber improved the high-temperature viscosity and reduced the low-temperature stiffness when compared to the original [20, 21, 30]. The fibers improved the high-temperature performance in the modified asphalt binder due to the physical properties of fibers, and different sizes of fibers (micro-fibers [31] or nano-fibers [32, 33]) were also applied to the modification of the asphalt binders and mixtures, including polymer fibers [24, 34], or carbon fibers [31-33]. The polystyrene and polyethylene-based copolymers were also used successfully in the modification of asphalt, and the mechanical properties of the modified asphalt were strongly enhanced [35, 36]. The morphological analysis of these asphalt binders was conducted by the Field Emission Scanning Electron Microscopy (FE-SEM) [31], and the chemical bonding information was observed by the Fourier Transform Infrared Spectroscopy (FTIR) [14].

Nanotechnology, a new material processing technology, emerged and nanomaterials were also adopted to enhance the performance of asphalt. The nanomaterials have nanoclay, nanosilica, carbon nano-fibers [33, 37], nano hydrated lime [38, 39], nanotubes [40], etc. The nanoclay largely reduced the rutting susceptibility in the asphalt matrix, and it is likely that the nanosilica had a positive effect on high-temperature performance and aging resistance [7, 8]. The carbon fibers improved the viscosity and complex shear modulus of asphalt binders, and the nano hydrated lime was designed to

reduce the moisture susceptibility [31, 39, 41]. The nano powdered rubbers also have a great improvement on the softening point and equivalent softening point of the modified asphalt binders [42]. These nanomaterials have a good dispersion in the asphalt matrix from the FE-SEM images, and the anti-aging properties of the modified binder were enhanced by FTIR results.

Some waste products cause environmental pressure, and it is also good to use waste materials in the asphalt to reduce environmental impact or alleviate the distress of asphalt pavement. The waste materials include electronic wastes [43, 44], waste fibers [24], waste glass [45], waste engineering oils [46], waste tires/rubber [21], recycled asphalt pavement [45, 47], etc. These waste materials have a good impact on the high- or low- temperature performance, as well as the resistance to moisture damage.

There are many types of modified asphalt binders under development. Different modification mechanisms were explored, and many analysis tools or tests were used to evaluate the properties and predict the field performance. It is common to use the Finite Element Method (FEM) or Discrete Element Method (DEM) to analyze or simulate the behaviors of the asphalt binders or mixtures. The FEM and DEM were developed for many years in material engineering, and many useful models or algorithms were used for different purposes or predictions. However, there are some limitations on the input parameters in these methods, which can be affected by different operators or methods in the laboratory. The analysis scale used in these methods is also a problem; they only focus on the macro or meso scale. Based on these limitations, the Molecular Dynamics (MD)

method emerged in the field of material engineering or physical areas with the rapid development of computational resources.

2.4 Multiscale Analysis

There are many numerical analysis methods to simulate the materials on different scales, different length/distance and time scales. Different algorithms are applied to solve various differential equations or simulation problems on computers based on physical theories. In 1687, Newton's Principia was published, and the calculus provided a new way to process the infinitesimal changes in movement. Newton's method in classical physics was used by researchers for several centuries, and the foundation for classical mechanics was laid out by Newton. Most models were built based on Newton's laws and methods. Quantum mechanics (QM) is also a branch of physics to process the actions or phenomena of atoms or photons, which is inexplicable by classic physics [48]. Most natural phenomena in theoretical science are substantially non-linear, and the iterated approximations are employed to solve the "non-linear" problem. Errors between the theory and experiments may occur due to some unknown parameters. However, the computer simulations bridge the connection between analytic theories and experiments. The computer simulations can also change the properties of components to analyze the response of the materials and structures, and it is one of the advantages for simulations compared to the experiments. In computer simulations, there are many length- and time- scales to fulfill different purposes and properties of materials (Figure 2.1), such as (1) simulations on the electronic/atomistic scale, which can be implemented by these methods: self-Consistent Hartree-Fock (SC-HF), self-Consistent Density Functional Theory (DFT) (SC-DFT), Car-Parinello (ab initio)

Molecular Dynamics (CPMD), Tight-Binding (TB), Quantum Monte Carlo (QMC), etc.; (2) simulations on the atomistic/microscopic scale by Molecular Dynamics (MD), Monte Carlo (MC) with classical force fields, Hybrid MD/MC, Embedded Atom Method (EAM), Particle in Cell (PIC), etc.; (3) simulations on the microscopic/mesoscopic scale by MD and MC with effective force fields, Dissipative Particle Dynamics (DPD), Phase Field Models, Cellular Automata (CA), Mean Field Theory (MFT), Finite Element Method (FEM), Smooth Particle Hydrodynamics (SPH), Lattice-Boltzmann Method (LBH), Dislocation Dynamics, Discrete Element Method (DEM), etc.; and (4) simulations on the mesoscopic/macroscopic scale by Hydrodynamics, Computational Fluid Dynamics (CFD), Finite Element Methods (FEM), Smooth Particle Hydrodynamics (SPH), Finite Difference Methods (FDM), Cluster and Percolation Models, etc [48].

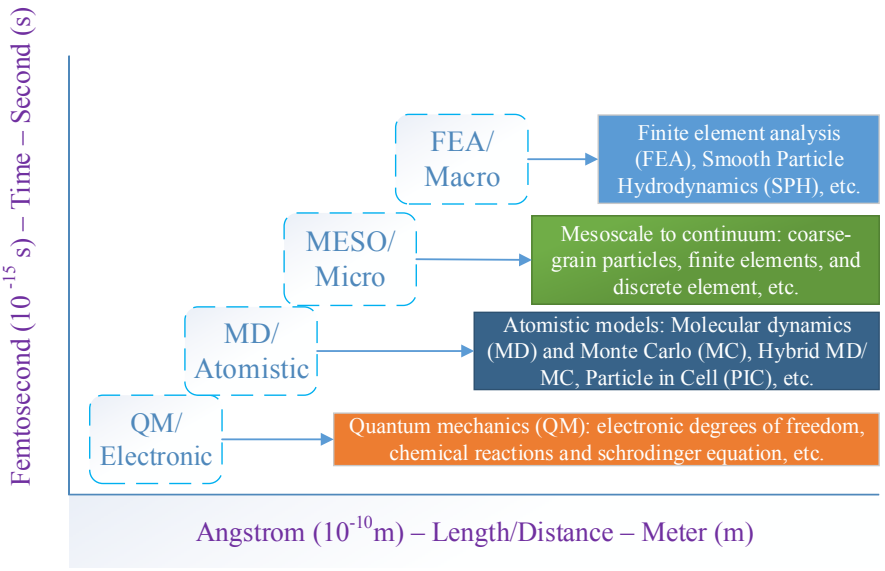

Figure 2.1. Range of different length/distance and time scales in computational simulations

In these simulation methods, the FEM and DEM were popularly used for the asphalt binders and mixtures for many years. Many researchers have contributions for different

simulations by FEM [49, 50] and DEM [51-53]. There are mainly two ways to conduct the simulations for asphalt binders and mixtures. (1) The structures of the asphalt binders and mixtures were generated by the DEM or FEM method; (2) The structures of the asphalt binders and mixtures were formed by the images from scanning real samples. Different properties and tests were simulated by different methods and algorithms, and different contact models were explored for different simulation requirements [54, 55], as well as two-dimensional (2D) [56] and three-dimensional (3D) [57] applications. The input parameters of DEM and FEM methods are from the test data, and the parameters can also be affected by many factors. The DEM and FEM methods are also validated as an effective way to understand and analyze the materials [53, 55].

The DEM and FEM methods focus on the mesoscopic/macroscopic scale to simulate the materials. However, in this study, the use of Molecular Dynamics is discussed for the asphalt material on the atomistic/microscopic scale. (1) The MD method is a new tool for researchers to understand the physical or chemical properties of materials, and explore the movements of molecules on an atomic scale. (2) The usage of MD can describe the details of molecules or atoms over a certain time, and it can be utilized to study the specific principles/problems of molecules/atoms or materials. It is easier and cheaper than doing experiments in the laboratory. (3) In MD simulation, a specific contribution or property can be altered, and it leads to analyze the effect of the changed property. The fundamental research/predictions in the old or newly developed materials are understood. (4) The material behaviors or responses can be analyzed and predicted under extreme conditions, such as very high and low pressures or dangerous situations. (5) The discovery time of new

materials is expedited, and the cost of the development of materials is reduced compared to that of the traditional material, because the extensive preliminary test data needs to be determined whether or not the new material works. The setup and difficulty/failure during testing are the factors used to obtain the experimental data. The cost of materials and labor and discovery time increase in the process of successfully obtaining the test data in early stages. In addition, the success rate of new material development can be improved using MD simulations.

2.5 Molecular Dynamics Method

Molecular dynamics is a computer simulation on the molecular movement of numerous N-body particles based on the physical principles of atoms and molecules. A given period of time is allowed for interaction between the atoms and molecules. The trajectories of atoms and molecules are determined by Newton's law and the forces between the atoms and molecules and are defined by the applied force field. The method originated and was further developed in the 1950s and is now applied in the chemical physics, material science and biomolecules [58, 59]. Due to the number of particles in a complex system, the experimental MD simulation generates cumulative errors in numerical integration. The errors could be minimized by proper algorithms and parameters, but cannot be eliminated. The ergodic hypothesis was obeyed in the system and all microstates in an isolated system are possible and equally probable over a long period of time [60]. The MD analysis provides a new way to fundamentally understand the material behaviors and properties from a particular standpoint. The behavior mechanism of materials can also be explored, and it is good for researchers to modify and improve the properties of materials.

The evolution of dynamics in molecules determines the properties of the systems. The “statistical mechanics” and “Laplace’s vision of Newtonian mechanics” describes the behaviors of molecular dynamics. The simulation size and time were elaborated so that the calculation time is reasonable (normally, less than one week) [61]. Currently, there are five kinds of MD simulations, which include Microcanonical ensemble (NVE ensemble), Canonical ensemble (NVT ensemble), Isothermal-isobaric ensemble (NPT ensemble), Isoenthalpic-isobaric ensemble (NPH ensemble), and Generalized ensembles [62]. (1) In the Microcanonical ensemble (NVE ensemble), the number of moles (N), volume (V) and energy (E) in the isolated system are not be changed. The system experiences an adiabatic process and no heat exchange occurs. In this situation, the total energy of the system is conserved and only the exchange between the kinetic and potential energy can proceed in the system. (2) In the Canonical ensemble (NVT ensemble), the number of moles (N), volume (V) and temperature (T) of the system will not be influenced by other parameters and it is considered to be constant temperature molecular dynamic (CTMD). In NVT, the energies of exothermic and endothermic processes are exchanged through a thermostat. Many thermostat methods are available for adding and removing the energy in the system through the system boundaries in a realistic way. The popular techniques used to control the temperature are the Nose-Hoover thermostat, Nose-Hoover chains, the Berendsen thermostat, the Andersen thermostat and Langevin dynamics. (3) In the Isothermal-isobaric ensemble (NPT ensemble), the number of moles (N), pressure (P) and temperature (T) will be conserved. The thermostat and barostat are needed in the system and its conditions close to the laboratory conditions (ambient temperature and pressure). The volume of the system can be changed freely. (4) In the Isoenthalpic-Isobaric ensemble (NPH ensemble), the

number of moles (N), pressure (P) and enthalpy (H) in the MD system are conserved. In NPH, the volume is available to be changed for the energy calculation, internal energy and kinetic energy. (5) The generalized ensembles is described by the replica exchange method. It was created for the slow dynamics in the disordered spin systems and can be considered to be parallel tempering.

Energy minimization or geometry optimization is another one, and the alternation of geometry leads to the low energy of the system. Different simulations will cause systems to reach a state of equilibrium. In addition, many kinds of software are available for MD simulations, for instance, Adun, Computer Simulation of Molecular Structures (COSMOS), Large-scale Atomic/Molecular Massively Parallel Simulator (LAMMPS), Monte Carlo Method (Towhee), Materials Processes and Simulations (MAPS), Materials Studio, Nanoscale Molecular Dynamics Program (NAMD), etc. The procedure of the MD simulation is shown in Figure 2.2.

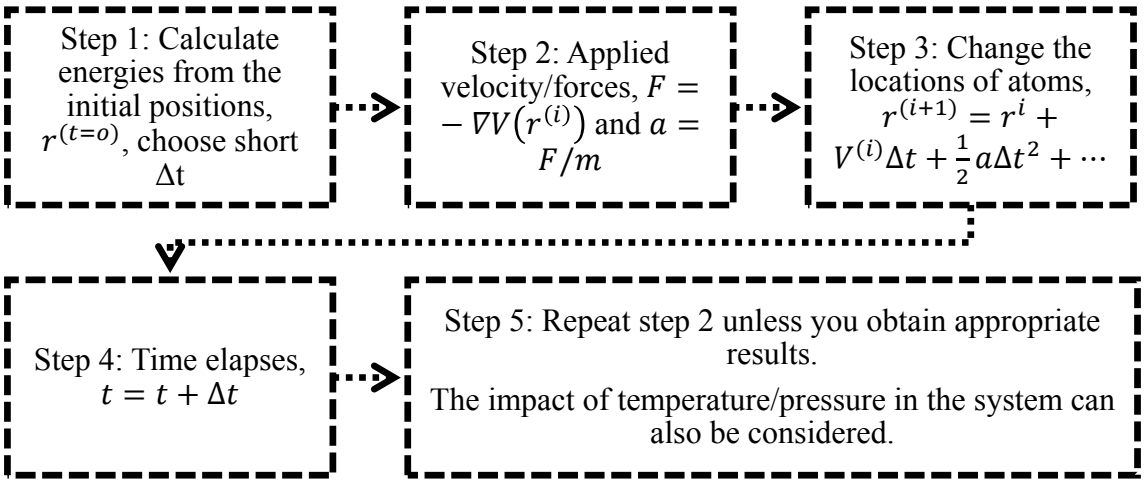

Figure 2.2. Calculation steps in MD simulations

2.6 Force Fields

A force field is used to define the energy calculations of the atoms in the systems. The parameters and functions in the force fields are based on the experimental test data and quantum mechanical calculations. There are many force fields developed by researchers for different materials and purposes, such as the Dreiding Force Field [63], General Amber Force Field (GAFF) [64, 65], Chemistry at HARvard Molecular Mechanics (CHARMM) Force Field [66], Condensed-phase Optimized Molecular Potential for Atomistic Simulation Studies (COMPASS) Force Field [67], Optimized Potential for Liquid Simulation (OPLS) Force Field [66], etc.

(1) DREIDING Force Field

The DREIDING Force Field [63], a generic force field for molecular dynamics and simulations, leads to an accurate prediction for organic systems. Different types of atoms are used in the DREIDING Force Field, and atoms with the same type of atom of the same element are identically treated in the force field. The five parameters are used to simulate the types of atoms and dynamics, and the parameters are as follows: the first two characters indicate the chemical elements, and the third character specifies hybridization: 1=linear (sp^1), 2=trigonal (sp^2), and 3=tetrahedral (sp^3). The fourth character is employed to describe the implicit hydrogen number. The fifth character is created for the function of alternative characteristics.

The potential energy (E) of molecules can be expressed by the summation of bonded interaction energy (E_{val}) and non-bonded interaction energy (E_{nb}), and it is shown in equation (2.1). The four part interactions are counted in the DREIDING Force Field,

such as bond stretch (E_B, two-body), bond-angle bend (E_A, three-body), dihedral angle torsion (E_T, four-body) and inversion terms (E_I, four-body). The expression is shown in equation (2.2). The non-bonded interactions are comprised by the van der Waals or dispersion (E_{vdw}), electrostatic (E_Q) and explicit hydrogen bond (E_{hb}) terms, and are shown in equation (2.3).

$$E = E_{val} + E_{nb} \tag{2.1}$$

$$E_{val} = E_B + E_A + E_T + E_I \tag{2.2}$$

$$E_{nb} = E_{vdw} + E_Q + E_{hb} \tag{2.3}$$

The bond stretch interaction would be expressed as a simple harmonic oscillator in the DREIDING Force Field [63], and it is shown in equation (2.4). For the two bonds IJ and JK sharing a common atom, the angle bend energy can be calculated using equation (2.5). For the torsion interactions between the two bonds IJ and KL connected through a common bond, JK, the energy expression is as shown in equation (2.6). For atom I bonded to three other atoms, J, K, and L, the inversion energy describes the energy required to force three bonds onto the same plane or keep bonds in the same plane. The energy expression is shown in equation (2.7).

$$E = \tfrac{1}{2}\, k_e\, (R - R_e)^2 \quad \text{and} \quad ke = (\delta^2 E/\delta R^2)_{R=Re} \tag{2.4}$$

$$E_{IJK} = \tfrac{1}{2}\, C_{IJK}\, [\cos\theta_{IJK} - \cos\theta^0_J]^2 \tag{2.5}$$

where θ is the angle between bond IJ and JK. The equilibrium angles θ^0_J can be extrapolated from the nearby element in the same column of the periodic table.

$$E_{IJKL} = \tfrac{1}{2}\, V_{JK}\, (1 - \cos\,[n_{JK}\, (\varphi - \varphi^0_{JK})]) \tag{2.6}$$

In the equation above, φ is the dihedral angle (angle between the IJK and JKL planes), n_{JK} is the periodicity (an integer), V_{JK} is the barrier to rotation (always positive), φ^0_{JK} is the equilibrium angle.

$$E^s_{inv}(\psi) = \tfrac{1}{2} K_{inv} (\psi - \psi_0)^2 \quad (2.7)$$

Referring to the equation above, ψ is the angle between the IL bond and JIK plane. K_{inv} is the force constant.

(2) General Amber Force Field

The General Amber Force Field (GAFF) is used for proteins and nucleic acids, and the parameters GAFF are primarily designed for organic molecules, which consists of hydrogen, carbon, nitrogen, oxygen, sulfur, etc. [64, 65]. The formula for GAFF is shown in equation (2.8).

$$E_{total} = \sum_{bonds} K_r(r - r_{eq})^2 + \sum_{angles} K_\theta(\theta - \theta_{eq})^2 + \sum_{dihedrals} \frac{V_n}{2}[1 + \cos(n\varphi - \gamma)] + \sum_{i<j}[\frac{A_{ij}}{R_{ij}^{12}} - \frac{B_{ij}}{R_{ij}^{6}} + \frac{q_i q_j}{\epsilon R_{ij}}] \quad (2.8)$$

where r_{eq} and θ_{eq} are the structural parameters at equilibrium; K_r and K_θ are the force constants; n and γ are the parameters for dihedrals; A, B and q are the potentials for non-bonded atoms; R_{ij} and ϵ are the distances and well depth for the van der Waals forces.

(3) Chemistry at HARvard Molecular Mechanics (CHARMM) Force Field

The CHARMM program is developed and maintained at Harvard, and the force field has been applied to many materials, such as proteins, Deoxyribonucleic acid (DNA), Ribonucleic acid (RNA), lipids, etc. The energy function of the CHARMM force field is shown in equation (2.9) [68].

$$V(\hat{R}) = \sum_{bonds} K_b(b - b_0)^2 + \sum_{angles} K_\Theta(\Theta - \Theta_0)^2 + \sum_{Urey-Bradley} K_{UB}(S - S_0)^2 + \sum_{dihedrals} K_\varphi(1 + \cos(n\varphi - \delta)) + \sum_{impropers} K_\omega(\omega - \omega_0)^2 + \sum_{non-bonded\ pairs}[\varepsilon_{ij}^{min}\left[\left(\frac{R_{min}}{r_{ij}}\right)^{12} - 2\left(\frac{R_{min}}{r_{ij}}\right)^{6}\right] + \frac{q_i q_j}{4\pi\varepsilon_0 \varepsilon r_{ij}}] + \sum_{residues} U_{CMAP}(\varphi, \psi) \quad (2.9)$$

where the parameters, K_b, K_Θ, K_{UB}, K_φ and K_ω are the force constants. b_0, Θ_0, S_0, ω_0 are structural parameters, Other parameters are the same as mentioned above in other force fields. CMAP energy is the numerical correction for proteins, and Urey-Bradley is a quadratic function of the distance.

(4) Condensed-phase Optimized Molecular Potential for Atomistic Simulation Studies (COMPASS) Force Field

The interactions in the COMPASS force field are complex compared to the other force fields [69]. The stretching bond and bending angles were represented by a polynomial with different orders. The formula of COMPASS force field is shown in equation (2.10).

$$E_{total} = \sum_b[K_2(\mathrm{b} - b_0)^2 + K_3(\mathrm{b} - b_0)^3 + K_4(\mathrm{b} - b_0)^4] + \sum_{angles}[K_2(\theta - \theta_0)^2 + K_3(\theta - \theta_0)^3 + K_4(\theta - \theta_0)^4] + \sum_\varphi[K_1(1 - \cos\varphi) + K_2(1 - \cos 2\varphi) + K_3(1 - \cos 3\varphi)] + \sum_\chi K_2\chi^2 + \sum_{b,b'} K(b - b_0)(b' - b'_0) + \sum_{b,\theta} K(b - b_0)(\theta - \theta_0) + \sum_{b,\varphi}(b - b_0)[K_1 cos\varphi + K_2 cos2\varphi + K_3 cos3\varphi] + \sum_{\theta,\varphi}(\theta - \theta_0)[K_1 cos\varphi + K_2 cos2\varphi + K_3 cos3\varphi] + \sum_{b,\theta}(\theta' - \theta'_0)(\theta - \theta_0) + \sum_{\theta,\theta,\varphi} K(\theta - \theta_0)(\theta' - \theta'_0) cos\varphi + \sum_{i,j}\frac{q_i q_j}{r_{ij}} + \sum_{i,j}\epsilon_{ij}[2\,(\frac{r_{ij}^0}{r_{ij}})^9 - 3\,(\frac{r_{ij}^0}{r_{ij}})^6] \quad (2.10)$$

where the energy function consists of two sections, valence terms and non-bond interaction terms. Other parameters are used in other force fields.

(5) Optimized Potential for Liquid Simulation (OPLS) Force Field

The OPLS all-atom force field was developed by Prof. Jorgensen, and it was used to describe the organic molecules, peptides and proteins [70]. The parameters of bonding

and angle were adopted from the Amber force field, and the torsion parameters were obtained from the ab inito calculations. The energy formula is shown in equation (2.11).

$$E_{total} = \sum_{bonds} K_r(r - r_0)^2 + \sum_{angles} K_\theta(\theta - \theta_0)^2 + \sum_{dihedrals}[\frac{V_1}{2}[1 + \cos(\varphi - \varphi_1)] + \frac{V_2}{2}[1 - \cos(2\varphi - \varphi_2)] + \frac{V_3}{2}[1 + \cos(3\varphi - \varphi_3)] + \frac{V_4}{2}[1 - \cos(4\varphi - \varphi_4)]] + \sum_{i>j} f_{ij}[\frac{A_{ij}}{r_{ij}^{12}} - \frac{C_{ij}}{r_{ij}^{6}} + \frac{q_i q_j e^2}{4\pi\epsilon_0 r_{ij}}] \quad (2.11)$$

where, the total energy is composed of two parts, bond interactions and non-bond interactions. f_{ij} is the fudge factor. Other parameters are presented above in other force fields.

2.7 Optimization Methods in Molecular Dynamics Simulation

When the molecular systems are built based on the components at a certain ratio, the energy optimization and data smoothing would be required to optimize the molecular systems. These procedures would help the researchers understand more about the systems they built and use more ways to calibrate and validate the systems. The methods used in these studies are as follows.

(1) Method of Steepest Descent

The method of steepest descent, also called stationary phase method, utilizes the Laplace's method to approximate an integral, where the targeted function deforms a contour integral in the complex plane and closely passes a stationary point through the steepest descent. The method was first brought out by Debye in the year 1909 and it is used to estimate the Bessel functions and Riemann-Siegel formula [71]. In the MD simulation, the steepest descent method was employed to find the minimum energy E_{min}.

$$E_{min} = \int_C f(z)e^{\lambda g(z)}dz \quad (2.12)$$

where C is a contour (graph of contour integral) and λ is large (real number) in Laplace's method. In other words, the required integral deforms the contour of integration where derivative g' (z) is zero (saddle point) so that the contour g possibly reaches the extreme point and is also a real number. However, the value in the saddle point does not mean that the extreme point is in the contour, or vice versa, due to the boundary condition.

(2) Conjugate gradient method

It is common that the conjugate gradient method is used for optimization problems in different systems with direct or iterative methods. It was developed by Hestenes and Stiefel in 1952 [72]. The formulas of the conjugate gradient method are shown below [72-74].

$$Ax = b,\ A \in R^{n\times n} \text{ and } u^T Av = 0, \text{(direct method)} \quad (2.13)$$

$$\mathrm{f(x)} = \frac{1}{2}\mathrm{x^T Ax} - \mathrm{x^T b},\ \mathrm{x} \in \mathrm{R^n}, \text{(iterative method)} \quad (2.14)$$

where A is symmetric, positive and real; b is a coefficient; and vectors u and v are non-zero.

(3) Savitzky-Golay Filter

The Savitzky-Golay filter is a digital filter to smooth the data points and increase the signal-to-noise ratio (SNR) without highly distorting the signal. In the convolution process, it is also used to fit adjacent data points with a low-degree polynomial by the method of linear least squares. If an analytical solution can be obtained by the least-squares equations through data processing, the convolution coefficients would be applied to

estimate the smoothed data/signals of two or three dimensions based on the mathematical procedures generalized by Abraham Savitzky and Marcel Golay [75-78].

$$Y_j^* = \frac{\sum_{i=-m}^{i=m} C_i Y_{j+i}}{N} \tag{2.15}$$

where Y_j is a running index of original data. Each C_i is equal to one and N is the number of convoluting integers for calculating the moving average. The Savitzky-Golay filter is also commonly used as a moving average filter to smooth the data fluctuations, and it can highlight the data trend or cycles.

(4) Particle-Particle-Particle-Mesh (PPPM)

The Particle-Particle-Particle-Mesh (PPPM) is a kind of Ewald summation based on the Fourier method, and two advantages from Particle-Particle (PP) and Particle-Mesh (PM) are combined in PPPM. The PP method is to find the short-range contribution, and the PM method is to find the total slowly varying force (TSVF) contribution. The forces in the PPPM method are separated into two parts (equation (2.16)), and these forces can be displayed by the inverse-square-law forces (equation (2.17) and equation (2.18)) [79].

$$F_{ij} = F_{ij}^{sr} + F_{ij}^{m} \tag{2.16}$$

$$F(r) = \frac{q^2}{4\pi\epsilon_0}\frac{1}{r^2} \; (r \gg a) \tag{2.17}$$

$$F(r) = \frac{q^2}{4\pi\epsilon_0 a^2}\left(\frac{8r}{a} - \frac{9r^2}{a^2} + \frac{2r^4}{a^4}\right) \; (r \ll a) \tag{2.18}$$

It describes two uniformly charged atom with total q and radius a/2, and Other parameters are presented above.

2.8 Molecular Dynamics Simulation on Asphalt model

Based on the Corbett and Rostler methods, the asphalt binder was separated into several components, and researchers created a relatively simple model to represent the asphalt with three components. Two asphaltene structures (asphaltene1 [80] and asphaltene2 [81]) were introduced from the studies of Artok [80] and Groenzin [81]. The n-docosane (n-$C_{22}H_{46}$) and 1, 7-Dimethylnaphthalene were treated as saturates and aromatics, respectively. The contents of these components are based on the molar mass of the asphalt model, and different percentages of these components were used in several references [13, 82]. The OPLS-aa force field was assigned in this asphalt model, and different properties of the asphalt model were analyzed through LAMMPS and the Monte Carlo (MC) Method [13]. The densities of the naphthalene and 1, 7-Dimethylnaphthalene are close to the experimental data. The density trend of the asphalt with different temperatures coincides with the laboratory trend, and there is still a minor difference between MD simulation and experimental data. The glass transition temperature was estimated from around 298.15 K (25^{o}C) to 353.15 K (80^{o}C) based on the results of the thermal expansion coefficient and isothermal compressibility. The low compressibility and high modulus were observed in the asphalt models, and it has a large difference between the experimental data and MD simulation [13].

The molecular orientations of different components were analyzed at different conditions. The molecules of asphaltene 1 stay parallel to each other at a low temperature, but T-shaped for molecules of asphaltene 2. The situation was reversed at high temperatures. The molecules of asphaltene 1 and asphaltene 2 keep intermolecular

orientation around 40°. The angle of fused aromatic rings in the naphthalene is around 0 to 20° [83]. The new seven components were used to model Canadian/Lloydminster (AAA-1) asphalt, and the physical properties and microstructure of the asphalt models were analyzed to better represent the real asphalt. The seven molecules of the AAA-1 model include n-C_{22}, 1, 7-dimethylnaphthalene, ethylbenzothiophene, 3-pentylthiophene, 7, 8-benzoquinoline, ethyltetralin and asphaltene 1 or 2. The density, thermal expansion coefficients, and solubility parameters agreed with the experimental data, and it is better than the prior study [84]. The asphatenes of the AAA-1 model remained parallel. However, the intermolecular orientation changed after polymer modification. The viscosities of the AAA-1 or modified one were calculated by Green-Kubo or Einstein methods [84]. A nonlinear regression was used to compute the rotational relaxation time in the asphalt system. The Green-Kubo and Einstein methods were used to calculate the viscosity at high temperatures. A modified Kohlrausch-Williams-Watts (KWW) described the results of the correlation function for asphalt models, and the Vogel-Fulcher-Tammann (VFT) equation also described the temperature dependence of relaxation time. The diffusion of each component was estimated, and the neat naphthalene moved fastest compared to the other components [85]. The dynamic properties of the model are contributed from each molecule. The relaxation time of molecules in the base or modified asphalt systems was computed and analyzed at the temperature range from 298. 15 (25°C) to 473.15 K (200°C). The KWW was also used to determine the correlation function for each component: asphaltene, polar aromatic, naphthene aromatic, C_{22} and polystyrene. The decrease in temperature led to the increase in relation time, and the modifier, polystyrene, reduced the correlation function. At low temperatures, the rotation of molecules slowed down more than translational

diffusion. The viscosities were estimated by the Debye-Stokes-Einstein equation, and the trend of viscosities was similar to that in literatures [86]. However, there is a huge difference between the MD simulation and test data.

The "cooee bitumen" was simulated by four types of molecules using the MD method: saturate hydrocarbon, resinous oil, resin, and asphaltene. One aging reaction was considered in this case, resins to asphaltenes, based on the trend of experimental data. The mass of the asphalt system is not constant during the reaction. The diffusion and stress autocorrelation function of the molecules in the "cooee bitumen" model were analyzed, as well as the rotational dynamics of the aromatics. The aging in the model causes the total mass to increase and leads asphaltenes to aggregate more and slow down dynamics [87].

Recently, twelve types of molecules were selected and mixed to represent the Canadian/Lloydminster (AAA-1), Venezuelan (AAK-1) and USA/West Texas (AAM-1) binder in order to improve the characteristics of the model compared to the previous model based on the contents of sulfur and carbon and ratio of carbon and hydrogen in aromatics and aliphatics. The asphaltene molecules were modified by Mullins [81, 88]; the rheological and physical properties of the asphalt model were analyzed by the MD method with the OPLS force field. The Hansen solubility parameters (HSP) of four components or each individual molecule were obtained with three-dimensional (3D) space fitting or Van Krevelen and Hoftyzer methods. There are similar HSPs observed with two approaches. However, it is difficult to predict the HSPs of sulfur-containing compositions. The difference in density between the new asphalt model and experimental data is around 0.06g/cm^3, and it is better than the previous model's result [89]. The wide molecular

weights were observed in these components, and six independent temperatures were used in this simulation from 298.15 K (25ºC) to 533.15 K (260ºC). The modified Kohlrausch-Williams-Watts function was used to regress the correlation time to estimate the relaxation times of each molecules. The increased size and decreased temperature caused the reduction of rotational relaxation rate in the molecules. It is interesting to obtain that the activation energy of these molecules is around 42 kJ/mol, and the diffusion coefficient and rotational relaxation time changes from 358.15 K (85ºC). The viscosities of the model at the temperature of 533.15 K are estimated through the Debye-Stokes-Einstein theory, and the results are consistent with the test data [90].

The self-healing mechanisms of the asphalt binder were researched using the MD method, and the binder model contains one asphaltene, 12 naphthene molecules, and 6 n-C_{23} at a ratio of 20:20:60 by the molecular mass. The self-diffusion function of molecules in asphalt covered the crack interface. The influence of chain length and branching of molecules on the self-diffusion was also studied in the asphalt model. The MD simulation results show that the increase of branching decreased the rate of diffusion in the crack interface, but the reversed trend was observed for the CH_2/CH_3 ratio in the model [91].

The effect of the antioxidants (eg, coniferyl-alcohol lignin) in the asphalt was studied based on Quantum Chemistry (QC), and the physical and chemical behaviors of the modification were developed [92]. The modification and aging mechanisms between the antioxidants and asphalt were explored through the chemical reactions using the Reactive Force Field (ReaxFF). The predication is also validated by the X-ray Photoelectron Spectroscopy (XPS) test. The aging effect of asphalt led to a chain-breaking

phenomena and reacted with oxygen. The molecules with a light molecular weight (alkanes and sulfoxides) were formed, and the oxidation and hardening of asphalt continued. Sulfoxides (initial stage) and ketones (following stage) are the major aging products from the reactions, and during the aging process, some intermediate chemicals were observed through MD simulation on an atomic scale. Therefore, the aging mechanisms include the oxidative hardening, chain-breaking of saturates, sulfoxidation, ketonization of benzylic carbons, etc. There is a positive effect of anti-aging of coniferyl-alcohol lignin in asphalt from the MD simulations and test results [92].

The intrinsic healing characteristics of asphalt binders have a correlation with thermodynamic properties and surface free energy, as well as the activation energy. The effect of chain length and branching of molecules for self-healing properties were also analyzed through MD simulations [93]. It can be verified by the FTIR results. The apparent activation energies (AAE) of the components (aromatic and aliphatic) in asphalt were tested based on the molecular movement, and the AAE of the aliphatic is higher than that of aromatic. It infers that the energy barrier of aromatic is low for movement of molecules. The explanations of this low energy can be demonstrated from two sides, (1) the spin-diffusion interaction, and (2) in-plane rotation [94].

The nanoaggregation of the asphaltene (one of the components of asphalt) was studied using the MD method, and four types of asphaltenes were modeled and layered by toluene and water, two uncharged asphaltenes, and two with a carboxylic group. The uncharged asphaltenes stayed around central positions of toluene layer, and two with a carboxylic group neared the interface between the toluene and water. The diffusions

direction of the asphaltenes in the toluene were parallel to the interface between the toluene and water, and the diffusion in other directions was suppressed [95]. The molecular oscillation behaviors of the asphaltenes were observed at the interface of oil and water based on the interfacial tension (IFT) results [96]. The aggregation mechanisms of the asphaltenes in different solvents (water, toluene and heptane) were investigated, and three different models with similar molecular weight represent asphaltenes. The MD results show that the asphaltenes aggregate with less surface-active in a pure solvent. The average structure of asphaltenes reflects the bulk properties, but not surface active properties [97].

The aggregation of the asphaltenes was also investigated with different aliphatic/aromatic ratios using MD simulations. There is no relationship between the aggregation level and aliphatic/aromatic ratios. The main aggregation force of asphaltene in toluene is from the attraction between the poly-aromatic cores, and the size and stability of asphaltenes were reduced in toluene relative to water [98]. The aggregation of the asphaltenes was investigated under heating using the MD method. The dissociation of the hydrogen bond in asphaltenes occurred at 523 K, and interactions between the aromatic-aromatic molecules were relatively stable. When the temperature increased to 673 K, the disruption of some aromatic-aromatic molecules started. The aliphatic chains and polar functional groups help stabilize the structure of the asphaltenes [99]. The influence of intermolecular interactions was evaluated during the aggregation process. A strong aggregation of asphaltenes was observed in heptane, and there is no further aggregation of asphaltenes peptized by resins based on the Molecular Mechanics (MM) and Molecular Dynamics (MD) methods [100]. There is also a relationship between the aliphatic side

chain length and aggregation level of asphaltenes in water. The aggregation is beneficial from the relative short or long aliphatic chains in asphaltenes, but not intermediate chains based on the MD simulations. The π-π interactions mainly led to the aggregation of asphatlenes with short aliphatic chains, and the θ-θ and π-θ interactions caused the asphaltenes with long aliphatic chains to aggregate together [101]. A linear trend between the hydrogen/carbon ratio and mean solubility parameter of the fractions in asphalt or oils was observed, and the solubility parameter can be deduced by the amount of hydrogen. No relationship between the amounts of heteroatom in asphalt and mean solubility parameter was found due to different contents in different asphalt or oils [102].

It is useful to calculate the density of the asphaltenes, as it relates to the structures of asphaltenes. In MD simulation, the density of asphaltenes with an average structure is lower than the experimental values, and the large aromatic rings and low hydrogen-carbon ratio lead to a high density of the asphaltenes from the calculated results with structural factors [103]. The aging issue of asphalt causes pavement distresses, and the aging effect of components of asphalt was studied, such as asphaltenes and resins. Different aging levels of asphaltenes and resins were considered in the MD systems, and the system energy, density and glass transition temperature were monitored and computed. The MD simulation results indicate that the amount of oxygen in asphaltenes affected the glass transition temperature (Tg), and Tg decreased when the oxidation level increased. However, there is no obvious trend between oxidation level of resins and glass transition temperature. The high temperature also provides more thermal energy to accelerate the movements of molecules and break the association between them [104].

Therefore, few components were used and mixed to represent the asphalt in MD simulations. The different properties of each component and asphalt models were simulated and analyzed. However, limited properties of the asphalt model were calculated, and there are still some properties that need to be explored.

2.9 Molecular Dynamics Simulation on Asphalt-aggregate model

The relationship between the asphalt and aggregate was developed and the asphalt-quartz structure model of the interface was used in the system. The CVFF_aug force field was considered in this simulation to characterize the inter-atom interactions. The shear stress and viscosity were evaluated and the acceptable simulation results were obtained in the study using the CVFF_aug force field. In the further study, the elastic properties, stiffness, shear modulus, Young's modulus and Poisson's ratio were calculated in the asphalt mixtures using molecular modeling. The deformation and failure of asphalt-rock systems were also researched when the system was subjected to uniaxial tension. The tensile strength and adhesion failure of this interface system was controlled by environmental conditions and shear stress rate [105].

Moisture damage is one of the major distresses in asphalt mixtures, and the effect of water on the interface between the asphalt and aggregates was investigated. Two asphalt models were composed either of asphaltene1 or asphaltene2, aromatics and saturates. The 1, 7-Dimethylnaphthalene and n-docosane (n-$C_{22}H_{46}$) represented the aromatics and saturates [13]. The structure of the quartz is used to represent aggregates. The asphalt-water-quartz (three-phase) system was generated to understand water diffusion and the mechanism of moisture damage. Different properties of the asphalt model with the CVFF

force field were calculated to calibrate the asphalt model, including density, thermal expansion coefficient, isothermal compressibility, and bulk modulus. The general trends of these results were similar to the references, but improvements are needed for future research. The adhesive stress of the interface model under the tension was recorded to quantify the adhesion stress between the asphalt and aggregate with or without water. From the simulation tests, the maximum strength around 250 MPa can make a gap with 2.8 angstrom between the asphalt and aggregates. It is different from the laboratory data, and it is caused by the defect-free atomic models and the spatial limitations. The surface texture and porosity of the real aggregates are also the reasons for the differences between the laboratory and simulation data. It is noticed that the loading rate on the interface model does not have much effect on the adhesion strength between the asphalt and aggregates in MD simulations. The model size effect of interface models was also considered, and the smallest size of the interface model has a largest adhesive stress. The stress decreased with the increase in model size. However, the adhesive stress between the asphalt and aggregates tends to be stable when the model size of model-3 is 3 times larger than the original one. In addition, different water contents in the interface models (three-phase systems: asphalt-aggregate and asphalt-water-aggregate) were used to investigate the effects of moisture. The simulation results indicate that the interface strength between the asphalt and aggregate decreased with the increase in water content in the interface models. The chemical compositions of the asphalt models also have an influence on the moisture susceptibility of interface models. It is observed that the temperature can also significantly affect the interface strength in the asphalt-aggregate and asphalt-water-aggregate models [106].

2.10 Molecular Dynamics Simulation on Asphalt-modifier model

Two types of modifiers were used to modify the asphalt model, Styrene-Butadiene-Styrene (SBS), and Maleic Anhydride Grafted SBS (MAH-g-SBS). The structures of asphaltenes determined the effect of modifiers based on the MD simulation results. The asphalt binder models with more alkanes tend to agglomerate together, as well as with more SBS modifiers [107]. A single polystyrene chain, with a molecular weight of 5223.6 g/mol was added into the asphalt model, which contains asphaltene2 [81], n-docosane (n-$C_{22}H_{46}$) and 1,7-Dimethylnaphthalene. The addition of the polymer in the base asphalt increases the density and bulk modulus, and decreases the thermal expansion coefficient and isothermal compressibility of the modified asphalt model [13]. The polystyrene molecules with 50 units were added to the AAA-1 model, and modified AAA-1 model was prepared. The density increased after the modification. The temperature susceptibility of the modified AAA-1 model decreased based on the results of the bulk modulus, isothermal compressibility, and expansion coefficients, and the diffusion slowed down after modification. The first peak positions of asphaltenes changed with the temperatures based on the radial distribution function (g(r)), as well as asphaltenes in the modified AAA-1 model. A high folding angle between aromatic rings in the AAA-1 model was observed with increasing temperatures, as well as rings in the modified AAA-1 model. The polymer modification did not change intermolecular orientations of small molecules and intramolecular orientation of molecules, or the packing and radial distribution. The polystyrene molecules changed the distribution of asphaltene 2, and low-temperature intermolecular orientations [84].

The base asphalt and asphalt with linear Styrene-Butadiene-Styrene (SBS) were simulated using the molecular dynamics method to understand the self-healing mechanism. The COMPASS (Condensed-phase Optimized Molecular Potentials for Atomistic Simulation Studies) Force Field was used for the base and SBS modified asphalt model. The structures of the linear SBS and modified asphalt are shown in Figure 2.3. The density and glass transition temperatures of the base and SBS modified asphalt models were calculated, and the results are identical to those of real asphalt. A simple crack interface model of the asphalt was generated, and the diffusion of asphalt was simulated. The diffusion coefficients were calculated from the mean square displacement (MSD). The presence of SBS in the base asphalt increases the diffusion under high temperatures. The activation energy and pre-exponential factors were also analyzed to define the self-healing properties of asphalt [108]. It is common to use the polymeric materials to enhance the thermos-mechanical properties of asphalt and reduce the period of pavement maintenance and increase the service life. Styrene-Butadiene Rubber (SBR) was used to modify the control asphalt, and the different properties of the control and modified systems were investigated, including the volumetric, structural and dynamic properties. In MD simulations, the addition of SBR did not affect the volumetric properties of the modified asphalt model, and it caused the aggregation of asphaltenes, as well as reducd the mobility of the asphalt components [109].

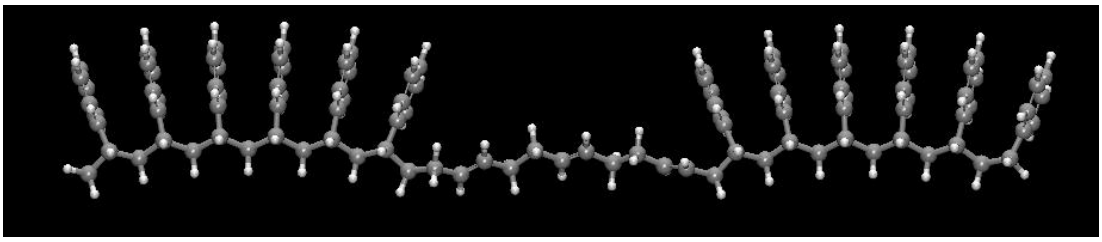

Figure 2.3. The molecular structure of linear Styrene-Butadiene-Styrene

Note: the black atom represents carbon and the white atom indicates hydrogen. The molar mass of SBS ($C_{108}H_{116}$) is 1414.08g/mol [108].

2.11 Summary and Recommendation

This study reviewed the application of molecular dynamics to understand the asphalt material in the field of civil engineering. Most of the references listed in this study focused on the property analysis and development of asphalt material. The application of molecular dynamics was divided into six parts: molecular dynamics method, force fields, optimization methods, molecular dynamics simulation on asphalt, and molecular dynamics simulation on asphalt-aggregate and asphalt-modifier. Based on the literature review, the primary viewpoints were summarized as follows.

(1) The application of the asphalt material was demonstrated in different areas. The components of the asphalt material were explicitly classified based on two methods, Corbett and Rostler methods. The properties of the asphalt changed with the ambient temperatures, and it consists of elastic and viscous parts. The element analysis in the asphalt material was also discussed.

(2) The performance of the asphalt material can be improved by different modifiers. The researchers tried to use various materials to enhance the performance to fulfill different

requirements. The modifiers include polymers, fibers, nanomaterials, and waste materials, etc. For instance, SBS, SBR, EGA, different kinds of rubbers with various sizes, fibers with different sizes (micro- and nano-fibers), different plastics, many kinds of nanomaterials (Nanoclay, nanosilica, nano-fibers, nano hydrated lime, nanotube, etc.), and waste materials (waste tire rubber, waste plastic, waste fibers, waste glass, waste oils, etc.) were used. These modifiers improved the properties of the asphalt material, or a specific property. The mechanisms of the modifiers in the asphalt materials are different and found by different tests and simulations, and the mechanism includes physical dispersion and enhancement, chemical reactions, physical dispersion and chemical reactions. The tests have Superpave Tests, Marshall Tests, SEM, FTIR, Gel permeation chromatography (GPC), Atomic-force microscopy (AFM), Nano indentation, etc. In the computer simulations, the DEM and FEM methods were commonly employed to disclose the mechanism and simulate the properties of the asphalt binders and mixtures.

(3) The asphalt material was analyzed and simulated on different scales, and there are electronic, atomic, microscopic, mesoscopic, and macroscopic scales. The length of the materials is from Angstrom to meter, and the timeframe is from femtosecond to second. Various methods and tools can be employed for analysis on different scales. The DEM and FEM methods primarily concentrated on the meso- and macro- scales. The MD discussed in the study essentially focused on the atomistic scale.

(4) The MD is a new method for material analysis due to the development of computational resources. The MD provides a fundamental view for different materials, and five kinds of simulations are commonly used including NVE, NVT, NPT, NPH, and generalized

ensemble. Many methods and algorithms were employed to realize different thoughts and analyses and better understand the materials and its development. The procedure of MD simulations was also discussed, and LAMMPS and MC methods were usually utilized for MD simulations.

(5) Force fields are the energy functions or parameters to define and calculate the energies or potentials in systems. All-atom force fields regulate coefficients for every atom in systems. Many force fields and the calculation equations were presented and explained. Different force fields may be suitable for different materials or properties. Different optimizations were also introduced to minimize the system energy and reach the equilibrium state. The optimization methods have 1) the method of steepest descent, 2) conjugate gradient method, 3) Davidon-Fletcher-Powell formula, 4) Broyden-Fletcher-Goldfarb-Shanno algoritm, etc.

(6) Different components (asphaltenes, napthene aromatics, polar aromatics, and saturates) were composed of the asphalt model in accordance with the Corbett method. Many properties of the asphalt models were calculated and inferred, and compared to the laboratory data, as well as the properties of each component in the asphalt models. The properties include the density, thermal expansion coefficient, glass transition temperature, isothermal compressibility, solution parameters, bulk modulus, etc. The molecular orientations of components were studied to analyze the effect of locations/positions of atoms or molecules, which can be linked to the changes of properties in the asphalt material. The relaxation time of each molecules was estimated by the modified Kohlrausch-Williams-Waats function. The viscosities of the asphalt models were estimated through the Debye-Stokes-Einstein theory. The self-healing

mechanisms of the asphalt material were studied, and the crack was recovered during the increase in temperature. The diffusion rate was related to the temperature, and the effect of the side chains of components on the properties was evaluated using the MD method, as well as the effect of the antioxidants and aging issue. In addition, the aggregations of each component (asphaltenes, napthene aromatics, polar aromatics, and saturates) were observed and analyzed under different conditions, solutions or interfaces.

(7) The relationship between the asphalt and aggregate is a major topic for researchers, and it relates to the performance and interaction mechanism of the asphalt mixtures. Few studies cover this topic using MD simulations. The asphalt-quartz system represents the asphalt mixture in MD simulations. The elastic properties of the asphalt-quartz system were calculated and the deformation and failure behavior of the asphalt-quartz system was simulated. The moisture mechanisms of the asphalt-quartz and asphalt-water-quartz system were revealed to understand the moisture damage. The effects of the stress, loading rate, model size and moisture content in the asphalt-quartz or asphalt-water-quartz system were investigated for analysis of moisture susceptibility in the asphalt mixtures.

(8) The relationship between the asphalt and modifier was also explored and studied through MD simulations. The polystyrene, SBS and SBR were added to modify the asphalt model. The properties of the modified systems were computed and analyzed and they included the density, diffusion coefficients, radial distribution function, glass transition temperature, etc. The results show the polystyrene changed the distribution of asphaltenes, and intermolecular orientation. SBS increased the diffusion coefficients

at high temperatures, and SBR induced the aggregation of asphaltenes, and reduced the mobility of components in asphalt models.

Based on the discussions and observations of the literature review, few studies on the properties of the asphalt model were carried out. There are still some additional properties of the asphalt model that need to be explored and discussed as follows.

(1) The potential use of a modified force field could be applied to the asphalt model in order to better define the energy of all atoms. The ESP or force field charges of the atoms can be used for the atoms. The properties of the asphalt model with a modified force field can be computed and analyzed, and the properties include density, glass transition temperature, viscosity, different modulus, thermal conductivity, etc. The comparison between the experimental and simulation data is conducted for evaluation and validation of the MD method.

(2) Various modifiers could be adopted for the modification of the asphalt model to obtain the preliminary data of the modified system. Different properties mentioned above can be calculated and compared to the base asphalt system.

(3) The adhesion relationship between the asphalt and aggregate is explored and analyzed through the MD simulation, and the effect of aging of the asphalt material can also be considered for adhesion energy. In addition, the diffusion of the asphalt material on aggregates can be studied for a self-healing mechanism using MD simulations; the activation energy of the asphalt is calculated and used to explain the movement of the molecules in the asphalt material. The contact angle between the asphalt and aggregate is explored to explain the process of self-healing of the asphalt on aggregates.

(4) More optimization methods can be used to optimize the system energy, such as Hessian-free truncated Newton algorithm and damped dynamics method.

(5) More components in the model can be added and optimized, and the molecular structure of each component can also be modified for different purposes.

(6) The calculation methods and boundary conditions will be explored during the property calculation of the asphalt model.

The authors recommend MD as an important research tool to understand more fundamental mechanisms of different materials or interfaces, such as the pharmaceutical development, explosion protection, surface treatment, etc. The MD method provides a special view for the material discovery and developments. The advantages of the MD method were discussed above in MD and multiscale analysis sections. It has a great potential to generalize the MD method for research, as well an excellent promotional value and social interests.

2.12 Acknowledgements

The authors appreciate the financial support of the U.S. National Science Foundation (NSF) under grant 1300286. The computational studies were performed using the computer cluster (Superior Research Center) at Michigan Technological University.

Chapter 3 Molecular Dynamics Simulation of Physicochemical Properties of the Asphalt Model

3.1 Overview

The objectives of this molecular dynamics study are to simulate the asphalt model using the common components from the references, and to predict the physical properties of asphalt material. The asphalt model consists of three components: the asphaltene, aromatic, and saturate, at the ratio of 5:27:41. The docosane and 1, 7-Dimethylnaphthalene represents the saturate and naphthene aromatic, respectively. The Amber Cornell Extension Force Field was adopted and utilized in the asphalt model system, and the experimental parameters associated with this force field were obtained from the General Amber Force Field (GAFF). The geometry and energy optimizations of the molecular components were used to establish the stable asphalt model system. The density of the asphalt model system was calculated with the Amber Cornell Extension Force Field. The predicted densities were compared with the laboratory data to verify the model. Moreover, the glass transition temperature range of the molecular asphalt model was computed from the relationship between the specific volumes and temperatures after the molecular dynamics experimental simulation.

The full text is reprinted with permission from Elsevier. "Molecular Dynamics Simulation of Physicochemical Properties of Asphalt Model, Fuel, 164, 83-93. Jan. 2016." by Hui Yao, Qingli Dai, and Zhanping You. See copyright clearance in Appendix A.

The glass transition temperature range had a good correlation with the experimental data. The viscosity data of the molecular asphalt model was calculated using the Muller-Plathe algorithm. The predicted viscosities at specific temperatures were also compared and discussed with the laboratory data and other published results. In addition, the bulk modulus of the molecular asphalt model was determined and obtained by applying the infinitesimal strain in the model boundaries. The results of the analysis of the bulk modulus in the asphalt model were compared to the reference data, and these predicted results were better than the reference values.

3.2 Introduction

Asphalt is widely applied in pavement engineering due to the good performance of pavement in asphalt mixtures. Asphalt material is the byproduct of petroleum refinement, and the petroleum is naturally generated from organic matter, which forms under the ground over millions of years, subjected to various conditions of very high pressures and temperatures. About 90 to 95 percent (by weight) of asphalt is comprised of carbon and hydrogen, and it is called a hydrocarbon (an organic material). The rest of the asphalt consists of two types of atoms, heteroatoms and metals, such as nitrogen, oxygen, and sulfur [7, 8, 14]. These interactions of atoms determine the physical and chemical properties of asphalt. The carbon content of asphalt is around 82.9% to 86.8%, and the hydrogen content ranges from 9.9% to 10.9%. The contents of nitrogen, sulfur, and oxygen range from 0.2% to 1.1%, 1.0% to 5.4%, and 0.2% to 0.8%, respectively [6]. In addition, some metal atoms can be found in the asphalt, such as nickel, iron, and vanadium. However, the quantities of all metals are less than 1 percent by weight of the asphalt. The existence

of these atoms that occur in small amounts depends on the locations and aging status of the asphalt. Currently, asphalt components can be separated by the Corbett and Rostler methods. Different absorption and desorption techniques are used in the Corbett method to separate the asphalt, and the four components are asphaltenes, saturates, napthene aromatics, and polar aromatics. Meanwhile, sulfuric acid is used in the Rostler method to separate the asphalt, and the five components are asphaltenes, paraffins, second acidiffins, first acidiffins, and nitrogen bases [6]. In addition, three types of molecules are presented in the asphalt: aliphatics, cyclics, and aromatics. These molecules interact with each other and directly affect the physical and chemical behaviors of asphalt.

Molecular dynamics (MD) is a computer simulation of the molecular movement of numerous N-body particles based on the physical principles of atoms and molecules. The trajectories of atoms and molecules are determined by Newton's law and the forces between the atoms and molecules, and are defined by the applied force field. A given period of time is allowed for the interaction between the atoms and molecules. Researchers have studied the asphalt material using the methods for molecular dynamics. Actually, investigations on the molecular level can increase the fundamental understanding of the properties of asphalt, as well as the modification mechanism. The asphalt binder models were recently established using the Large-scale Atomic/Molecular Massively Parallel Simulator (LAMMPS) and the Monte Carlo Method (Towhee) [13, 83, 85]. Two asphaltene structures (asphaltene1 [80] and asphaltene2 [81]) were modeled by following by the results of Artok [80] and Groenzin [81]. The n-docosane (n-$C_{22}H_{46}$) and 1,7-Dimethylnaphthalene were adopted to model the saturate and aromatic compositions in the

asphalt binder, respectively. The number of molecules, mass fraction, and mass percent by atom in the asphalt binder models were calculated to fit the parameters of the references. The OPLS-aa (all-atom optimized parameters for liquid simulations) Force Field was employed in this study to analyze the properties of asphaltene1 and asphaltene2, as well as other components in the asphalt models, such as the density and thermal expansion. The computational results showed that the OPLS-aa Force Field can efficiently supply the parameters and provide sufficient accuracy for the simulation. The temperature-density results between the simulations and experimental test data were correct. The effect of polymer modification in the asphalt binder was proven in the simulation through the property changes of the modified asphalt in the model [13]. They also studied the molecular orientations of three components in the asphalt binder models. The results showed that the orientations of the molecules near the asphaltenes were affected by the molecular structures and temperatures [83].

The tests for the relaxation time and diffusion of the asphalt components were conducted using the molecular dynamics simulation over different temperatures. The viscosity of the asphalt was computed by the Green-Kubo and Einstein methods at different temperatures [84]. A modified Kohlrausch-Williams-Watts function was employed and the results were regressed to obtain the relaxation times for the asphalt model. The Vogel-Fulcher-Tammann and Debye-Stokes-Einstein equations were adopted to evaluate the viscosity and the diffusion of the asphalt model. The computational results revealed that the neat naphthalene diffused faster than the other components of asphalt binders and the asphaltene molecules diffused slowest in the asphalt models [85].

Recently, a new MD model was proposed to represent the Canadian/Lloydminster (AAA-1), Venezuelan (AAK-1), and USA/West Texas (AAM-1) asphalt, utilizing three kinds of asphalt molecular compositions in accordance with the element, molecular types, and composition fractions. The new model has 12 molecular components based on the common three-component model. The new model, with longer branches, contains four molecular groups: saturates, naphthene aromatics, polar aromatics, and asphaltenes [89]. In this model, the asphaltene molecules were obtained by Mullins [81, 88]; the saturate fractions were represented by the squalane and hopane; the naphthene aromatic molecules were simulated by the perhydrophenanthrene-naphthalene (PHPN) and dioctyl-cyclohexane-naphthalene (DOCHN); the polar aromatic molecules were displayed by modified quinolinohopane, thio-isorenieratane, benzobisbenzothiophene, pyridinohopane, and trimethylbenzene-oxane. The new asphalt model overcame the weaknesses of previous models, such as the low density and fast relaxation time, and showed a better representation and property prediction [89].

The dynamic modulus and shift factors were also simulated in the asphalt binder model. The horizontal shift factors were fitted into the Williams-Landel-Ferry equation with parameters [104], and the dynamic modulus data was interpreted using the Maxwell models. The thermodynamic properties of asphalt binder components were analyzed by Tarefder and Arisa [104]. The results of the simulation include the density, glass transition temperature and potential energy of the systems. The results showed that the resin and asphaltene systems had a different relationship over a range of temperatures. The percentage of oxygen influenced the glass transition temperature. Oxidation levels affected

the glass transition temperature of asphaltenes and did not affect the glass transition temperature of resin in the study [104]. In this study, MD was employed to calculate the physical properties of asphalt. The validated asphalt model helps us to understand the components of the asphalt and the interaction/relationship between the components from a molecular aspect.

3.3 Scopes and Objectives

The objectives of this study are to simulate the asphalt model using the common components from the references and to predict the physical properties of asphalt material. The Amber Cornell Extension Force Field was applied to the molecular systems, and the Electrostatic Potential (ESP) charges were allocated to these components with the NWChem analysis using quantum mechanics (QM). The densities of the molecular asphalt model were used for the verification of the asphalt model. After verifying the model, the property simulations of the asphalt model were carried out, including the glass transition temperatures, viscosity, and bulk modulus. Different calculation methods were employed to simulate and predict these properties of the asphalt model. The comparisons of the predicted results with the laboratory or reference model data were conducted. In addition, these calculation and optimization methods used in this study are useful for simulating other materials, and these are also the references for generating a new asphalt model.

3.4 Molecular Dynamics Simulation Theory and Force Field Potentials

3.4.1 Classic MD simulation procedures

Normally, five kinds of simulations were adapted in the experimental MD simulation including the Microcanonical ensemble (NVE ensemble), Canonical ensemble

(NVT ensemble), Isothermal-isobaric ensemble (NPT ensemble), Isoenthalpic-isobaric ensemble (NPH ensemble), and Generalized ensembles [62]. Energy minimization (also called geometry optimization) is another kind of MD simulation, and the geometric change in the model leads to a low energy of the system. In this research, the energy minimization, and NVT and NPT simulations have been used to bring the system to equilibrium. In addition, the procedure of the experimental MD simulation is shown in Figure 3.1.

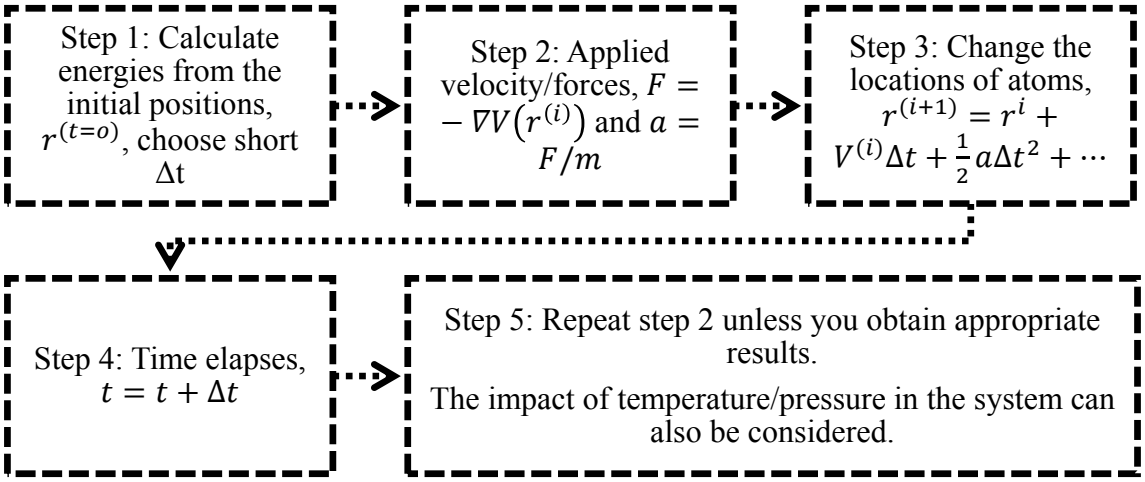

Figure 3.1. Simple procedure of experimental MD simulations

3.4.2 Force Fields

Amber (Assisted Model Building with Energy Refinement) Force Field was first developed for nucleic acids, proteins, and organic molecules. Due to the limited parameters of the original Amber Force Field, the researchers made efforts to add the parameters to the Amber Force Field to apply it for different purposes, such as in the energy calculation and MD simulations. The Amber Cornell Force Field and General Amber Force Field (GAFF) were used for many organic molecules and biological molecules [64, 65]. Equation

(3.1) is often used to describe structures and bonded and non-bonded energies in molecular systems. In this study, the parameters of GAFF were added into the Amber Cornell Force Field, and it is called the "Amber Cornell Extension Force Field" for the energy calculation.

$$E_{total} = \sum_{bonds} K_r(r - r_{eq})^2 + \sum_{angles} K_\theta(\theta - \theta_{eq})^2 + \sum_{dihedrals} \frac{V_n}{2}[1 + \cos(n\varphi - \gamma)] + \sum_{i<j}[\frac{A_{ij}}{R_{ij}^{12}} - \frac{B_{ij}}{R_{ij}^{6}} + \frac{q_i q_j}{\epsilon R_{ij}}] \quad (3.1)$$

where the first term, bonds, is the energy between the covalently bonded atoms (two atoms); the second term, angles, is the energy caused by the geometry of electron orbitals (three atoms); the third term is the energy from twisting a bond (four atoms); and the fourth term is non-bonded energy from van der Waals and electrostatic energies (atom pairs). r_{eq} and θ_{eq} are the equilibrium structural parameters; K_r and K_θ are the force constants; n and γ are the multiplicity and phase angle for the torsional angle parameters, respectively; A, B and q are the non-bonded potentials between all atom pairs; and finally, R_{ij} and ϵ are the distances of the atoms and well depth for the van der Waals energy calculation.

3.4.3 Optimization Methods in Experimental MD Simulation

(1) Conjugate Gradient Method

The conjugate gradient method, with an iterative or direct algorithm, is used for numerical solutions of particular systems with linear equations. The conjugate gradient method with a direct algorithm is normally used in small and simple systems, as well as in Cholesky decomposition [110]. However, the partial differential equations and optimization problems are common in large sparse systems, and the conjugate gradient

method with an iterative algorithm can be applied in these large and complex systems for solutions and optimizations [111]. The computing equations are shown below.

$Ax = b,\ A \in R^{n\times n}$ and $u^T Av = 0$, (direct method) (3.2)

$f(x) = \frac{1}{2}x^T Ax - x^T b$, $x \in R^n$, (iterative method) (3.3)

where A is symmetric, positive and real; b is a coefficient; and vectors u and v are non-zero.

(2) Particle Mesh Ewald Method

The Particle Mesh Ewald (PME) method is a kind of Ewald summation. Ewald summation, named after Paul Peter Ewald, is a method to compute the long-range interactions in periodic systems. In Ewald summation, the long-range interactions can be separated into short-range and long-range contributions. The short-range interaction potential is calculated in real space, and the long-range interaction potential is calculated by a Fourier transform [112-114].

In the Particle Mesh Ewald (PME) method [113, 114], the generic interaction potential can also be divided into two parts, short-range and long-range interactions. In this method, the direct summation will be replaced by a particle mesh Ewald summation between particles. The PME method has several advantages for calculating the long-range forces in largely molecular systems, these being high accuracy, continuity, and efficiency. Additionally, the PME method can be integrated into conventional MD algorithms.

$E_{Tot} = \sum_{i,j} \varphi(r_j - r_i) = E_{sr} + E_{lr}$ (3.4)

$$E_{sr} = \sum_{i,j} \varphi_{sr}(r_j + r_i) \text{ and } E_{lr} = \sum_k \widetilde{\Phi_{lr}}(K)\,|\tilde{\rho}(K)| \quad (3.5)$$

where E_{Tot} is the total Ewald summation in the system; E_{sr} is the short-range potential in real space; E_{lr} is the long-range potential in the Fourier space; $\widetilde{\Phi_{lr}}(K)$ is the potential of Fourier transforms; and $\tilde{\rho}(K)$ is the charge density of Fourier transforms.

3.5 Asphalt Model

Based on the Corbett method [115] in asphalt extraction, the asphalt has four components: asphaltenes, saturates, naphthene aromatics, and polar aromatics. In this study, the asphaltene structure proposed by Artok et al. [80] and Zhang et al. [13] has moderate aromatic rings with small branches. They used a group of molecular structures at a certain ratio to represent the asphaltene component in the asphalt model. The asphaltene structure used in this study is shown in Figure 3.2a. The number of carbon rings and chains of naphthene aromatics are smaller than the asphaltene's from the reference of Zhang and Groenzin [13, 81]. The 1,7-Dimethylnaphthalene could be represented as the naphthene aromatics based on the ratio of alkane and aromatic. The structure of 1,7-Dimethylnaphthalene is shown in Figure 3.2b. Zhang and Storm [13, 116] also mentioned that the nuclear magnetic resonance (NMR) was used to analyze the asphalt, and a balance between the aromatic and alkane carbons was observed in the asphaltenes, resins, and saturates. Docosane, reported by Zhang and Kowalwski [13, 117], is a normal alkane. The melting and boiling points of docosane are 317 K and 642 K, respectively. The melting and boiling points are consistent with those of saturates in the asphalt. The docosane can represent the saturate in the asphalt model. The chemical structure of docosane is shown in Figure 3.2c.

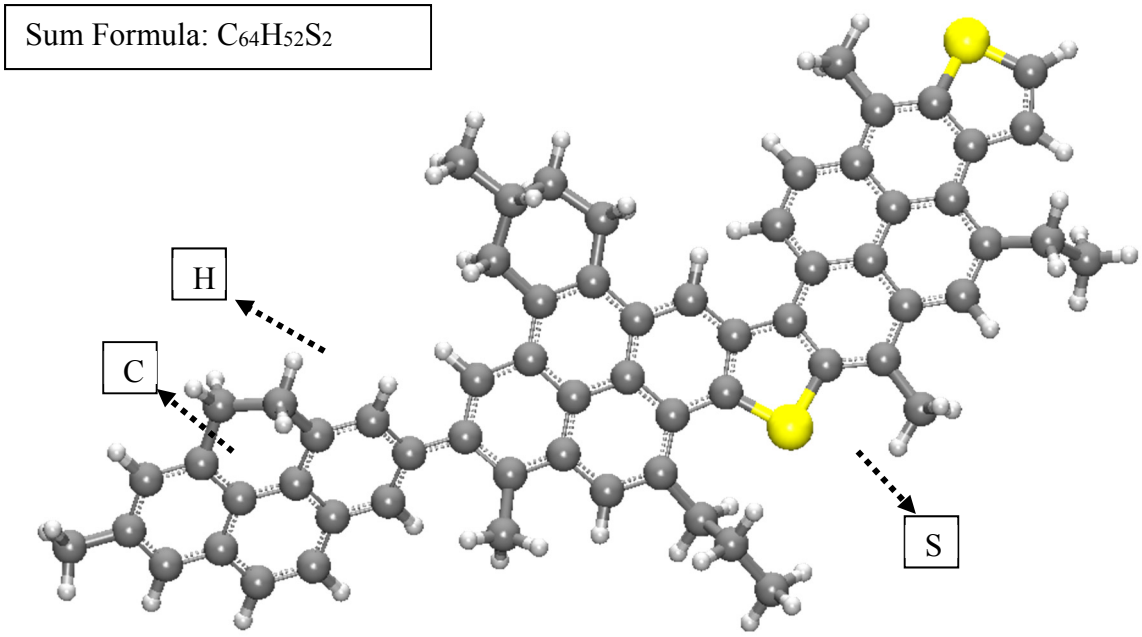

(a) Chemical structure of the asphaltene in the ball and stick model: black color balls indicate carbon atoms; white color balls represent hydrogen atoms; and the yellow color balls stand for sulfur atoms.

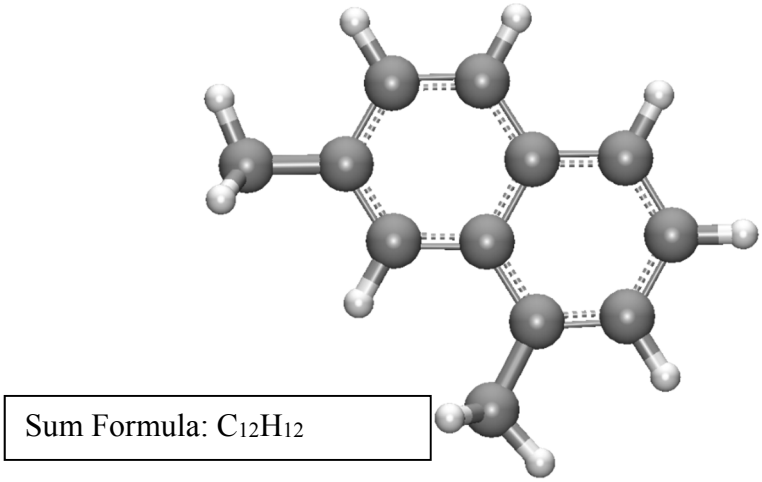

(b) Chemical structure of 1,7-dimethylnaphtalene in the ball and stick model: black balls indicate carbon atoms; white balls represent hydrogen atoms. It represents the naphthene aromatic.

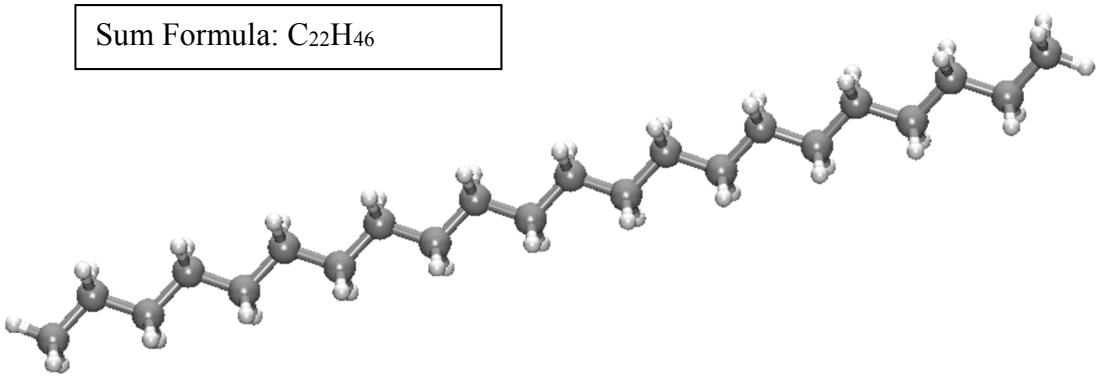

(c) Chemical structure of docosane in the ball and stick model: black balls indicate carbon atoms; white balls represent hydrogen atoms. It represents as a saturate.

Figure 3.2. Three components in the asphalt model

In the simulation, it is common that many explicit atoms represent a single molecule in a complex system, which results in a more accurate computation. All parameters for each atom in the complex system are supplied by the Amber Cornell Extension Force Field in this study, such as bonds between two atoms, angles between three atoms, and a dihedral setting between four atoms. The experimental MD simulations were conducted using computation programs such as LAMMPS and optimizations [118, 119] in the study, as well as the utilization of computer clusters.

The components of the asphalt model were determined, and the optimization of the components were done before building the asphalt model. The components of the asphalt model were optimized by NWChem (a plugin in the Materials Processes and Simulations (MAPS)), and Electrostatic Potential (ESP) charges were also assigned to the components [120]. After the optimization of each component system, the three components were ready to represent the asphaltene, saturate, and naphthene aromatic. The asphalt model was built with these components at a ratio of 5:41:27, respectively. The details of the molecular components in the asphalt are shown in Table 3.1. The 5 asphaltenes, 27 aromatics and 41

saturates were placed randomly in the periodic unit cell, and the periodic boundary conditions were used in the asphalt system, named the asphalt model. A Periodic boundary condition (PBC) is a kind of boundary condition that uses a small system/unit cell to approximate the large/infinite system. When the particles pass through one side of the unit cell, they appear on the other side with the same statue. In topological terms, the outside particles of the unit cell can be thought of as being mapped into the inside of a unit cell or torus. If the PBC is applied in three directions, the unit cell can be thought of as mimicking a bulk phase to possibly avoid the boundary conditions. The PBC can be combined with Ewald summation methods (usually with the particle mesh Ewald) to calculate the electrostatic forces in molecular systems [121]. When building the model, the asphalt model was built at a density of 0.1 g/cm^3 in the initial stage (Figure 3.3(a)). There is potential to make the components more random with a low density of the asphalt model. A low density is better for adjusting the position of molecules when optimizing the energy.

Table 3.1. The overall composition of the asphalt model

Asphalt model	Mass (g/mol)	Sum Formula	Numbers of atoms	Numbers of bonds	Number of molecules	Total Mass (g/mol)	Mass fraction (%)
Asphaltene	885.23	$C_{64}H_{52}S_2$	118	132	5	4426.15	20.685
1,7-dimethylnaphthalene	156.22	$C_{12}H_{12}$	24	25	27	4217.94	19.734
Docosane	310.6	$C_{22}H_{46}$	68	67	41	12734.6	59.581
Asphalt binder					73	21378.81	

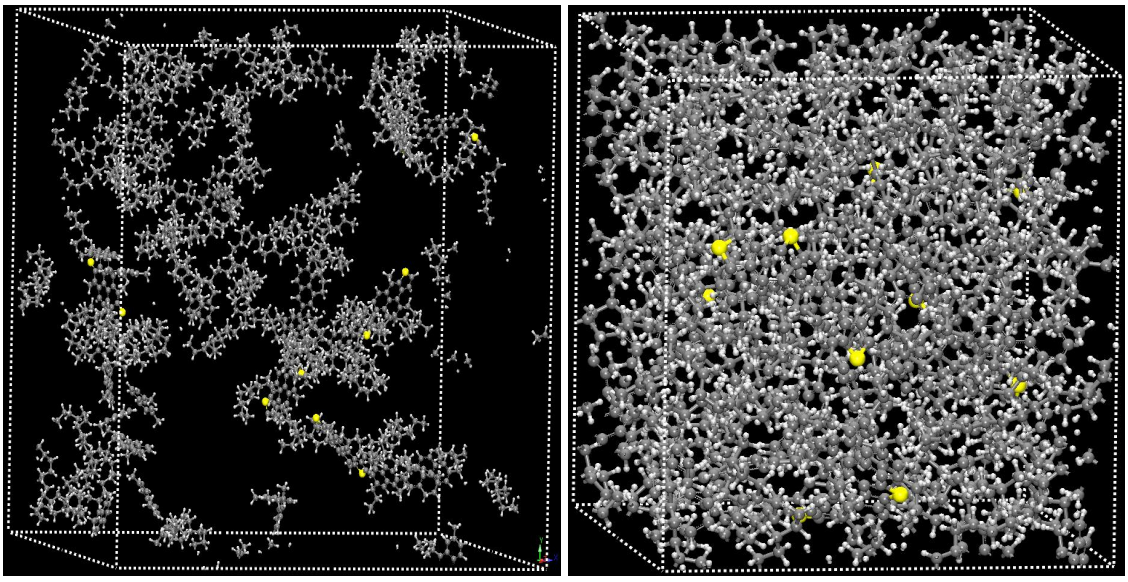

(a)The asphalt model generation in the initial stage; (b) Asphalt model after NPT simulations

Figure 3.3. Molecular images of the asphalt model with the Amber Cornell Extension Force Field at different states

3.6 MD simulation of physical properties with the asphalt binder model

3.6.1 Density Prediction and Model Verification

The asphalt model was built using the Amber Cornell Extension Force Field (Figure 3.3(a)). Once the asphalt model was built with the Amber Cornell Extension Force Field, the conjugate gradient method was used to optimize the system. The NPT ensemble was applied to compress the asphalt model to obtain the density of the molecular system and unit cell dimensions under the conditions of a 1 atm pressure and 298.15 Kelvin temperature. It is common that the density is used to validate the system in MD simulations, and this density was close to matching the density of the real state. The asphalt model (Figure 3.3(b)) with the Amber Cornell Extension Force Field was equilibrated in four steps: 1) optimize the energy at 5000 max iterations using the conjugate gradient method; 2) subject it to 100 atm and 298.15 K for 20 ps (picosecond); 3) run with 200 ps at 1 atm

and 298.15 K; and 4) follow with 500 ps at the same condition (Figure 3.4(a) and Figure 3.4(b)). The aim of high pressure in the system is to help the atoms speed up their positional adjustments and the network structure formation of intermolecular contacts, and also to quickly find good geometric locations in the unit cell. In the fourth step, the system can reach the equilibrium state smoothly under normal air pressure (1 atm) and room temperature (298.15 K). During the experimental MD simulation, the MD data trajectories were recorded every 100 fs (femtosecond). During the NPT simulation, the Nose-Hoover thermostat and barostat were applied to the system to maintain the system at the condition of 298.15±10 K and 1 atm pressure. The asphalt model reached the relative equilibrium state after these steps, and the molecular structure of the asphalt model is shown in Figure 3.3(b). Figure 3.3 displays the difference of the asphalt model before and after the NPT simulations, and all of the atoms are mapped into the unit cell. The spatial structure of the asphalt model before the NPT ensemble is loose and becomes dense after the NPT ensemble (constant molecules, constant pressure and temperature in the simulation).

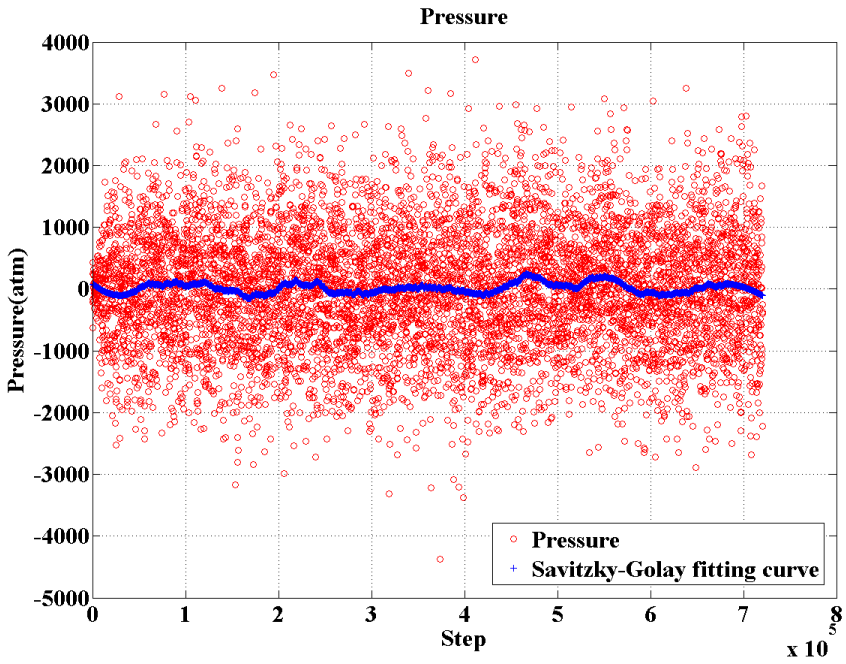

(a) Pressure (atm) results of the asphalt model (7,200 data points)

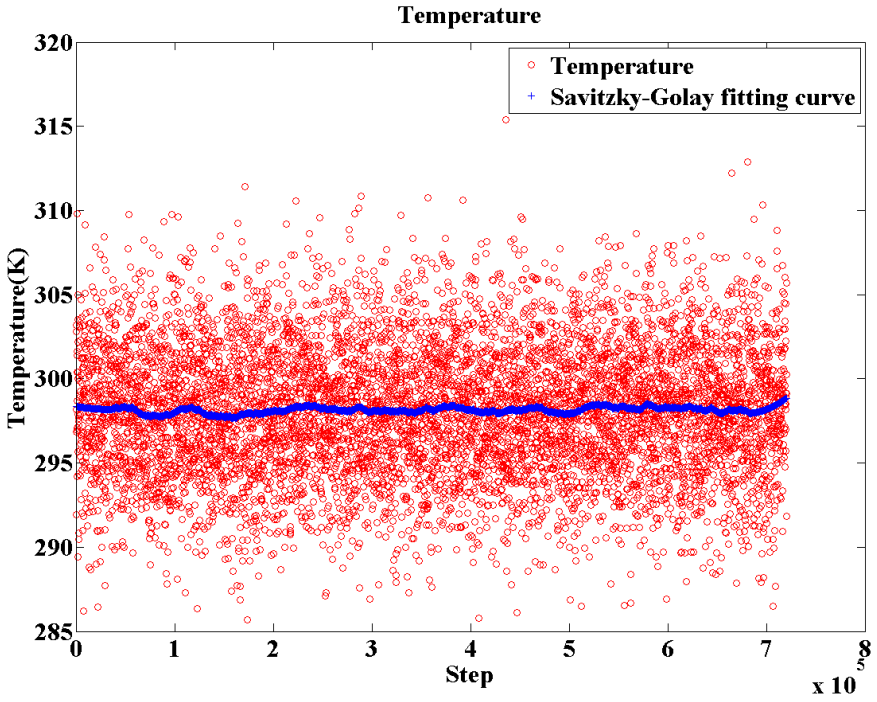

(b) Temperature (Kelvin) results of the asphalt model (7,200 data points)

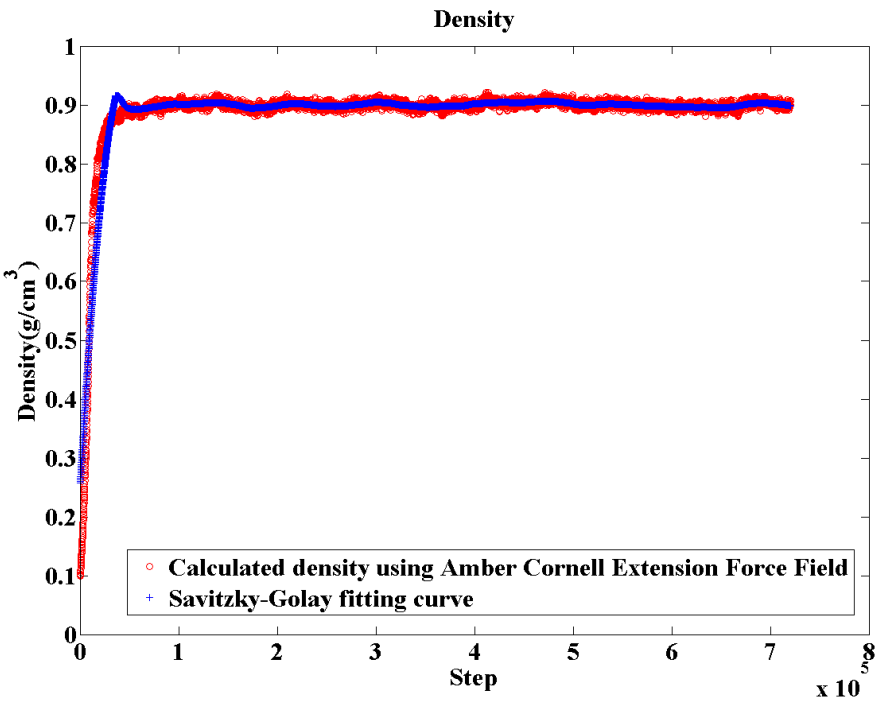

(c) Density results of the asphalt model (7,200 data points)

Figure 3.4. Computational results of the asphalt model during the NPT simulation

Figure 3.4(a) and Figure 3.4(b) reveal the pressure and temperature range during the NPT simulation of the asphatl1 model. The pressure results fluctuate due to the large attractive and repulsive forces in the system when the NPT ensemble is applied. The data was processed by a Savitzky-Golay filter [76] with a span of 10% to evaluate the moving average of the simulated data. The pressure and temperature of the system are around 1 atm and 298 K, respectively, from the moving average data. Compared to the moving average data, the pressure fluctuations are possibly caused by the small amount of molecules in the system in contrast to the large amount of molecules in the real state. The small number of molecules in the system definitely causes the large deviation. The same situation occurs in the references [13, 122]. The fluctuation amplitude varies within $1/\sqrt{N}$ relative to the moving average, where N is the molecular number in the simulated system

[122]. Based on Avogadro's number [123], there are $10^{23} \sim 10^{24}$ molecules/atoms per mole in the substances, so the variation in data fluctuation is inappreciable. However, the rate of fluctuation is remarkable for 10^2 molecular numbers in the system. The temperature range in Figure 3.4(b) is within a 10 K variation, and it corresponds with the user requirement in the simulation. In addition, the asphalt model was clearly condensed. The calculated densities during the NPT simulation are shown in Figure 3.4(c).

Figure 3.4(c) demonstrates the changes in density of the asphalt model in the processing of the NPT ensemble. The density is rapidly changed through the NPT simulation with the PME method, which is usually combined with periodic boundary conditions, and the stable state is reached after 2 ps. The density data was also processed by a Savitzky-Golay filter with a span of 10%, and the data moving average was presented. The stable density results are around 0.91 g/cm^3 at the conditions of room temperature and normal air pressure. It is close to the laboratory data (0.95 g/cm^3 – 1.05 g/cm^3) [13, 89, 122], and the density of actual asphalt varies from the components and source of the asphalt. The average density of the asphalt model is slightly higher than the data of the reference at different temperatures, but not significantly so (0.01 g/cm^3 amplitude). Actually, it is hard to improve any further when using the same molecular structure. In addition, the trend in density of the asphalt model is smoother than that of the reference. This indicates that the asphalt model with the Amber Cornell Extension Force Field is valid, and the asphalt model can be represented as an asphalt in the simulation. Furthermore, the relationships between the density and running temperature in the asphalt model were calculated through the NPT ensemble, and the computational results are shown in Figure 3.5.

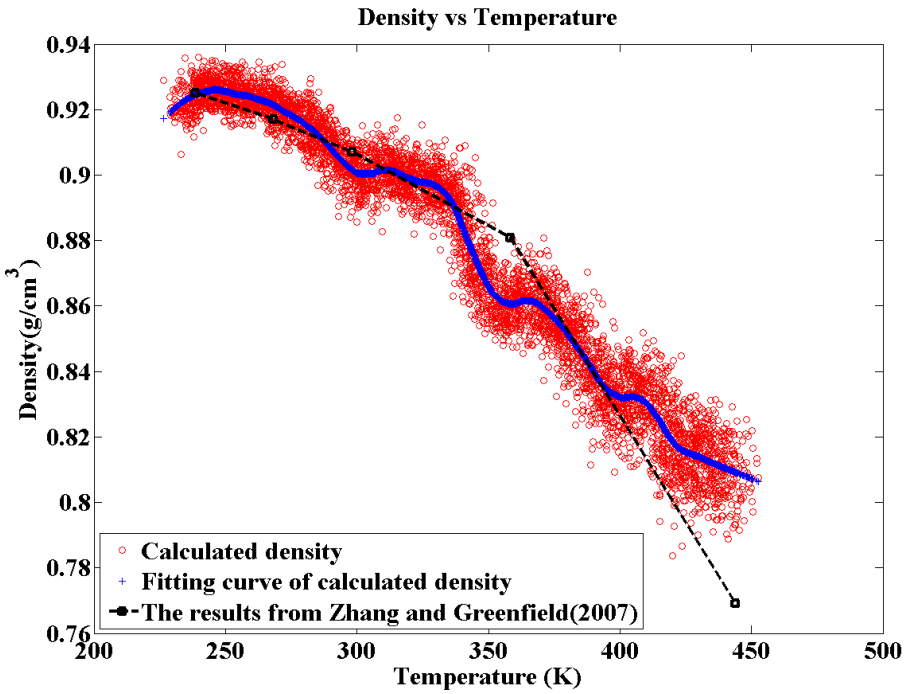

Figure 3.5. Density results of the asphalt model with the Amber Cornell Extension Force Field compared to the reference data (12,000 data points)

Figure 3.5 shows the densities at different temperatures and the density comparisons between the asphalt model data and the reference data [13]. The NPT ensemble was applied to the asphatl1 model for 500 ps at the conditions of 1 atm pressure and a temperature range of 233.15 K to 443.15 K. The densities were also processed by a Savitzky-Golay filter with a span of 10% to obtain the moving average. From this figure, it is clear that the densities decrease when the temperature in the system increases, and it coincides with the reference data from Zhang and Greenfield 2007 [13]. The densities of the asphalt model using the Amber Cornell Extension Force Field (Figure 3.5) are slightly higher than those of the reference data from Zhang and Greenfield 2007 [13]. This means that the densities of the asphalt model are close to the actual density of the asphalt, and the data of the asphalt model with the Amber Cornell Extension Force Field is better than the

reference results. The trend in density of the asphalt model is smoother than that of the reference data. Therefore, the asphalt model with the Amber Cornell Extension Force Field can be represented as the actual asphalt and can also be used for the property calculation.

3.6.2 MD Prediction of the Glass Transition Temperature (Tg)

The glass transition is a reversible process in the materials when amorphous materials are heated or cooled, and the materials change from a hard or brittle state into a molten or rubber-like state [124]. It is called vitrification when a viscous liquid is cooled into a glass state. When the materials go through a glass transition, the physical properties are changed massively, but it is not considered a phase transition [125]. The coefficient of thermal expansion of many materials may also be smoothly changed throughout the glass transition [126]. The glass transition temperature (Tg) is the temperature at the intersection where two asymptotes or thermodynamic equilibrium lines intersect in the curve of the specific volume and temperature (Figure 3.6). The specific volume is the ratio of material volume to mass, and is also the reciprocal of density. The glass transition process may start before the temperature Tg, seen in Figure 6, and the physical hardening may occur when the materials are in the transition area based on the free volume concept [124]. The glass transition temperature can be measured using the Differential Scanning Calorimetry (DSC)/Dilatometric measurements. The first order properties (entropy) of asphalt during the glass transition phase are continuous, but second order properties (heat capacity) are discontinuous [124]. It is also observed that multiple glass transitions occur in the asphalt binder material and the glass transition temperature can be an overlap in result of several transitions due to the complex compositions of asphalt. The reference shows that a broad

temperature range of 223.15 K to 303.15 K could be a glass transition temperature range of asphalt based on the dilatometric analysis [124]. In the MD simulation, the estimated results between the specific volume and temperature of the asphalt model are shown in Figure 3.7.

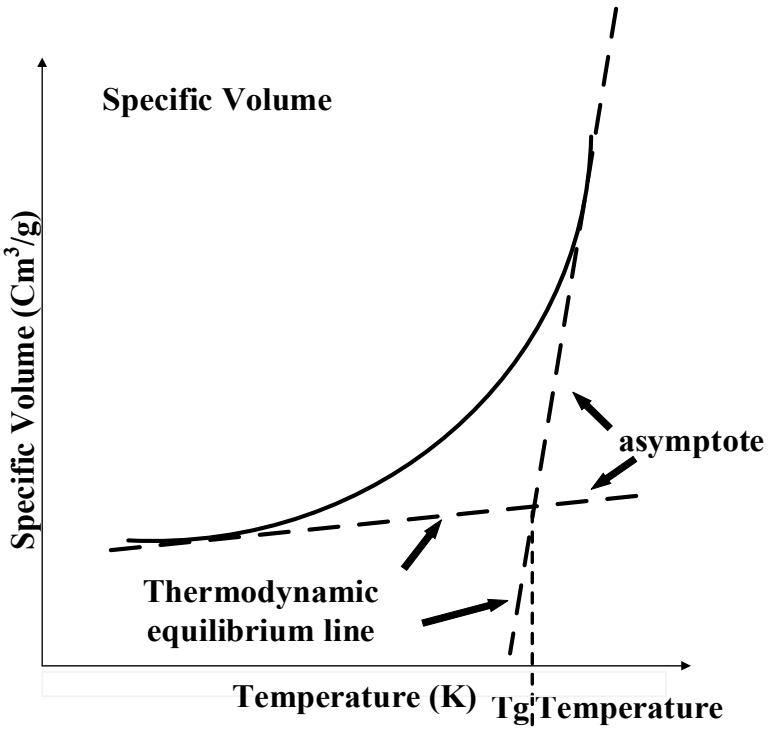

Figure 3.6. Material behavior in the glass transition temperature region

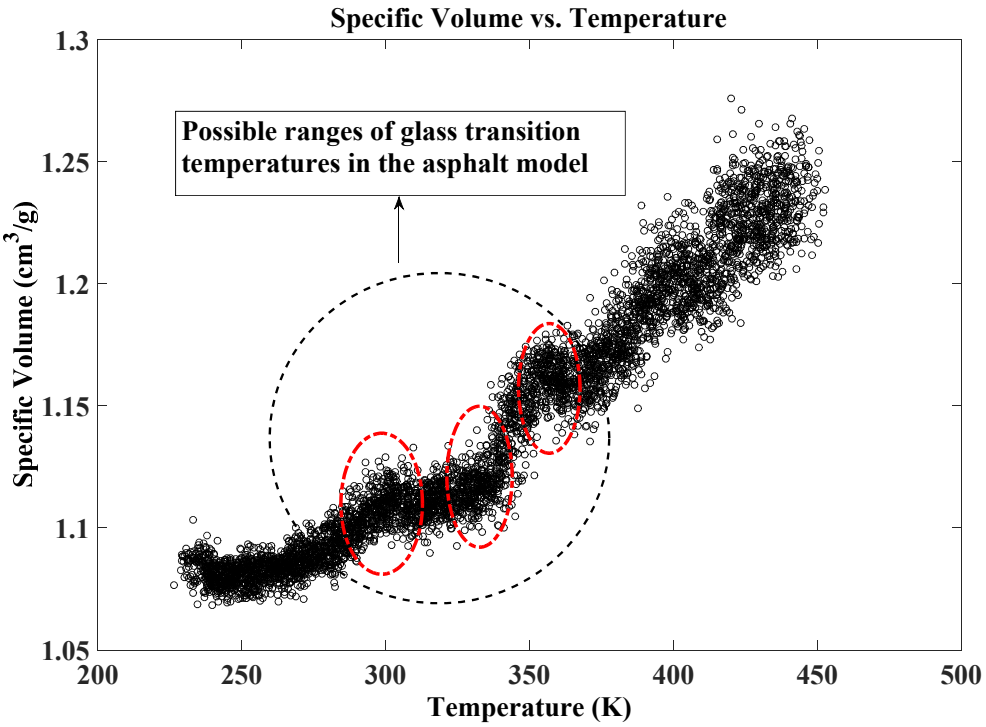

Figure 3.7. Relationship between the specific volume and temperature (10,000 data points)

Figure 3.7 shows the relationship between the specific volume and temperature in the asphalt model. The specific volume increases with the increase in temperatures in the model. There is an interval where the slope of the specific volume and temperature curve changed significantly. Based on the definition of glass transition temperature, two asymptotes intersect and the estimated temperature range is from 275 K to 425 K in the figure. Therefore, the temperature range of the asphalt model needs to be narrowed down. The individual NPT simulation was adopted. The simulations were conducted at individually selected temperatures from high temperatures to low temperatures at the condition of 1 atm pressure. It was simulated that one asphalt sample could be tested from high temperatures to low temperatures. These selected temperatures were 443.15 K, 425.15

K, 400.15 K, 375.15 K, 350.15 K, 325.15 K, 300.15 K, 275.15 K, 250.15 K and 233.15 K. The specific volumes of the asphatl1 model at 233.15K are shown in Figure 3.8(a). In addition, the specific volumes at other temperatures were similar to the data trend in Figure 3.8(a). Due to page limits, the figures at other temperatures were not presented in this paper. The specific volume under each specific temperature was averaged, and the average results of the specific volume of the aspahlt1 model at several separate temperatures are plotted as shown in Figure 3.8(b).

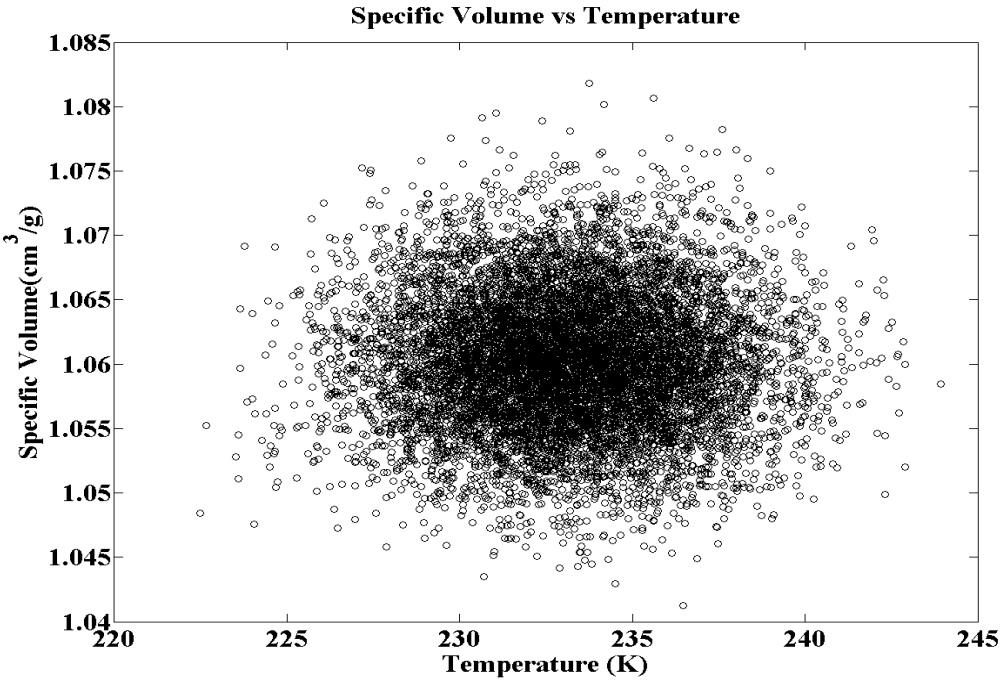

(a) The specific volume of the asphalt model at a temperature of 233 K (10,000 data points)

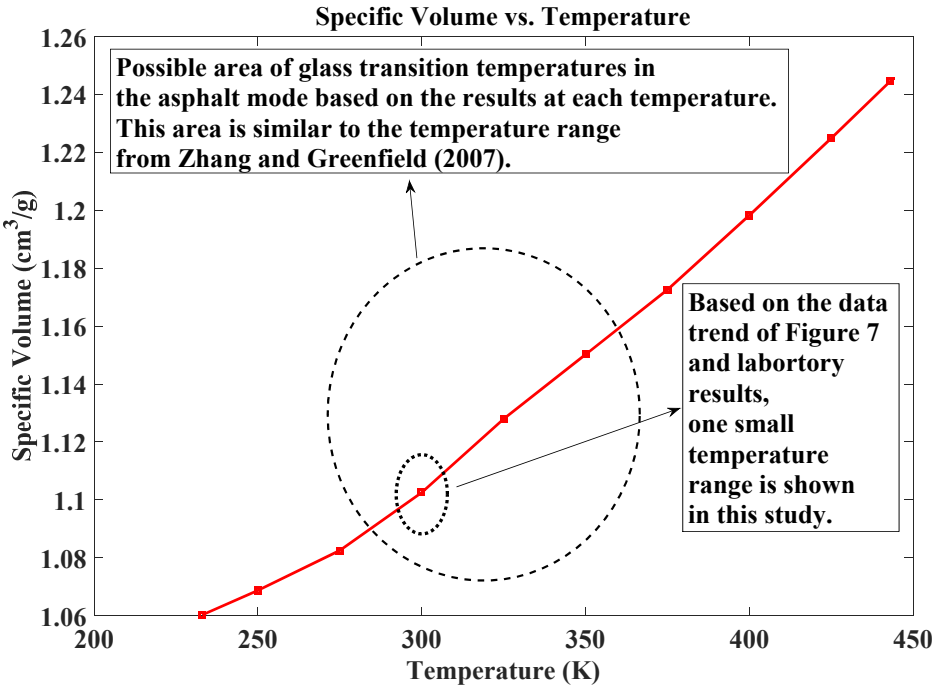

(b) The relationship between the specific volume and temperature at different temperatures in the asphalt model

Figure 3.8. The glass transition temperature results of the asphalt model using MD simulation

Figure 3.8(a) demonstrates the results of the specific volume of the asphalt model at the temperature of 233.15 K. The temperature of the simulation maintains a variance of 10 K and is consistent with the requirements. The data of specific volume is focused around 233.15 K, and the data also shows an amplitude of 2.5%. The data was averaged to represent the results of the specific volume at 233.15K. Likewise, the results of the specific volume at other temperatures were calculated using the same process. However, the computational results of others temperatures are not included in this paper since the data figures are similar. Figure 3.8(b) displays the average specific volumes of the asphalt model at different temperatures. The possible area of the glass transition temperature is pointed out in the figure. The glass transition temperatures can consist of many small transitions

due to the complex components of asphalt. The glass transition temperature of the asphalt model is about 300 K, synthesizing the specific volumes associated with the data of Figure 3.7 and the laboratory results [124]. The results stay consistent with the laboratory data ranging from 223 K to 303 K [124] and are better than the range of the reference (298 K to 353 K) from Zhang and Greenfield [13].

3.6.3 MD Prediction of Asphalt Viscosity and Comparison with Reference Data

Viscosity of a fluid is a measurement of resistance to gradual deformations due to the shear or tensile stress in the fluid. When shear force is applied to the fluid, the resistance to shear flow represents the dynamic shear viscosity of the fluid. The adjacent layer, which is close to the flow layer, moves in a parallel direction with a different speed. The velocity gradient occurs in this idealized Couette flow. The viscosity calculation can be expressed as equation (3.6) [127]. In addition, the Brookfield DV-II plus viscometer was used to test the viscosity of the asphalt, and the test procedure was followed by the Superpave™ specification. Asphalt is a Newtonian fluid at high temperatures, and this indicates that the viscosity of asphalt does not depend on the rate of shear strain [4].

$$F = \eta A \frac{u}{y} \tag{3.6}$$

where F is the applied force in the fluid, A is the area of the plate, η is the dynamic viscosity (proportionality factor), and u/y is the velocity gradient.

In the MD simulation, there are at least four methods to calculate the viscosity using LAMMPS [118]. The first method is to set up non-equilibrium MD (NEMD) simulations through shearing the unit box in the simulation, then set the temperature of the fluid through

the SLLOD equations [128] of motion. The second method is to use one or more moving walls to shear the fluid, then thermostat the temperature of the fluid. In the third method, the Muller-Plathe algorithm [129] is used to perform a reverse non-equilibrium MD (rNEMD) simulation. The momentum flux in one direction is transferred between atoms from one layer to a different layer in a different dimension, and the velocity gradient is also monitored (Figure 3.9). In the fourth method, the Green-Kubo (GK) formula or Einstein relations are used to calculate the transport coefficients by equilibrium MD. In this study, the third method (Muller-Plathe Method) was used to calculate the viscosity of the asphalt model.

In the experimental rNEMD simulation, the Muller-Plathe method was used to calculate the viscosity [129]. The total energy and linear momentum are conserved in this method. The shear viscosity, a proportionality coefficient, is caused by a momentum flux in the shear field, which is a velocity gradient. The mathematical calculation is shown in equation (3.7). The momentum flux is determined by a momentum flowing perpendicular through a surface area A in a certain time t. The calculation formula of momentum flux is shown in equation (3.7). When the momentum flux is imposed on the fluid, the periodic unit box is divided into many layers in the z-direction (Figure 3.9). Due to the periodic boundary conditions in the unit box, it is accurately known that the amount of momentum is transferred from the $z = 0$ layer to the $z = L_z/2$ layer, and the transfer swaps are repeated periodically. In the NEMD simulation, the momentum flow in the opposite direction is allowed for the physical frictions in the unit box. Then, the momentums in the atom layers

z = L_z/2 and z = 0 are largest (Figure 3.9). Therefore, the momentums transferred from the z = L_z layer to z = L_z/2 layer are equal to those from the z = 0 layer to z = L_z/2 layer.

$$j_z(p_x) = -\eta \frac{\partial v_x}{\partial_z}, \text{ and } j(p_x) = \frac{P_x}{2tA} \tag{3.7}$$

where η is the shear viscosity; $\frac{\partial v_x}{\partial_z}$ is the shear rate; $j(p_x)$ is the momentum flux; P_x is the momentum; t is the length of simulation; $A = L_x L_y$, L_x is the length of the simulation box (x direction); and L_y is the length of simulation box (y direction).

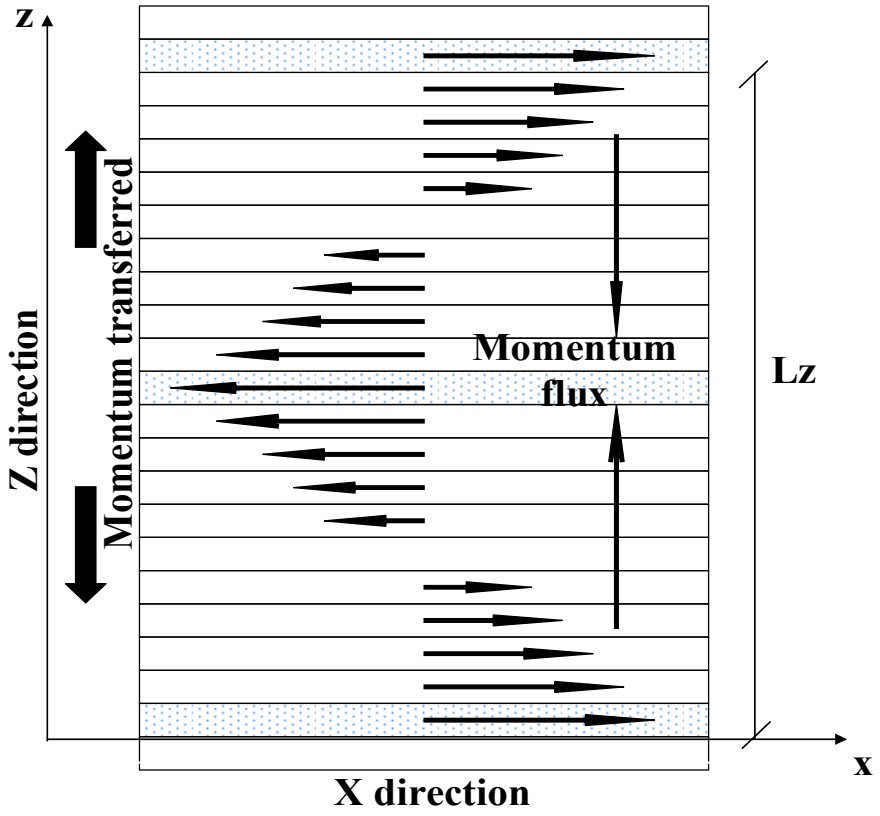

Figure 3.9. Schematic image of momentum flux transfer in the periodic unit box

In the usual NEMD simulation, the shear velocity is imposed on the system and the stress response is measured. However, in this experimental rNEMD simulation, the

momentum flux was imposed on the asphalt system. The response of the shear velocity was recorded every 100 steps. The momentum transferred to the asphalt system at the temperature of 443.15 K was shown in Figure 3.10(a). Furthermore, the viscosity unit in the MD system is gram/mol/angstrom/femtosecond and the rotational viscosity unit in the actual asphalt is kilogram/meter/second. The unit converting parameter of results in the experimental MD simulation is computed, and the conversion coefficient and Avogadro's constant are used to balance the asphalt system. The viscosities of the asphalt system at the temperature of 443.15 K are shown in Figure 3.10(b), and the viscosities of the asphatl1 system at different temperatures are displayed in Figure 3.10(c).

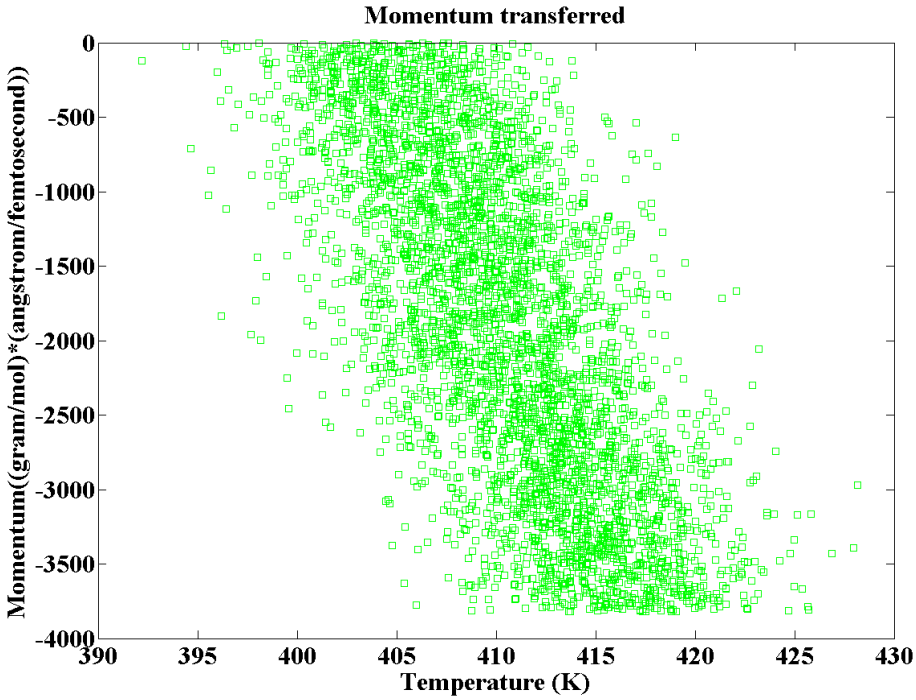

(a) Momentum transferred in the asphalt model at the temperature of 443.15K (40,000 data points)

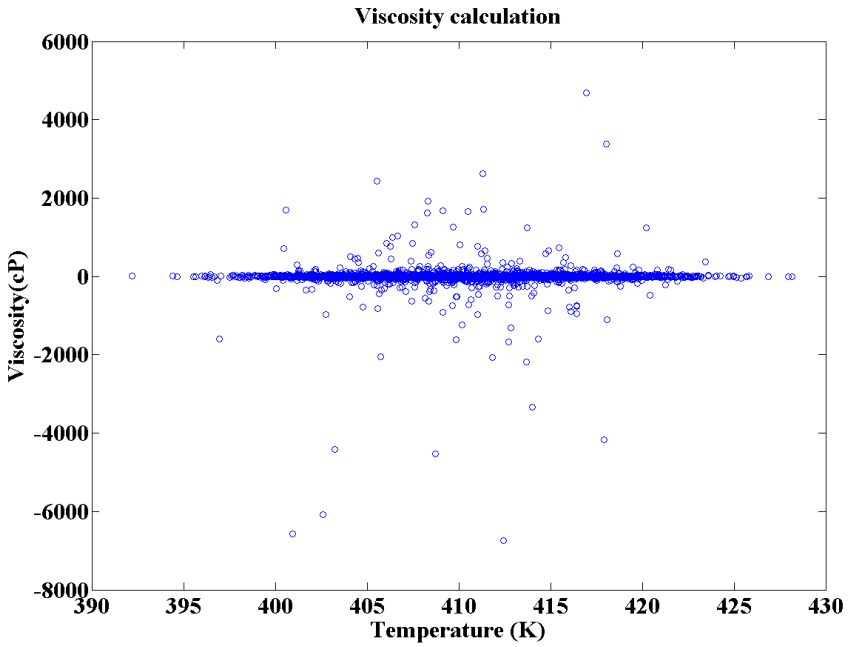

(b) The viscosity values of asphatl1 model at the temperature of 443.15K (40,000 data points)

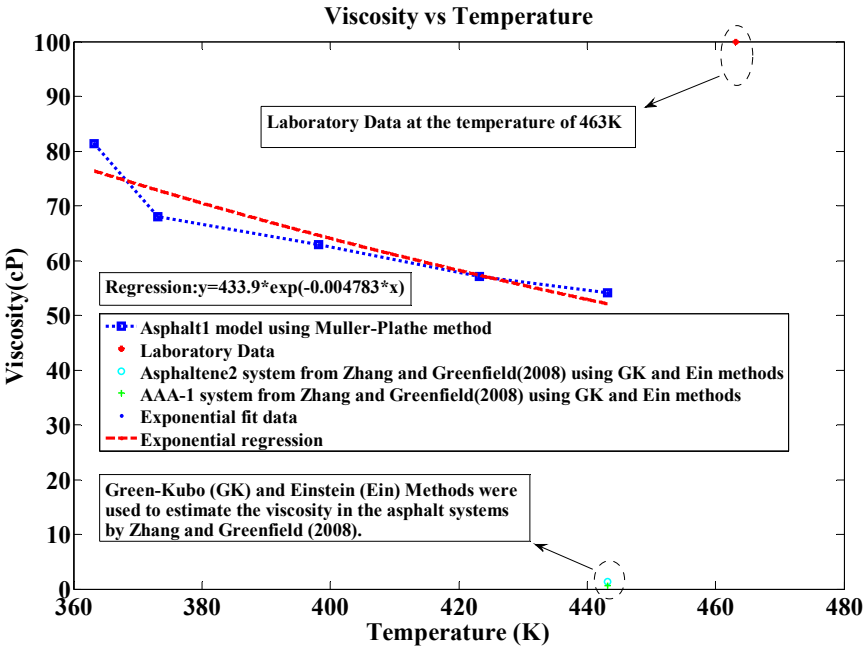

(c) The viscosity values of the asphalt model at the different temperatures

Figure 3.10. The viscosity calculation of the asphalt model using MD simulation

Figure 3.10(a) shows the momentum transferred between the layers in the rNEMD simulation at a temperature of 443.15 K. The linear trend and acceptable amplitude of the momentum transferred can be observed from the figure in the small molecular system compared to the macroscopic state. Similar results are also represented at different temperatures and are not presented due to the repeatability. It is extrapolated that the shear velocity response between the layers is also linear from equation (3.7). The requirement of rNEMD is fulfilled in the viscosity simulation. Furthermore, the momentum transferred rises with an increase in temperatures. The temperature range was maintained around 20 K in the experimental MD simulation. Figure 3.10(b) demonstrates the viscosities at the temperature of 443.15 K after converting units. Similar results are also presented at other temperatures. The viscosities stay consistent and maintain a certain magnitude. It is common that the fluctuation in data occurs due to the small system used in the MD simulation compared to the macroscopic scale. The viscosities at one temperature were averaged to obtain the relationship between the temperatures and viscosities in the MD system. Figure 10(c) reveals the viscosities of the asphalt model at different temperatures. The calculated viscosities were compared with the laboratory data [8] at the temperature of 463 K and the reference data at the temperature of 443.15 K conducted by Zhang and Greenfield [84] using the Green-Kubo (GK) and Einstein (Ein) methods. The viscosity decreases in the asphalt model with increasing temperatures. The viscosities in the system represent the exponential trend against the temperatures, and it coincides with the exponential trend in the laboratory data [130]. The viscosities computed at the temperature of 443.15 K are 0.65 cp and 1.35 cp from the reference data [84] (Zhang and Greenfield 2008) using two different asphalt systems as shown in Figure 3.10(c), respectively. The

viscosity of the PG 58-34 asphalt tested in the laboratory is around 100 cp at the temperature of 463 K [8]. The viscosity (54.16 cp) at the temperature of 443.15 K in this MD simulation is higher than the reference data, but it is lower than the laboratory data. It is demonstrated that the computational results in this experimental MD simulation are better than the reference data. This also indicates that the MD simulation of the asphalt system with the Amber Cornell Extension Force Field and Muller-Plathe method has better predictions for computing the physical property in this case. However, there is still a slight difference between the simulation and laboratory data. The new asphalt model and methods may be explored to narrow the difference in the ongoing research.

3.6.4 Bulk Modulus

The bulk modulus (K) is the basic property of materials to measure the resistance to uniform compression. It is defined by the quotient of the normal stress to volumetric strain in the substance. The bulk modulus also relates to the compressibility of materials [131]. In this MD simulation, infinitesimal strains in three directions were applied to the asphalt model. The NVT integration was performed in the asphalt system using the Nose/Hoover thermostat with SLLOD motion equations [128], and the positions and velocities of atoms in the model were updated during the NVT simulation. The corresponding stress values were monitored and recorded during the stress-strain response cycle. In addition, the NVT simulations were run at different temperatures for at least 2 nanoseconds with a timestep of 1 femtosecond, and millions of data points were produced to compute the bulk modulus of the asphalt model.

During the MD simulations, positive and negative strains were imposed in three coordinate directions [12] (equation (3.8)), namely tension and compression in the asphalt model. The overall volumetric change was shown in equation (3.9). The averaged stresses in both tension and compression were calculated with equation (3.10). The values of the bulk modulus of the asphalt model under positive and negative dilations were computed and averaged by equation (3.11). After several NVT simulations of the asphalt model, the stresses in three coordinate directions of the asphalt model under the temperature of 273.15 K are demonstrated in Figure 3.11(a). The bulk moduli of the asphalt model are calculated and shown in Figure 3.11(b). Furthermore, the relationship between the stress and strain of the asphalt model in the x-direction is illustrated in Figure 3.11(c). However, the similar stress and strain results of the asphalt model under different temperatures and other coordinate directions are not presented in this paper.

$$\varepsilon_{xx} = \varepsilon_{yy} = \varepsilon_{zz} = \pm 0.005 \tag{3.8}$$

$$\Delta = \varepsilon_{xx} + \varepsilon_{yy} + \varepsilon_{zz} \tag{3.9}$$

$$\sigma_{average} = \frac{1}{3}(\sigma_{xx} + \sigma_{yy} + \sigma_{zz}) \tag{3.10}$$

$$K = \frac{\sigma_{average}}{\Delta} \tag{3.11}$$

where, ε_{xx}, ε_{yy}, ε_{zz} is the infinitesimal strain in all three coordinate directions; σ_{xx}, σ_{yy}, σ_{zz} is the average normal stress in all three coordinate directions; Δ is the overall dilatation of the simulation box; $\sigma_{average}$ is the average stress in the MD simulation; and K is the bulk modulus in the MD system.

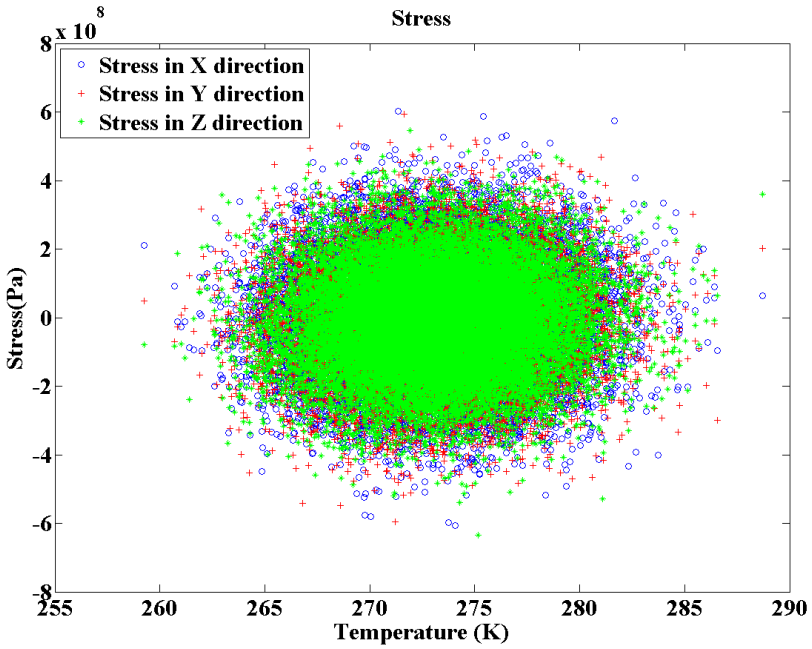

(a) Stress magnitude under the negative volumetric strain at the temperature of 273.15K (60,000 data points)

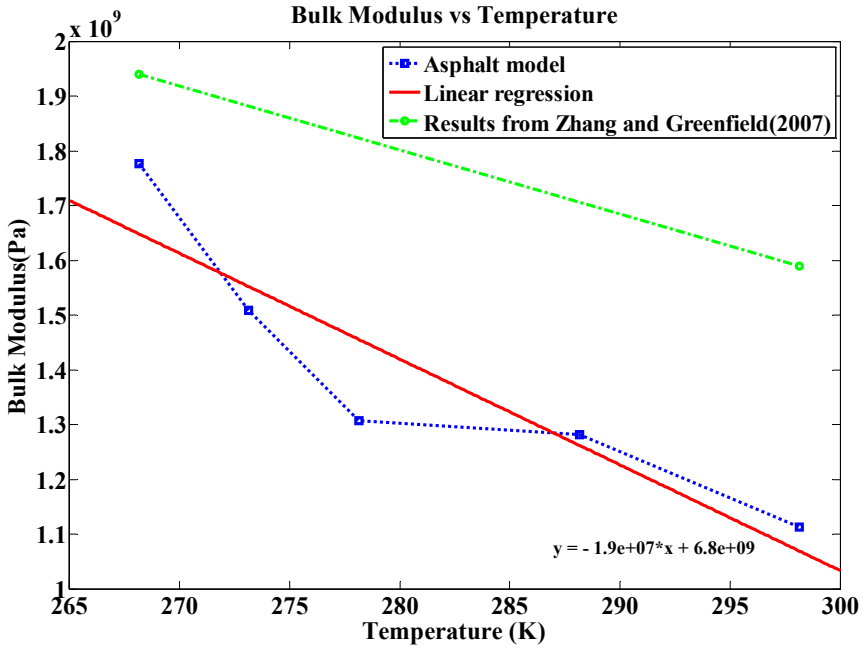

(b) Bulk modulus of the asphalt model under different temperatures

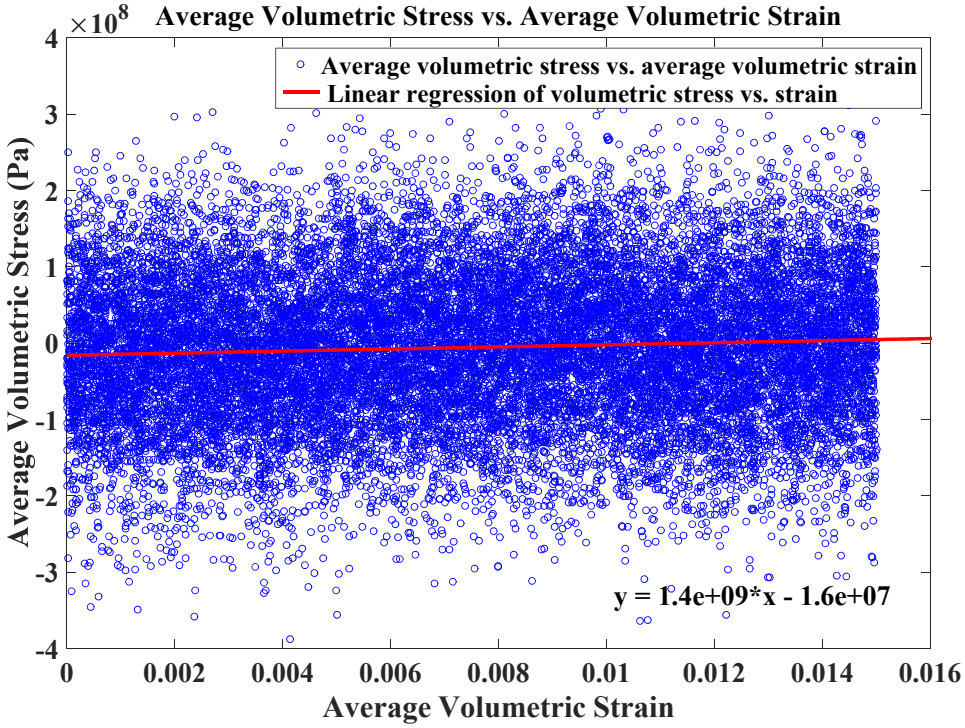

(c) Average volumetric stress-strain relationship in the asphalt model under the negative strain at the temperature of 273.15K

Figure 3.11. Average volumetric strain levels and bulk modulus results in the asphalt model

Figure 3.11(a) reveals the amplitude of the stress response of the asphalt model when negative strains in three coordinates are applied to the model at a temperature of 273.15 K. The variation in temperature of the data points maintains a 10 K difference, which agrees with the input temperature range. The stress magnitude of the model stays at a $\pm 10^8$ Pa level. Due to the small molecular system relative to the real asphalt, the response of stress in the model presents a high level and fluctuation within a wide range, even the infinitesimal strain is imposed on this system. The reasonable or possible amplitude of the response stress falls within a $1/\sqrt{N}$ variation (N represents the molecular number in the system) [122]. The stress is also concentrated and homogenously distributed in the three axial directions of the asphalt models. Figure 3.11(b) demonstrates the bulk moduli of the

asphalt model at different temperatures with a linear regression. The bulk modulus of the asphalt model decreases by increasing the temperatures, and the data trend agrees with the reference [13]. In addition, in Figure 3.11(c), the relationship between the average volumetric stress and strain in the asphatl1 model is presented with a linear regression. The volumetric strain (overall dilatation) ranges along three coordinates, from 0 to 0.015 in the model, and the stress response level of the asphatl1 system is demonstrated within a magnitude of 10^8 Pa. Based on the laboratory bulk moduli of asphalt [132], the bulk modulus of asphalt at the temperature of 293.15 K is around 3 MPa using the poker-chip test. The bulk modulus in the asphalt model is larger than the laboratory data. This can be due to two reasons: (1) the current molecular model (asphalt system) with limited molecular numbers have a difference in the bulk materials with a much higher number of molecules; (2) the simulation time is in the range of several femtoseconds, which cannot represent the relaxation behavior that occurred within seconds or minutes. All these factors lead to much stiffer moduli than the lab measured data. The trend or modulus changing with temperature have a similar trend as the experimental data. The simulation time and molecular numbers are restricted with current computational capacities. A new asphalt model under development will be expected to have a closer prediction. However, the bulk moduli in this study are still slightly better than the results from Zhang and Greenfield [13] and closer to the laboratory testing results [132].

3.7 Discussions and Conclusions

The asphalt model with three components was used to mimic the asphalt in this experimental MD simulation, and the Amber Cornell Extension Force Field was employed

in the asphalt model. The NWChem analysis was applied to calculate and assign the ESP charge to the asphalt components. The conjugate gradient method, particle mesh Ewald method, and Savitzky-Golay filter were used to optimize the system energy and data smoothing. The physical properties of the asphatl1 model were computed including density, glass transition temperatures, viscosity, and bulk modulus. The computational results and conclusions in the asphatl1 model are drawn.

1) During the asphalt model building process, the three components, asphaltenes, aromatics and saturates, were represented by asphaltene, dimethylnaphthalene, and docosane, respectively, and the ratio of the three components in the asphalt model was 5:27:41. The conjugate gradient and NWChem were applied to the asphatl1 model with the Amber Cornell Extension Force Field for optimizing the energy and geometry.
2) The densities at different temperatures of the asphalt model using the Amber Cornell Extension Force Field were closer to the laboratory densities and reference data from Zhang and Greenfield [13]. The density property was also used to validate the asphalt model.
3) The glass transition temperatures of asphalt can be a small temperature range due to the complex compositions of the asphalt and the temperatures can be varied from the sources and components. The glass transition temperatures were computed based on the relationship between the temperatures and specific volumes. The glass transition temperature of the asphalt model with the Amber Cornell Extension Force Field was narrowed down into one small temperature ranges (around 300 K) compared to the

wide reference range (298 K to 353 K) from Zhang and Greenfield [13] based on the laboratory testing data.

4) There were four methods to calculate the viscosity in material engineering [118], and the Muller-Plathe algorithm was utilized to compute the viscosity of the asphalt model in this experimental MD simulation. The results of the asphalt model using the Muller-Plathe method in the rNEMD simulation are closer to the laboratory testing data compared to the reference data from Zhang and Greenfield [13] using the Green-Kubo and Einstein methods.
5) The bulk modulus was computed by applying volumetric and small strains in three coordinates of the asphatl1 model. The stress response in the mode was monitored, and the stress results in three coordinates were averaged for the calculation of the bulk modulus. The bulk modulus of the asphalt model is closer to the laboratory data than the reference data from Zhang and Greenfield [13].

The physical properties of the asphalt model computed in the experimental MD simulation include density, glass transition temperature, viscosity, and the bulk modulus. The computational results of the physical properties of the asphalt model are generally better than the reference data from Zhang and Greenfield [13]. Therefore, the asphalt model with the Amber Cornell Extension Force Field has a relatively good prediction for the properties compared to the reference model [13]. Furthermore, the calculation and optimization methods used in this manuscript are promising ways to simulate the materials, such as the numerical procedures to generate the asphalt model and optimize the system energy, and to calculate the physical properties and process the data of the simulation. In

addition, future work will mainly focus on the calculation of the shear modulus or diffusion coefficients. It is evident that there is still a difference between the simulation and the laboratory results. New asphalt models or methods will be developed to narrow these differences. This work is currently ongoing.

3.8 Acknowledgements

The authors appreciate Dr. Andreas Bick's valuable suggestions and help on the generation of the asphalt model and property calculations. The authors appreciate the financial support of the U.S. National Science Foundation (NSF) under the grant 1300286. The computational studies were performed using Scienomics MAPS software suite (MAPS, Version 3.4, Scienomics, Paris, France, 2014) and computer cluster (Superior Research Center) at Michigan Technological University. Any opinion, finding, and conclusion expressed in this paper are those of the authors and do not necessarily represent the view of any organization.

Chapter 4 Chemo-physical Analysis and Molecular Dynamics (MD) Simulation of Moisture Susceptibility of Nano Hydrated Lime Modified Asphalt Mixtures

4.1.Overview

The purpose of this study is to investigate the moisture susceptibility of nano hydrated lime (NHL) modified asphalt mixtures and determine the fundamental factors of moisture damage in asphalt mixtures using the molecular dynamics (MD), as well as analyze the effect that the aging of asphalt binders has on the moisture damage in asphalt mixtures. The NHL was added to the control asphalt to make NHL modified asphalt. The modified asphalt was mixed with aggregates to form NHL modified asphalt mixtures. The tensile strength ratio (TSR) test was used to evaluate the moisture susceptibility of asphalt mixtures. When the TSR test was done, different solutions were used to extract the polar groups from the tested asphalt mixtures, and the polar groups were analyzed using Fourier transform infrared spectroscopy (FTIR) attenuated total reflection (ATR). When asphalt oxidizes, the six functional groups (ketones, carboxylic acids, anhydrides, aldehydes, amides and esters) with the carbonyl group can be found in the polar part of asphalt based on FTIR ATR spectral data and references. The polar groups with the carbonyl group also

---

indicate the oxidation extent of asphalt binders. The FTIR test results indicate that carboxylic acids and ketones were the primary aging products in asphalt, and these two carbonyl groups relate to the rutting resistance and moisture susceptibility of asphalt mixtures. Furthermore, the MD interface systems of asphalt-aggregate and aggregate-water were created, as well as the separated systems (asphalt, water, and aggregates). The essential mechanisms for the moisture susceptibility of asphalt mixtures were explored with MD simulations. The potential energies of the interface systems and each separated system were computed to obtain the adhesion energies of the interface MD models. The differences in adhesion energy between the asphalt-aggregate and aggregate-water systems show that water tends to bond to the aggregate rather than the asphalt. This also explains the displacement of water that occurs in asphalt mixtures when there is moisture damage. In addition, the effect of asphalt aging on the moisture susceptibility of the asphalt mixture was also analyzed using MD interface models. The MD results demonstrate that the aging group in asphalt is helpful in reducing the moisture damage in asphalt mixtures.

4.2. Introduction

The oxidation hardens the asphalt and increases the viscosity of the asphalt. The exposure to ultraviolet radiation (UV), oxygen, and heat due to nature are the main causes of asphalt aging. The carbonyl and sulfoxide groups increase in the asphalt as oxidation occurs. The carbonyl groups include ketones, carboxylic acids, anhydrides, aldehydes, amides and esters. During the aging of asphalt, the aromatic components of the asphalt agglomerated and caused a reduction in the mobility and reactivity of the asphalt [133-135]. An earlier study on asphalt aging with oxygen focused on the relationship between the

properties of asphalt and the extent of oxidation. Asphaltene is the main component that affects the viscosity of asphalt [136]. Oxidation increased the spatial variations of asphalt on the nanoscale. The aging of asphalt also increased the adhesive and cohesive strengths of the asphalt in the early aging state. This indicates that the resistance to rutting and the moisture susceptibility in asphalt mixtures improved. However, the adhesive and cohesive strengths of the asphalt were not enhanced after aging with the pressure aging vessel (PAV). The micromechanical properties of asphalt were determined by the asphaltene content and the size of the microstructures [137]. In addition, some modifiers have an anti-aging performance, such as crumb rubber with styrene-butadiene-styrene (SBS), and nanomaterials [14, 138].

Modified asphalt binders have been widely used in road construction to improve the performance of pavement. Researchers have been searching for innovative materials to improve the performance of asphalt binders and asphalt mixtures. The use of non-modified nanoclay (NMN) and polymer modified nanoclay (PMN) in the control asphalt binder improved the complex shear modulus (G*) and viscosity [8, 14, 15]. The micro- or nano-sized materials (Nanoclay and carbon microfiber) improved the moisture susceptibility of the modified asphalt mixtures or decreased the potential of moisture damage [139]. The recycled asphalt pavement (RAP) was also used to reduce the moisture susceptibility of the hot mix asphalt (HMA) and warm mix asphalt (WMA) [140-142]. In accordance with the literature review [38, 143-146], hydrated lime improved the moisture susceptibility of asphalt mixtures. The addition of the hydrated lime allowed for the precipitation of calcium ions onto the aggregate surface, making it more favorable to the asphalt binder and

improving the binder-to-aggregate adhesion [147, 148]. The hydrated lime was either added into the asphalt directly or into the asphalt mixtures as filler, and both ways were shown to improve the resistance to moisture damage and frost, as well as a resistance to chemical aging [144]. That was the motivation to select the nano hydrated lime (NHL) in this study.

Molecular mechanics is when classical mechanics (Newtonian mechanics) is used to model molecular systems. The appropriate force field is assigned to the molecular systems, and the potential energies of these systems are calculated. The physical movements of atoms and molecules are simulated by the computer program in the Molecular Dynamics (MD) simulation. These atoms and molecules move and interact to mimic the response to external forces or environments. The MD program, Large-scale Atomic/Molecular Massively Parallel Simulator (LAMMPS) [118], is used to study the interaction between the asphalt and aggregates, as well as the reciprocity between the water and aggregates. Five kinds of MD simulations are usually used to model the different states in the systems, such as Microcanonical ensemble (NVE ensemble), Canonical ensemble (NVT ensemble), Isothermal-isobaric ensemble (NPT ensemble), Isoenthalpic-isobaric ensemble (NPH ensemble), and Generalized ensembles [62]. The relationship between the asphalt and aggregate was developed, and the asphalt-quartz structure model of the interface was used in the system [105]. The Consistent Valence force field (CVFF_aug) was considered in this simulation to characterize the inter-atom interactions. The shear stress and viscosity were evaluated and acceptable simulation results were obtained using the CVFF_aug force field [105].

In this moisture susceptibility study of asphalt mixtures, the NHL was used to improve the moisture damage in the asphalt mixtures. The polar groups in the NHL modified and control asphalt binder were extracted from the damaged asphalt mixtures and analyzed. The aging effect of asphalt was evaluated on the water damage in asphalt mixtures. The fundamental mechanism of moisture damage in the asphalt mixtures was explored with the MD simulation.

4.3.Research Objectives

The objectives of this study are to analyze the effect aging of the NHL modified asphalt binders has on the moisture damage in asphalt mixtures, and to understand the fundamental factors or chemical groups in the asphalt, which link to the moisture susceptibility of asphalt mixtures. The functional groups with the carbonyl group in the asphalt can be found to relate to the water damage of asphalt mixtures. The six functional groups (ketones, carboxylic acids, anhydrides, aldehydes, amides and esters) containing the carbonyl group in the asphalt were demonstrated and studied. Furthermore, the molecular dynamics were applied to analyze the relationships and interactions of three interface systems: asphalt-aggregate system, aggregate-water system and aggregate-asphalt with the carboxylic acid (aging group), as well as the impact of asphalt aging on the moisture damage in asphalt mixtures.

4.4.Materials and Experimental Design

4.4.1 Chemistry of carbonyl groups

During asphalt oxidation, the six functional groups with the carbonyl group are formed including carboxylic acids, aldehydes, amides, anhydrides, esters, and ketones. 1)

Carboxylic acid in the organic compound consists of a carboxyl group (C (O) OH) and R (the rest of the molecules) [149], and it is easily detected and identified by the FTIR. Carboxylic acid is a weak acid and can only donate H^+ cations [150]. 2) Ketones are the organic components with the structure of RC (=O) R', where the R and R' are the hydrocarbon groups. They do not have a reactive group due to their structures [150]. The ketone carbon is often demonstrated as being "sp^2 hybridized" (electron and molecular structures), and ketones are trigonal and planar around the ketonic carbons. The ketones are different from the functional groups with a carbonyl group, such as carboxylic acids, amides, and esters [151]. 3) Anhydrides consist of two acyl groups (RCO-, carbonyl and alkyl groups) connected to the oxygen atom in the acid anhydrides [149]. It is also a reactive acyl group, so it can produce carboxylic acid and acetate esters [152]. 4) Aldehydes are also an organic group with the structure R-CHO. This structure is called the formyl group when the R is replaced by H. The sp^{2-} hybridized and planar carbon connects oxygen with a double bond. The aldehydes and carboxylic acids can be produced from the oxidations of alcohol, and they are polar groups [149, 153, 154]. 5) Amides are a group with the structure $R_nEO_xNR'_2$, where E represents different elements and n and x denote the number of atoms [149]. Amide can be the hydrogen bond acceptor and donor, due to the carbonyl bond. This characteristic of the hydrogen bond acceptor and donor also makes it soluble in water [155]. 6) Esters are chemical compounds with the structure RCO_2R', where R and R' are the hydrocarbons in the organic esters. Esters can be derived from the condensation of the carboxylic acids, such as formate, hexyl octanoate and acetate. The reactions include alcoholysis of acyl chlorides and acid anhydrides, esterification of carboxylic acids, and so on [149, 156-158].

4.4.2 Preparation of polar groups in the asphalt

The control asphalt used was a PG 58-28 asphalt binder. Nano hydrated lime (NHL) with a particle size of 100nm (Figure 4.1a) was shipped from, Sha Highland Network Tech Company of China, in Shanghai city. The micro-image of NHL was observed by the field emission scanning electron microscopy (FE-SEM). In Figure 4.1b, the NHL materials were agglomerated. The NHL consists of 90% calcium hydroxide, 3% calcium carbonate, 1.5% calcium oxide, 1.5% silicon dioxide and some insoluble matters. The density of NHL is 2.24 g/cm^3. Amounts of 10% and 20% NHL by weight of asphalt were added to the control asphalt.

The NHL material was slowly added into the control asphalt and the modified asphalt binders were blended for two hours in the high shear machine. The asphalt binders and aggregates were blended in the drum mixer and compacted by a Superpave Gyratory Compactor (SGC). Then, the indirect tensile test of asphalt mixtures was performed, and the tensile strength ratio (TSR) of asphalt mixtures was evaluated. When the TSR test was done, the tested samples were immersed and extracted by different solutions. Firstly, the cyclohexane solution was used to extract the non-polar part of the asphalt in the tested asphalt mixtures. Then, the toluene and ethanol were mixed at a ratio of 9:1 to dissolve the remaining part of the asphalt mixture samples. The non-polar and polar parts of the asphalt were obtained through these steps.

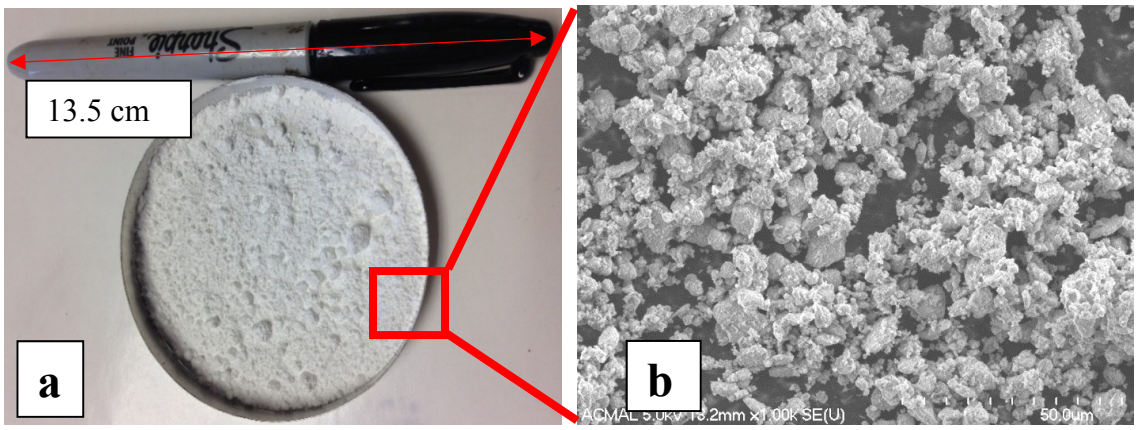

Figure 4.1. Appearance and FE-SEM image of nano hydrated lime materials: a) white powder, b) the FE-SEM image at the magnitude of 1,000x

4.4.3 Polar group analysis

Infrared spectrometry (IR) is a useful tool in analyzing the chemical composition and molecular bonds of materials. The Fourier Transform Infrared Spectroscopy (FTIR) is a piece of technical equipment used for detecting the infrared absorption of tested materials with a wide range of wavelengths. The FTIR attenuated total reflection (ATR) was used to test different types of samples [159]. The organic asphalt is composed of 90% carbon and hydrogen, and small amounts of other elements [6]. It is known that six movements in the CH_2 groups are common in organic materials, such as symmetrical stretching, rocking, anti-symmetrical stretching, twisting, scissoring, and wagging [160]. Of these movements, the symmetrical and anti-symmetrical stretching movements are most common in asphalt. The Jasco IRT 3000 FTIR spectrometer was employed to test the samples. The non-polar and polar parts of asphalt were tested by FTIR ATR, and the spectra of samples were analyzed.

4.5.Moisture Susceptibility Test of NHL Modified Asphalt Mixtures

The NHL was slowly added to the PG 58-28 asphalt and the modified asphalt was mixed in the high shear mixer at 135ºC and 5000rpm. Due to the high amount of NHL in the asphalt, the shear speed was increased slightly when the sample was blended. The modified asphalt binders were prepared for the asphalt mixture after about two hours of mixing. The aggregates were also pre-heated for approximately two hours to dry. The gradation 5E3 of aggregates was also used to compact the asphalt mixtures by a SGC. The mixing and compaction temperatures were 150ºC and 135ºC, respectively. Mixing was followed by the Superpave compaction, and the loose asphalt mixtures were heated in the oven (135ºC) for at least two hours. The samples were cured at room temperature for at least 72 hours after the asphalt mixtures were compacted.

When the asphalt mixtures were ready, the indirect tensile test was conducted and the tensile strength ratios (TSR) of the control and modified asphalt mixtures were evaluated. The test was based on AASHTO's procedure T283. The air voids were maintained between 6% and 8%. The height of the sample was about 63.5 mm and the diameter was about 100 mm. The thaw cycles were applied to the asphalt mixtures by immersing the sample in the 60ºC water for different periods of time. All of the samples were measured, using the Universal Testing Machine (UTM), for the indirect tensile strength and its ratio under the conditions of the room temperature and constant loading rate. These parameters were calculated by equation (4.1), and the results are shown in Figure 4.2.

$$S_t = \frac{2P}{\pi tD}\ ,\ TSR = \frac{S_2}{S_1} \tag{4.1}$$

Where S_t is the tensile strength (Pa), P is the maximum load (N), t is the sample thickness (mm), D is the sample diameter (mm), TSR is the tensile strength ratio, S_1 is the average dry tensile strength, and S_2 is the average conditioned tensile strength.

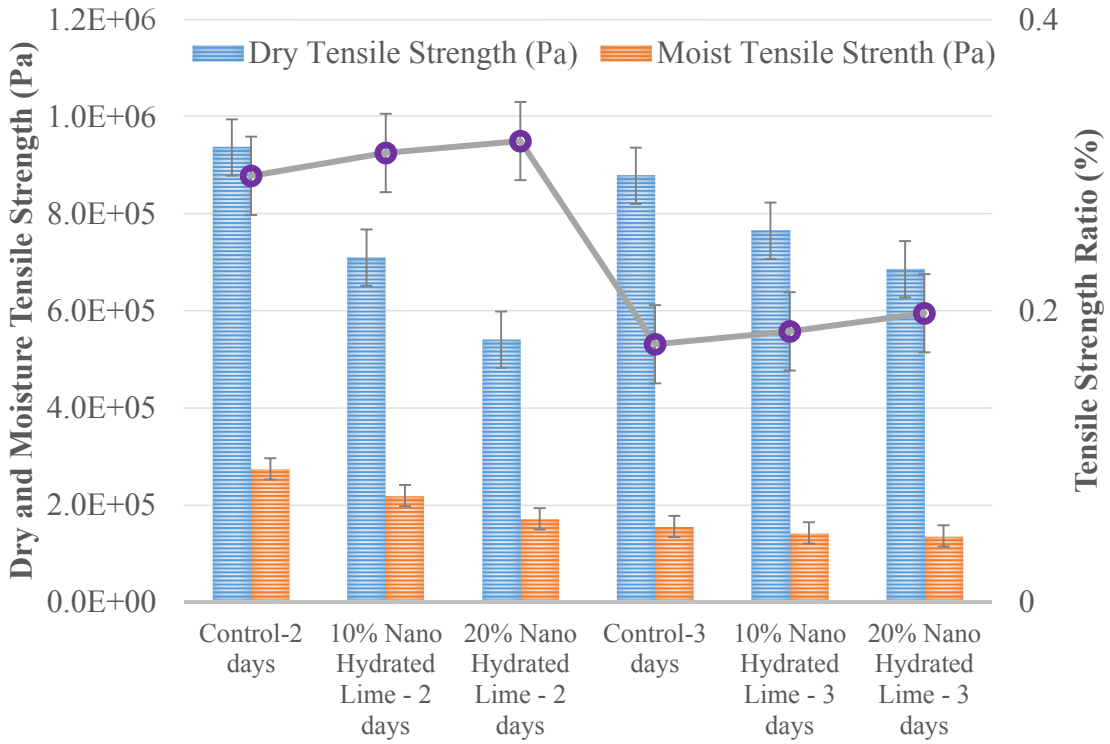

Figure 4.2. Tensile strength ratio (TSR) of the control and NHL modified asphalt mixtures

Figure 4.2 shows the tensile strengths of the control and NHL modified asphalt mixtures. The results show that the addition of NHL into the asphalt mixtures decreases the dry tensile strength, as well as the wet tensile strength. The results also coincide with the trend of the reference [143]. However, the TSR of nano hydrated lime modified asphalt mixtures increases slightly. The moisture susceptibility of nano hydrated lime modified asphalt mixtures improves relative to the control asphalt binder from the TSR data. The wet tensile strength of the control asphalt mixture decreases faster than that of hydrated

lime modified asphalt mixtures. Meanwhile, the dry tensile strength at 3 days for the hydrated lime modified asphalt mixtures increases compared to the dry tensile strengths at 2 days. This indicates that the addition of the nano hydrated lime delays the moisture damage of modified asphalt mixtures. The calcium ions from the NHL can prevent the displacement of water at the asphalt binder-aggregate interfaces. Seen from the reference [143], if the hydrated lime was blended with the asphalt prior to the asphalt mixture, it can effectively reduce the moisture damage of modified asphalt mixtures. In addition, the trends of mixing and compaction temperatures of the control and modified asphalt mixtures were followed by the temperatures of the control asphalt mixture. If the mixing and compaction temperatures and the oxidation time of modified asphalt increases, the strengths of modified asphalt mixtures increase more, as expected. This also explains the low values for strengths of the dry and wet NHL modified asphalt mixtures compared to the control mixture.

4.6.FTIR Sample Preparation and Characterization Results

The asphalt mixture samples were tested by UTM and the tensile strength of the asphalt mixtures was measured. The tested samples were dried at room temperature. Then, a small amount (around 20 grams) of the tested samples was soaked in cyclohexane solution (around 100 ml). The non-polar compounds in the asphalt melted in the cyclohexane. The first extraction of the asphalt mixtures was done after the solution was mixed for about half an hour and settled for a half hour. The second extraction of the asphalt mixtures was performed using the solvent (around 40 ml) mixed with toluene-ethanol at a ratio of 9:1. The polar components in the asphalt were absorbed by the solvent, not by the

cyclohexane. The solution was also mixed for about half an hour and settled for a half hour. The weights of the samples and solutions were recorded, as well as the non-polar and polar parts of the asphalt. The weight of the polar components of the asphalt comprised less than 2% of the weight of the tested asphalt mixtures.

4.6.1 Functional components in the asphalt

The polar components of the control asphalt were tested at the liquid state by the FTIR ATR. The spectrum data of the polar parts of the control asphalt was analyzed to show the number of carbonyl groups in the asphalt. The evidence of six functional groups with a carbonyl group was found from the spectral images and references. The polar parts of the asphalt in the solution were examined by FTIR ATR, and the FTIR results are shown in Figure 4.3. In addition, the carbon-oxygen (C-O) single bond can be observed in the ethanol spectrum [161-163]. One of the solutions used in the FTIR ATR test was mixed with toluene and ethanol, and the bonding features of toluene and ethanol are shown in the spectra of the solution (Figure 4.3). The features of six functional groups with carbonyl are as follows.

(1) There are different types of ketones, such as acyclic, cyclic, α, β-unsaturated, and aryl ketone. The ketones can be detected at a range of 1665 cm^{-1} - 1850 cm^{-1} [164, 165], shown in Figure 4.3a. Ketones can reinforce the intensity of the carbonyl group in asphalt at around 1700 cm^{-1} [134]. They also have a close relationship to the performance of asphalt binders and mixtures [143-145, 166].

(2) Three bonds, carbon-oxygen double stretching bond (C=O), carbon-oxygen single stretching bond (C-O), and oxygen-hydrogen bond (O-H), are observed in carboxylic

acid [164, 165]. Figure 4.3a shows that the C=O peak of carboxylic acids is detected at a range of 1700 cm^{-1} - 1725 cm^{-1} [14] in the polar groups of asphalt. Figure 4.3b and Figure 4.3c demonstrate the peaks of the carbon-oxygen single stretching bond (C-O) and hydroxyl group (O-H) are observed at a range of 1210 cm^{-1} - 1320 cm^{-1} and 2500 cm^{-1} - 3300 cm^{-1}, respectively. The carboxylic acids in the asphalt were also studied by Campbell [134], and the results show that carboxylic acids are also aging products of asphalt.

(3) Figure 4.3a shows that two main carbonyl groups are detected at the bands [164, 165] around 1800 cm^{-1} - 1830 cm^{-1} and 1740 cm^{-1} - 1775 cm^{-1}, respectively. The anhydrides are also produced during the oxidation of asphalt and the two carbonyl groups observed should be anhydrides. A limited anhydrides were observed during oxidation, but large amounts of anhydrides were detected in the long-term aged asphalt [167]. Stronger absorbance appeared at a range of 1740 cm^{-1} - 1775 cm^{-1}, and this peak area was used to represent the anhydrides in this study.

(4) The references [164, 165] display that there are two obvious bonds, carbonyl (C=O) and carbon-hydrogen bonds (C-H), in the aldehydes. The peak of the carbonyl group in the aldehyde is detected at a range of 1720 cm^{-1} - 1740 cm^{-1}, as shown in Figure 4.3a. It is easy to identify two peaks of carbon-hydrogen bonds of organic materials at a range of 2820 cm^{-1} - 2850 cm^{-1} and 2720 cm^{-1} - 2750 cm^{-1} in Figure 4.3c. Campbell studied asphalt oxidation, and the results reveal that the aldehydes also increased the carbonyl absorbance in the oxidized asphalt [134].

(5) The carbon-oxygen double stretching bond (C=O) and carbon-oxygen single stretching bond (C-O) are observed in the ester group [164, 165]. The peak of the carbonyl group

(C=O) of esters is found in a region of 1735 cm^{-1} - 1750 cm^{-1} from Figure 4.3a in the polar part of the asphalt. The peak of the carbon-oxygen single bond (C-O) in the esters can be detected in an area of 1000 cm^{-1} - 1300 cm^{-1} from Figure 4.3b. Due to the small amount of esters in the oxidized asphalt, there is a limited contribution to the aging of the asphalt [134].

(6) Figure 4.3a reveals that the peak of carbonyl groups (C=O) in the amide is observed at a range of 1640 cm^{-1} - 1690 cm^{-1}. Figure 4.3b and Figure 4.3c also show that the N-H stretching and bending bonds are found in a region of 3100 cm^{-1} - 3500 cm^{-1} (including a shoulder band) and 1550 cm^{-1} - 1640 cm^{-1}, respectively, in the asphalt at the liquid state. Due to the small amount of amide [134] in the asphalt, the amide may not be easily detected.

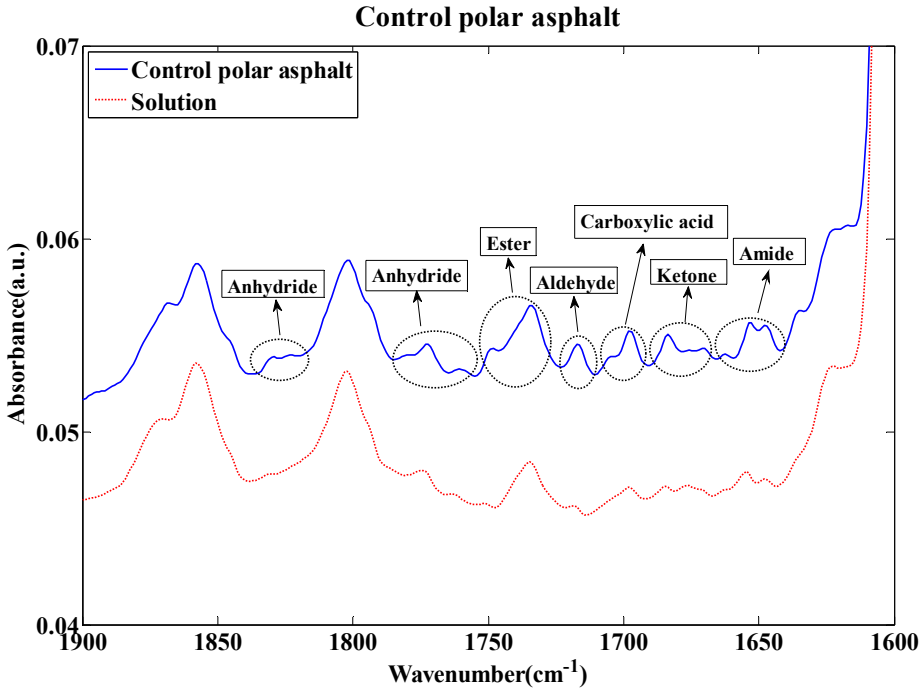

(a) Functional groups containing the carbonyl group in the polar asphalt (liquid state)

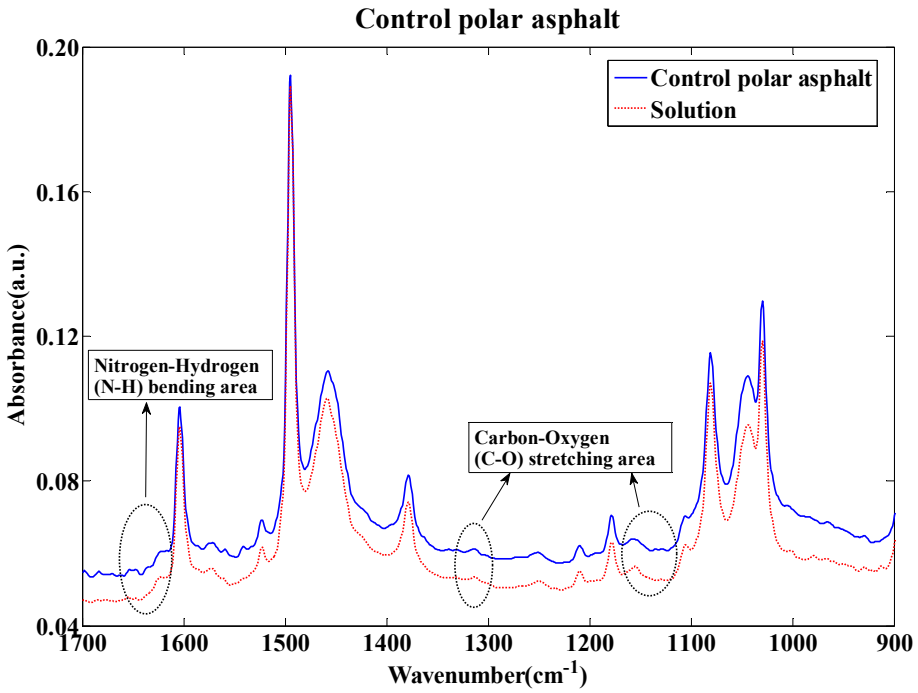

(b) Nitrogen-hydrogen and carbon-oxygen bonds in the polar asphalt (liquid state)

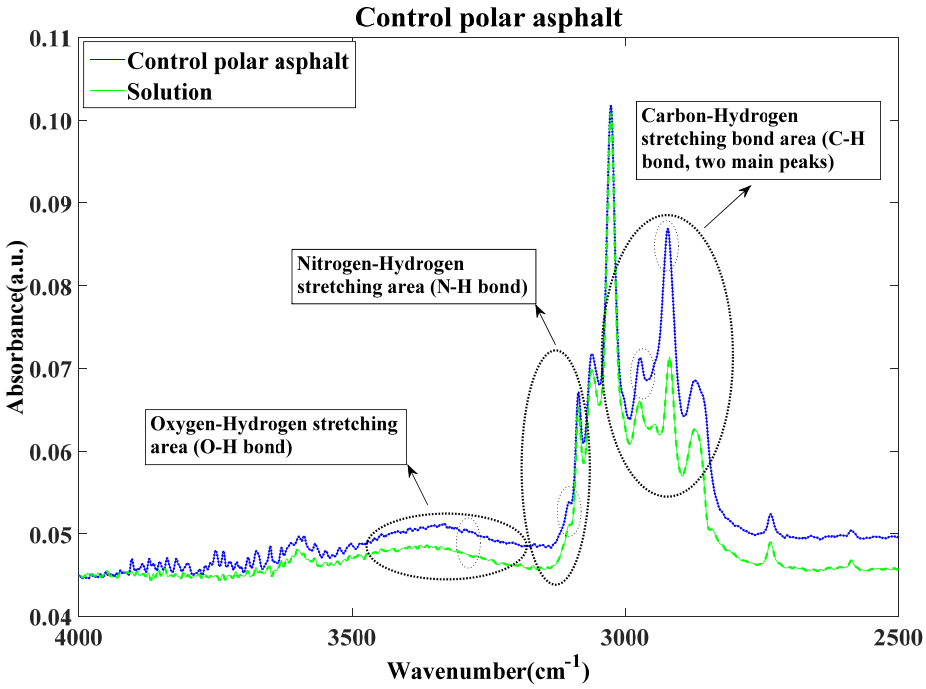

(c) Oxygen-hydrogen and Nitrogen-hydrogen bonds in the polar asphalt (liquid state)

Figure 4.3. Chemical bonds in the asphalt binders

4.6.2 FTIR results of polar groups in the control and NHL modified asphalt

After identifying the functional groups in the polar parts of the control asphalt, the liquid asphalt samples were dropped into the groove of FTIR and tested by FTIR ATR. The FTIR spectra were recorded with the accumulation of 256 scans, with a resolution of $4cm^{-1}$. The peak range of functional polar carbonyl groups in the asphalt is demonstrated in Table 4.1. The polar compounds were tested by the FTIR ATR at liquid state. The results of the FTIR spectra are shown in Figure 4.4. The carbonyl groups in the polar part of the asphalt were analyzed, and these groups may relate to the performance of the asphalt mixtures [143].

Table 4.1. Functional groups containing a carbonyl in the asphalt binder

Functional Groups	**Absorption Frequency Region, Wavenumber (cm^{-1})**
Carbonyl: C=O	1670-1820, stretching vibration, strong intensity [7, 164, 165]
Functional Groups: Carboxylic Acid	
C=O	1700-1725, stretching vibration [7, 164, 165]
O-H	2500-3300, stretching vibration, strong intensity [7, 164, 165]
C-O	1210-1320, stretching vibration, strong intensity [7, 164, 165]
Functional Groups: Aldehyde	
C=O	1720-1740, stretching vibration, strong intensity [7, 164, 165]
=C-H	2820-2850 & 2720-2750, stretching vibration, medium intensity [7, 164, 165]
Functional Groups: Amide	
C=O	1640-1690, stretching vibration, strong intensity [7, 164, 165]
N-H	3100-3500, stretching vibration, unsubstituted [164, 165]
N-H	1550-1640, bending vibration [164, 165]
Functional Groups: Ketone	
Acyclic	1705-1725, stretching vibration, strong intensity [164, 165]
Cyclic	3-membered-1850, stretching vibration, strong intensity [164, 165]
	4-membered-1780, stretching vibration, strong intensity [164, 165]
	5-membered-1745, stretching vibration, strong intensity [164, 165]
	6-membered-1715, stretching vibration, strong intensity [164, 165]
	7-membered-1705, stretching vibration, strong intensity [164, 165]
α, β - unsaturated	1665-1685, stretching vibration, strong intensity [164, 165]
Aryl ketone	1680-1700, stretching vibration, strong intensity [164, 165]
Functional Groups: Anhydride	
C=O	1800-1830&1740-1775, stretching vibration [7, 164, 165]
Functional Groups: Ester	
C=O	1735-1750, stretching vibration, strong intensity [7, 164, 165]
C-O	1000-1300, stretching vibration, two bands or more [7, 164, 165]

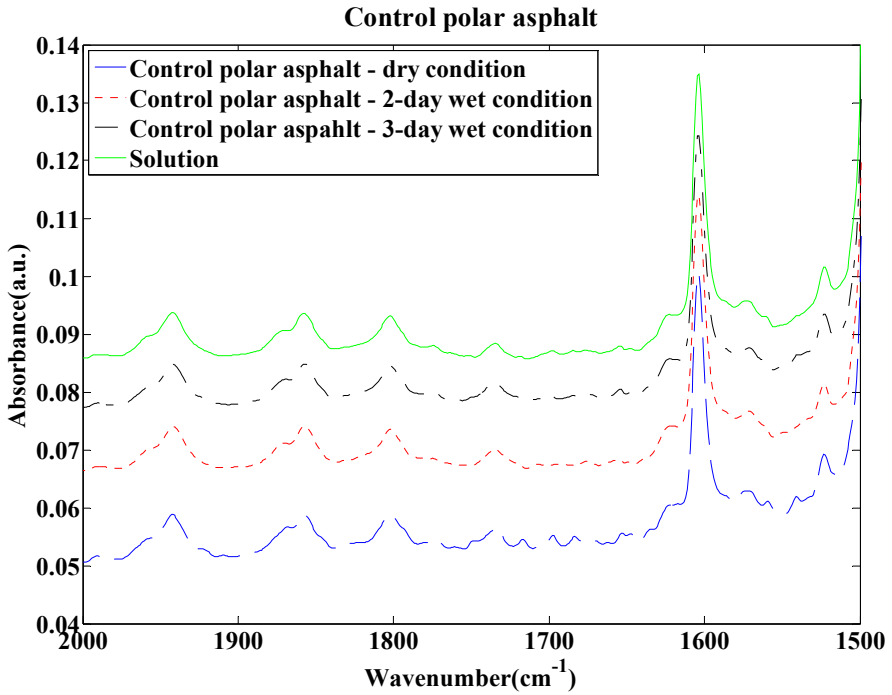

(a) FTIR spectra of the polar parts in the control asphalt at a range of 1500-2000cm^{-1}

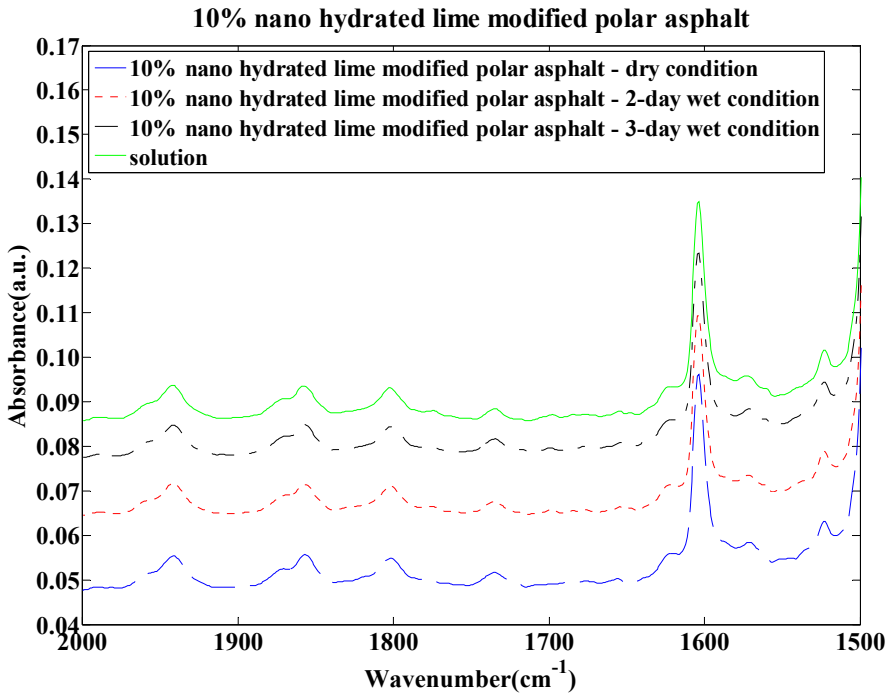

(b) FTIR Spectra of the polar parts in 10% NHL modified asphalt at a range of 1500-2000cm^{-1}

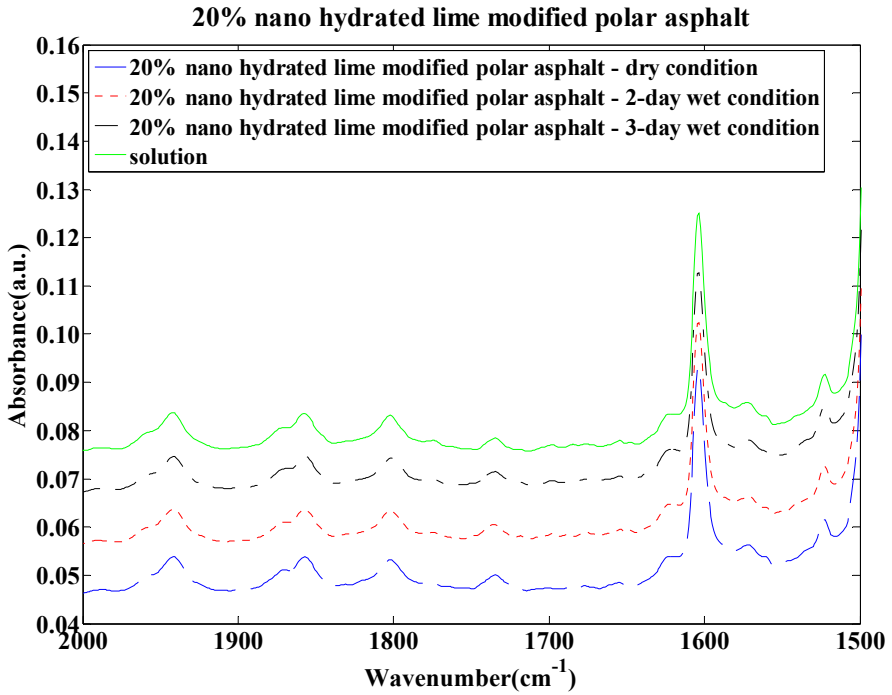

(c) FTIR spectra of the polar parts in 20% NHL modified asphalt at the range of 1500-2000cm^{-1}

Figure 4.4. FTIR results of polar parts in the asphalt binders

Figures 4.4 shows the FTIR spectra of polar compounds in the asphalt at the liquid state. The solvents used were also tested with the FTIR ATR. The FTIR spectra of the control and NHL modified asphalt were compared, and the polar compositions in the asphalt were analyzed. Based on the literature review [143-145], the hydrated lime can enhance the adhesion between the aggregate and asphalt. The hydrated lime particles melted in the asphalt and the carboxylic acids/carbonyl groups in the asphalt improved the moisture susceptibility of the asphalt mixtures including the mixture with siliceous aggregates. Compared to the spectra of the solutions, the peaks of the functional polar groups in asphalt were clearly displayed (section: functional group components). The ratios of carbonyl groups in the asphalt were calculated using equation (4.2) through equation

(4.8). The results of the ratio calculations of the control and NHL modified asphalt at the liquid state are shown in Figure 4.5.

$$I_{acids} = \frac{\text{Area of the carboxylic acid bands between 1720 cm}^{-1}\text{and 1700 cm}^{-1}}{\sum \text{Area of the spectral bands between 2000 cm}^{-1}\text{ and 600 cm}^{-1}} \quad (4.2)$$

$$I_{aldehydes} = \frac{\text{Area of the aldehyde bands between 1735 cm}^{-1}\text{and 1720 cm}^{-1}}{\sum \text{Area of the spectral bands between 2000 cm}^{-1}\text{ and 600 cm}^{-1}} \quad (4.3)$$

$$I_{amides} = \frac{\text{Area of the amide bands between 1660 cm}^{-1}\text{and 1645 cm}^{-1}}{\sum \text{Area of the spectral bands between 2000 cm}^{-1}\text{ and 600 cm}^{-1}} \quad (4.4)$$

$$I_{anhydrides} = \frac{\text{Area of the anhydride bands between 1775 cm}^{-1}\text{and 1750 cm}^{-1}}{\sum \text{Area of the spectral bands between 2000 cm}^{-1}\text{ and 600 cm}^{-1}} \quad (4.5)$$

$$I_{esters} = \frac{\text{Area of the ester bands between 1750 cm}^{-1}\text{and 1735 cm}^{-1}}{\sum \text{Area of the spectral bands between 2000 cm}^{-1}\text{ and 600 cm}^{-1}} \quad (4.6)$$

$$I_{aryl\ ketones} = \frac{\text{Area of the aryl ketone bands between 1700 cm}^{-1}\text{and 1685 cm}^{-1}}{\sum \text{Area of the spectral bands between 2000 cm}^{-1}\text{ and 600 cm}^{-1}} \quad (4.7)$$

$$I_{\alpha,\beta\ unsaturated\ ketones} =$$

$$\frac{\text{Area of the } \alpha,\beta \text{ unsaturated ketone bands between 1680 cm}^{-1}\text{and 1665 cm}^{-1}}{\sum \text{Area of the spectral bands between 2000 cm}^{-1}\text{ and 600 cm}^{-1}} \quad (4.8)$$

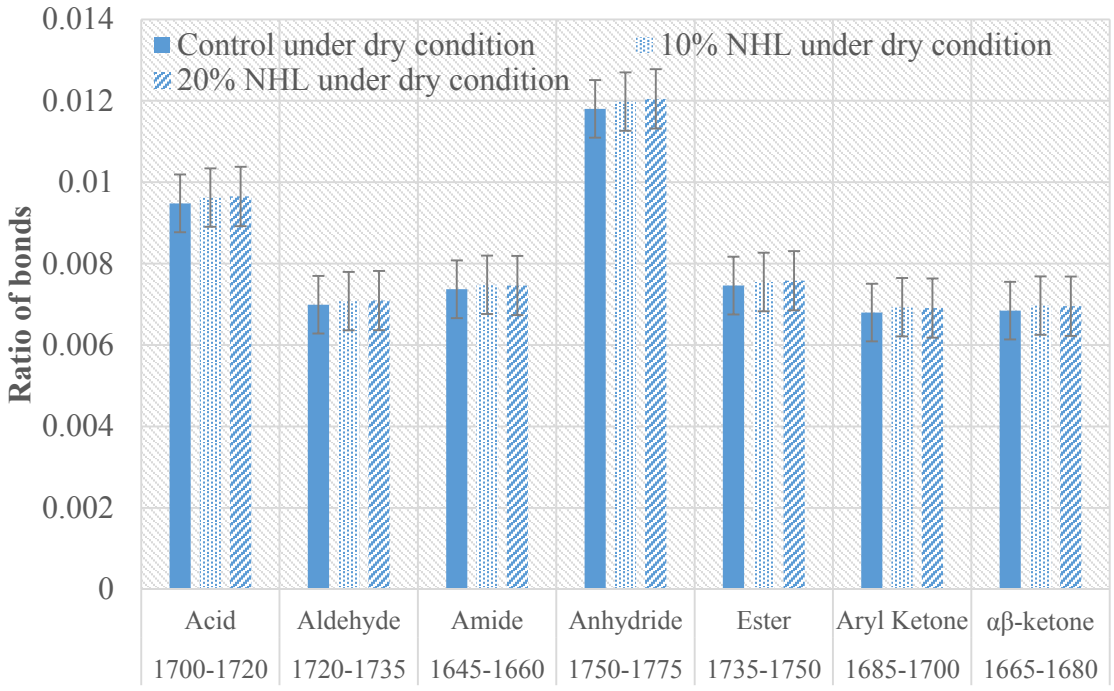

(a) Ratio calculations of functional polar groups in the control and NHL modified asphalt at the dry condition (liquid state)

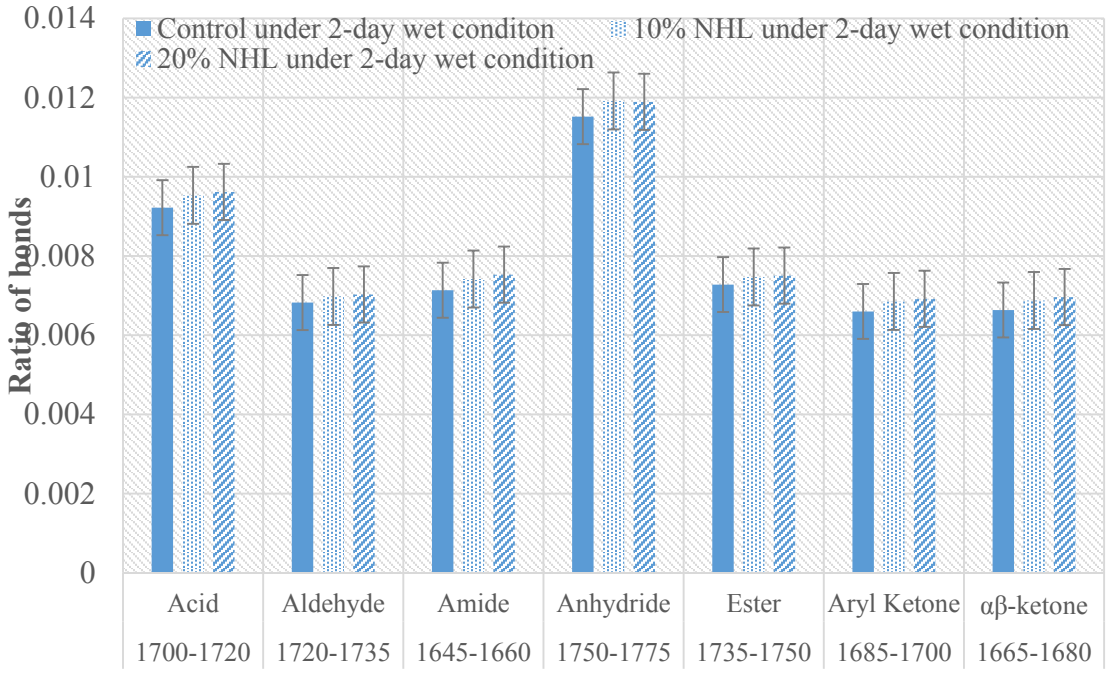

(b) Ratio calculations of functional polar groups in the control and NHL modified asphalt after a 2-day wet condition (liquid state)

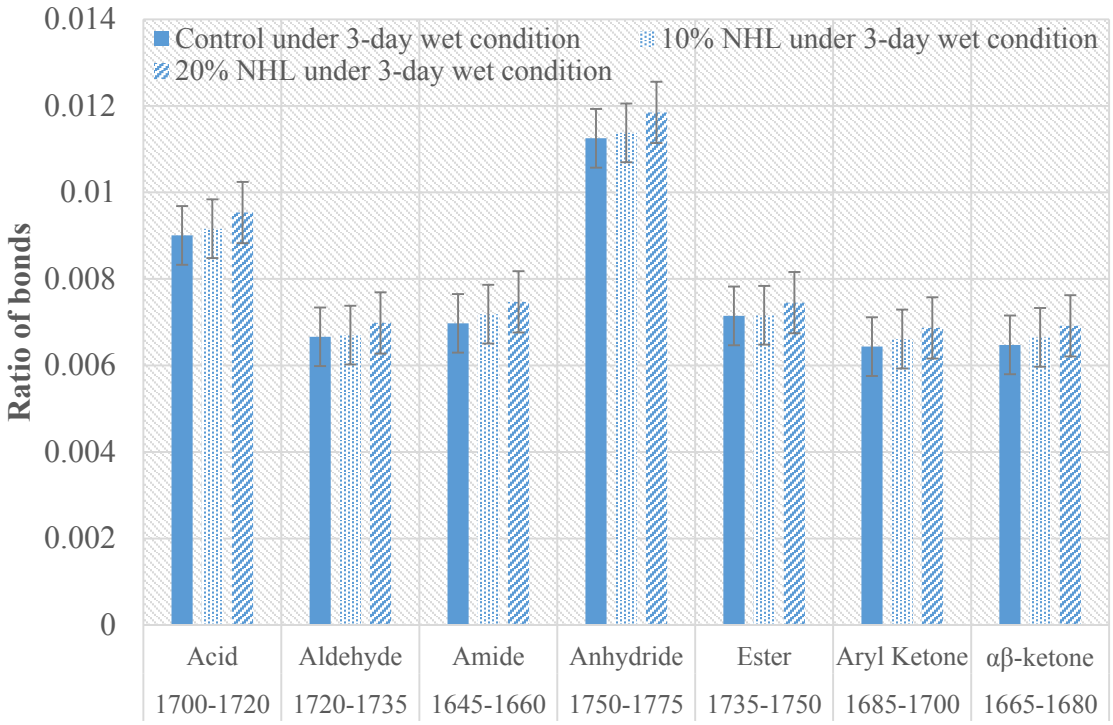

(c) Ratio calculations of functional polar groups in the control and NHL modified asphalt after a 3-day wet condition (liquid state)

Figure 4.5. Ratio calculations of functional polar groups in the control and NHL modified asphalt

During the FTIR sample preparations, it is possible that the concentrations of polar groups in the asphalt were affected by the solutions. However, the trends of these functional groups were not changed. It is likely that the composition produced by the asphalt oxidation may be changed by different conditions. Figure 4.5a shows the ratios of functional polar groups in the control and NHL modified asphalt at the dry condition. The amount of anhydride is the highest in the polar groups in the asphalt. If the sum of aryl ketones and α,β-unsaturated ketones are considered as ketones, then, the ketones are the main products in the functional polar groups of asphalt. After the asphalt mixture tests, it is determined that the carboxylic acids in the polar groups of asphalt are also a major part of the asphalt

oxidation products. The amount of esters, aldehydes and amides is less than the three primary groups (anhydrides, ketones and carboxylic acids) in the oxidized asphalt. Seen from Figure 4.5a, the amounts of functional carbonyl groups in the 20% NHL modified asphalt are more than the control and the 10% NHL modified asphalt. The quantity of carbonyl groups in the 10% NHL modified asphalt is slightly more than that of the control asphalt. The addition of NHL into the control asphalt increases the functional groups in the modified asphalt in the dry condition.

Figure 4.5b and Figure 4.5c reveal the ratios of the functional groups in the control and NHL modified asphalt after 2- and 3- day wet conditions. The amount of carbonyl groups in the 20% NHL modified asphalt is more than those in the control and 10% NHL modified asphalt, and the quantity of carbonyl groups in the 10% NHL modified asphalt is more than that of the control asphalt under the wet condition. The anhydrides, carboxylic acids and ketones are still the leading products during the aging process in the polar asphalt at a liquid state. Considering the TSR results of the control and NHL modified asphalt mixtures, the more polar groups that are in the asphalt, the better the TSR results are. This indicates that asphalt aging under the wet condition helps the asphalt mixture to resist moisture damage, especially the ketones, carboxylic acids, and anhydride in this case. The calcium ions in the NHL modified asphalt may be the reason for the improvement of the moisture damage in the asphalt mixtures.

Therefore, the ketones and carboxylic acids increased more after the oxidation of asphalt, and the anhydrides and amides increased, in this case. The aging groups in the asphalt enhance the resistance to permanent deformation in the asphalt pavement at an

earlier stage and also help to improve the moisture susceptibility of asphalt mixtures. Furthermore, the effect of NHL materials on the resistance to moisture damage in asphalt mixtures is positive.

4.7.Molecular Dynamics (MD) Analysis

The bonding strength between the aggregates and the asphalt determines the performance of the rutting resistance and moisture susceptibility in asphalt mixtures [8, 168]. The mechanism of water replacement in the moisture damage in asphalt mixtures is demonstrated in Figure 4.6, from the initiation to the propagation stage. The bonding strength is related to the adhesion energy between the asphalt and aggregates, which varies with the interfacial interactions among asphalt, water, and aggregates. Therefore, the adhesion energy calculation is important to explain the mechanism of moisture distresses in the asphalt mixtures. In this study, the interaction between the asphalt and aggregates, as well as the interaction between the water and aggregates, was first simulated using the molecular dynamics method. Through MD simulations of the potential energies of the interface and individual models, the adhesion energies were computed to explain the cause of moisture damage in asphalt mixtures. The aging effects of asphalt binders were demonstrated for the mitigation of water damage in asphalt mixtures.

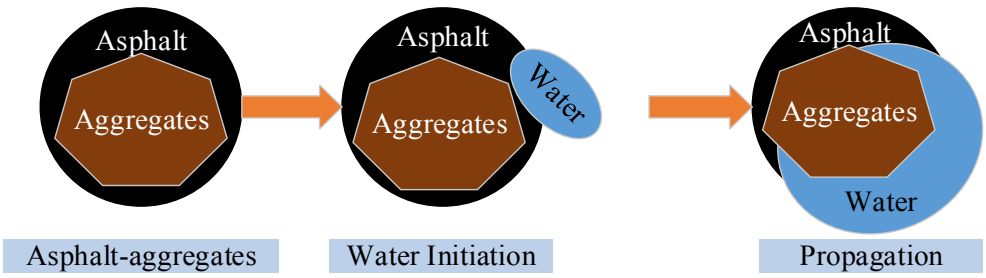

Figure 4.6. Stages of water displacement in the moisture damage of asphalt mixtures

When the asphalt and aggregates are mixed, the aggregates are heated in the oven for at least two hours. It is assumed that water on the surface or in the porous holes of the aggregates is vaporized and escapes from the aggregates. This confirms that the water inducing the damage in the asphalt mixtures is from the external environment. The repeated traffic loads and changes in environmental conditions decrease the strength of adhesion between the aggregates and asphalt/asphalt mastic and the cohesive bonding strength within the asphalt binder [169, 170]. It is also assumed that the asphalt mastic consists of the asphalt binder and fine aggregates (aggregate size is normally smaller than 2.36 mm), and the asphalt mastic is in the transition state to form the asphalt mixtures [53, 171]. When the adhesive and cohesive bonds are reduced in the asphalt mixtures, water starts to intrude into the aggregates, and moisture damage in asphalt mixtures develops from the initiation stage to the propagation stage (Figure 4.6).

In these interface models, the crystal quartz (SiO_2) structure is represented as the aggregate in the asphalt mixtures. Based on the Corbett method [6], the asphalt material is composed of asphaltenes, polar aromatics, naphthene aromatics, and saturates through different absorption and desorption. Based on the references [83, 85], the asphalt model consists of asphatenes, saturates, and aromatics at the ratio of 5:41:27, respectively. The

structure of asphaltenes in the asphalt model was proposed by Artok et al. [80] and Zhang et al. [13]. These saturates were represented by docosane molecules and the aromatics were replaced by the 1, 7-dimethylnaphthalene in the asphalt model from the references [13, 81, 84, 117]. In addition, based on the structure of asphalt components from the references [13], the aging effects on these components were investigated and one of the asphalt aging groups (the carboxylic acid group) was attached in the structure of the components (Figure 4.7). The possible structures of asphaltenes (Figure 4.7a) and aromatics (Figure 4.7b) with the carboxylic acid group are proposed and displayed in Figure 7. However, the structure of docosane (Figure 4.7c) is relatively stable, and it is likely that the docosane is not compatible with other oxidizing agents.

Three interface models among the asphalt, water, and aggregates were created by the Materials Processes and Simulations (MAPS) software with the Amber Cornell Extension Force Field [64, 65]. These interface models include the interaction systems of 1) asphalt-aggregate, 2) aggregate-water, and 3) aggregate-asphalt with carboxylic acid (aging group) (Figure 4.8). The density of asphalt in the interface model is around 1.04 g/cm^3, which matches the physical properties of asphalt. Parts of bond parameters of the Amber Cornell Extension Force Field are from the Amber Cornell Force Field and General Amber Force Field (GAFF) [64, 65]. The system energy formula in the Amber Cornell Extension Force Field is shown in equation (4.9).

$$E_{total} = \sum_{bonds} K_r(r - r_{eq})^2 + \sum_{angles} K_\theta(\theta - \theta_{eq})^2 + \sum_{dihedrals} \frac{V_n}{2}[1 + \cos(n\varphi - \gamma)] + \sum_{i<j}[\frac{A_{ij}}{R_{ij}^{12}} - \frac{B_{ij}}{R_{ij}^{6}} + \frac{q_i q_j}{\epsilon R_{ij}}] \quad (4.9)$$

Where the first term is the energy between the covalently bonded atoms; the second term is the energy caused by the geometry of electron orbitals; the third term is the energy from twisting a bond; the fourth term is a non-bonded energy from van der Waals and electrostatic energies (atom pairs). r_{eq} and θ_{eq} are the equilibrium structural parameters; K_r and K_θ are the force constants; n is the multiplicity and γ is the phase angle for the torsional angle parameters; A, B and q are the non-bonded potentials between all atom pairs; and finally, R_{ij} is the distance of atoms and ϵ is the well depth for van der Waals energy.

In the interaction models, the Electrostatic Potential (ESP) charges were allotted to the asphalt components by using the quantum mechanics module NWChem in the MAPS software [120]. The Conjugate Gradient method and the Particle Mesh Ewald (PME) method were used to optimize the energy of the system. The Conjugate Gradient method was used to optimize the energy in the large and complex systems. The optimization calculation formula is shown in equation (4.10).

$$f(x) = \frac{1}{2}x^T Ax - x^T b,\ x \in R^n,\ \text{(iterations)} \tag{4.10}$$

Where A is symmetric, positive and real, b is a known coefficient.

PME is an Ewald summation for the long-range potential computation in the periodic systems. In the PME method, the long-range part is divided into two sections: short-range and long-range contributions. The calculations of two-part energies are expressed in equation (4.11).

$$\varphi(r) \stackrel{\text{def}}{=} \varphi_{sr}(r) + \varphi_{lr}(r) \tag{4.11}$$

Where $\varphi_{sr}(r)$ is the short-range term potential energy which quickly converges in the real space, and $\varphi_{lr}(r)$ is the long-range term potential which quickly converges in the Fourier space.

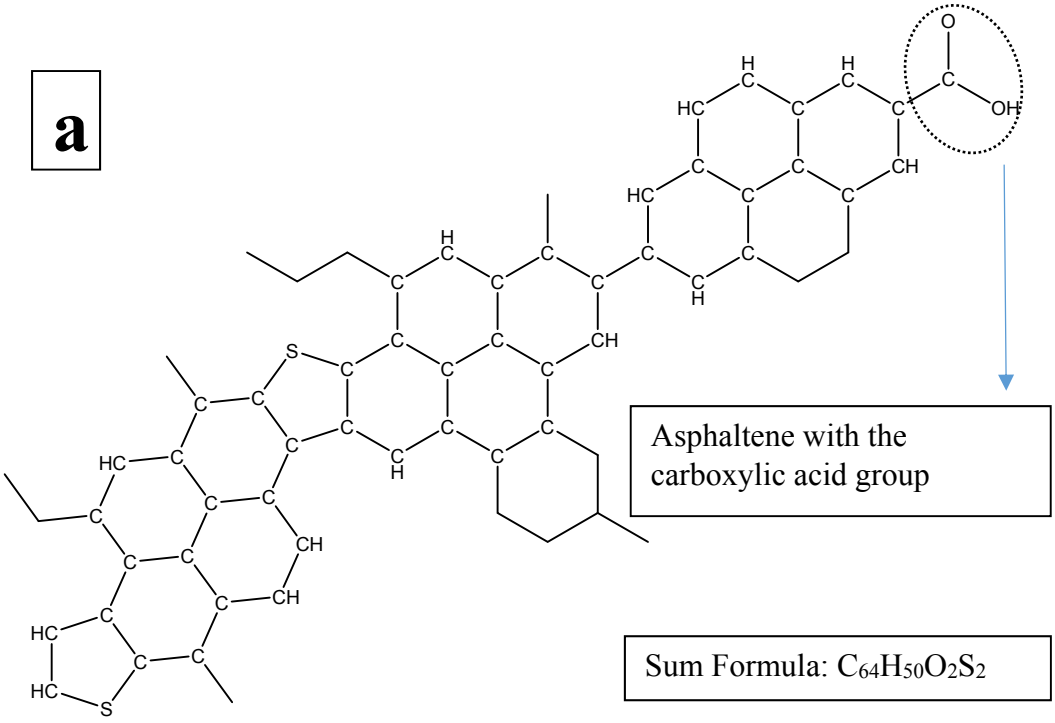

a) asphaltene structure with the carboxylic acid group (aging group)

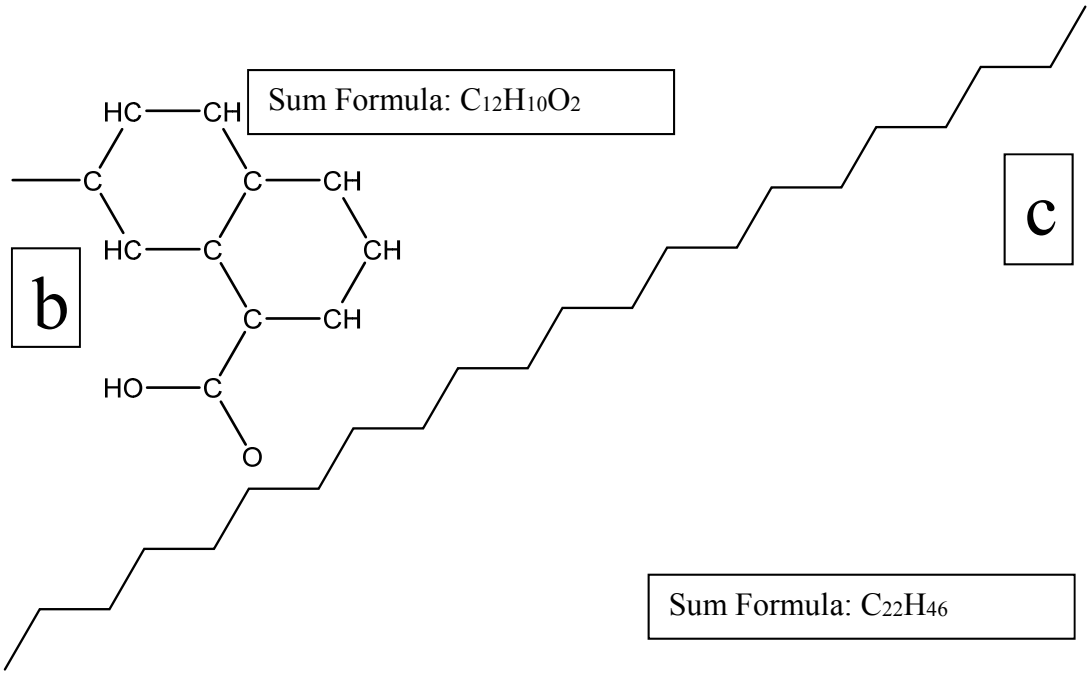

b) 1, 7-dimethylnaphthalene with the carboxylic acid group (aging group)
c) Docosane structure, represents a saturate.

Figure 4.7. Three components in the asphalt model with the carboxylic acid group (aging group)

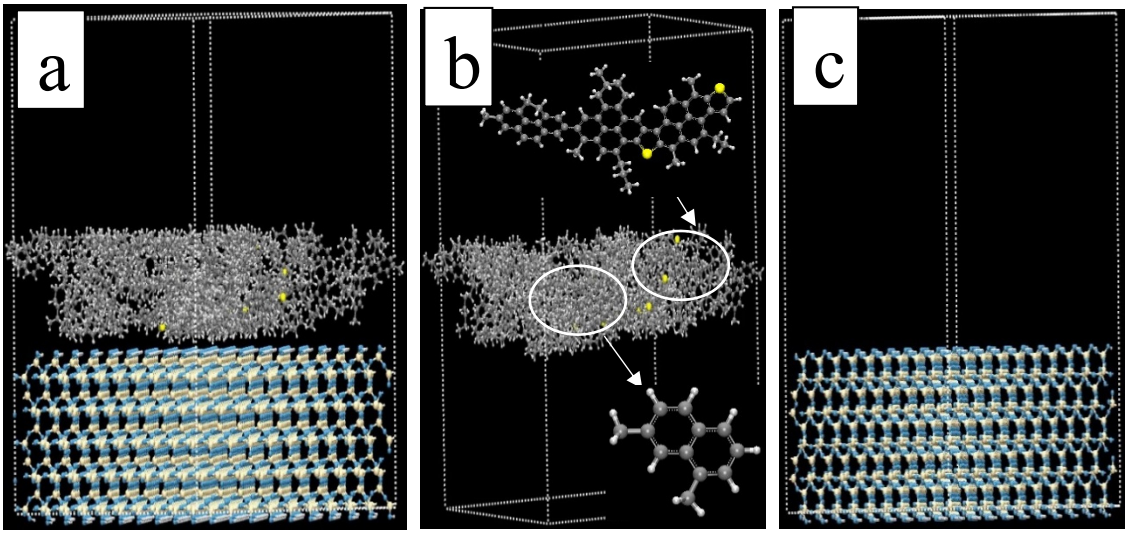

1) The molecular structures of the asphalt-aggregate system: (a) aggregate-asphalt system; (b) only the asphalt system; and (c) only the aggregate system with functional group OH on the surface layer.

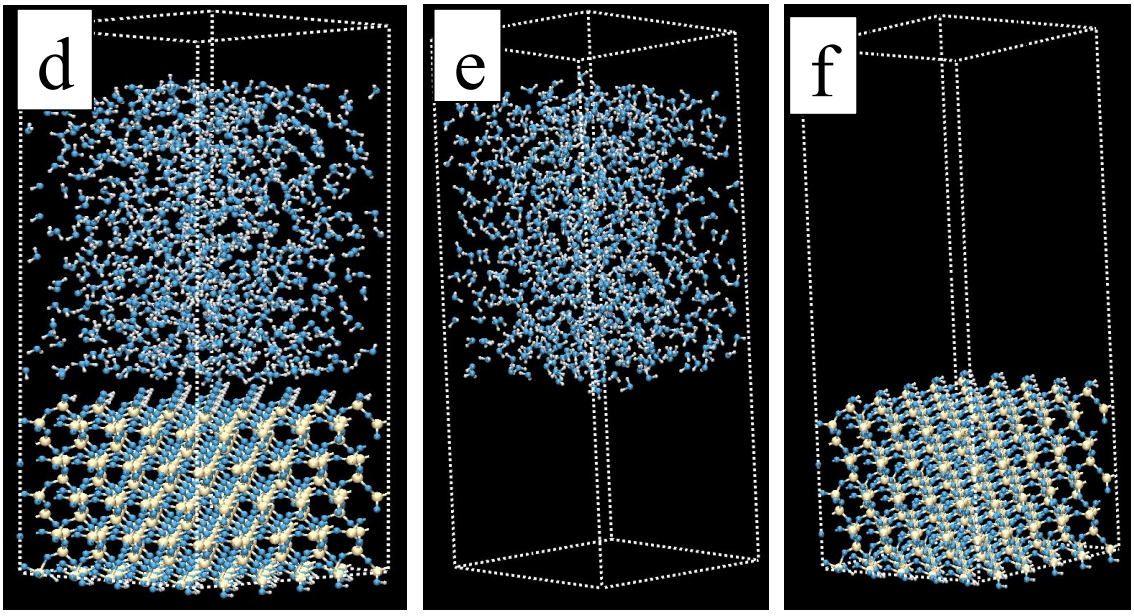

2) The molecular structures of the aggregate-water system: (d) aggregate-water system; (e) only the water system; and (f) only the aggregate system with functional group OH on the surface layer.

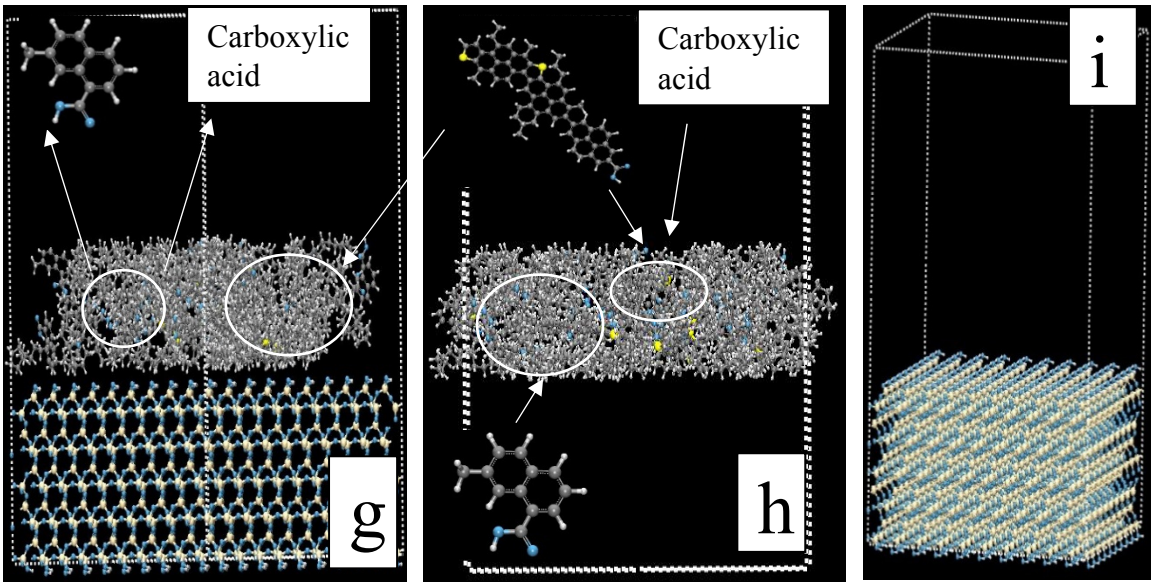

3) The molecular structures of the asphalt-aggregate system with aging groups: (a) aggregate-asphalt system with the carboxylic acid group; (b) only the asphalt system with the carboxylic acid group; and (c) only the aggregate system with functional group OH on the surface layer.

Figure 4.8. MD models for 1) Asphalt-aggregate interactions; 2) water-aggregate interactions and 3) aggregate-asphalt with the carboxylic acid group systems

Figure 4.8 shows the interface MD models of asphalt-aggregate, water-aggregate, aggregate-asphalt with the carboxylic acid group systems. The adhesion energy of each system directly relates to the bonding strength of the system. The adhesion energy of each interface system is computed using equation (4.12).

$$E_{adhesion} = \frac{E_{interface} - (E_{top} + E_{substrate})}{A} \quad (4.12)$$

Where $E_{adhesion}$ is the adhesion energy of the interface system (kcal/mol); $E_{interface}$ is the potential energy of the interface system (kcal/mol); E_{top} is the potential energy of the top layer system, asphalt, or water system (kcal/mol); $E_{substrate}$ is the potential energy of the substrate system, and aggregate system (kcal/mol); A is the area of each interface system (Angstrom^2).

To calculate the adhesive energy for the asphalt-aggregate, an interface model with a specific vacuum layer and periodic boundary condition was applied as shown in Figure 4.8a. The aggregate model includes a surface layer with the hydroxyl group (-OH) for the following study. The separate aggregate models with the surface function group (-OH) and asphalt model were developed as shown in Figure 4.8b and Figure 4.8c. The NVT simulation was conducted in three interface systems and in each separate system. The potential energies of these systems were computed and outputted. The energy conversion factor was used to present the adhesion energy (conversion factor: $1\frac{kcal}{mol} = 6.95 \times 10^{-21} J$). Avogadro's number was used to convert the energy unit. After computing and unit conversion, the adhesion energy of the asphalt-aggregate system is -0.1446295 J/m^2. Similarly, the adhesion energy calculation of the water-aggregate interface was conducted

with the interface model and two separate systems of the water layer and aggregate substrate, shown in Figure 4.8d, Figure 4.8e, and Figure 4.8f. The adhesion energy of the aggregate-water system was calculated as -1.86955 J/m^2. In order to demonstrate the effects of aging on the asphalt, on the adhesion energy interface, the interface model of the aggregate-asphalt with the carboxylic acid group and two separate systems were developed as shown in Figure 4.8g, Figure 4.8h, and Figure 4.8i. The adhesion energy of the aggregate-asphalt with the carboxylic acid group system was evaluated as -0.151371 J/m^2.

The different adhesion energies of asphalt-aggregate and aggregate-water systems indicate that the bonding strength between the asphalt and aggregate is lower than the attraction force between aggregate and water. The energy difference is also the reason why water bonds to the aggregates easier than the asphalt in asphalt mixtures. Therefore, coating the aggregates with asphalt is the key process in making asphalt mixture samples or paving asphalt pavement. It is also very important to dry the aggregates prior to mixing. These procedures make sure that water completely vaporizes from the aggregate pores and surfaces. These are also preventive measures/practices to reduce the moisture damage in asphalt mixtures. Furthermore, the energy of adhesion of the aggregate-asphalt (with the carboxylic acid group) system is greater than that of the asphalt-aggregate system. The varying energies of two systems imply that the presence of the aging group in asphalt causes a stronger adhesion force between the asphalt and aggregate. This phenomenon also reasonably interprets that studying the mildly aged asphalt is helpful in improving the water susceptibility of asphalt mixtures.

4.8.Discussions and Conclusions

The control and NHL modified asphalt were tested by FTIR ATR to analyze the polar groups with carbonyl in the asphalt at a liquid state. Parts of the control and the NHL modified asphalt mixture samples tested by TSR were also used to be extracted by solutions. These solutions contained the polar functional groups that were detected by the FTIR ATR to analyze the carbonyl groups in the asphalt. The mechanical driving forces for water damage between the asphalt-aggregate and aggregate-water systems in asphalt mixtures were explored and discussed using molecular dynamics simulations. Based on the data analysis of the extracted control and the NHL modified asphalt, the following conclusions can be drawn.

1) During the oxidation of asphalt, the resins and maltenes in the asphalt helped to generate polar group components, including carbonyl groups, sulfoxide groups, and nitrogen oxides. Carboxylic acids and ketones were the major products of the oxidized asphalt, which also produces high amounts of anhydrides. The limited amount of amides, esters, and aldehydes in the oxidized and extracted asphalt was detected. Carboxylic acids, ketones and anhydrides are the pivotal components in the asphalt that link to the rutting and moisture resistance in asphalt mixtures, as well as the bonding strength between the asphalt and aggregates. The aging of asphalt definitely improves the resistance to moisture damage in wet environment at an early stage according to these research findings. However, the long-term aging of asphalt causes the degradation of the bonding strength between the asphalt and aggregates, as well as the fatigue life and resistance to moisture.

2) The interface MD models of asphalt-aggregate and aggregate-water systems were generated to simulate the mechanism that produces adhesive energy, and also to mimic the interactions between aggregates and asphalt/water. The potential energies of each MD interface system and separated systems (asphalt, water, and aggregate) were computed to determine the bonding energy of each system. The difference of adhesive energies between the asphalt-aggregate and aggregate-water systems is the fundamental reason for moisture damage in asphalt mixtures. The water tends to adhere to aggregates rather than to asphalt under the same condition. In addition, from investigating the different adhesion energies between the aggregate and asphalt with or without the carboxylic acid group (aging group), the moderately aged asphalt improves the energy of adhesion and, thus, helps resist moisture damage in asphalt mixtures.

With chemical extraction, the polar and non-polar components in the asphalt were separated and analyzed to link the moisture susceptibility of asphalt mixtures with FTIR characterization. Ketones, carboxylic acids and anhydrides are the main compounds present during asphalt oxidation in this study, and these also relate to the performance of the pavement. MD simulations discovered the adhesion energy difference between asphalt-aggregate and aggregate-water systems. The analysis results explain the chemo-physical properties of asphalt related to the moisture damage in asphalt mixtures. In addition, the future research of our group will focus on simulating asphalt aging.

4.9 Acknowledgements

The authors appreciate the help of Dr. Andreas Bick on generating the molecular dynamics model. The experimental work was completed at the Transportation Materials

Research Center of Michigan Technological University. The authors appreciate the financial support of the U.S. National Science Foundation (NSF) under the grant number: 1300286. Any opinion, finding, and conclusion or recommendation expressed in this material are those of the authors and do not necessarily reflect the view of any organization.

Chapter 5 Property Analysis of Exfoliated Graphite Nanoplatelets Modified Asphalt Model Using Molecular Dynamics (MD) Method

5.1 Overview

The molecular model of the exfoliated multi-layered graphite nanoplatelets (xGNP) was created for the modification of the asphalt model, and the control asphalt model consists of three components: asphaltenes, aromatics, and saturates, based on our group's previous study. This modified asphalt model was verified through the density calculations and comparisons. The properties of the control and xGNP modified asphalt models were computed and analyzed using the Molecular Dynamics (MD) method, and the properties include the glass transition temperature, viscosity and thermal conductivity. The test and MD simulation results show that: (1) the density of the xGNP modified model is higher than that of the control model; (2) the glass transition temperature of the xGNP modified model is closer to the laboratory data of the Strategic Highway Research Program (SHRP) asphalt binders than that of the control model; (3) the viscosities of the xGNP modified model at different temperatures are higher than those of the control model, and it coincides with the trend in the laboratory data; (4) the thermal conductivities of the xGNP modified asphalt model are higher than those of the control asphalt model at different temperatures, and it is consistent with the trend in the laboratory data.

The full text of this chapter will be submitted to the journal of "Construction and Building Materials" for publication.

5.2 Introduction

5.2.1 Asphalt material

Asphalt is a byproduct of petroleum refinement and is also widely applied to many fields such as transportation, recreation, building construction, etc. Around 90% of asphalt consists of carbon and hydrogen. Based on the Corbett method, asphalt can be separated into four components: asphaltenes, saturates, napthene aromatics, and polar aromatics. Asphalt is composed of asphaltenes, paraffins, first acidiffins, second acidiffins, and nitrogen bases using the Rostler method [6]. These different types of molecules in asphalt interact with each other and affect the chemo-physical properties of asphalt [6].

Modifiers are commonly used to improve the performance of asphalt in industry and research areas. Recently, asphalt binders and mixtures modified with carbon fiber and crumb rubber were tested and evaluated [21, 23, 30, 31, 172, 173]. The base asphalt blended with carbon fibers or crumb rubber showed that the high-temperature performance improved, and the resistance to rutting of asphalt mixtures was enhanced. The carbon fibers and crumb rubber also improved the viscosity. The microstructure and performance of the crumb rubber and carbon modified asphalt binders were tested by the Scanning Electron Microscope (SEM) or fluorescence microscope. From the microstructural images of the asphalt binder, the compatibility and dispersion between modifiers and the asphalt binders were observed [23, 172]. In addition, water damage is a main distress for asphalt pavement, and the lime material has been studied as a modifier for improving the water damage of asphalt mixtures for many years. The resistance to rutting and fatigue cracking in lime modified mixtures was investigated in both moisture-damaged and undamaged states. In

the evaluation process, the advanced test methods (triaxial repeated-load permanent deformation and constant crosshead-rate direct tension tests) and models were adopted. The performance test results indicate that the moisture susceptibility of lime modified mixtures improved [39, 143, 174].

Due to special properties, nanomaterials were introduced and used in different fields to enhance the composite materials [42]. Different types of nanoclay have been widely used in the modification of asphalt. The test results show that the layered structure of nanoclay improved the high-temperature performance of asphalt and the resistance to rutting and fatigue cracking [8, 14]. The nanosilica material was also used and added into the asphalt matrix for the improvement in the performance. The microimages of the nanosilica modified asphalt were observed, and the test results indicate that the resistance to permanent deformation in the modified asphalt improved [7]. The literature shows that graphite was used for the modification of asphalt, and the addition of graphite improved the electrical property of asphalt [175]. In this study, the multi-layer graphite sheets were applied to modify the asphalt in consideration of the high thermal stability, self-lubrication, and high electrical conductivity of multi-layer graphite sheets [176-179]. This is also the motivation to use the material for the modification of the asphalt model.

5.2.2 Molecular Dynamics (MD) method

Molecular Dynamics (MD), initially originated in theoretical physics, was applied widely in materials science [58, 59]. MD is a kind of computer program to simulate the movements of atoms in materials, and the atoms and molecules interact for a designed time based on the Newton's law of motion. The trajectories of atoms and molecules are

monitored, and the energy of the system is computed. In physics, MD was used to examine physical properties [58, 59]. The evolution of dynamics in a single molecule is used to determine the macro properties of the system. The "statistical mechanics by number" and "Laplace's vision of Newtonian mechanics" were also used to describe the molecular dynamics. The simulation size and total duration time were selected so that the calculation can be finished within a reasonable time [61]. The Large-scale Atomic/Molecular Massively Parallel Simulator (LAMMPS) [118] and the Monte Carlo for Complex Chemical Systems (MCCCS) program [180] were commonly used for MD simulations. The computation algorithm of the MD simulation is shown in Figure 5.1.

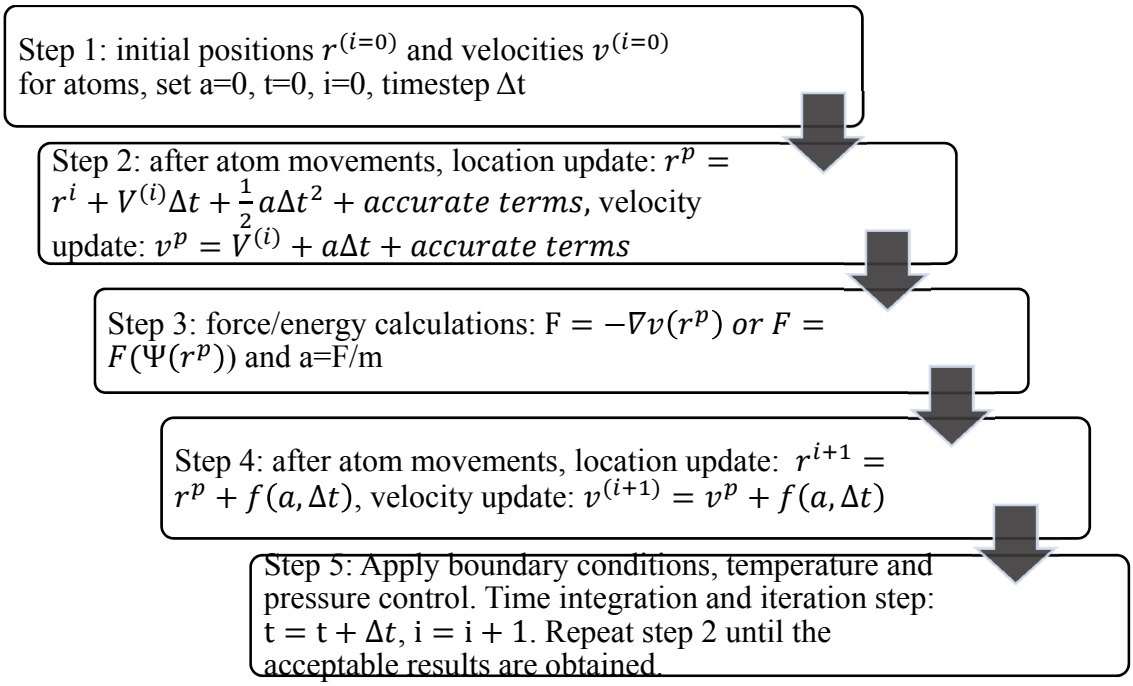

Figure 5.1. Computation algorithm of Molecular Dynamics (MD) simulation

Recently, three components of mixtures (asphaltenes, aromatics, and saturates) were chosen to represent the asphalt using MD simulation. In this reference model, 1,7-

dimethylnaphthalene ($C_{12}H_{12}$) and docosane (n-$C_{22}H_{46}$) were represented as naphthene aromatics and saturates, respectively [13]. Two kinds of asphaltene structures were used, and the density of each component was calculated using the MD method. From the simulation results, there are still many differences between the test and the simulation data in the calculations of the glass transition temperature and bulk modulus [13]. A new asphalt model with four components (asphaltenes, polar aromatics, naphthene aromatics and saturates) was created, and the density and thermal expansion coefficient of the asphalt model were calculated. The MD simulation results agreed with the laboratory data [84]. In addition, polystyrene was added to this asphalt model for polymer modification analysis. The radial distribution functions g(r) of components of the asphalt model were computed [84]. The MD simulation was also applied to study the self-diffusivity properties of asphalt binders, recently. The effect of healing on the fatigue performance of binders was studied, and the MD model of an asphalt binder was created to predict the healing effect. The self-diffusion effect caused the binder molecules to flow across the crack interface. The correlation between the length and branching of molecules and self-diffusion of asphalt molecules were investigated [91]. The relationship between the asphalt and aggregate was developed and the asphalt-quartz structure model of the interface was used in the system. The Consistent-Valence Force Field (CVFF_aug) was considered in this simulation to characterize the inter-atom interactions [105].

Based on literature review, few researchers used MD to simulate modified asphalt and studied the physical properties of modified asphalt models in engineering disciplines. In this study, the common multi-layer graphite model was adopted, and the components of

the control asphalt model was composed of asphaltenes, saturates and aromatics. The Amber Cornell Extension Force Field (ACEFF) was developed and used to simulate the asphalt modified with exfoliated multi-layered graphite nanoplatelets (xGNP). The energies of the asphalt systems were calculated, and the properties of control and modified asphalt models were computed. The comparisons of properties between the control and modified asphalt models were conducted, as well as the comparisons between the simulation and laboratory results.

5.3 Force Field and Optimization Methods

5.3.1 Force field

A force field, presented as parameters of mathematical functions in molecular mechanics, was used to describe the energies of the atoms. Force field parameters and functions are obtained from experimental tests and quantum mechanical calculations. Many force fields were developed and introduced by the researchers, such as the Chemistry at HARvard Molecular Mechanics (CHARMM) Force Field [66], Assisted Model Building and Energy Refinement (AMBER) Force Field [181], Condensed-phase Optimized Molecular Potential for Atomistic Simulation Studies (COMPASS) Force Field [67], Optimized Potential for Liquid Simulation (OPLS) Force Field [66] and DREIDING Force Field [63]. Different ensembles were used in the MD method, including the Microcanonical ensemble (NVE ensemble), Canonical ensemble (NVT ensemble), Isothermal-isobaric ensemble (NPT ensemble), Isoenthalpic-isobaric ensemble (NPH ensemble), and Generalized ensembles [62]. In this study, the Amber Cornell Extension Force Field was used to define the movement in the molecular system, and the experimental parameters in

this force field were referenced from the General Amber Force Field (GAFF). The formula is shown in equation (5.1).

$$E_{total} = \sum_{bonds} K_r(r - r_{eq})^2 + \sum_{angles} K_\theta(\theta - \theta_{eq})^2 + \sum_{dihedrals} \frac{V_n}{2}[1 + \cos(n\varphi - \gamma)] + \sum_{i<j}[\frac{A_{ij}}{R_{ij}^{12}} - \frac{B_{ij}}{R_{ij}^{6}} + \frac{q_i q_j}{\epsilon R_{ij}}] \quad (5.1)$$

where r_{eq} and θ_{eq} are the equilibrium structural data from an x-ray test; K_r is the force coefficient determined by linear interpolation between the single and double bond values; K_θ is the force coefficient from vibrational analysis of a simple sp2 atom; n is the multiplicity for dihedrals; γ is the phase angle for the torsional angle parameters; A, B and q are the non-bonded potentials between atom pairs; R_{ij} is the distance between the atoms; and ϵ is the well depth for van der Waals energy.

5.3.2 Optimization methods

When the molecular systems are built, energy optimization and data smoothing are required to optimize the molecular systems and output results, respectively. These procedures help the researchers understand more about the systems. The following methods were used in this study.

1) Conjugate Gradient Method

The conjugate gradient method is a kind of iterative algorithm to solve the partial differential equations. The solutions for unconstrained optimization problems like energy minimizations were also developed by Hestenes and Stiefel [111]. The formula is shown in equation (5.2).

$u^T Av = 0$, (direct method) or $f(x) = \frac{1}{2}x^T Ax - x^T b, x \in R^n$ (iterative method) (5.2)

where A is symmetric, positive and real; b is a known coefficient; and vectors u and v are non-zero.

2) Particle-Particle-Particle-Mesh Method (PPPM)

The Particle-Particle-Particle-Mesh Method (PPPM) is used to compute long-range electrostatic force, which can be divided into two parts: short- and long-range interparticle forces [79]. The formula is shown in equation (5.3).

$$F_{ij} = F_{ij}^{sr} + F_{ij}^{m} \quad (5.3)$$

where F_{ij} is the interparticle forces in the system; F_{ij}^{sr} is the rapid varying short-range component; F_{ij}^{m} is the slowly varying component.

5.4 Objectives and Scopes

The objectives of this study are to use MD method to simulate the multi-layer graphite/graphene modified asphalt model, and the properties of the asphalt models are calculated and compared. The components of the control asphalt model consists of asphaltenes, aromatics, and saturates, and it was built in the previous work [182] of authors. The common multi-layer graphite/graphene model was used to represent the modifier (xGNP graphene nanoplatelets). The Amber Cornell Extension Force Field and Electrostatic Potential (ESP) charges were assigned to the components of the control and modified asphalt models. Different properties of the asphalt models were computed including the density, glass transition temperature (Tg), viscosity and thermal conductivity.

The MD simulation data of the control and modified models and their laboratory results were compared.

5.5 Model Generation

Based on previous work of the authors [182], three components were used in the control asphalt including the asphaltenes, aromatics, and saturates at a ratio of 5:27:41. The 1, 7-Dimethylnaphthalene and docosane were used to represent the aromatics and saturates, respectively. The asphaltene structure is from the reference, $C_{64}H_{52}S_2$. The control asphalt model was generated to represent the control asphalt PG 58-28. In the laboratory tests, the modifier, xGNP graphene nanoplatelets, used in this study is produced by XG Sciences Inc., and its micro-image (Figure 5.2a) was obtained by the field emission scanning electron microscope (FE-SEM). The distance between the graphene layers is around 3.35 Å, and the mole mass content of xGNP nanoplatelets in the modified asphalt is 2% by the weight of the control asphalt. During the preparation of xGNP modified asphalt in the laboratory, 2% xGNP multi-layer graphite particles were slowly added in the asphalt matrix at the temperature of 145ºC. The modified asphalt was sheared in the high shear machine for two hours to ensure that particles were well dispersed. Similarly, in the simulation test, the common multi-layer graphite model (Figure 5.2b) was used to represent the xGNP nanoplatelets, and 2% xGNP nanoplatelets were randomly added to the control model. The xGNP modified asphalt model was generated and is shown in Figure 5.2c.

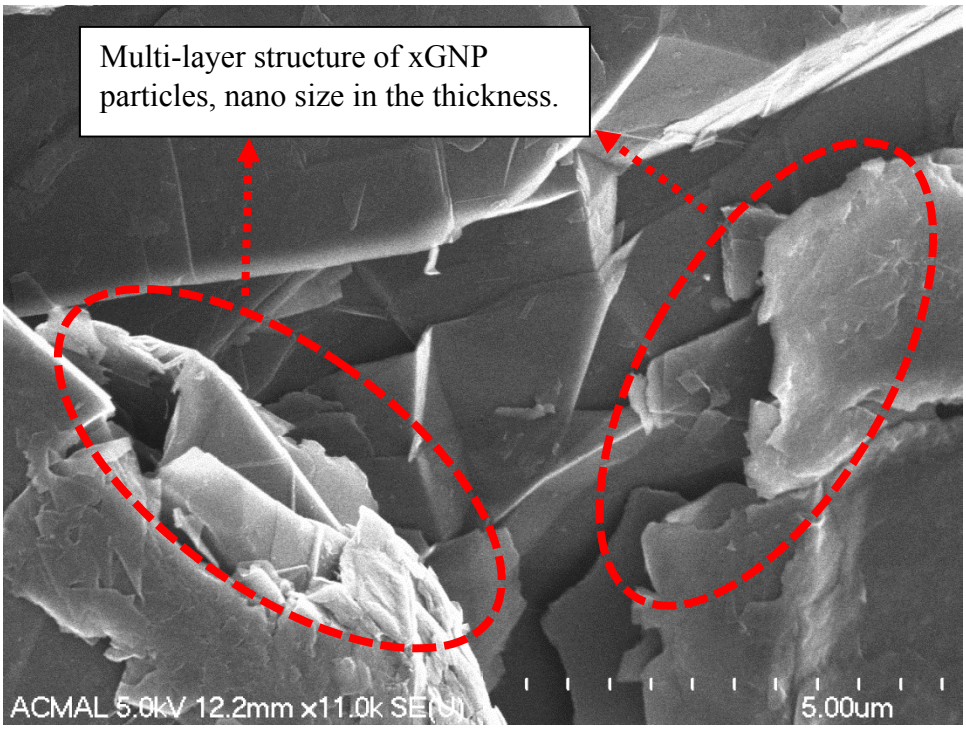

(a) FE-SEM image of multi-layer xGNP nanoplatelets

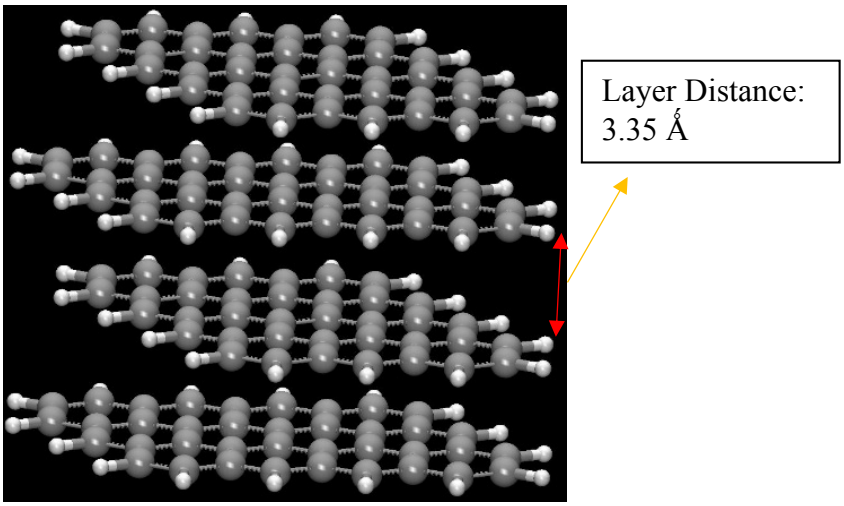

(b) Multi-layer graphite model: white color for hydrogen atom; grey color for carbon atom

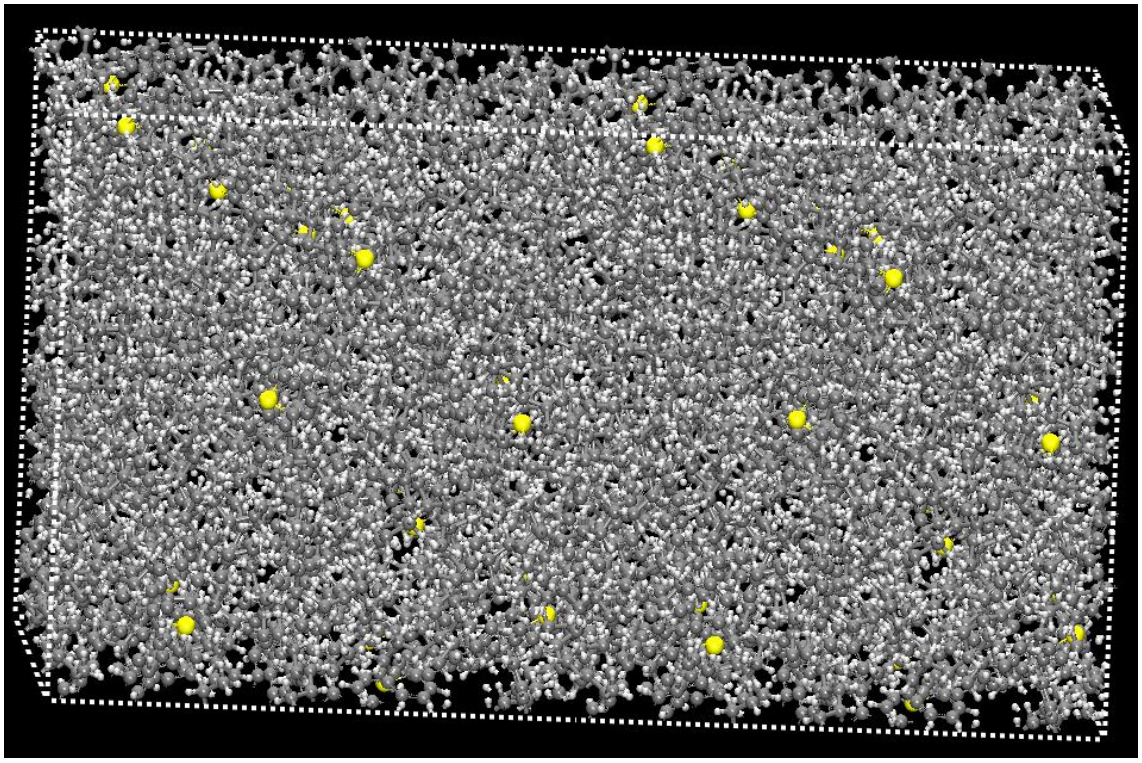

(c) Molecular structures of xGNP modified asphalt model: white color for hydrogen atom; grey color for carbon atom and yellow color for sulfur atom.

Figure 5.2. The SEM image of multi-layer xGNP particles, molecular structures of xGNP modified asphalt model and exfoliated multi-layer xGNP graphite model

5.6 Physical Properties of the Control and xGNP Modified Asphalt Models

5.6.1 Density

When the control asphalt and modified asphalt models were generated using molecular dynamics, the densities of these models were computed at the conditions of room temperature and air pressure to verify the model. The LAMMPS and optimization methods mentioned above were used to conduct the experimental MD simulations. The NPT ensemble simulations were employed to compress or relax the unit cell. The temperatures,

pressures, and densities of the control and xGNP modified asphalt models are shown in Figure 5.3.

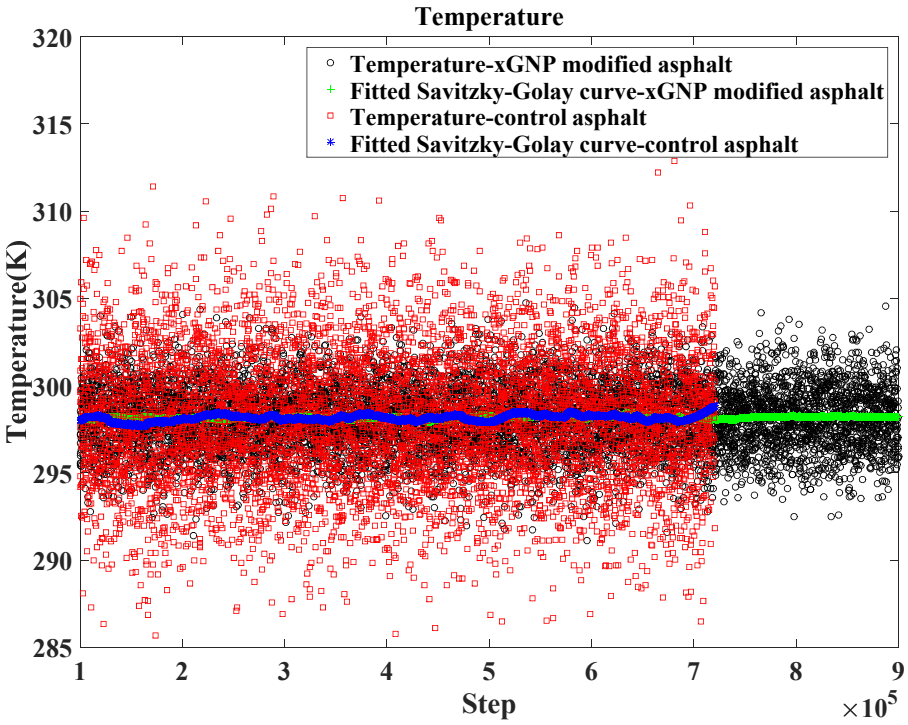

(a) Temperatures in the xGNP modified asphalt system through these steps

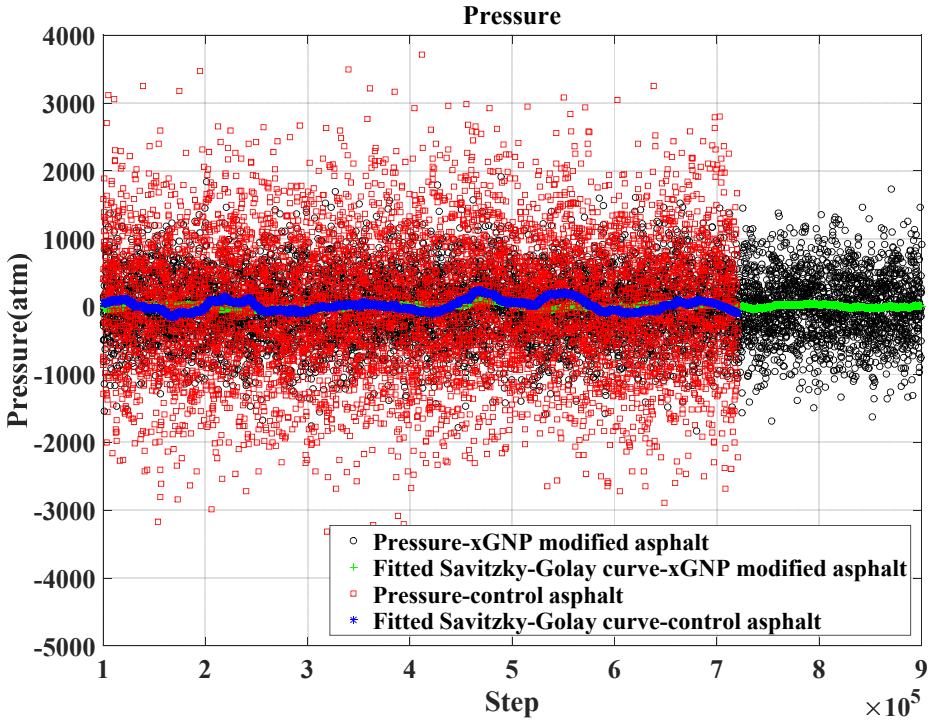

(b) Pressures in the xGNP modified asphalt system through these steps

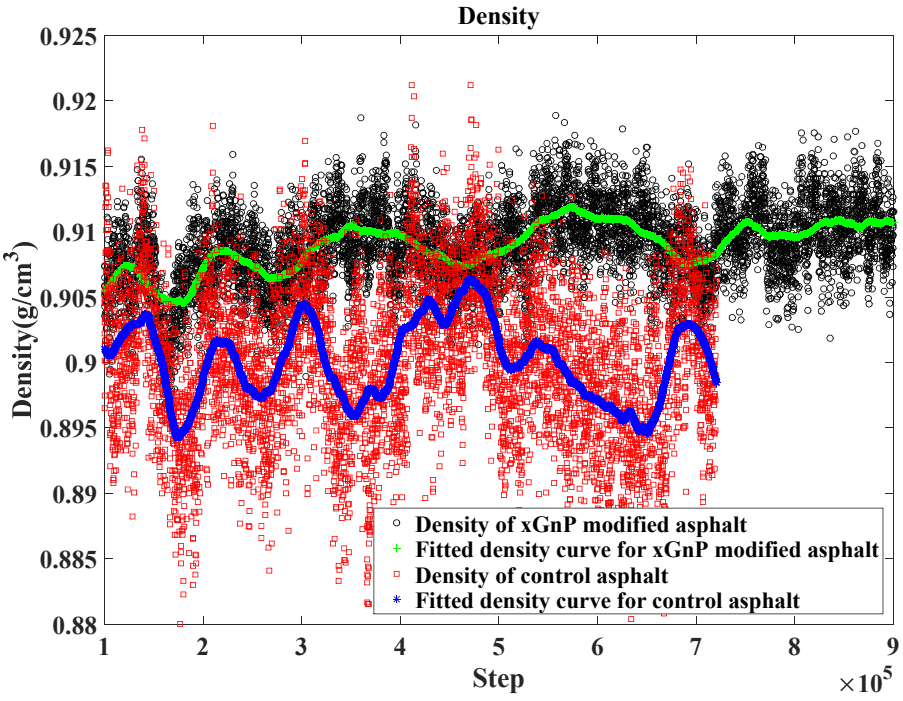

(c) Densities of the control and xGNP modified asphalt systems

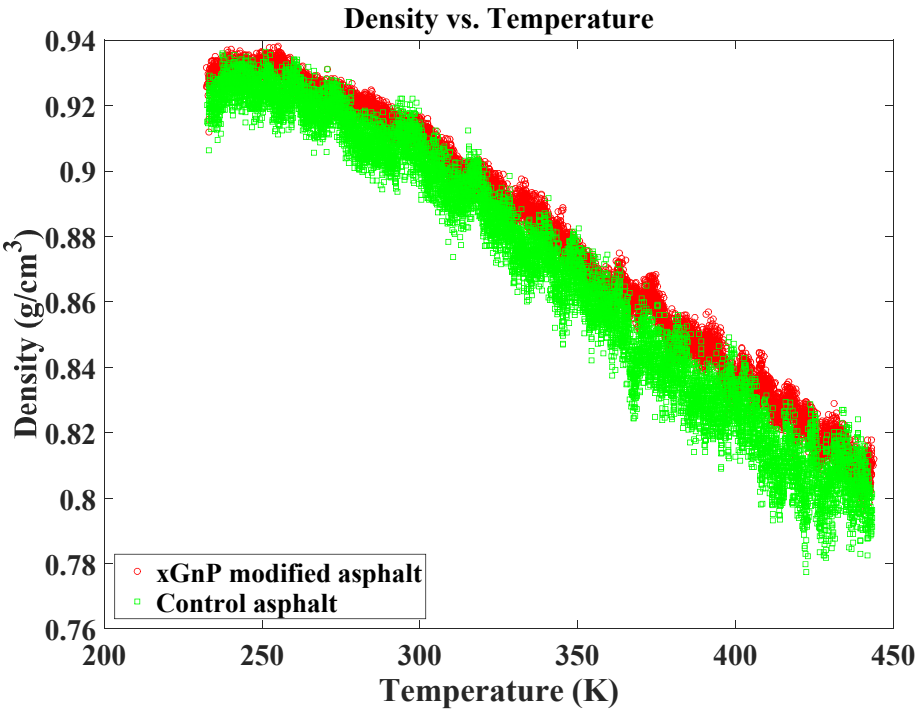

(d) Densities of the control and xGNP modified asphalt systems at different temperatures

Figure 5.3. Density curves of the control and xGNP modified asphalt models

Figure 5.3a and Figure 5.3b show the temperatures and pressures in the control and modified asphalt systems under the NPT ensemble. The systems were run more than 1ns to be stable and optimized. Parts of results are shown. The data was fitted by a Savitzky-Golay filter [76] with a span of 10%, and the moving average is also clear for data analysis. The temperatures of the control and xGNP modified asphalt are close to 298 K during these steps, and the pressures fluctuate around 1 atmosphere (atm). Meanwhile, it is interesting to note that the data fluctuation of the control model is obviously greater than that of the modified asphalt model due to the difference in the molecular number. The fluctuated data range varies with a $1/\sqrt{N}$ variation based on the baseline of the moving average, where N is the number of molecules in the MD system [122]. According to Avogadro's number

[123], the substances normally have around 10^{24} molecules per mole. Compared to the real substances, it is hard to reach such a number in the MD simulation. Therefore, the data fluctuation is acceptable, and it explains the reason why the data fluctuation of the control system is larger than that of xGNP modified asphalt.

Figure 5.3c shows densities of the control and xGNP modified asphalt systems, and the data was fitted by a Savitzky-Golay filter [76] with a span of 10%. The densities of the xGNP modified asphalt system are larger than those of the control asphalt model. It is reasonable that the addition of xGNP particles in the control system increases the density of the modified system. It is apparent that the density data amplitude of the control system is larger than that of xGNP modified asphalt model, as well as the stability due to more molecules. In addition, the densities of the control and xGNP modified asphalt systems are also close to the laboratory (0.95 g/cm^3 – 1.05 g/cm^3) [13, 89, 122] and reference data [13]. Therefore, the modified asphalt model is verified. Figure 5.3d displays the density curve of the control and xGNP modified asphalt with different temperatures, which range from 233.15 K to 443.15 K. The densities of the asphalt models decrease with the increase in temperature, and the density of xGNP modified system is slightly greater than that of the control model under different temperatures. Meanwhile, the density trends of the control and xGNP modified models are similar to that of the reference model [13]. In addition, the data amplitude of xGNP modified model is smaller than that of the control system.

5.6.2 Glass transition temperature

The low-temperature crack is one of the problems for building materials, especially for asphalt, and it is caused by the reduction in temperature and thermal stress. When the

ambient temperature drops to a certain point, the asphalt has to deform to relax the thermal stress due to the hindrance of the large-scale molecular motion [115]. Meanwhile, the glass transition temperatures (Tg) of materials are influenced by their components, and the addition of new component in the material results in a difference in the glass transition temperature. The formula [115] of the glass transition temperatures of composite materials is shown in equation (5.4).

$$\frac{1}{T_g} = \sum \frac{w_i}{T_{gi}} \tag{5.4}$$

where T_g and T_{gi} are the glass transition temperature of the composite material and its component, respectively; and w_i is the mass fraction of the component.

The asphalt transfers from the viscoelastic state to a brittle one. The internal stress increases and thermal energy is insufficient below the glass transition temperature in the materials. Therefore, the glass transition temperature is an important parameter or property for amorphous materials, and it should be low for a good low-temperature performance [115]. The glass transition temperature is the temperature where two asymptotes intersect on the specific volume-temperature curve. In the laboratory, the glass transition temperature of materials can be tested by differential scanning calorimetry (DSC). In this MD simulation study, the control and xGNP modified asphalt systems were relaxed under NPT ensemble with a temperature range of 233.15 K to 443.15 K. The specific volumes of these systems were calculated and the glass transition temperatures of the models were determined. The MD simulation results of the control and xGNP modified asphalt models are shown in Figure 5.4.

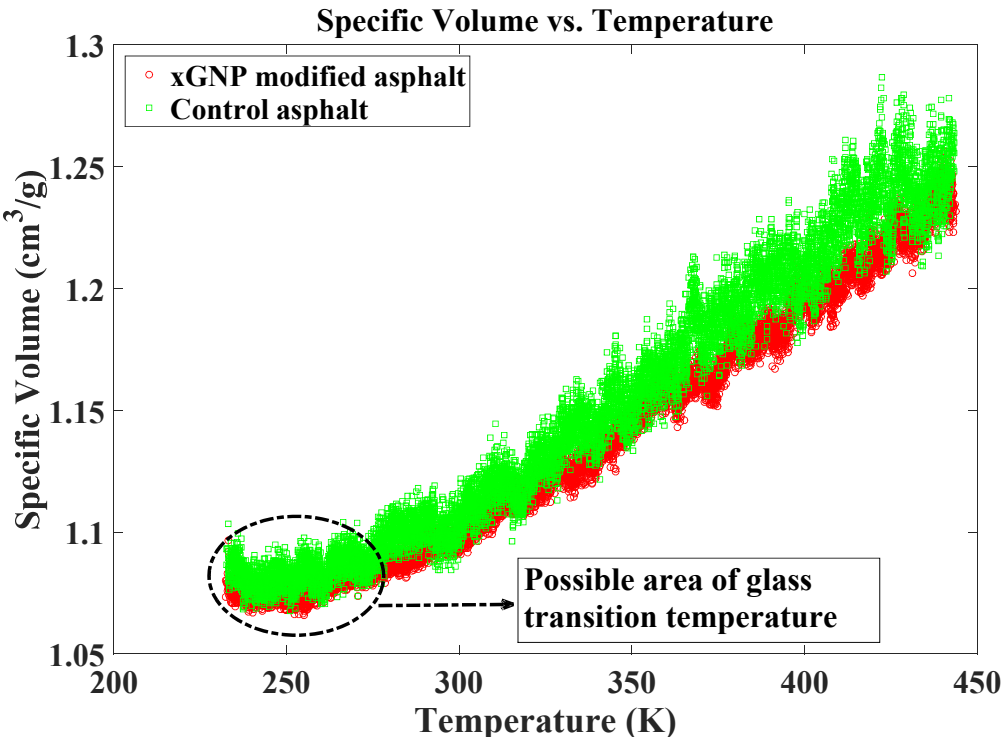

(a) specific volumes of the xGNP modified asphalt system

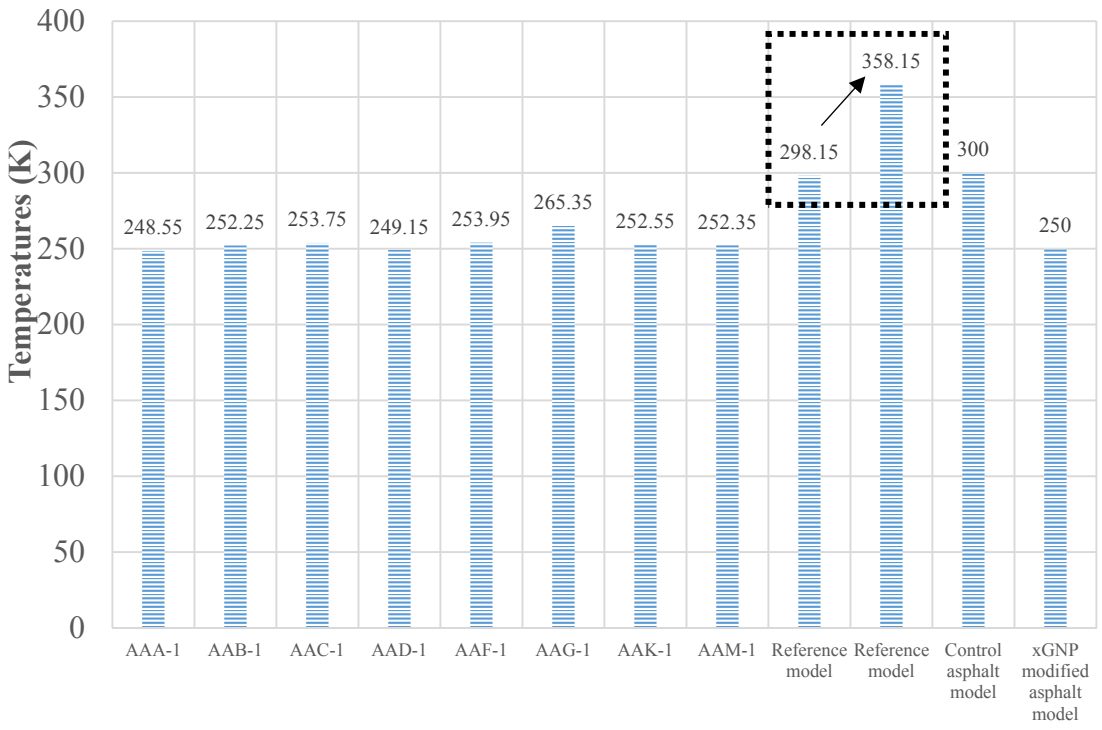

(b) Glass transition temperatures of different asphalt types and models (the data of the glass transition temperature of different binders is from the reference [13, 115, 182]: 248.55ºC for AAA-1 binder, 252.25ºC for AAB-1, 253.75ºC for AAC-1, 249.15ºC for AAD-1, 253.95ºC for AAF-1, 265.35ºC for AAG-1, 252.55ºC for AAK-1, 252.35ºC for AAM-1, 300ºC for control asphalt model [182], and temperature range from 298.15ºC to 358.15ºC for the reference model [13])

Figure 5.4. Specific volumes and temperatures of control and xGNP modified asphalt systems

Figure 5.4a shows the specific volumes of the control and xGNP modified asphalt models. The specific volumes increase with increasing temperatures of the models. The glass transition temperature of the control asphalt model is around 300 K [182]. As shown in the Figure, it is deduced that the Tg of the xGNP modified asphalt system is around 250

K. Based on the laboratory data in the reference [124], the range of the Tg of asphalt is from 223 K to 303 K. The Tg of the modified asphalt model is within the laboratory data range, and it is also better than the reference data [13] (298 K to 358 K) of the asphalt model. In order to get better thermal relaxation in the asphalt, a low Tg of asphalt is expected. In addition, the xGNP modified asphalt model has a better low-temperature performance than the control asphalt system. Figure 5.4b shows the comparisons of glass transition temperatures of the references and MD simulations. The glass transition temperatures of the Strategic Highway Research Program (SHRP) asphalt binders are all around 250 K [115], including SHRP asphalt AAA-1, AAB-1, AAC-1, AAD-1, AAF-1, AAG-1, AAK-1 and AAM-1. The Tg of xGNP modified asphalt model is close to glass transition temperatures of SHRP asphalt binders. Therefore, the Tg of xGNP modified asphalt is reasonable and better than the results of the control and reference asphalt models.

5.7 Rheological Properties of the Control and xGNP Modified Asphalt Models

5.7.1 Viscosity measurement and simulation methods

Dynamic shear viscosity is an important parameter of fluids to measure the resistance to gradual deformation induced by shear stress. If the shear speed caused by the external force is appropriate, the fluid particles move parallel to the particles sheared. The speed varies linearly from the sheared layers to different layers. The resistance between these layers is caused by friction. The formula to calculate viscosity is shown in equation (5.5).

$$\eta = \frac{Fy}{Au} \tag{5.5}$$

where F is the applied force; A is the area of the plate; η is the dynamic shear viscosity; and u/y is the shear gradient.

During the construction of asphalt pavement, the viscosity determines the mixing and compaction temperatures, which relates to the pump ability, mix ability and workability of asphalt. Based on the American Society for Testing and Materials (ASTM) D4402, the Brookfield DV-II plus viscometer (Figure 5.5a) was selected to test the viscosity of asphalt in the laboratory. The viscosity test results are shown in section 6.3. In the MD experimental simulation, there are four common methods to calculate the dynamic shear viscosity in the MD systems [118]: 1) a non-equilibrium MD (NEMD): the unit cell is sheared by "fix deform" and the temperature is controlled; 2) a NEMD: the viscosity is computed through the velocity and pressure in the systems; 3) a reverse non-equilibrium MD (rNEMD): the momentum flux is transferred between different layers in the unit cell through the Muller-Plathe algorithm; 4) equilibrium MD (EMD): the Green-Kubo (GK) formula is used to compute the viscosity, and continuous momentum flows are applied in the unit cell.

In this MD study, the Muller-Plathe method was used to calculate the viscosities of the control and xGNP modified asphalt systems. The unit cell of asphalt models was split into twenty layers. The viscosity calculation is shown in equation (5.6). During the calculation of viscosity in MD simulation, unit conversion is needed. The viscosity unit in the MD simulation is gram/mol/angstrom/femtosecond, but the unit in the laboratory test is kilogram/meter/second. Avogadro's constant is used to convert from microscopic to macroscopic states. In addition, the momentums transferred in the control and xGNP

modified systems at the temperature of 443 K are shown in Figure 5.5b. The viscosities of the control and xGNP modified asphalt systems at temperature of 423 K are shown in Figure 5.5c. The MD and laboratory viscosity results of the control and xGNP modified asphalt systems at different temperatures are shown in section 6.3.

$$j_z(p_x) = -\eta \frac{\partial v_x}{\partial_z} \text{ and } j(p_x) = \frac{P_x}{2tA} \tag{5.6}$$

where η is the dynamic shear viscosity; $\frac{\partial v_x}{\partial_z}$ is the shear rate; $j(p_x)$ is the input momentum flux; P_x is the input momentum; t is the simulation time; $A = L_x L_y$, L_x is the length of unit cell in the x direction; and L_y is the length of unit cell in the y direction.

(a) Brookfield DV-II plus viscometer for testing viscosity of asphalt

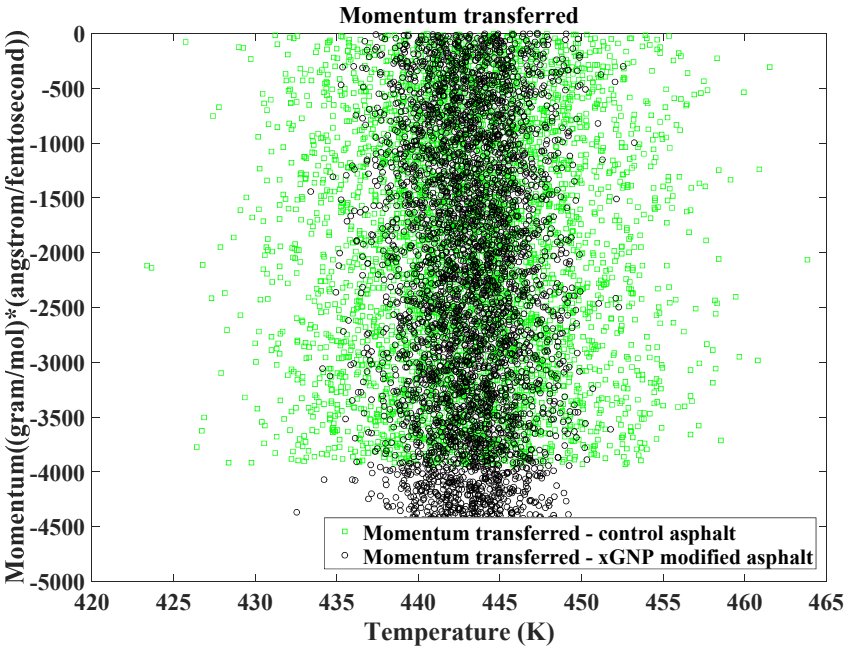

(b) Momentum transferred in the control and xGNP modified systems at the temperature of 443K

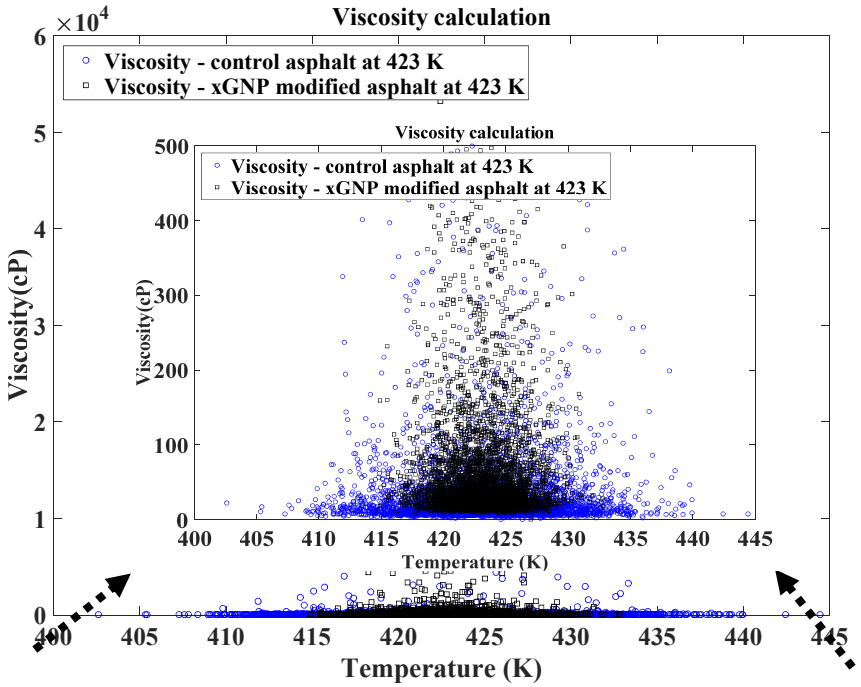

(c) Viscosities of the control and xGNP modified systems at the temperature of 423K

Figure 5.5. Viscosity test and MD calculation for the control and xGNP modified asphalt systems

Figure 5.5b displays the momentum transferred in the control and xGNP modified systems at the temperature of 443 K, and it is part of the results under different temperatures due to repeatability. The momentum transferred in the xGNP modified model is more than that of the control model. The temperatures in the control asphalt model fluctuate more than those of the xGNP modified asphalt model due to fewer molecules. The temperatures are also around 443 K, and do not have large variations. It indicates that more molecules in the MD system lead to less data variation and a stable structure of materials. It coincides with the conclusion that the vibrating range of MD data is within a $1/\sqrt{N}$ variation [122] (N is the number of molecules in the system). Figure 5.5c demonstrates viscosities of the control and xGNP modified asphalt systems at a temperature of 423 K, and it is also part of data analysis under different temperatures. The temperature fluctuation of the control model is larger than that of xGNP modified model due to fewer molecules compared to xGNP modified asphalt system. The temperatures are also centered at 423 K and have a range of 20 K variation. It coincides with the temperature setting of simulations. Furthermore, the statistical analysis of viscosities of the control and xGNP modified asphalt models was performed to analyze the distributions of viscosity data in MD simulation.

5.7.2 Statistical analysis for viscosities of the control and xGNP modified asphalt models

The variation of data in the viscosity calculation is observed in last section 6.2. The statistical analysis was used to better understand the data distribution, and it is also good for describing and reproducing the data. It is well known that many experimental or observational data arising in engineering is shaped by a lognormal distribution due to its

various appealing properties. If a random variable x follows a lognormal distribution, the random variable Y = log(X) is distributed as a normal. The probability density function (pdf) of a lognormal distribution with parameters μ and σ is given by

$$f(x) = \frac{1}{x\sigma\sqrt{2\pi}} e^{-\frac{(\log x-\mu)^2}{2\sigma^2}} \tag{5.7}$$

where $x > 0, -\infty < \mu < \infty,$ and $\sigma > 0.$ In this study, we consider the lognormal distribution, because it provides heavier tails compared with the normal one and is thus more flexible to experimental data when studying robustness to outliers. Due to large variations of data from 7.375894 to 53239.325870, we consider the more appropriate fits based on data ranging from 0 to 300, and from 0 to 500. The parameter estimates of μ and σ with their standard errors in parenthesis are presented in Table 5.1. The histograms with the fitted lognormal distributions are depicted in the top two figures (Figure 5.6). It can be seen from the two figures that with different choices of truncations, the lognormal distribution provides more flexible fits to xGNP data. A similar conclusion can also been drawn for the fitness of the lognormal distribution to Control data (Figure 5.6). Consequently, we may conclude that the data departure from the lognormality is acceptable or slight, the lognormal distribution is more robust and flexible model, allowing a better fitting as shown above.

Table 5.1. Parameter estimates of μ and σ with their standard errors

	μ	σ
xGNP (<500)	3.81542596 (0.01393144)	0.85901818 (0.00985102)
Control (<500)	3.01951678 (0.01529361)	0.95801986 (0.01081422)

Note: xGNP: viscosity data of the xGNP modified asphalt model; Control: viscosity data of the control modified asphalt model

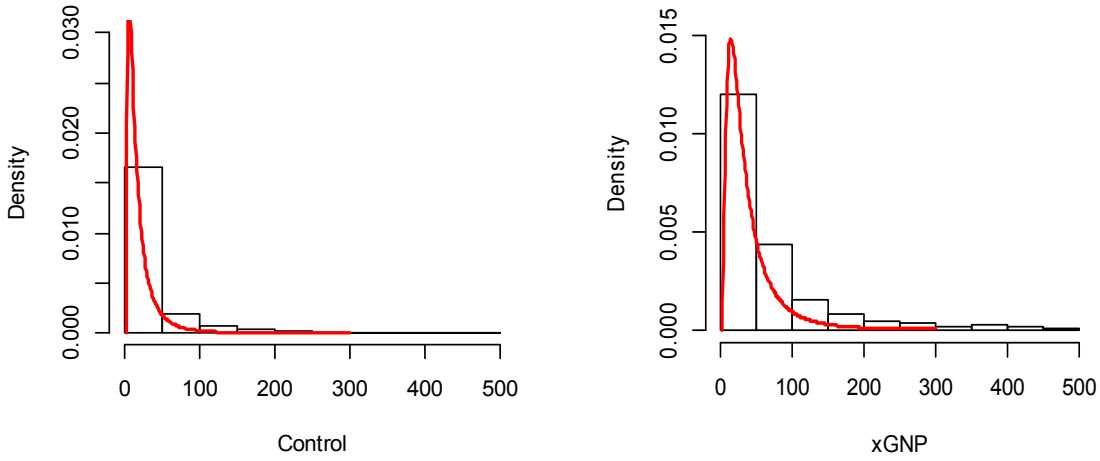

Figure 5.6. The histogram with the fitted lognormal distributions (the right plot for xGNP data, and the left plot from Control data; Bars represent the MD simulation data, and the red lines represent fitted lognormal curves)

5.7.3 Comparison of viscosity predictions of the control and xGNP modified asphalt models

Based on the data analysis from the MD simulation and laboratory data, the viscosity data between the control and xGNP modified asphalt models was compared and analyzed, as well as the experimental results. The exponential regressions were used to fit the viscosity

data of the control and xGNP modified asphalt models. The comparisons between the control and xGNP modified models were conducted, as shown in Figure 5.7, including the experimental and reference data.

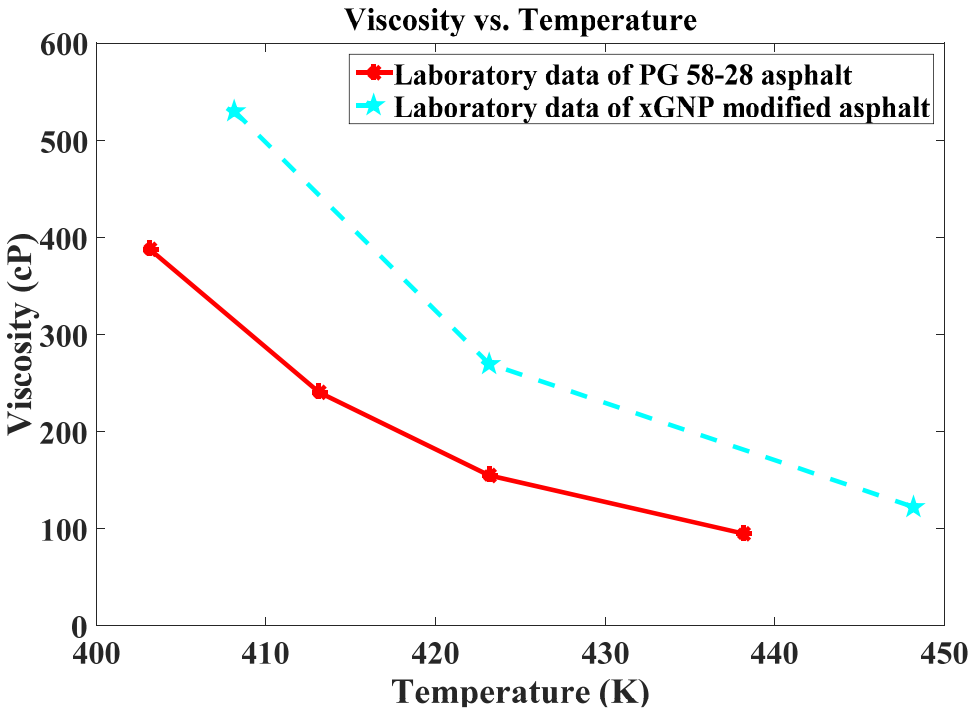

(a) viscosities of the control and xGNP modified asphalt in the laboratory

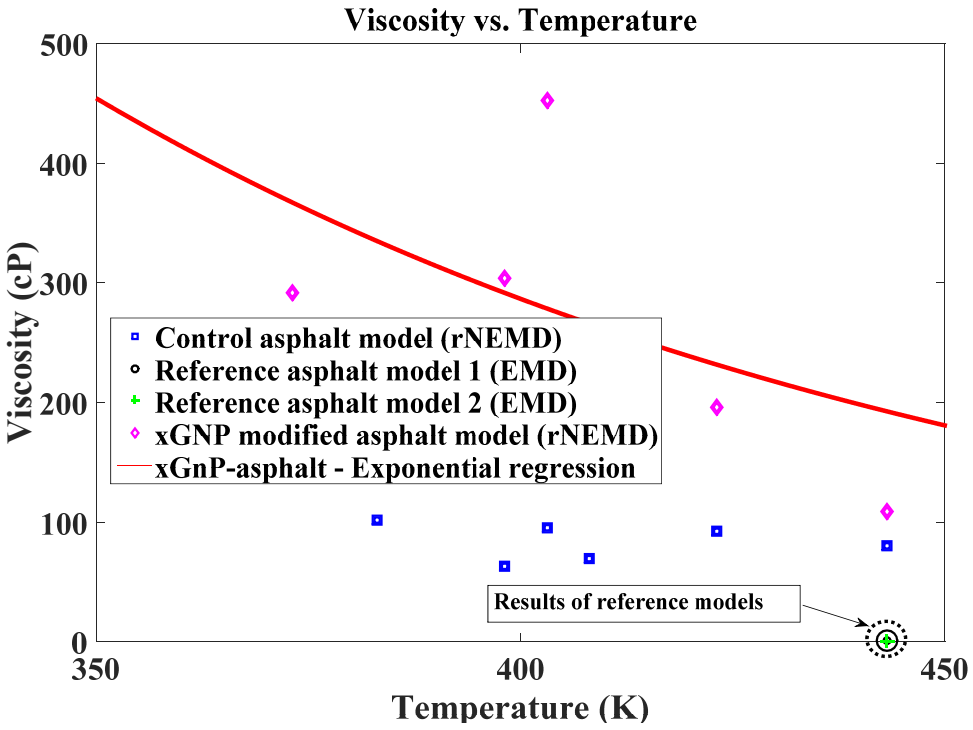

(b) viscosities of the control and xGNP modified asphalt models

Figure 5.7. MD and laboratory results of the control and xGNP modified asphalt systems

Figure 5.7 shows the viscosities of the control and xGNP modified asphalt models, as well as the laboratory data of the xGNP modified asphalt and control. From the test data, the viscosities of xGNP modified asphalt (Figure 5.7a) are higher than those of the control asphalt (red line). It indicates that multi-layer xGNP particles increase the viscosity of the modified asphalt. In addition, the viscosity decreases with the increase in temperatures of the asphalt. Meanwhile, the viscosities of MD simulations in Figure 5.7b were averaged from the calculations under each separate temperature. The MD simulation viscosities of the xGNP modified asphalt model (red line in Figure 5.7b) are also higher than those of the control asphalt model. It is similar to the trend in the laboratory data. The exponential trends are observed to be fitted for the MD simulation results due to the same trend in the laboratory data [130]. In this figure, it is obvious that the viscosities of the control and

xGNP modified asphalt models are higher than those of the reference models [84] (0.65 cp and 1.35 cp at 443.15 K) using Green-Kubo and Einstein (Ein) EMD methods. The relatively flat line is observed in the viscosity data of the control asphalt model, and the viscosity results (92.47 cp and 80.13 cp) at 423.15 K and 443.15 K are close to the laboratory data (155.0 cp and 95.0 cp) at two different temperatures for the control asphalt model, respectively. It is noticed that there is some improvement between the results of the control asphalt and the model in the reference [182]. However, for the xGNP modified asphalt model, the viscosities (452.42 cp, 195.98 cp and 108.96 cp) at 403.15 K, 423.15 K, and 443.15 K, respectively, are very close to the laboratory data (530.0 cp, 270.0 cp and 122.5 cp). The simulation results of the xGNP modified asphalt system are better than those of control asphalt system, and the trend in viscosity of the xGNP modified asphalt system is similar to that of the laboratory data. It is caused by the increase in the molecular number in the xGNP modified asphalt model compared to the control asphalt model. It is expected that more molecules in the MD asphalt system improve the accuracy of data prediction. Therefore, the viscosity calculation of MD simulations in the xGNP modified asphalt system with the Amber Cornell Extension Force Field provide a better prediction using the Muller-Plathe method compared to the results of the references [84] and the control asphalt model.

5.8 Thermal Property of the Control and xGNP Modified Asphalt Models

The thermal conductivity is a kind of measures of materials to transmit the heat energy in a diffusive manner based on Fourier's law. The materials with a high thermal conductivity are applied to the heat sink, and the materials with a low thermal conductivity

are manufactured for thermal insulation. In the laboratory, the xGNP modified asphalt was mixed with ultrasonic stirring during the process of high shear so that the xGNP particles can be homogenously dispersed in the asphalt matrix. The thermal properties analyzer (KD2 Pro) was employed to measure the thermal conductivity of asphalt based on the transient line heat source method [183]. The asphalt was placed in the glass tube as shown in Figures 5.8a and 5.8b, and the single needle TR-1, with a 2.4 mm diameter and 60 mm in length was used to test the thermal conductivity. During the heating and cooling processes, the temperature-time relationship is monitored by the sensor located in the needle. The thermal conductivity is calculated with the parameters from the fitted curve of the temperature-time. The formula for thermal conductivity is shown in equation (5.8).

$T = m_0 + m_2 t + m_3 lnt$ (Heating process); $T = m_1 + m_2 t + m_3 ln\frac{t}{(t-t_h)}$ (Cooling process) and $k = \frac{q}{4\pi m_3}$ (5.8)

where m_0 and m_1 are the ambient temperatures in the heating and cooling processes, respectively; m_2 is the rate of drift of the background temperature; m_3 is the slope of a line relating temperature rise to the logarithm of temperature; q is the heat input and k is the thermal conductivity.

In the MD simulations, there are four methods to compute the thermal conductivity for MD systems: 1) NEMD: energy is applied to the hot region, and an equal energy is subtracted from the cold area in the simulation cell. The heat flux is monitored between different temperature layers; 2) NEMD: Energy is added or subtracted in two regions, and the temperature difference of the intermediate region is monitored; 3) rNEMD: The kinetic

energies of two atoms in different layers are swapped, and the temperature gradient is monitored; 4) EMD: the heat flux can be computed from the fluctuations of per-atom potential and kinetic energies, as well as the stress tensor. It is common in NEMD (non-equilibrium MD) for calculating the thermal conductivity of systems to impose the temperature gradient and the responded heat flux is measured. However, a reverse non-equilibrium MD (rNEMD) algorithm is used in the Muller-Plathe method [184]. The heat flux is applied in the system and the temperature gradient is measured. When the heat flux is imposed in the simulation cell, which is divided into N slabs (N is an even number, twenty was used in this study) with identical thickness. Energy transfer (Figure 5.8c) is produced from hot to cold slabs through the z-direction and it causes the temperature difference (Figure 5.8d) between these two slabs. Velocity exchange occurs in two particles, and the energy conservation is satisfied. The formulas for thermal conductivity and heat flux are shown in equation (5.9). In addition, the Avogadro constant was used to complete the unit conversion due to different scales from microscopic to macroscopic states based on equation (5.9). The mass/volume effect in the MD simulation was also considered in the unit conversion. The results of thermal conductivity of the xGNP modified and control models are presented in Figure 8e. Also, the thermal conductivities of asphalt under different temperatures in the laboratory are shown in Figure 5.8e.

$$J = -\lambda \nabla T \text{ and } \lambda = -\frac{\sum_{transfers} \frac{m}{2}(v_{hot}^2 - v_{cold}^2)}{2tL_xL_y\langle \partial T/\partial z \rangle} \quad (5.9)$$

where ∇T is the temperature gradient (scalar) in the simulation cell; J is the energy transferred (scalar) through the surface of layers; λ is the thermal conductivity; t is the

simulation time; v_{hot} is the velocity of the hot particle; v_{cold} is the velocity of the cold particle; m is the identical mass of particles; L_x is the length of the simulation box in the x-direction; and L_y is the length of the simulation box in the y-direction; and $\partial T/\partial z$ is the temperature gradient in the z-direction.

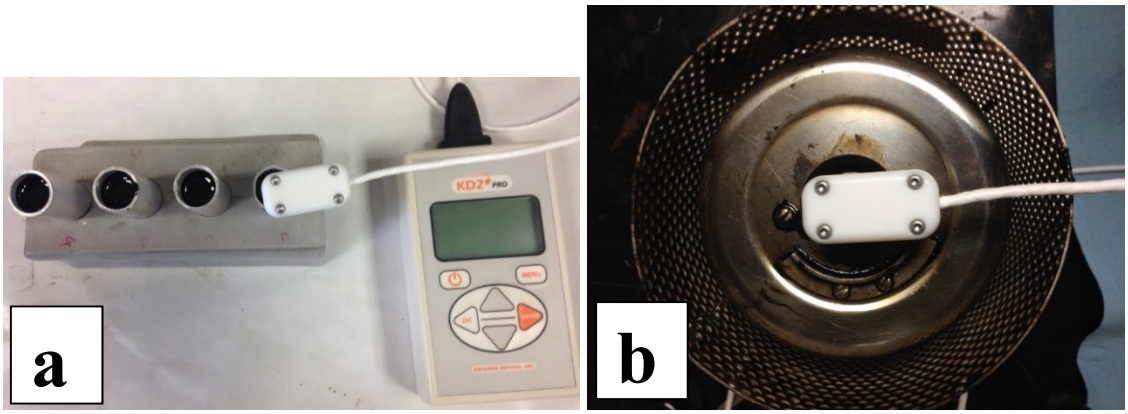

(a) KD2 Pro thermal conductivity tester in the laboratory
(b) the chamber for temperature control in the thermal conductivity test

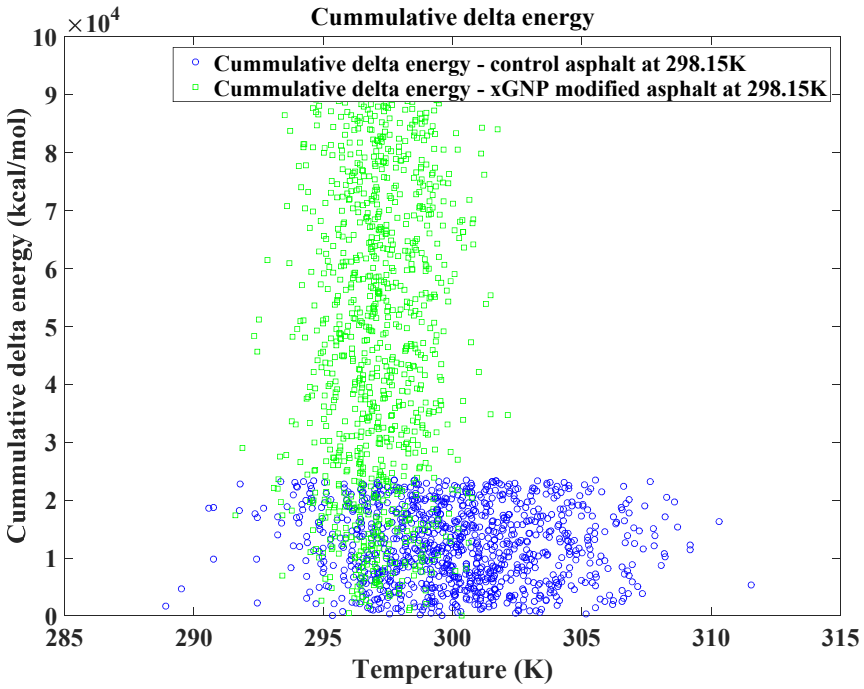

(c) Cumulative delta energies of the control and xGNP modified asphalt systems at a temperature of 298.15K

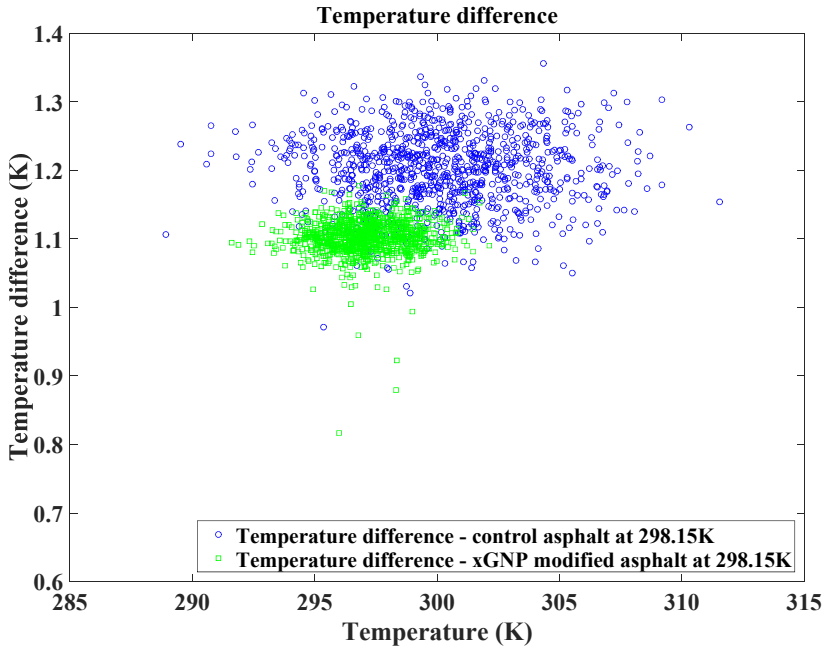

(d) Temperature difference of the control and xGNP modified asphalt systems at a temperature of 298.15K

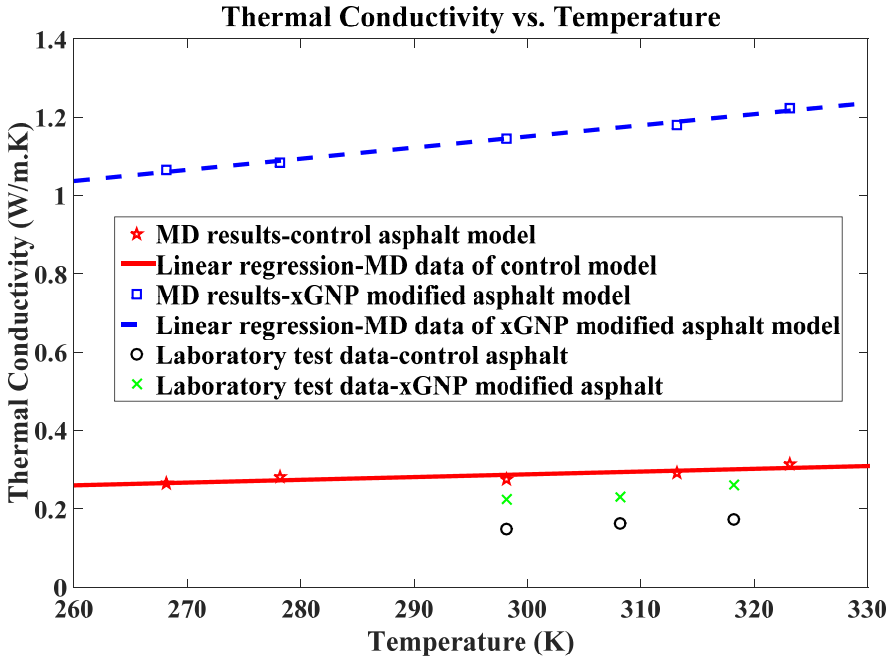

(e) Thermal conductivity results of laboratory tests and MD simulations

Figure 5.8. Thermal conductivity calculations in the laboratory and MD simulation

Figure 5.8a and Figure 5.8b display the KD2 Pro thermal conductivity apparatus and the temperature control chamber used in the laboratory, respectively. Figure 5.8c shows the cumulative energy input in different molecular systems. The control asphalt system has a relative low energy input in contrast to the energy of the xGNP modified asphalt system due to the small number of molecules and low volume in the control system. The energy of the xGNP modified asphalt system is four times greater than that of the control asphalt system, and it is the same as the mass ratio of the xGNP modified asphalt system to the control system. The temperature variation of the xGNP modified asphalt model is also lower than that of control system due to the large number of molecules. Figure 5.8d shows the temperature difference in different asphalt systems after the input of the heat flux. The variation in the temperature difference of the xGNP modified model is less than that of the control asphalt model, as well as the temperature variation in the MD simulation. It is likely that more molecules in the system result in better stress and heating responses and produce a stable system. Figure 5.8e demonstrates the thermal conductivity results through laboratory tests and MD simulations. The thermal conductivity of the control asphalt at room temperature is 0.148 W/m·K, and it is close to the reference data of asphalt [185] (0.170 W/m·K). The thermal conductivity of the xGNP modified asphalt at room temperature is 0.226 W/m·K, and it is near to the reference data [185] from 0.396 W/m·K to 0.934 W/m·K with different amounts of graphite (different types from the multi-layer graphite used in this study). It is reasonable that the thermal conductivity of the control and xGNP modified asphalt models at room temperature is around 0.275 W/m·K and 1.146 W/m·K, respectively. There is still an insignificant difference between this laboratory data and the data from the MD simulation.

The xGNP particles in the control asphalt improves the thermal conductivity of the modified asphalt from the experimental data. The same trend of thermal conductivity is also observed in the data from the MD simulation after the addition of the multi-layer graphite xGNP model in the control asphalt model. The thermal conductivities of control and xGNP modified asphalt increase with the increase in temperatures of the experimental tests, and the thermal conductivities of the control and xGNP modified asphalt models also increase by increasing the temperatures of the systems. However, there are minor differences between the experimental data and the MD simulation results. It is probably caused by a few reasons: (1) in the preparation of the samples and laboratory testing, the xGNP particles in the modified asphalt were not perfectly dispersed in the tested area due to the mixing method and not operational errors, and this causes inhomogeneous heating of the modified asphalt during testing; (2) the test area of the thermal conductivity is relatively small; (3) the multi-layer graphite xGNP model does not fully represent the xGNP particles in the asphalt matrix for the calculation of thermal conductivity, and there are some improvements needed for models of xGNP particles and asphalt. After the analysis of laboratory and MD data, it is confirmed that xGNP particles can improve the thermal conductivity of asphalt, and the multi-layer graphite xGNP model can also enhance the thermal conductivity of the control asphalt model. The trend in temperature versus thermal conductivity of the MD simulation results is the same as the trend in the experimental data.

5.9 Discussions and Conclusions

The MD model of multi-layer graphite xGNP nanoplatelets was created and used for the investigation of the effect of modification on the control asphalt model. The control asphalt model was composed of three components: asphaltenes, aromatics, and saturates. The xGNP modified asphalt model was generated from the addition of the xGNP model in the control asphalt model. The conjugate gradient method and PPPM were used for energy optimization, and the Savitzky-Golay filter was used for smoothing data. The Amber Cornell Extension Force Field was used in these asphalt models, and the physical properties of the models were calculated including density, the glass transition temperature, viscosity, and thermal conductivity.

(1) The densities of these asphalt models were computed, and the addition of the multi-layer xGNP model increased the density of the xGNP modified asphalt model compared to that of the control asphalt model. The molecular number in MD systems significantly affects the data variation for density calculation. The density of MD asphalt systems decreases with the increase in temperatures.

(2) The glass transition temperature of the xGNP modified asphalt model is around 250 K, and it is better than the results of the reference, 298 K to 358 K [13]. This glass transition temperature is better than previous results (around 300 K [182]) for the control asphalt model, because it is the same as the glass transition temperature of SHRP asphalt binders, around 250 K, from laboratory results [115].

(3) The Muller-Plathe method was used to calculate the viscosity of the control and xGNP modified asphalt models. The twenty layers in the MD asphalt models were separated

for this calculation. The addition of xGNP particles in the control asphalt matrix improves viscosities of the modified asphalt at different temperatures, and the same effect of multi-layer xGNP models in the control asphalt model was observed. Compared to the experimental viscosities of the xGNP modified asphalt, the viscosities of the MD simulation is close to the experimental results at the temperatures of 403 K, 423 K, and 443 K. The relationship between viscosities and temperatures in the data of the MD simulation is also the same as that of the laboratory results.

(4) The experimental data shows that the xGNP particles in the control asphalt increase the thermal conductivity of the modified asphalt at room temperature. During the calculation of thermal conductivity, the Muller-Plathe method was used in these MD simulations, and the multi-layer xGNP model in the control model also improves the thermal conductivity of the xGNP model at room temperature. The thermal conductivity of the control and xGNP modified asphalt increase with increasing temperatures, and the same trend is observed in the data of MD simulations.

Therefore, the multi-layer xGNP graphite particles in asphalt can improve viscosity and thermal conductivity of the modified asphalt, and the xGNP graphite model in the control asphalt model can also enhance the density, glass transition temperature, viscosity and thermal conductivity. It is obvious that the same trend of experimental data and MD results is observed during the testing and MD calculation of different properties of asphalt. It is likely that the xGNP particles can be utilized and generalized for pavement construction and heat sink. In addition, more properties of asphalt and its models will be tested and calculated for future research.

5.10 Acknowledgements

The authors appreciate the financial support of the U.S. National Science Foundation (NSF) under grant 1300286. The computational studies were performed using computer cluster (Superior research center) at Michigan Technological University. Any opinion, finding, and conclusion expressed in this paper are those of the authors and do not necessarily represent the view of any organization.

Chapter 6 Modulus predictions of the asphalt model with multi-layer graphite nanoplatelet model using Molecular Dynamics (MD) method

6.1 Overview

The objective of this study is to simulate the exfoliated multi-layered graphite nanoplatelets (xGNP) modified asphalt using the Molecular Dynamics (MD) method, and to analyze different modulus properties of these asphalt models compared with those of the control asphalt model. The multi-layered graphene model was used to represent the xGNP particles, which was used to modify the control asphalt in the laboratory. The control asphalt model was used in the previous study by the authors. The xGNP model was randomly placed in the control asphalt model to prepare the xGNP modified asphalt model using the same conditions and procedures in the laboratory preparation. When the xGNP modified asphalt model was generated, the densities of the control and xGNP modified asphalt models were computed and verified. Different properties of these models were simulated and calculated in MD simulations using procedures similar to those in the experiments, which include the bulk modulus, Young's modulus, shear modulus and Poisson's ratio. The simulation results indicate that the modulus trends of these asphalt models are the same as those of laboratory data.

The full text of this chapter will be submitted to "ASCE Journal of Materials in Civil Engineering" for publication.

The MD simulation data is larger than the laboratory results due to several reasons discussed in the study. In addition, Poisson's ratios calculated from MD simulations coincide with the laboratory results.

6.2 Introduction

Nowadays, asphalt pavement is the main pavement type around the world, and the performance and properties of asphalt are studied by researchers, as well as the composition of asphalt. The asphalt is composed of carbon, hydrogen and some trace elements [6, 13, 182, 186]. The performance of asphalt also depends on the source and ambient temperatures. Different modifiers have been applied to the original asphalt in order to obtain better pavement performance. Rubbers [21, 187-191] and fibers with different sizes [31, 33, 192] were widely utilized to enhance the high-temperature performance of asphalt binders and mixtures, and, recently, nanomaterials [7, 8, 14, 33]. The modification mechanism of these modifiers was also explored and the microstructure of the modified asphalt was examined by researchers [7, 21, 30, 37, 44, 193, 194]. However, the fundamental understanding of the modification and interaction between the modifiers and asphalt are still unclear on a nano scale or on the atomic scale in the modified asphalt.

Molecular dynamics (MD), originating from physics, is widely applied in different research areas, and it is a computer program to simulate the materials and its behaviors on the atom scale [195]. At present, the molecular dynamics (MD) method is a new tool for researchers to understand the physical properties of materials and functions of macromolecules on the atom scale. MD describes the details of each particle/atom motion over a period of time, and it helps address some specific problems or principles of atoms

or materials. It is easier than doing the experiments in the laboratory. In MD simulation, a specific property of materials can be solely studied by altering the specific contributions, and it can be used for fundamental research or functional predictions in a new material.

Two asphaltene structures were used, and saturates and naphthene aromatics were added to the asphalt model. Different properties of the asphalt models with All-atom Optimized Parameters for Liquid Simulation (OPLS-aa) force field were calculated and evaluated, such as density, thermal expansion, isothermal compressibility, and bulk modulus [13]. An asphalt model, which is similar to the asphalt AAA-1 of the Strategic Highway Research Program (SHRP), was generated, and the composition of asphalt consists of asphaltene, polar aromatic, naphthene aromatic, and saturate. The Hansen solubility parameters of components in the asphalt models were calculated, and the radial distribution function and intramolecular orientation of components were also analyzed [84]. Based on the literature review, few researchers researched the modified asphalt model and different modulus properties. In this study, the control asphalt model was composed of asphaltenes, naphthene aromatics, and saturates based on the Corbett method. The graphite model with the multi-layer structure was used to represent the modifier, exfoliated multi-layered graphite nanoplatelets (xGNP) particles, selected in the study. The modifier model was randomly added to the control asphalt model, and different modulus properties were mimicked and analyzed.

6.3 Force Field

The force field provides the parameters for atoms in the system to calculate the energy of systems. The Amber Cornell Extension Force Field (ACEFF) was used in this

study, and some experimental parameters were obtained from the General Amber Force Field (GAFF) [64]. The formula of energy calculation of ACEFF is shown in equation (6.1).

$$E_{total} = \sum_{bonds} K_r(r - r_{eq})^2 + \sum_{angles} K_\theta(\theta - \theta_{eq})^2 + \sum_{dihedrals} \frac{V_n}{2}[1 + \cos(n\varphi - \gamma)] + \sum_{i<j}[\frac{A_{ij}}{R_{ij}^{12}} - \frac{B_{ij}}{R_{ij}^{6}} + \frac{q_i q_j}{\epsilon R_{ij}}] \quad (6.1)$$

where r_{eq} or θ_{eq} is the equilibrium of the structural data; K_r is the force coefficient between double bonds; K_θ is the force coefficient from vibrational analysis; n is the multiplicity for dihedrals; γ is the phase angle for the torsional angle parameters; A, B and q are the non-bonded potentials; R_{ij} is the distance between atoms; and ϵ is the depth of the van der Waals energy well.

6.4 Objectives and scopes

The objectives of this study are to apply the molecular dynamics (MD) method to simulate the control and xGNP modified asphalt, and the moduli of the control and xGNP modified asphalt models are calculated and compared with the laboratory results. The modulus properties include the bulk modulus, Young's modulus and shear modulus. The bulk modulus of the asphalt models is computed through compression and tension in the model, and the Young's modulus of the models is simulated by applying the negative and positive strain in one direction, not in the other two directions, at different temperatures. The shear modulus of the models is also calculated by applying a shear strain in the XY direction at different temperatures. These moduli are computed and compared with the experimental data, as well as Poisson's ratio.

6.5 Model Generation

In the laboratory, the xGNP graphene nanoplatelets were used to improve the performance of the modified asphalt, and the PG grade of the control asphalt is PG 58-28. The 2% xGNP particles were slowly added to the control asphalt, and the modified asphalt was mixed in the high shear machine for around two hours at the temperature of 450 K. In MD simulation, the asphalt model was composed of three components, asphaltenes, naphthene aromatics, and saturates, at a ratio of 5:27:41 [13]. The docosane (n-$C_{22}H_{46}$) and 1, 7- dimethylnaphthalene ($C_{12}H_{12}$) represent saturates and naphthene aromatics, respectively. The structure of the asphaltene ($C_{64}H_{52}S_2$) was introduced from the references [13, 80, 182], and the control asphalt model was built in the previous study [182]. The model of multi-layer graphene sheets (Figure 6.1a) was used to represent the xGNP particles, and this model was randomly added to the control asphalt model at the temperature of 450 K. The 2% (by molar mass) xGNP model was dispersed in the matrix of the control asphalt model, and the molecules of the control asphalt model were four times those of the previous asphalt model [182] in order to maintain the mass ratio of the xGNP model of the control asphalt model. The percentage of the xGNP particles in the base asphalt model is based on the molar mass of the base asphalt model. It is commonly used in the references [82, 108, 109]. The 2% xGNP particles was used in the modification of asphalt for laboratory tests. The mass of the xGNP modified asphalt model is around 87405.39 g/mol. It is also beneficial to analyze the variation in data due to mass in MD simulations.

In addition, the xGNP modified asphalt model (Figure 1b) with the force field charge was optimized by the conjugate gradient method (a kind of algorithm to solve optimization problems) and the Particle-Particle-Particle-Mesh Method (PPPM) (an accurate and efficient method to calculate interactions in MD simulation) [79].The conjugate gradient method was used to relocate the positions of atoms and reallocate the velocities of atoms in asphalt binder models [110, 111]. The PPPM (a kind of Ewald summation) was used to optimize the system energy by mapping charges to a three-dimensional mesh and interpolating the electric fields back to atoms [79].

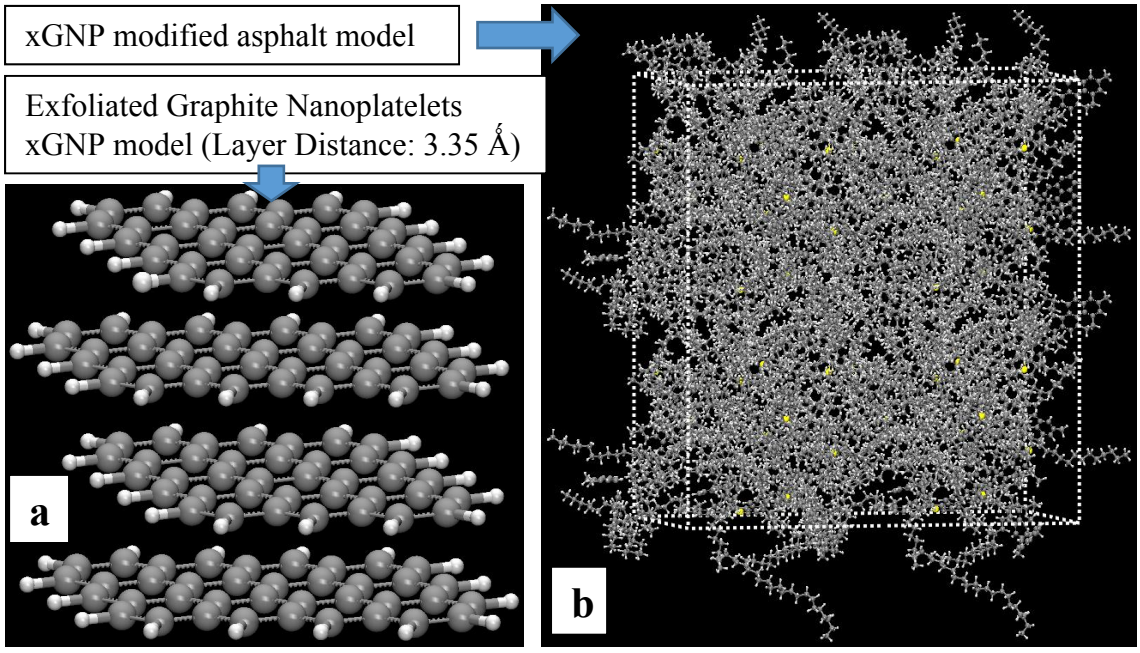

Figure 6.1. The molecular model of multi-layer graphene sheets and xGNP modified asphalt model, (a) the molecular model of exfoliated graphite nanoplatelets (xGNP model); (b) xGNP modified asphalt model.

6.6 Modulus Calculations

Different moduli were calculated for the asphalt models using MD simulations, such as bulk modulus, Young's modulus and shear modulus. The test procedures of these

moduli were simulated in the asphalt models. Before the modulus calculations, the densities of the asphalt models were computed and verified (Figure 6.2). The NPT (isothermal-isobaric ensemble) simulation was employed to compress and relax these asphalt models. The densities of the control and xGNP modified asphalt models are around 0.903 g/cm^3 and 0.911 g/cm^3, respectively. The densities of these asphalt models are stable after several picoseconds. After energy optimizations and NPT simulation, the modulus calculations were carried out, and the results of MD simulations were as follows.

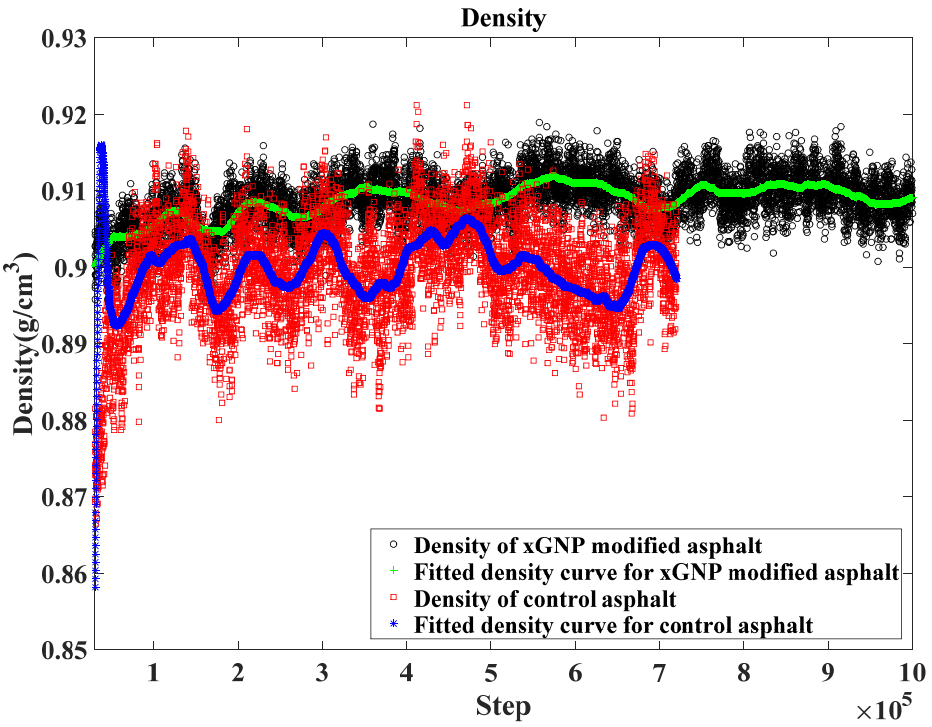

Figure 6.2. Densities of the control and xGNP modified asphalt models

6.6.1 Bulk modulus

Bulk modulus, a kind of numerical constant, is a measure of the ability of the materials to withstand the changes in volume under compression or tension in three directions. The bulk modulus is defined by equation (6.2). In the laboratory, there are four

approaches to test the bulk modulus: two separate tests (uniaxial and shear), long cylindrical test in tension and compression, confined compression test, and poker-chip geometry in tension and compression. In the MD simulation, the small volumetric strains were applied to the control and xGNP modified asphalt models, and the negative and positive strains were applied using equation (6.3) [62]. The Nose/Hoover thermostat and SLLOD algorithm (Lee-Edwards boundary conditions) were employed for these asphalt models when performing NVT (canonical ensemble) simulations in these models. The positions and velocities of atoms were updated during the simulation time, and pressure changes were also updated and recorded by pressure tensors. These models were fixed by NVT simulations for at least 2 ns, and millions of data was produced. During the MD simulations, the dilatation and shrinkage of volumes are shown in equation (6.4), and the averaged stresses under tension and compression are calculated using equation (6.5). The average values of bulk modulus for these asphalt models are computed by equation (6.6) at different temperatures from three directions.

After few ns NVT simulations, the corresponding stress results in three directions of these asphalt models were calculated, and one of the stress results (under different temperatures, three directions, and negative and positive strains) was presented. The stress results of the control and xGNP modified asphalt models under negative strain at the temperature of 298.15 K are shown in Figure 6.3a. There are two methods to calculate the bulk modulus in MD simulation, one is to directly use the applied strain and responding stress (the first calculation method), and another one is to use the regression function to compute the bulk modulus (the second regression method). The average volumetric stress-

strain relationships in these asphalt models are shown in Figure 6.3b based on the second method. Consequently, the bulk moduli of these asphalt models at different temperatures are shown in Figure 6.3c after averaging based on the first method.

$$K = -V\frac{dP}{dV} \tag{6.2}$$

$$\varepsilon_{xx} = \varepsilon_{yy} = \varepsilon_{zz} = \pm 0.005 \tag{6.3}$$

$$\Delta = (1 \pm \varepsilon_{xx})\big(1 \pm \varepsilon_{yy}\big)(1 \pm \varepsilon_{zz}) - 1 \tag{6.4}$$

$$\sigma_h = \frac{1}{3}(\sigma_{xx} + \sigma_{yy} + \sigma_{zz}) \tag{6.5}$$

$$K = \frac{\sigma_h}{\Delta} \tag{6.6}$$

where P is the pressure, and V is the volume, ε_{xx}, ε_{yy}, $and\ \varepsilon_{zz}$ are the small strain in all three coordinate directions; σ_{xx}, σ_{yy}, $and\ \sigma_{zz}$ are the volume averaged stress in all three coordinate directions; Δ is the overall dilatation of the simulation box; σ_h is the averaged stress in the MD simulation; and K is the bulk modulus in the MD system.

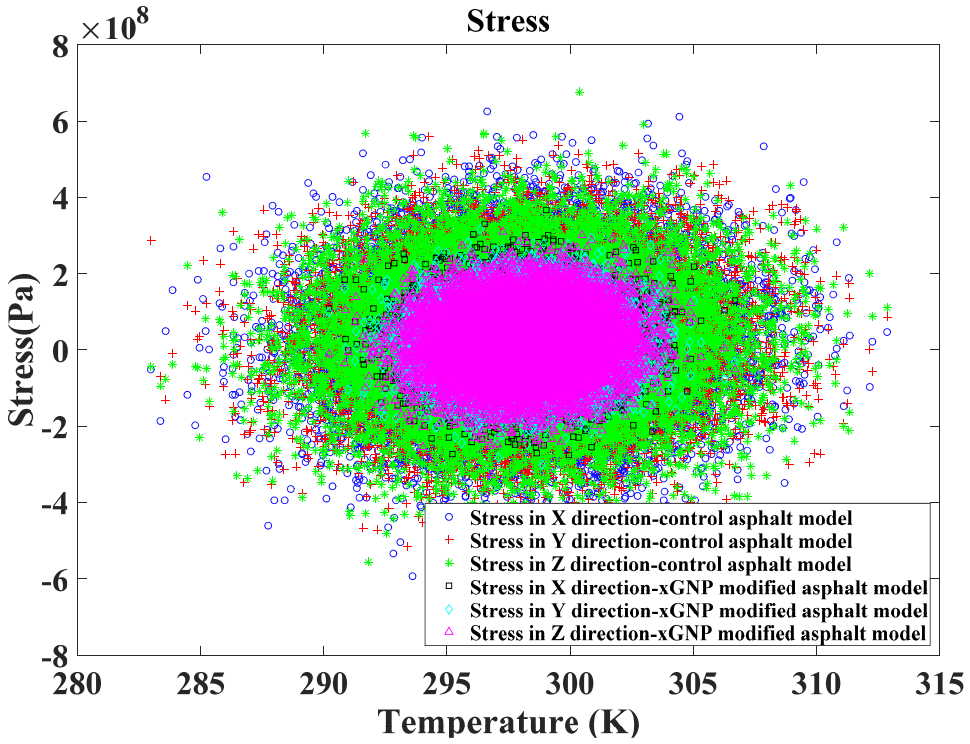

(a) Stress level of the control and xGNP modified asphalt models under negative strain at the temperature of 298.15 K (1.2×10^5 data)

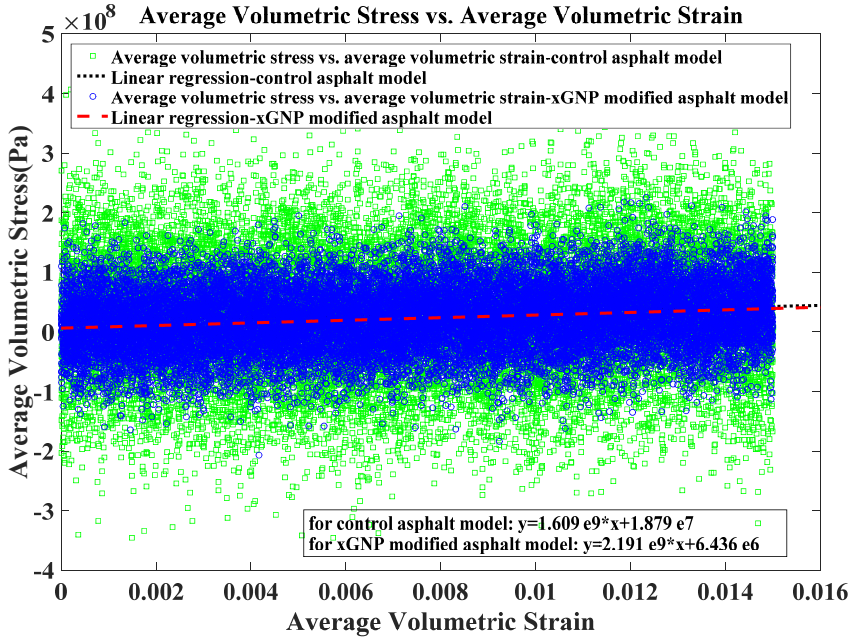

(b) Average volumetric stress-strain relationship between the control and xGNP modified asphalt models under the negative strain at the temperature of 298.15 K

Note: Two regression lines are so close, one is a black dotted line for the control asphalt model, and another line is a red dashed line for the xGNP modified asphalt model. The regression function is designed to determine the bulk moduli of these asphalt models.

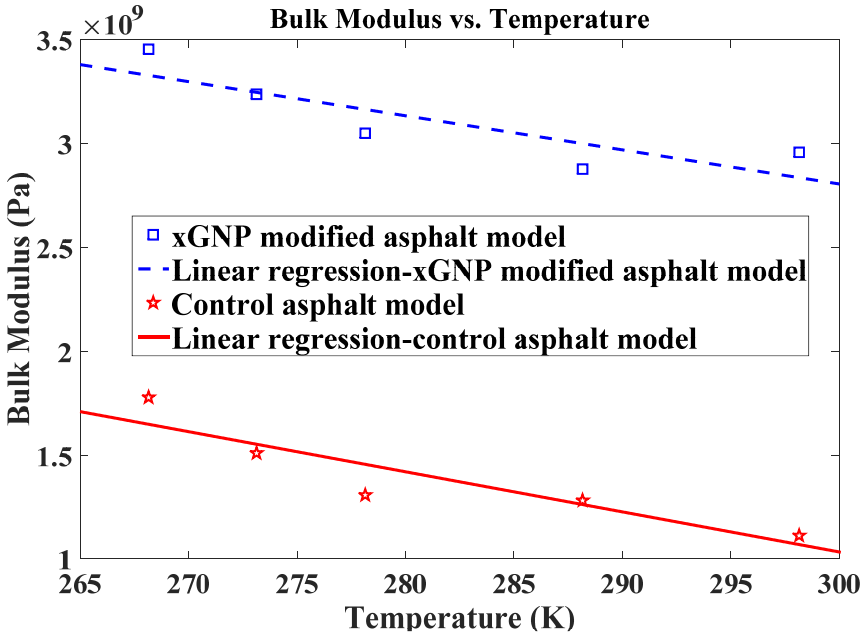

(c) Bulk moduli of the control and xGNP modified asphalt models at different temperatures

Figure 6.3. The modulus calculations for the control and xGNP modified asphalt

The loading process in the laboratory was simulated in this MD simulation. Figure 6.3a shows the stress magnitudes of the control and xGNP modified asphalt models under negative strain at a temperature of 298.15 K. The data amplitudes of asphalt models in different directions are different and relatively stable around $\pm 10^8$ Pa, and the data of the xGNP modified asphalt model fluctuates less than that of the control asphalt model due to different numbers of molecules or atoms. Figure 6.3b shows the relationships between volumetric stresses and strains of these asphalt models and their regression lines for the asphalt models under negative strain at the temperature of 298.15 K after averaging every 100 steps. The linear regression is fit for a stress-strain relationship in the modulus

calculations. The changes in volumetric strains range from 0 to 0.015 in two asphalt models, and they are consistent with the applied strains. Actually, the magnitude of the bulk modulus from the two methods used in this MD simulation is the same, and it is around 10^9 Pa. Figure 6.3c displays the bulk moduli of the control and xGNP modified asphalt models at different temperatures based on the first method. The moduli of the control and xGNP modified asphalt models decrease by increasing the system temperatures. The moduli of the xGNP modified asphalt model are higher than those of the control asphalt model at different temperatures. The addition of the xGNP model in the control asphalt model increases the bulk modulus. Based on the reference [132], the bulk modulus of the asphalt binder was tested in the laboratory using the poker-chip test, and it is around 3 MPa at the temperature of 293 K. There is still a difference between the simulation and laboratory data. In this MD simulation, the actual strain was applied to the asphalt model, and it is similar to the laboratory test procedure. The time frame of the applied strain is around a femtosecond, and it is really short compared to real time. It is reasonable that the response of the asphalt model is rigid and elastic, and the asphalt can be considered an elastic material when the temperature is relatively low. The limited number of molecules could be one of the reasons for this simulation data. In addition, it is likely that if a different MD simulation method was used for the bulk modulus, which does not apply actual strain in the model, the simulation data may be close to the laboratory data.

6.6.2 Young's modulus

(1) Calculation of Young's modulus

Young's modulus is a stiffness measurement for elastic materials and it is the ratio of the responding stress to the (responding) strain along an axis under Hooke's law [127]. The Young's modulus is different from the bulk modulus and shear modulus, sometimes called the modulus of elasticity. The asphalt can be treated as elastic material under low temperatures because most materials exhibit nearly Hookean characteristics for a small strain or stress. Considering that, the test temperature in this MD simulation is lower than room temperature. In the laboratory, the nano-indentation test was used to evaluate the Young's modulus of asphalt. Both the loading and depth control modes can be used in the test. Considering the influence of the indenter tip, the reduced Young's modulus was introduced, and the Young's modulus Es of the sample is calculated using equation (6.7). The reduced modulus is calculated from the slope of the load-indentation curve when unloading by equation (6.8) [196]. The Young's moduli of PG 70-22 and PG 76-28 asphalt binders are around 0.76 MPa and 5.22 MPa at room temperature, respectively [196].

$$\frac{1}{E_r} = \frac{1-v_s^2}{E_s} - \frac{1-v_i^2}{E_i} \tag{6.7}$$

$$E_r = \frac{\sqrt{\pi}}{2}\frac{S}{\sqrt{A}} \tag{6.8}$$

where E_r is the reduced modulus; E_s is the Young's modulus of the tested sample; E_i is the Young's modulus of the indenter tip; v_s is Poisson's ratio of the tested sample; v_i is Poisson's ratio of the indenter tip; S is the initial unloading stiffness, and A is the contact area during the test.

During the MD simulation, the small strains (positive and negative 5‰) were applied to these asphalt models in one direction. The NPH (isoenthalpic-isobaric ensemble) simulation, which maintains constant enthalpy, pressure and number of particles in the systems, was performed in these asphalt models with the temperature control (temp/rescale). Meanwhile, the uniaxial tensile or compressive stress was applied in one direction and no stress in the other directions. The position and velocities of atoms in the systems were updated at different temperatures, and the pressure or stress was recorded during the application of strain. The MD simulation time is at least 1 ns, and every 100 timesteps were averaged. The averaged pressures in the control and xGNP modified asphalt models were calculated under the positive and negative strains in independently different directions at different temperatures. The pressure results of the control and xGNP modified asphalt models in six MD simulations are shown in Figure 6.4a (under positive strain) and Figure 6.4b (under negative strain). The relationship between the applied strain and stress in these asphalt models and the linear regression are shown in Figure 6.4c (under positive strain) and Figure 6.4d (under negative strain) based on the second regression method. The Young's moduli of these asphalt models at different temperatures are shown in Figure 6.4e.

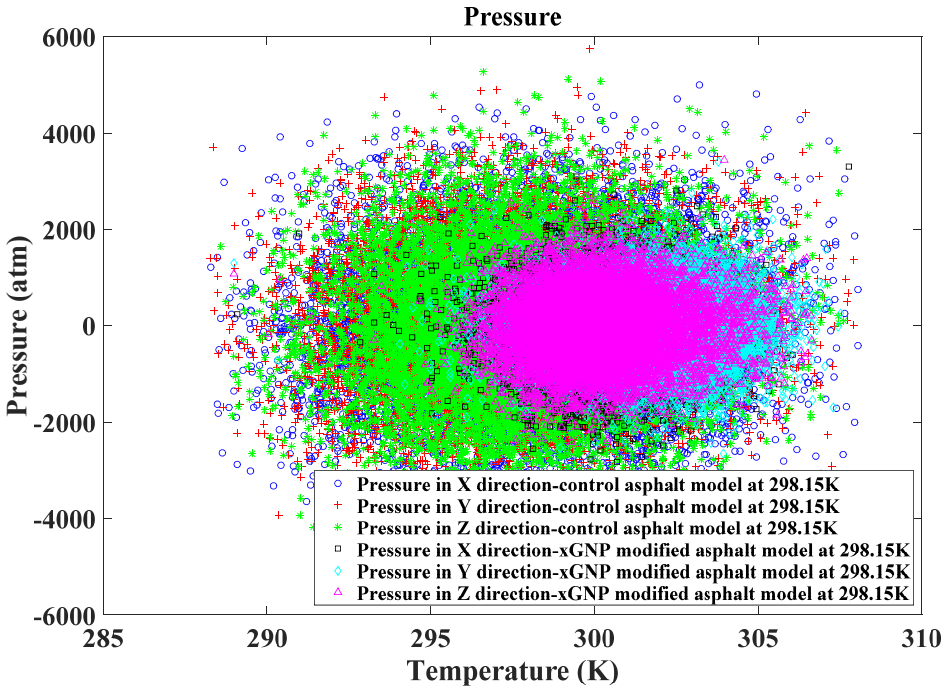

(a) Pressures of the control and xGNP modified asphalt models under **positive** strain: the label "Pressure in X direction – control asphalt model at 298.15 K" represents the pressure in the control asphalt model when **positive** strain was applied in the x direction at the temperature of 298.15 K, and no strain or stress in the other directions.

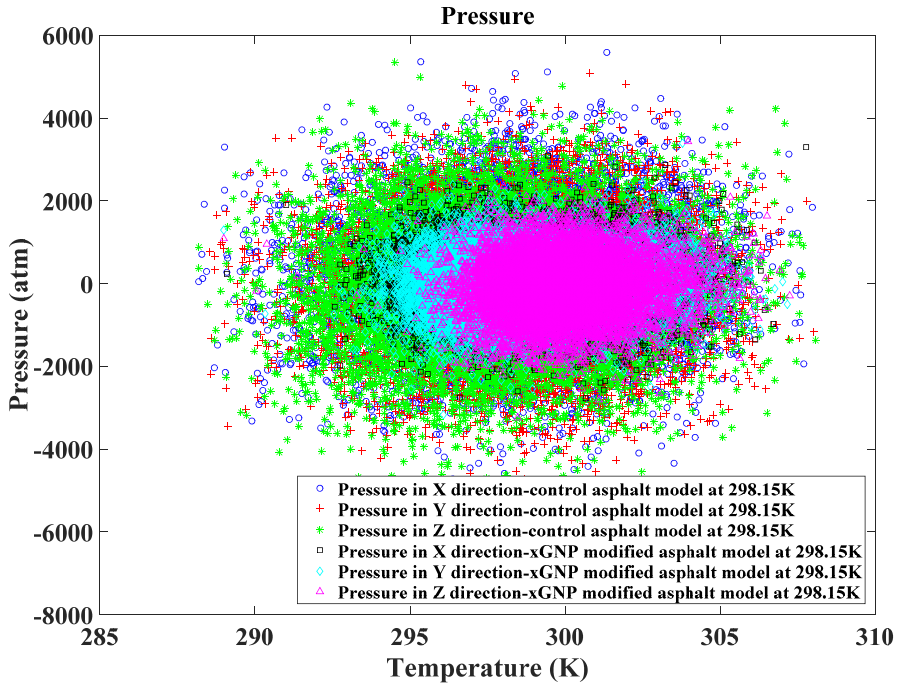

(b) Pressures of the control and xGNP modified asphalt models under **negative** strain: the label "Pressure in X direction – control asphalt model at 298.15 K" represents the pressure in the control asphalt model when **negative** strain was applied in the x direction at the temperature of 298.15 K, and no strain or stress in the other directions.

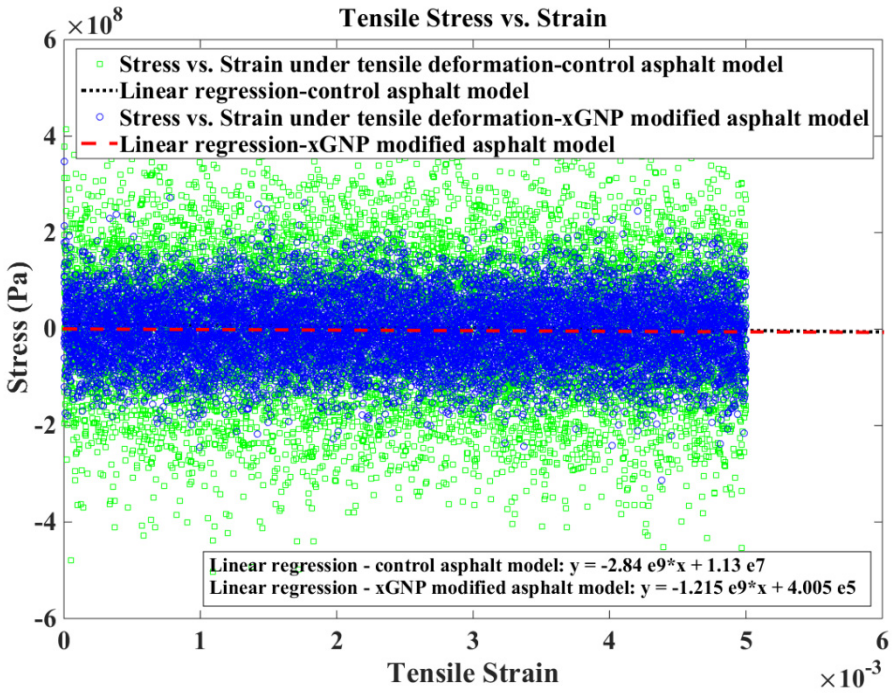

(c) Stress-strain relationship of the control and xGNP modified asphalt models under **positive** strain in the z direction at the temperature of 298.15 K, and the linear regression.

Note: Two regression lines are close, one is a black dotted line for the control asphalt model and the other is a red dashed line for the xGNP modified asphalt model. The regression analysis is used to calculate the Young's modulus of these asphalt models under positive strain.

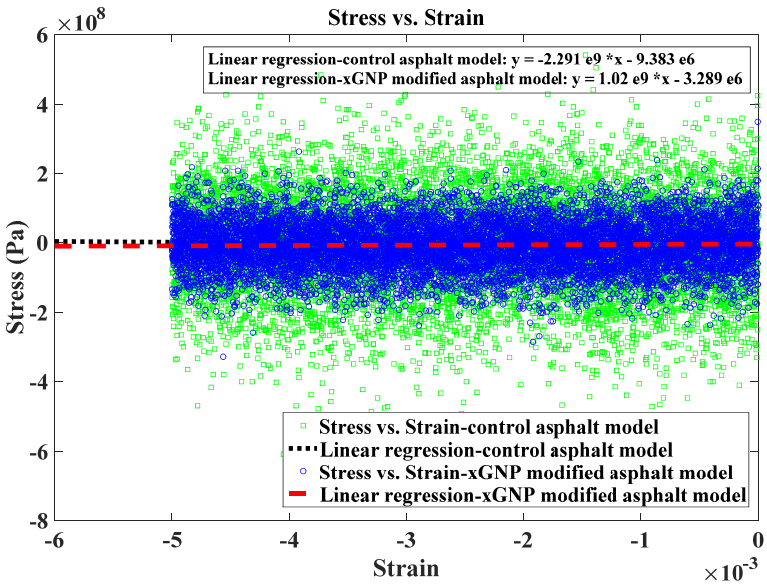

(d) Stress-strain relationship of the control and xGNP modified asphalt models under **negative** strain in the z direction at the temperature of 298.15 K and the linear regression.

Note: Two regression lines are close, one is a black dotted line for the control asphalt model and the other is a red dashed line for the xGNP modified asphalt model. The regression analysis is employed to compute the Young's modulus of these asphalt models under negative strain.

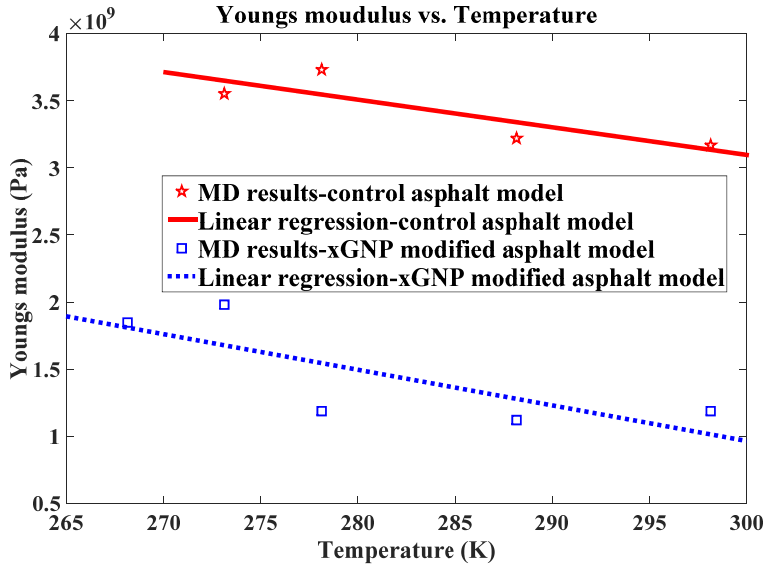

(e) Young's modulus versus temperature of the control and xGNP modified asphalt models

Figure 6.4. Young's modulus calculation of the control and xGNP modified asphalt models

Figure 6.4a shows the pressures of these asphalt models in the six different simulations at the temperature of 298.15 K in three different directions when positive strain is applied. Figure 6.4b displays the pressures of these asphalt models in the six different simulations at the temperature of 298.15 K in three different directions when negative strain is applied. It is noted that the pressures of the xGNP modified asphalt model have less fluctuations than those of the control asphalt model due to the numbers of molecules and atoms and more concentrated data. The pressures from different directions (x, y, and z) in the control asphalt model are within the same magnitude and range. It indicates that there is no difference in pressures among three different directions when applying the same strain in the asphalt model. The same situation occurs in the xGNP modified asphalt model.

Figure 6.4c shows the relationship between the tensile stress and strain of the control (green squares) and xGNP (blue circles) asphalt models in the z direction at the temperature of 298.15 K under positive strain. Figure 6.4d displays the relationship between the stress and strain of these asphalt models in the z direction at the temperature of 298.15 K under negative strain. The amplitude of variation in the stress-strain data of the xGNP modified asphalt model (blue circles) is less than that of the control asphalt model (green squares), and the numbers of atoms and molecules definitely influence the variation of results. The regression function in Figure 4c and 4d was also used to calculate the Young's modulus of the control (a black dotted line) and xGNP (a red dashed line) asphalt models based on the linear relationship between stress and strain.

Figure 6.4e demonstrates the Young's modulus of the control (a red solid line) and xGNP (a blue dotted line) asphalt models at different temperatures. The Young's moduli

of these asphalt models are averaged from the results of negative or positive strain in different directions. The Young's modulus of these asphalt models decreases with increasing ambient temperatures in the models. Compared to the laboratory testing results (0.76 MPa for PG 70-22 asphalt and 5.22 MPa for PG 76-28 asphalt) of Young's modulus at room temperature [196], there is a wide gap between the experimental and simulation data (around 10^9 Pa). Negative or positive strain was applied in these asphalt models at a short time, a few thousand time steps. It is reasonable that the small deformation at a very short time results in a large stress in an assumed elastic model at low temperatures. Meanwhile, the simulation or interaction time and numbers of atoms or molar mass in these models are also the determining factors for the calculation of the Young's modulus. It is obvious that the Young's moduli of the xGNP modified asphalt model are lower than those of the control asphalt models at different temperatures, and the Young's modulus of the xGNP modified asphalt is close to the experimental results relative to the control asphalt model. It is likely due to a large number of atoms and molecules in the xGNP modified asphalt model compared to the control asphalt model. When negative or positive strain was applied in a short time, more atoms or molecular numbers in the model helped relax the responding stress caused by the small strain applied in one direction when the other directions were not confined. If the simulation cell is confined or the strains are applied in three directions, the responding stress would be higher than the stress at the condition of no confinement or strain in one direction since it is hard to relax the stress in the confined system.

(2) Statistical analysis

The regression method was used to calculate the Young's modulus, and the correlation analysis was used to measure and interpret the strength of the relationship between two continuous variables (strain and stress). We mainly focus on the Pearson's product-moment correlation coefficients, whose value ranges from -1 to +1. This correlation is commonly used for measuring the linear relationship between two variables [197]. For example, the Pearson correlation, r, between two variables X_i and Y_i (i = 1, 2, …, n) can be computed by equation (6.9).

$$r = \frac{\sum_{i=1}^{n}(X_i-\bar{X})(Y_i-\bar{Y})}{\sqrt{\sum_{i=1}^{n}(X_i-\bar{X})^2 \sum_{i=1}^{n}(Y_i-\bar{Y})^2}} \tag{6.9}$$

where $\bar{X}$ and $\bar{Y}$ are the sample means of the X_i and Y_i values, respectively, and n is the sample size. We also conduct the t-test for the population correlation ρ to check whether or not a linear relationship exists between the two variables. More specifically, we are interested in testing. $H_0: \rho = 0$ vs $H_a: \rho \neq 0$ (6.10)

We obtain the Pearson correlation between strain and stress, which is r = -0.02868321. To test the above hypothesis, we obtain the t-statistic given by equation (6.11).

$$t^* = \frac{r\sqrt{n-2}}{\sqrt{1-r^2}} = -2.8692 \tag{6.11}$$

From the results, with degrees of freedom df = 9998, the corresponding p-value from this t-statistic is 0.004124 (< 0.01). We can thus reject the null hypothesis. Thus, there is sufficient statistical evidence at the $\alpha = 0.01$ significance level to conclude that there is a significant linear relationship between strain and stress.

6.6.3 Shear modulus

The shear modulus is designed to describe the response of the materials to the shear stress and to measure the stiffness of materials based on the generalized Hooke's law. The shear modulus can be calculated from equation (6.12). The shear modulus of asphalt is related to the field performance of asphalt pavement. In the laboratory, the shear modulus of the asphalt binders is tested by a Modular Compact Rheometer (MCR) (Figure 6.5a) with different plates (Figure 6.5b) for different temperatures, and the temperatures can range from 253 K to 355 K. The round plate with a diameter of 25 mm was selected to test the complex shear modulus using the oscillatory mode. The testing data of the control (PG 58 -28) and the modified asphalt with 2% xGNP particles under the condition of temperatures of 319.15 K to 343.15 K and frequency of 45 Hz is shown in Figure 6.5c.

In the MD simulation, the small shear strains (positive and negative 5‰) were applied to the asphalt models in the XY direction, and it is similar to the procedure used in the laboratory test. The applied strain between the laboratory and simulation is different, because the asphalt model is assumed to be a pure elastic material in this study. The NVT ensemble was used with the SLLOD algorithm when the shear strain (equation (6.12)) was applied to the asphalt models. The positions and velocities of atoms in the asphalt models were updated at every step, and the pressures and temperatures were recorded. The pressure results of these asphalt models under positive and negative results are shown in Figure 6.6a and Figure 6.6b. The shear moduli of these asphalt models are shown in Figure 6.6c based on the first calculation method.

$$G = \frac{\tau_{xy}}{\gamma_{xy}} \text{ and } \gamma_{xy} = \pm 0.005 \quad (6.12)$$

where G is the shear modulus of the sample; τ_{xy} is the shear stress in the XY direction; γ_{xy} is the shear strain in the XY direction.

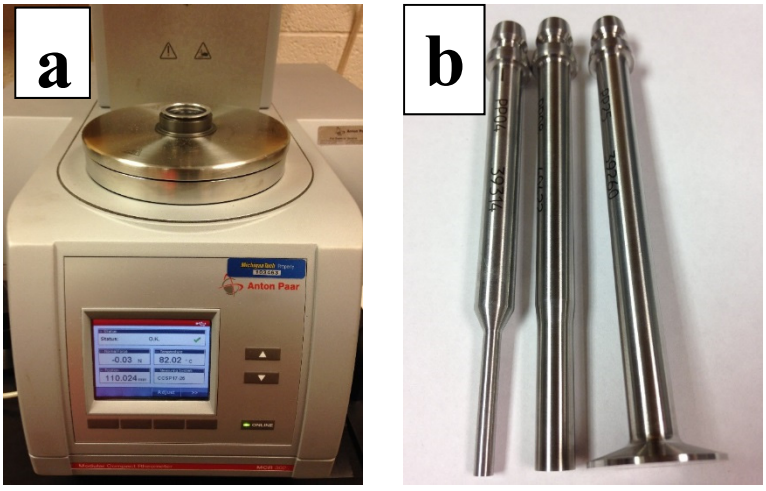

(a) Modular Compact Rheometer (MCR); (b) Accessories for testing plates with different diameters and temperatures

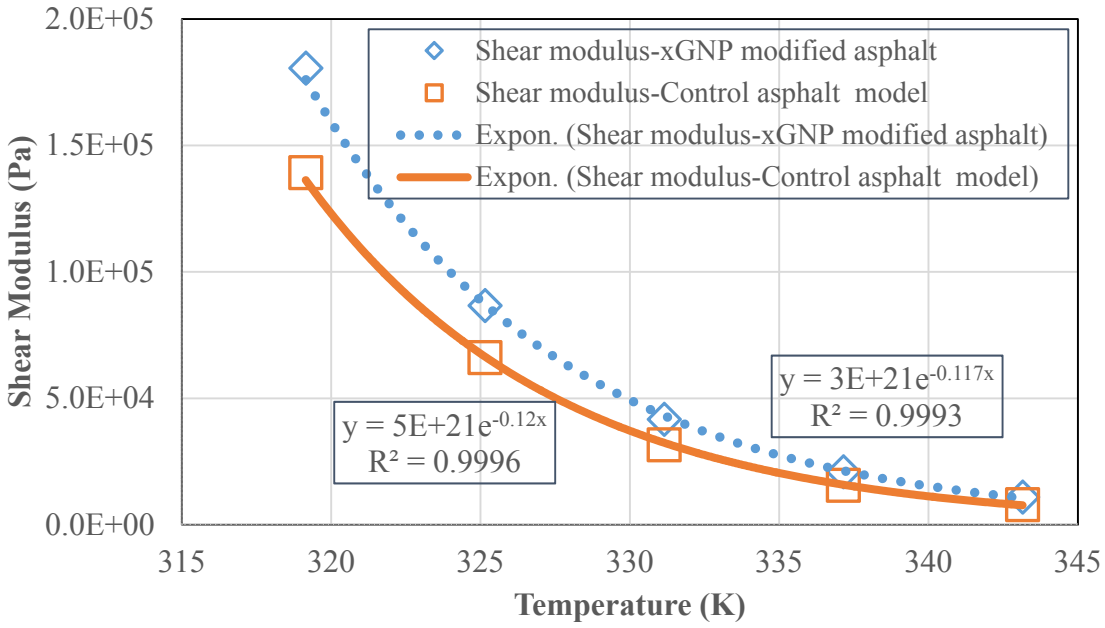

(c) Shear moduli of the control (PG 58-28) and modified asphalt binders with 2% xGNP particles

Figure 6.5. The modular compact rheometer (MCR) for the shear modulus of asphalt binders

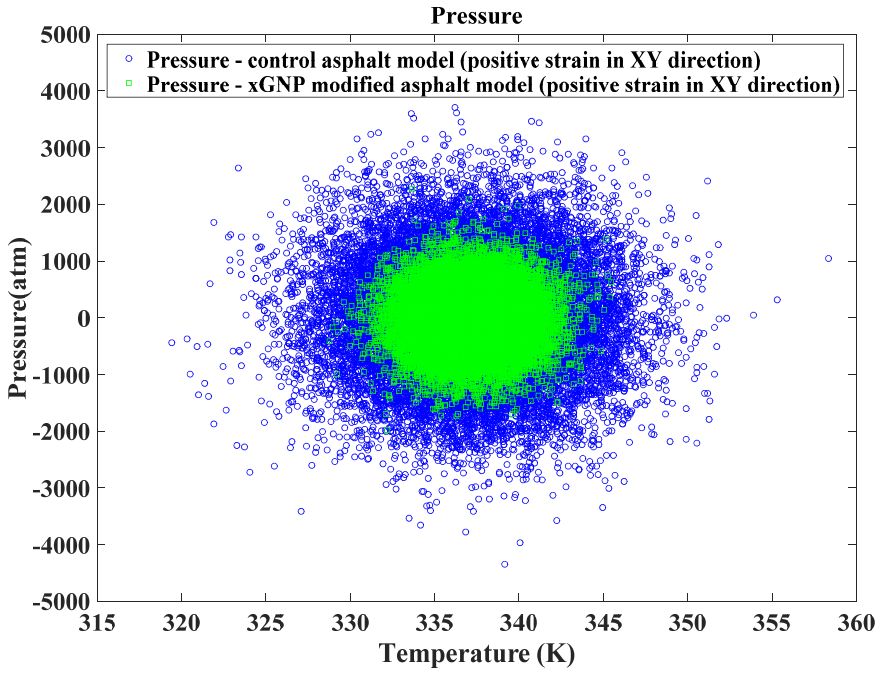

(a) Pressures of the control and xGNP modified asphalt models under positive shear strain in the XY direction at a temperature of 337.15 K

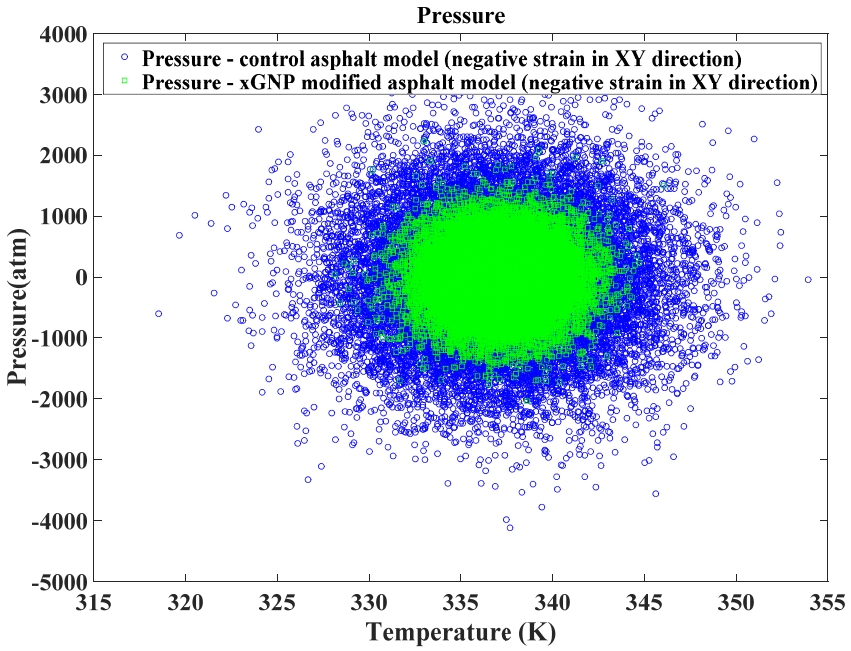

(b) Pressures of the control and xGNP modified asphalt models under negative shear strain in the XY direction at a temperature of 337.15 K

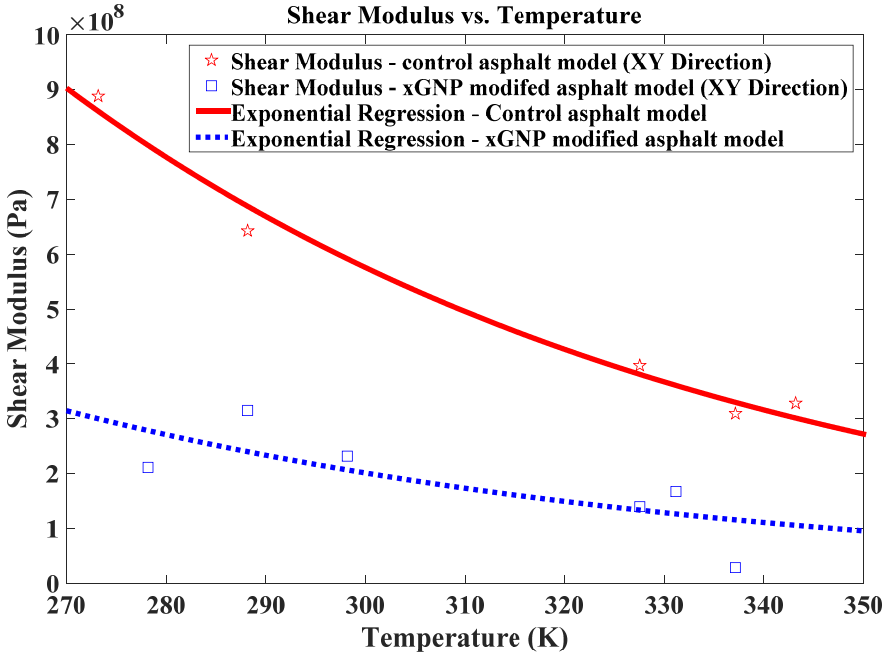

(c) Shear moduli of the control and xGNP modified asphalt models under different temperatures

Figure 6.6. Shear modulus calculation of the control and xGNP modified asphalt models

Figure 6.5c shows the shear moduli of the control and xGNP modified asphalt at different temperatures. The laboratory data of the shear modulus was regressed and fitted by the exponential curve, and the value of R squared is around 0.99. The shear modulus of the control and xGNP modified asphalt decreases with increasing test temperatures. The magnitude of the shear modulus of unaged asphalt is around 10^5 Pa. However, the magnitude of the shear modulus of aged asphalt can reach more than around 10^7 Pa [8]. Figure 6.6a displays the pressures of the control and xGNP modified asphalt models under positive shear strain in the XY direction at the temperature of 337.15 K. The variation of the control asphalt model is larger than that of the xGNP modified asphalt, and it is due to fewer molecules/atoms. The average pressures of the control and xGNP modified asphalt models are around 1.4 atm and 15 atm, respectively, due to the applied strain. The pressure data in these MD systems is relative concentrated, and the center of the temperature is around 337 K. It is also observed in Figure 6.6b where pressures of these models under negative strain in the XY direction are at the temperature of 337 K.

Figure 6.6c shows the shear moduli of the control and xGNP modified asphalt models under different temperatures after averaging. In these MD simulations, the simulation data of the shear modulus of these asphalt models decreases with the increase in the test temperature, and the exponential regression is excellently fitted to the simulation results. The trends of the shear modulus of these asphalt models agree with that of the experimental data. However, the magnitude of the shear modulus is around 10^8 Pa, and it is larger than the laboratory results. The shear modulus of the control asphalt model in the MD simulation is higher than that of the xGNP modified asphalt. There are several reasons

for the large shear modulus: (1) the interaction time for applying the strain to these models is really short, several femtoseconds, and the running time of these simulations, a few nanoseconds, is also very short compared to the real time scale in laboratory tests. It is a reasonable response for elastic materials in asphalt models. (2) Asphalt is a viscoelastic material at medium and high temperatures. The response of the asphalt models is elastic, and the results tend to approach the laboratory results when the test temperature is relatively low. (3) The molecular numbers of these asphalt models are limited, and from the trend, the more molecules or atoms in the model, the more the results are close to laboratory data. In addition, when the strain was applied to these asphalt models, the xGNP modified asphalt model expanded and relaxed the strain and responding stress effects due to more molecules and atoms compared to the control asphalt model. This is also the explanation as to why the shear modulus of xGNP modified asphalt is less than that of the control asphalt model. It indicates that if there are more molecules/atoms in the model, the modulus can approach the experimental results.

6.6.4 Poisson's ratio

When materials are compressed in one direction, the materials normally expand in the other two directions; this phenomenon is usually called "Poisson effect". Poisson's ratio is used to measure the effect, and it can be calculated using equation (6.13). The Poisson's ratio of isotropic and linear elastic materials ranges from -1.0 to 0.5 due to the positive values of these moduli. Poisson's ratio can also be calculated from the bulk modulus and shear modulus after determining these values in the asphalt models, and the

formula for Poisson's ratio is shown in equation (6.14) [62, 132]. The results of Poisson's ratio of these asphalt models are shown in Figure 6.7.

$$v = -\frac{d\varepsilon_{trans}}{d\varepsilon_{axial}} \tag{6.13}$$

$$v = \frac{3K-2G}{6K+2G} \tag{6.14}$$

where, v is the Poisson's ratio; $d\varepsilon_{trans}$ is the transverse strain; $d\varepsilon_{axial}$ is the axial strain; K is the bulk modulus and G is the shear modulus.

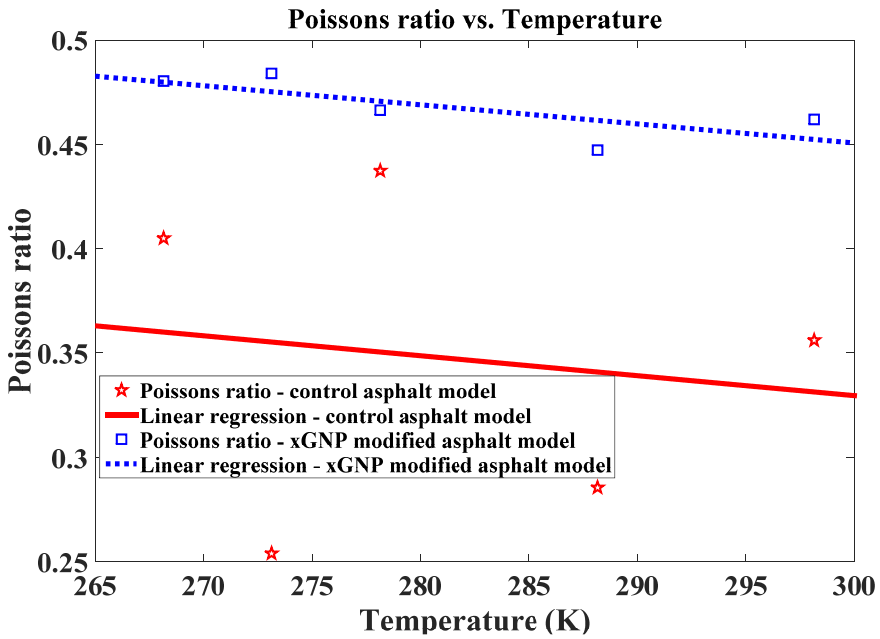

Figure 6.7. Poisson's ratios of the control and xGNP modified asphalt models at different temperatures

Figure 6.7 shows the results of Poisson's ratio of the control and xGNP modified asphalt models at a temperature range from 268.15 K to 298.15 K. Poisson's ratio of the control asphalt model is around 0.35, and the Poisson's ratio of the xGNP modified asphalt model is around 0.45 at temperatures from 268.15 K to 298.15 K. It falls within the area of theoretical values. The variation of Poisson's ratio of the control asphalt model is larger

than that of the xGNP modified asphalt, and it is likely due to the fewer number of molecules or atoms in the control asphalt model. Considering different loading times and temperatures, the Poisson's ratio of a typical asphalt binder was from 0.35 to 0.5 based on the reference [198]. Recently, the Poisson's ratio of two types of asphalt binders was tested at 20^{o}C, and it starts from around 0.25 to 0.5 under different loading times [132]. It can be seen that Poisson's ratios of the control and xGNP modified asphalt models are reasonable and agree with the reference and experimental data. It indicates that the responses of asphalt models are acceptable when applying strain in these asphalt models and calculating moduli in MD simulations.

6.7 Discussions and Conclusions

The control and xGNP modified asphalt binders were simulated in this study using the Molecular Dynamics (MD) method, and different properties of these asphalt models were simulated and computed. The multi-layer graphene model was generated to represent the xGNP particles, which were used to modify the control asphalt in the experiments. The components of the control asphalt model were based on the previous study by the authors. The xGNP modified asphalt model was prepared using the same conditions and procedures from the experiments. After calculating different properties, the following summaries can be drawn.

(1) The density of the xGNP modified asphalt model is higher than that of the control asphalt, and it indicates that the addition of xGNP model increases the density of the asphalt model. The test process of the bulk modulus in the laboratory was simulated using MD algorithm, and the bulk moduli of the control and xGNP modified asphalt

were calculated with two methods. There is no difference between the results from the two methods. The bulk moduli of the models linearly decrease with the increase in temperature. The trends of the bulk modulus in the MD simulations agree with those of the reference and laboratory data. The difference between the simulation and experimental results was observed due to the time scale and limited molecules.

(2) The test process of the Young's modulus in these asphalt models was simulated using the MD method, and the Young's modulus of the models was calculated based on the second regression method. The Young's moduli of these models increase linearly with decreasing test temperature. The trend of Young's modulus in MD simulations is similar as the predicted trend in the experiments. The Young's moduli of the control and xGNP modified asphalt models are larger than laboratory data, and it is caused by several factors: time steps, simulation time, and molecular numbers.

(3) The shear modulus of these asphalt models was calculated by applying the small shear strain in one direction (XY direction) to these models based on the first method mentioned above. The shear moduli of these asphalt models decrease exponentially with increasing test temperature. The trends in the MD simulation data of these asphalt models fit the regressed curves of the experimental results. The Young's moduli of these models are higher than the experimental results. The large modulus of the models is induced by the time scale and limited molecules in MD simulations. However, it can be predicted that if the test temperature is lower than 273 K, the shear modulus of the asphalt models would be close to the experimental data, as well as the Young's modulus and bulk modulus.

(4) Poisson's ratios of these asphalt models are also obtained from different modulus results. The range of Poisson's ratio is the same as that of the experimental data. It implies that the stress response of asphalt models is reasonable after applying the small strain to these models.

In this chapter, the modulus properties of the control and xGNP modified asphalt models were analyzed and compared. The trends in different moduli of the asphalt models were the same as those of the experimental results, and good predications of Poisson's ratio in the asphalt models were observed. The contributions of this study include (1) the use of the NPH ensemble to obtain the Young's modulus of the asphalt models with the Amber Cornell Extension Force Field, (2) a method using NVT and SLLOD algorithm to calculate the bulk and shear moduli of the asphalt models with the Lee-Edwards boundary conditions, and (3) the rules for producing data in MD simulation by applying a correlation analysis. Even though a large difference between the simulation and experimental data was observed, which is likely due to the time frame and complexity as well as the elastic response of the model materials, the research method is useful for the simulation of other materials. In addition, future research of our group would focus on the self-healing properties of the asphalt models and lessening differences between the simulation and laboratory results.

6.8 Acknowledgements

The authors appreciate the financial support of the U.S. National Science Foundation (NSF) under grant 1300286. The computational studies were performed using computer cluster (Superior Research Center) at Michigan Technological University. Any

opinion, finding, and conclusion expressed in this paper are those of the authors and do not necessarily represent the view of any organization.

Chapter 7 Molecular Dynamics (MD) simulations of the diffusion of the asphalt binder on aggregates

7.1 Overview

This study aims to understand the mechanism of the self-healing and diffusion of the asphalt on aggregates. The microscale asphalt mastic samples were prepared with asphalt and fine aggregates of a small size (below 0.3 mm). The microscale dynamic X-ray computed tomography were conducted to capture the asphalt self-diffusion process in a microscale asphalt mastic sample controlled at 80^{o}C using the Advanced Photon Source (APS) beamline 2-BM at Argonne National Laboratory. The contact angle, activation energy and Mean Squared Displacement (MSD) were analyzed to describe the self-healing behaviors of the asphalt materials. The Molecular Dynamics (MD) method was employed to simulate the asphalt molecular diffusion process at different temperatures, and to compute the contact angle between the asphalt and aggregate models. The contact angle goniometer was selected to measure the contact angle between the asphalt droplet and aggregates at different temperatures. The results of tests and MD simulations show that (1) the asphalt diffused after heating from the x-ray images, and the stages and mechanism of the diffusion process of the asphalt on the aggregates were investigated; (2) the low contact angle was observed in the interface model of asphalt and aggregates at high temperatures using the MD method. The wetting condition changed from partial non-wetting to wetting

---

The full text of this chapter will be submitted for publication.

after heating in the interface model. The molecules of the asphalt model at high temperatures moved faster than under low temperatures; (3) the test results of the contact angle between the asphalt and aggregates demonstrated self-diffusion process of the asphalt material. The test data was also compared with the MD simulation results at different temperatures.

7.2 Introduction

7.2.1 Self-healing of asphalt materials

Asphalt is a kind of temperature-dependent material, and research for the self-healing properties of the asphalt materials has been studied for many years since the concept of the autonomic healing was brought up by S. R. White in Nature magazine in 2001. The cracking of the materials can lead to mechanical degradation and electrical failure. A new structural polymer material with the self-healing function was invented, and a microencapsulated healing agent was released once the crack occurred in this polymer. The toughness of this polymer can be recovered up to 75% [199]. The self-healing concept was introduced and extended to other materials, such as polymers, metals, and asphalt materials. Recently, the fracture-healing-re-fracture test (FHR) with the morphological analysis was used and developed to understand the self-healing capability of the asphalt materials [200]. The increased temperature and time were useful for the self-healing capability, and a master curve for the recovery strength was developed. The healing process of the asphalt binder was also observed by the fluorescence microscopy [200]. However, it is better to use the scanning electron microscope (SEM) to understand the microstructure changes of the healing process, and more details may be elaborated [8, 41]. During the self-

healing evaluation tests, it is common that the repeated loads and recoveries of the asphalt binders or mixtures were used. Two healing indices (the modulus ratio and cycle number ratio) of the asphalt binder were introduced and studied for the self-healing properties [201].

The asphalt mastic is also a self-healing material, and the properties and healing rate are largely affected by the temperature. The differential equations for equilibrium temperatures in the asphalt mastic surface were developed, and the model parameters were derived from the infrared cameras [202]. The steel wool was also used to reinforce the asphalt mixture/concrete, and the fatigue resistance of the modified asphalt mixture was studied. The extension ratio of the fatigue life and stiffness recovery were introduced to evaluate the self-healing effect, and the induction healing can improve the self-healing effect and durability of the asphalt mixtures [203].

Molecular Dynamics (MD) is a kind of new method to understand and explore the materials on an atomic scale. Currently, few researchers studied the physical properties of the asphalt binder or asphalt mixtures using MD method [182], as well as self-healing properties. At the University of Texas at Austin, the self-healing properties were recently modeled by the researchers. The influence of healing on the fatigue-cracking of asphalt binders was studied and the MD model of an asphalt binder was created to predict the healing effect. The self-diffusion effect of binder molecules flowed across the crack interface. The relationship of the molecular length or branching to the self-diffusivity property in asphalt was studied [91]. The interface model between the asphalt and aggregate was also created to study and analyze the mechanism of the moisture damage of asphalt mixtures, and the adhesion energy was adopted to explain the moisture

susceptibility [39]. It is a promising way to use the MD method to study and analyze the self-healing properties of the asphalt material. In this paper, the MD method was employed to study the self-healing properties (contact angle) and the diffusion (Mean Squared Displacement) to understand the molecular movement of the asphalt material.

7.2.2 Wetting theory

Wettability is the tendency of a liquid (asphalt) to spread on the solid substrate (aggregates), and it can be related to the diffusion and healing properties of asphalt. It is commonly measured by the contact angle (equation (7.1)) among three phases: solid, liquid and gas. The degree of the wetting is balanced by the adhesive and cohesive forces (Figure 7.1). When a liquid drop is on a solid substrate, the contact angle is zero, and it means the liquid is perfectly wetting on the solid substrate. If the contact angle is 180^o, it indicates perfectly non-wetting [204]. The wetting condition relates to the properties of the interface between the liquid and substrate. It is acceptable that this concept was generalized to the asphalt material for the interface evaluation. It is known that the macro performance of asphalt mixtures can be predicted and speculated from the wettability of the asphalt binder on the aggregates. It is common that there are two kinds of wettings, non-reactive or reactive wetting. The non-reactive wetting is discussed in this case since the PG 58-28 base asphalt is used on the aggregates and it is likely that there is no chemical reaction between the base asphalt and aggregates.

$$\gamma_{SG} = \gamma_{SL} + \gamma_{LG} cos\theta \tag{7.1}$$

where, γ_{SG} is the surface tension/energy between the solid and gas; γ_{SL} is the surface tension/energy between the solid and liquid; γ_{LG} is the surface tension/energy between the liquid and gas; and θ is the contact angle between the three phases.

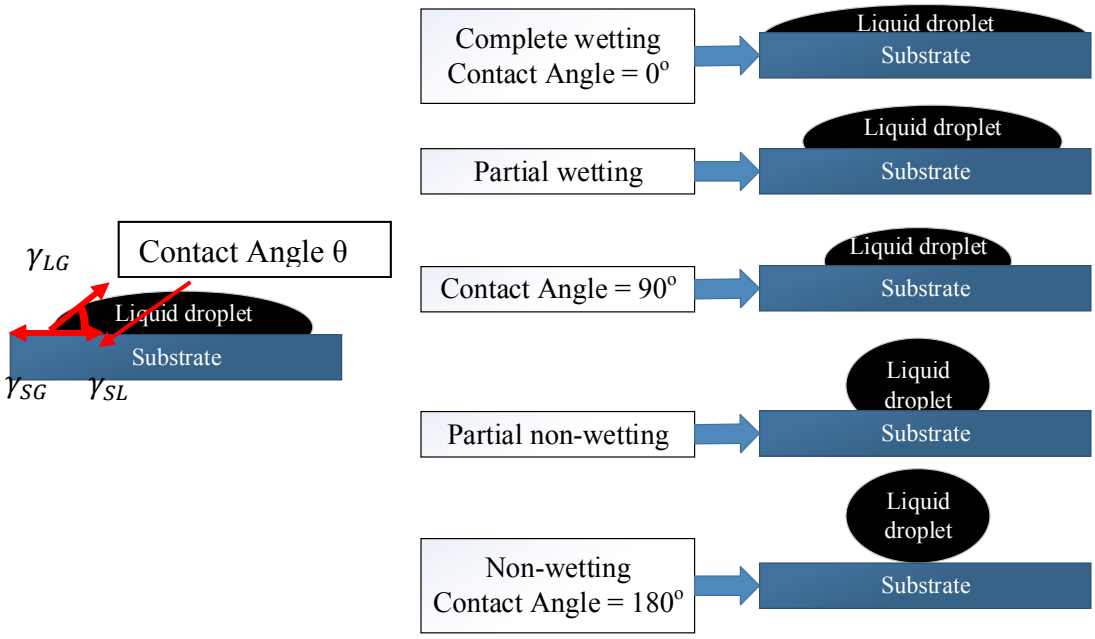

Figure 7.1. A liquid droplet on a solid substrate under different conditions

7.3 Scopes and Objectives

The objective of this study is to explore and understand the mechanism of the self-healing and diffusion of the asphalt materials. The flow of the asphalt binder in the asphalt mastic was studied from the images obtained by the x-ray beamline in Argonne National Laboratory around 353.15 K (80°C). The self-diffusion of the asphalt binder on the aggregates was investigated both computationally and experimentally. The MD interface model was created, and the MD method was used to calculate the contact angle between the asphalt and aggregate models, and analyze the diffusion of the asphalt model on the aggregate model. In addition, the contact angle goniometer was used to test the contact

angle between the asphalt and aggregates in the laboratory in order to compare with the MD simulation results.

7.4 Morphological Analysis

The self-diffusion of asphalt is a key component for self-healing of the asphalt binder in asphalt mixtures, and the self-healing properties can be directly affected by the ambient temperature. The self-diffusion of the asphalt was conducted in Argonne National Laboratory, and the x-ray beamlines can be customized by the need of research. It is also known that the interface interaction between the aggregates and asphalt is complicated, and the asphalt mastic samples are selected to study the self-diffusion of asphalt. In the x-ray tests, the PG 58-28 asphalt binder was used and 10% content of the asphalt was adopted by the weight of aggregates. The aggregate size used to make the asphalt mastic is below 0.3mm and the gradation of the aggregates in the mastic samples are shown in Table 7.1. The asphalt mastic samples were mixed and filled into a small tube with a diameter of 1.63 mm and a height of around 2 cm. The small tube was installed on the base, and placed in the furnace with the desired temperatures. The samples were tested by the x-ray beam line at different temperatures in Advanced Photon Source of Argonne National Laboratory. The x-ray test results of the asphalt mastic samples are shown in Figure 7.2 through Figure 7.3. After scanning the samples, the asphalt mastic samples were reconstructed and are shown in Figure 7.2. The reconstructed samples were easily visualized before and after heating, and the dimensions of samples were displayed. Through these visualized samples, the separated slices from visualized samples were extracted and analyzed. The two positions in the visualized samples were observed and analyzed, the images are shown in Figure 7.3.

Table 7.1. The aggregates size and mass used to make the asphalt mastic samples

Aggregate Size	Weight used in the sample (gram)	Details
No.50	343.91	0.3mm
No.100	185.18	0.15mm
No.200	198.41	0.075mm
Dust Filler	145.5	<0.075mm
PG 58-28 Asphalt	87.3	10% wt by the aggregates

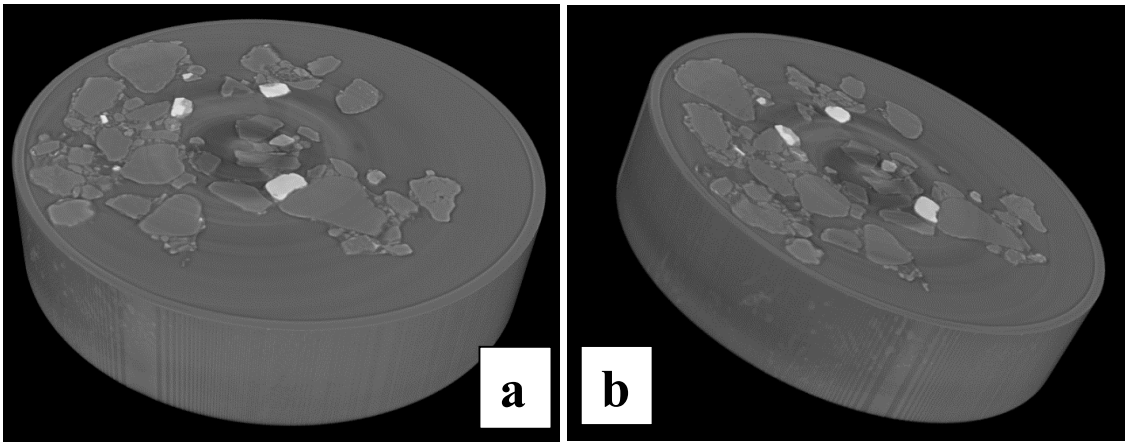

Figure 7.2. Reconstructed images for the tested asphalt mastics (diameter: 1.63mm, height: 0.4mm): a) initial state of the asphalt mastic; b) the asphalt mastic at 353.15 K (80^{o}C) after three and half hours heating

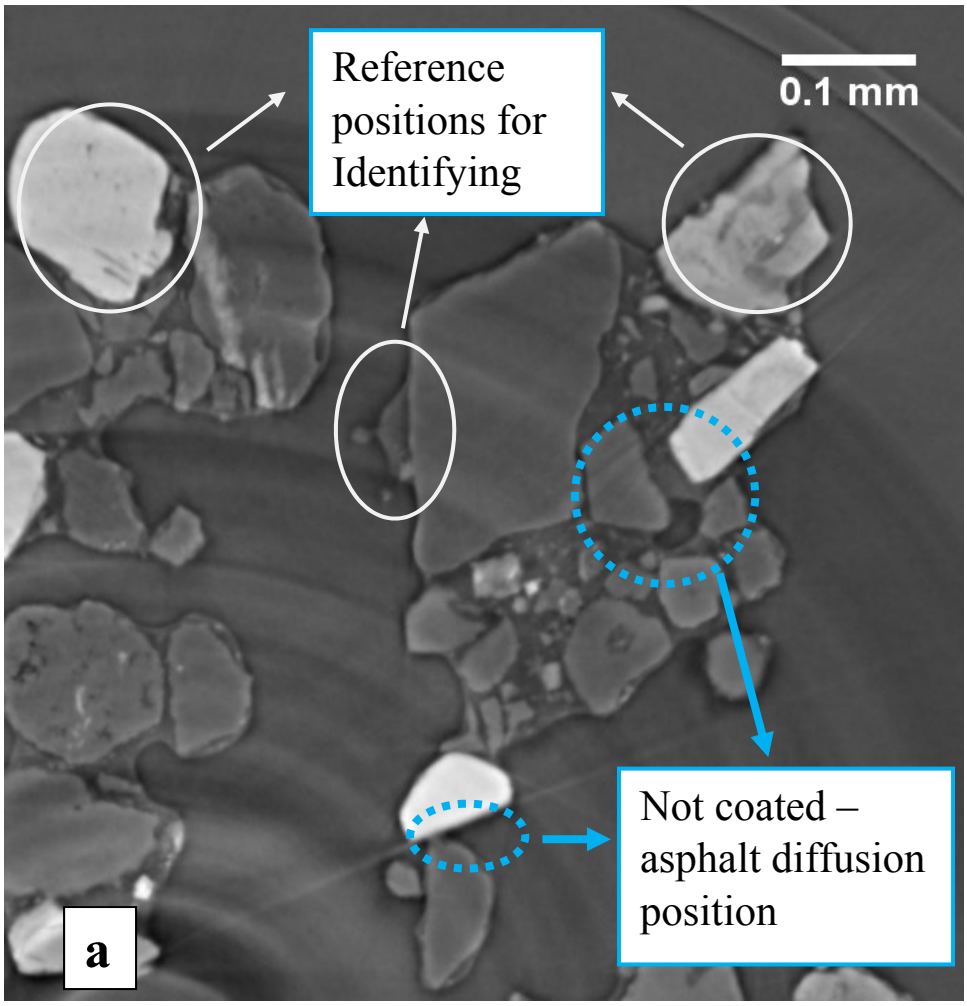
Reference positions for Identifying
0.1 mm
Not coated – asphalt diffusion position
a

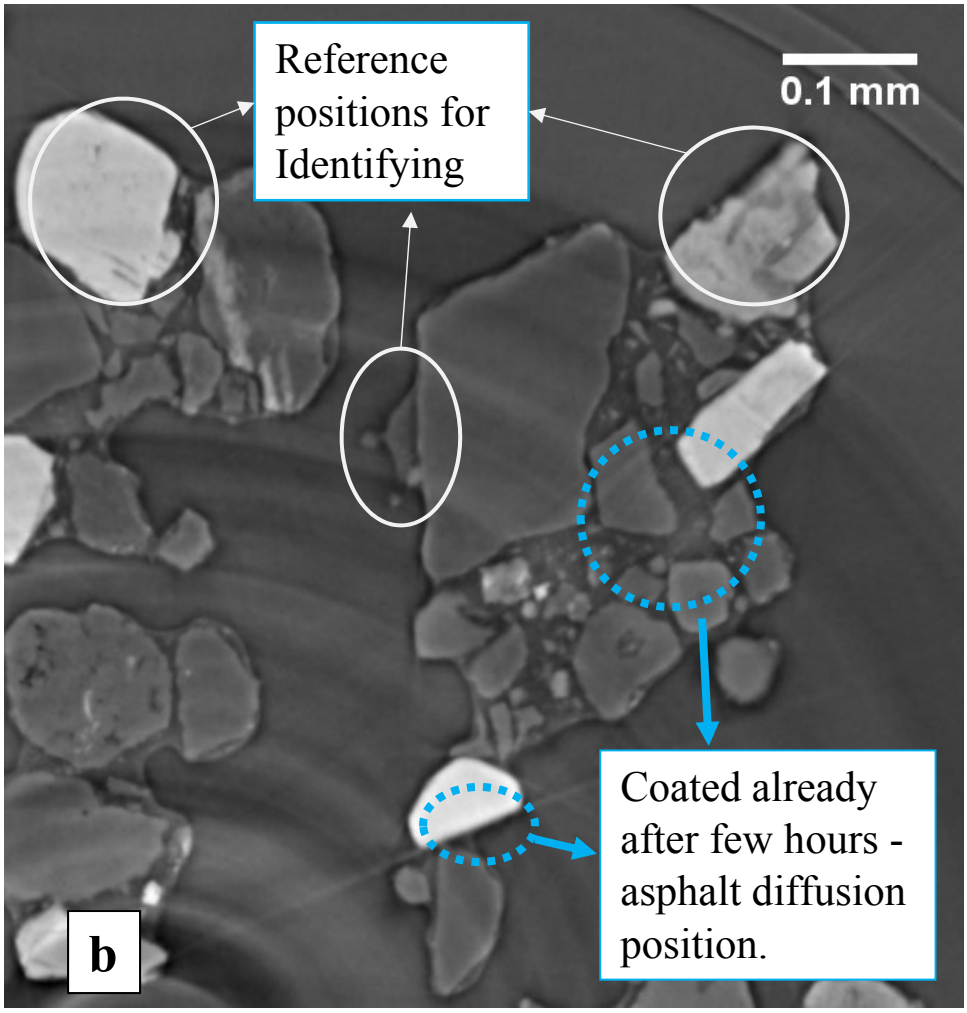

Figure 7.3. Asphalt diffusion in the small tube during heating – position 2: a) the initial image of the asphalt mastic; b) the image of the asphalt mastic at 353.15 K (80°C) after three and half hours heating

Figure 7.3 shows the self-diffusion positons of the asphalt binder through identifying the reference positions of aggregates in the asphalt mastics. The initial and healed states of the asphalt mastics were compared, the asphalt binder flowed definitely after heating. During heating for hours, the asphalt moved to coat aggregates at the micro level (Figure 7.3b). It indicates that the self-diffusion effect is a key part for self-healing properties, and it also helps coat aggregates in the mixing and compaction. Based on the literature review [200, 205, 206], the normal asphalt content for the asphalt mastic ranges

from 18% to 50% by weight of aggregates. In this case, the 10% asphalt by the weight of aggregates was adopted to prove the asphalt binder flow at the high temperatures, even at the condition of the low amount of the asphalt binder in the asphalt mastic. The cross sections of the sample in the figures were cut along with the tube length direction. In these figures, (1) the asphalt binder on the aggregates trended to the uniform state; (2) few areas on the aggregates are not coated by the asphalt (Figure 7.3a); (3) the aggregates are assumed as the substrate relative to the asphalt, and it is a liquid-air system at the high temperatures; (4) the free asphalt binder exists in this system and it is enough to coat all aggregates. The temperature dependence property of asphalt determines the states of asphalt from liquid to solid at different temperatures. The asphalt binder would be in the liquid state at high temperatures. From these images, it is inferred that the heating processing provided enough energies (necessary activation energy and kinetic energy) to force more free asphalt to squeeze the air and move to coat the aggregate. It is assumed that the first step of this movement is that the asphalt in the tube moves from the high coating areas of asphalt to low coating areas of asphalt (Figure 7.4). The activation energy of the asphalt was required for starting to move. The necessary activation energy of the asphalt binder can be calculated from the Arrhenius equation [207] (equation (7.2)). The second step of this movement is that the contact area between the asphalt and aggregates increases, and the contact angle between the asphalt and aggregates decreases after heating or energy input due to the balance of adhesive and cohesive forces of asphalt and aggregates (Figure 7.4).

$$\eta = Ae^{\frac{E_f}{RT}} \quad \text{and} \quad ln\eta = \frac{E_f}{RT} + lnA \tag{7.2}$$

Where η is the viscosity index of the asphalt (Pa.s), T is the kelvin absolute temperature (K), A is a fitting coefficient, E_f is the activation energy for initiating the asphalt flow (J), and R is the universal gas constant (8.314 $J.mol^{-1}.K^{-1}$).

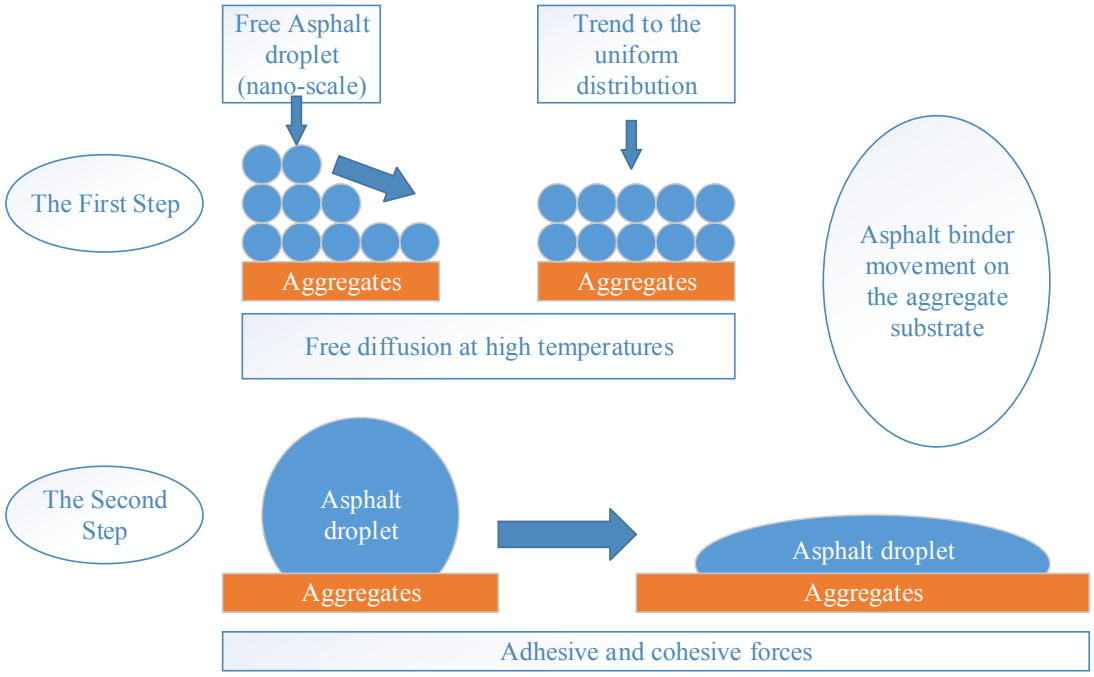

Figure 7.4. A diagram of the diffusion of the asphalt binder on the aggregates

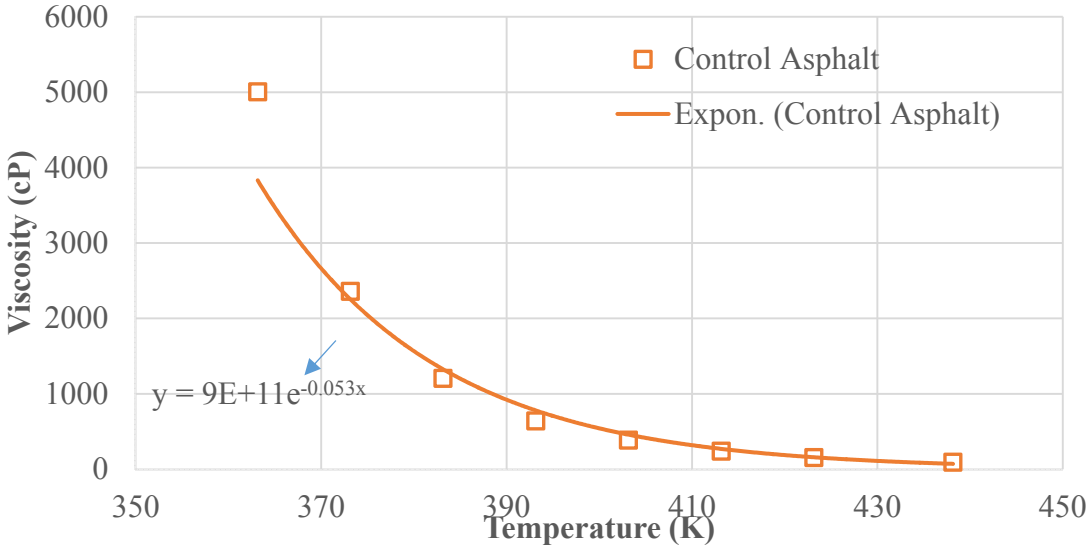

(a) the viscosity results of the asphalt binder

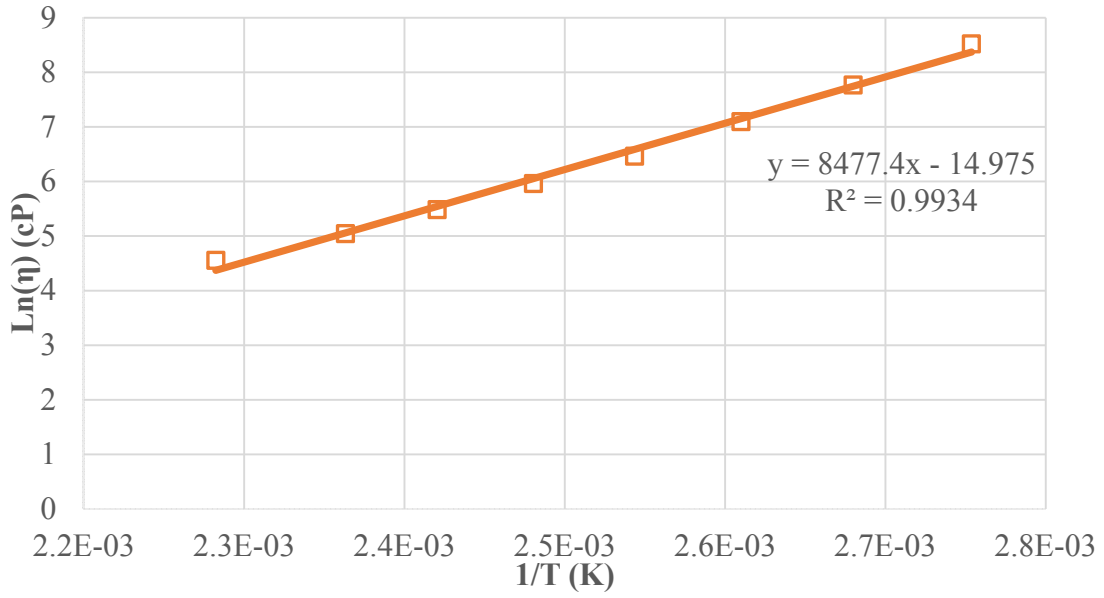

(b) the regression calculation between the ln η and 1/T

Figure 7.5. The viscosity and activation energy calculation of the asphalt binder

The viscosity of the asphalt binder was required to calculate the activation energy, and the viscosity of the asphalt was tested by the rotational viscometer in the laboratory. The viscosity and activation energy of the asphalt binder were calculated based on the equation (1). The calculation results are shown in Figure 7.5. Figure 7.5 shows the viscosity results and regression calculation of the asphalt binder. The activation energy of the asphalt binder is 70481.1036 J/mol after the calculation. It means the threshold energy for flowing of asphalt. It is better to have a lower activation energy for self-healing functions.

It is envisaged that if the tube is filled by the water, the water cannot move freely in the tube. The density of water is close to the asphalt. The gravity of materials in the tube can be ignored in this case. Therefore, the surface tensions or adhesive and cohesive forces could be one of explanation directions for flowing (Figure 7.4). These forces make asphalt

have a contractive tendency of the surface that allows it to resist an external force caused by kinetic energies. The heating of asphalt increases the kinetic energy of asphalt binder. The asphalt fluid needs to maximize the contact surface areas against the inward attractive/cohesive forces, the asphalt is also attracted by the adhesion energy between the asphalt binder and aggregates. Then, the asphalt binder trends to coat the aggregates more, and the contact angle between the asphalt and aggregates decreases. The added energy leads to the asphalt flow and aggregate coatings, and the increased contact area between the asphalt and aggregates causes the decrease of adhesion energy. The predictions and explanations for the asphalt flow can also be verified and validated by Molecular Dynamics method and contact angle goniometry.

7.5 Molecular Dynamics (MD) method on asphalt diffusion

7.5.1 MD study for contact angles

The asphalt flows on the aggregates during heating, and the contact angle between the asphalt and aggregates decreases. The Molecular Dynamics method was employed in this study to verify the predictions and explanation mentioned above. The interface model between the asphalt and aggregates was created, and there are two models, top (asphalt) and down (aggregates) models. The model of the silicon dioxide (SiO_2) was used to represent the aggregate in the interface model, and the asphalt model was created with a density of around 1.0 g/cm^3 based on the previous study of the authors [182]. The asphalt model consists of three components: asphaltenes, aromatics and saturates with the Amber Cornell Extension Force Field (ACEFF, equation (7.3) [182]), at a ratio of 5:27:41. The distance between the asphalt and aggregates is around 2 Å in the interface model, and the

interface model (total 12026 atoms) with a periodic boundary condition (PBC) is shown in Figure 7.6.

$$E_{total} = \sum_{bonds} K_r(r - r_{eq})^2 + \sum_{angles} K_\theta(\theta - \theta_{eq})^2 + \sum_{dihedrals} \frac{V_n}{2}[1 + \cos(n\varphi - \gamma)] + \sum_{i<j}[\frac{A_{ij}}{R_{ij}^{12}} - \frac{B_{ij}}{R_{ij}^{6}} + \frac{q_i q_j}{\epsilon R_{ij}}] \quad (7.3)$$

where, r_{eq} and θ_{eq} are the structural parameters under the equilibrium state; K_r and K_θ are the force coefficients; n and γ are the torsional angle parameters; A, B and q are the non-bonded potentials for all atom pairs; R_{ij} is the distances of the atoms and ϵ is the well depth for the van der Waals energy.

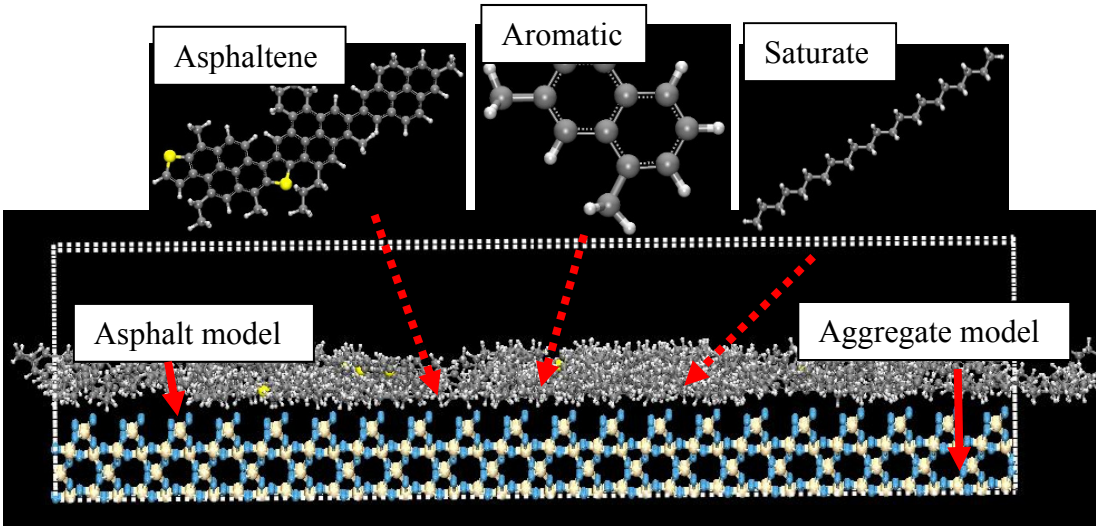

Figure 7.6. Interface model between the asphalt and aggregates. Note: the grey atom for Carbon; the white atom for Hydrogen; the yellow atom for Sulfur; the blue atom for Oxygen; and the brown atom for silicon.

After the generation of the MD interface model, the conjugate gradient [72] and particle-particle particle-Mesh Ewald (PPPM) methods [79] were used to optimize the system energy and calculate the long-range coulombic interactions. The canonical

ensemble (NVT) was applied to the interface system with the Nose-Hoover thermostat. The positions and velocities of atoms in the interface model were updated each timestep. There are two ways to simulate the healing process during heating in the asphalt-aggregate system: (1) the temperature ramp in the interface was set from 298.15 K (25^{o}C) to 353.15 K (80^{o}C) in one simulation during the running time (5ns), and it is similar to the test process in the laboratory (Method One); (2) the different temperatures were selected, and each single temperature was set up in each MD simulation (Method Two). The specific locations (left corner marked in Figure 7.7) of the interface model were monitored during the MD simulation, and the contact angle between the aggregates and asphalt in the interface model was calculated at the final timestep. The locations of the atoms were recorded in the interface model based on the calculation method one (temperature ramp), and the images from OVITO (Open Visualization Tool) [208] are output and shown in Figure 7.7 (Method One).

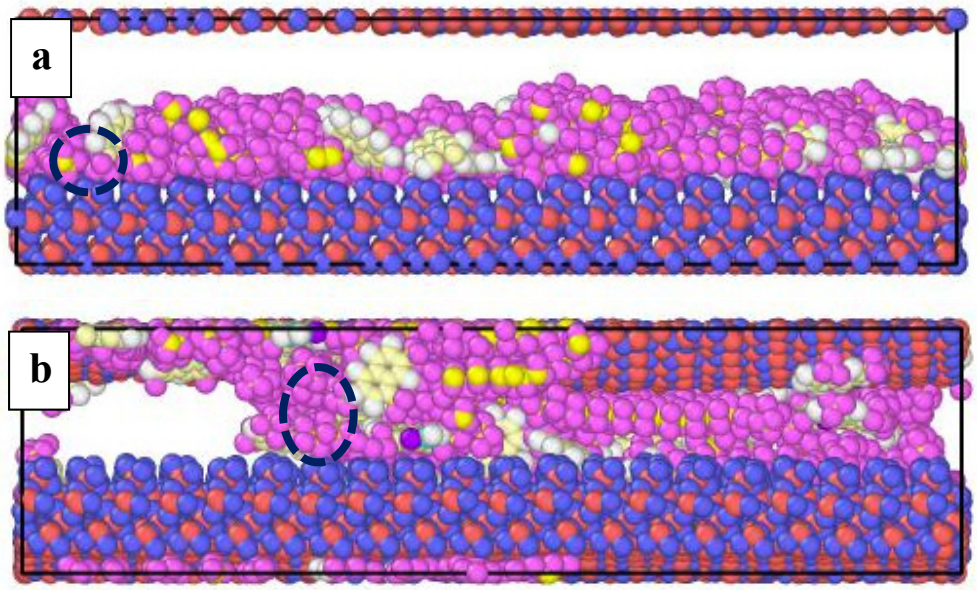

Figure 7.7. The images of the interface model under different conditions: a) the initial interface structure before heating; b) the interface structure after 5ns heating. Note: Eight types of atoms in the interface model (OS (blue), Si (red), CA (light yellow), CT (Yellow), HC (light purple), HA (white), SS (purple), and CC (light blue) with different colors), OS type for the ether or ester oxygen; Si type for the silicon atom. CA type for sp2 aromatic carbon in 6-membered ring with 1 substituent; CC type for sp2 aromatic carbon in a 5-membered ring with 1 substituent and next to a nitrogen; CT type for aliphatic carbon (tetrahedral); HC type for hydrogen bonding hydrogen (charged group); HA type for aliphatic or aromatic hydrogen; and S type for sulfur in disulfide linkage or methionine.

Figure 7.7 shows the structures of the interface model: a) after the energy optimization, and b) after the NVT simulation during 5ns heating in the system. In Figure 7.7a, the locations and velocities of molecules of the asphalt model in the top level were updated after the optimization of the conjugate method. The molecules in the asphalt model were relatively stable, and the structure of the asphalt model was monitored. The contact angle between the asphalt and aggregates in the interface model was estimated in the left corner (constant position, circled in Figure 7.7a), and it was averaged, 140.7^{o}. This is the initial step for the NVT simulation for self-diffusion of the molecules of asphalt. In Figure 7.7b, the molecules of the asphalt model moved up after heating, and adhered to the upper aggregate model due to the adhesion energy between the asphalt and aggregate models in

the periodic boundary condition. It indicates that the self-diffusion of the molecules of the asphalt occurs in these MD models. The molecules of the asphalt model diffused, and aggregated together like a circle, which is similar to the asphalt droplet in the contact angle test (mentioned in the following section). A long simulation time, 5ns, was set up in the model, and it is enough time for the models to relax in the temperature ramp (298.15 K to 353.15 K). The structure of the interface model was imaged at the final timestep, and the contact angle between the asphalt and aggregate in the interface model at the left corner was also computed. The angle data was averaged, 52.6^{o}. Based on the theory of wetting tendency (Figure 7.1), the wetting condition between the asphalt and aggregates is partial non-wetting at the initial state, and the wetting condition changes to the partial wetting at the end state after heating. It indicates that there is a non-reactive wetting between the asphalt and aggregates, and the asphalt does not tend to spread on aggregates under the equilibrium state at room temperature. However, after heating, the contact angle of asphalt-aggregate changes, and the asphalt spreads on the aggregate substrate. It is consistent with the assumption made in section: morphological analysis. The heating provides the kinetic energy for asphalt, and the energy reaches the activation energy. The asphalt starts to move and spread on the aggregates. In addition, the NVT was applied to the interface model under each single temperature for the calculation and verification of the contact angle (Method Two). The molecular structures of MD interface models at the end timestep are shown in Figure 7.8.

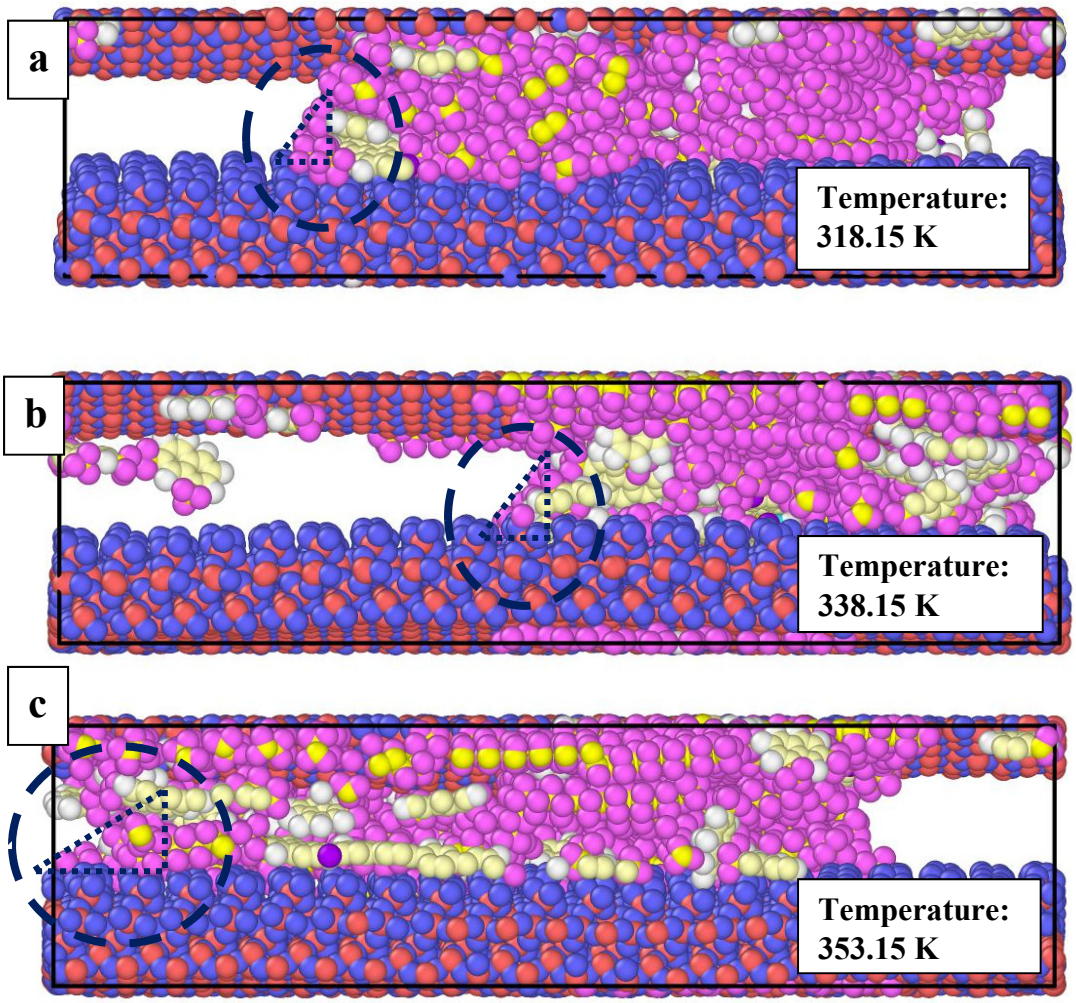
a
Temperature:
318.15 K
b
Temperature:
338.15 K
c
Temperature:
353.15 K

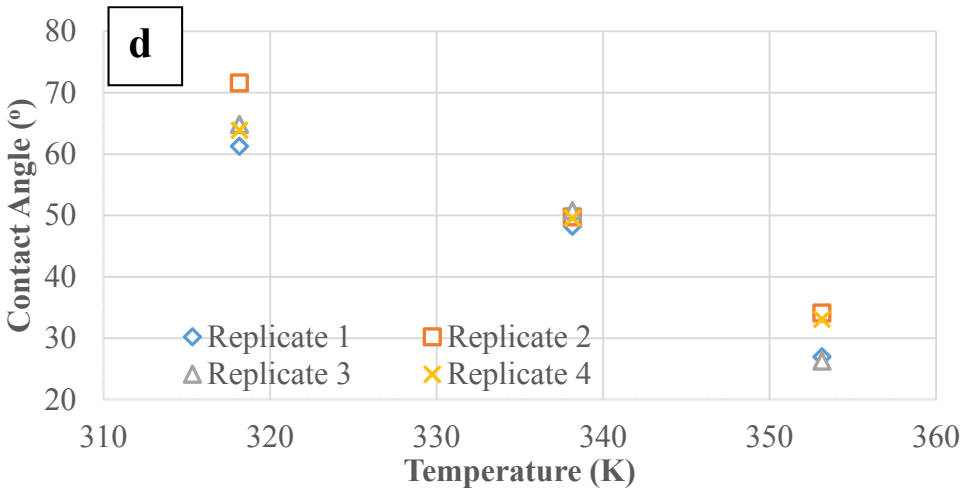

Figure 7.8. The images of the interface model at different temperatures: a) the image of the final timestep (5ns) at 318.15 K; b) the image of the final timestep (5ns) at 338.15 K; c) the image of the final timestep (5ns) at 353.15 K; d) contact angles at different temperatures.

Figure 7.8 shows that the molecular structures of the interface models under different temperatures at the final timestep, as well as the contact angles. The contact angles from Figure 7.8a to Figure 7.8c were calculated at left corner of the interface model at different temperature, and the angles were averaged and shown in Figure 7.8d. In Figure 7.8d, the contact angle of asphalt-aggregate decreases with the increase of the temperature in the interface model from 318.15 K to 353.15 K. The averaged contact angle of the interface model at 318.15 K is 65.9°, 49.6° at 338.15 K, and 29.1° at 353.15 K. The asphalt-aggregate interface is partial wetting at these temperatures. It also coincides with the assumption made in section: morphological analysis. When heating the asphalt on aggregates, the energy of asphalt reach the activation energy and diffuses. The contact area between the asphalt and aggregates increases, and the contact angle of asphalt-aggregate decreases. It is extrapolated that the contact angle decreases linearly when heating asphalt on the aggregate substrate. In addition, the MD simulation on diffusion of the interface

model can also explain the diffusion of the asphalt binder on aggregates in the images obtained from Argonne National Laboratory.

7.5.2 MD study for movements of the asphalt binder

Mean square displacement (MSD) is to measure the deviation or movement over time of atoms/molecules between the targeted and reference positions (equation (7.4)). It is common to understand the spatial distribution of molecules under random motions in the molecular structures. The MSD over time can relate to the diffusion coefficients of the materials, and the activation energy can also be linked using Arrhenius law from diffusion coefficients. In the self-healing process of asphalt, the activation energy can be considered as the energy required for the movement of molecules. The motions of molecules in the interface model were updated, and the mobility and activity of molecules were also monitored, as well as the orientation. It is useful for understanding the molecular properties of the materials. In this study, the squared displacements (dx, dy and dz, three directions) were recorded at different temperatures during NVT simulations for interface models, as well as total squared displacement. The MSD results of asphalt molecules in interface models are shown in Figure 7.9.

$$MSD = \frac{1}{T}\sum_{t=1}^{T}(x(t) - x_0)^2 = dx^2 + dy^2 + dz^2 \quad (7.4)$$

where, T is the averaged time; x_0 is the reference position of the particles/atoms.

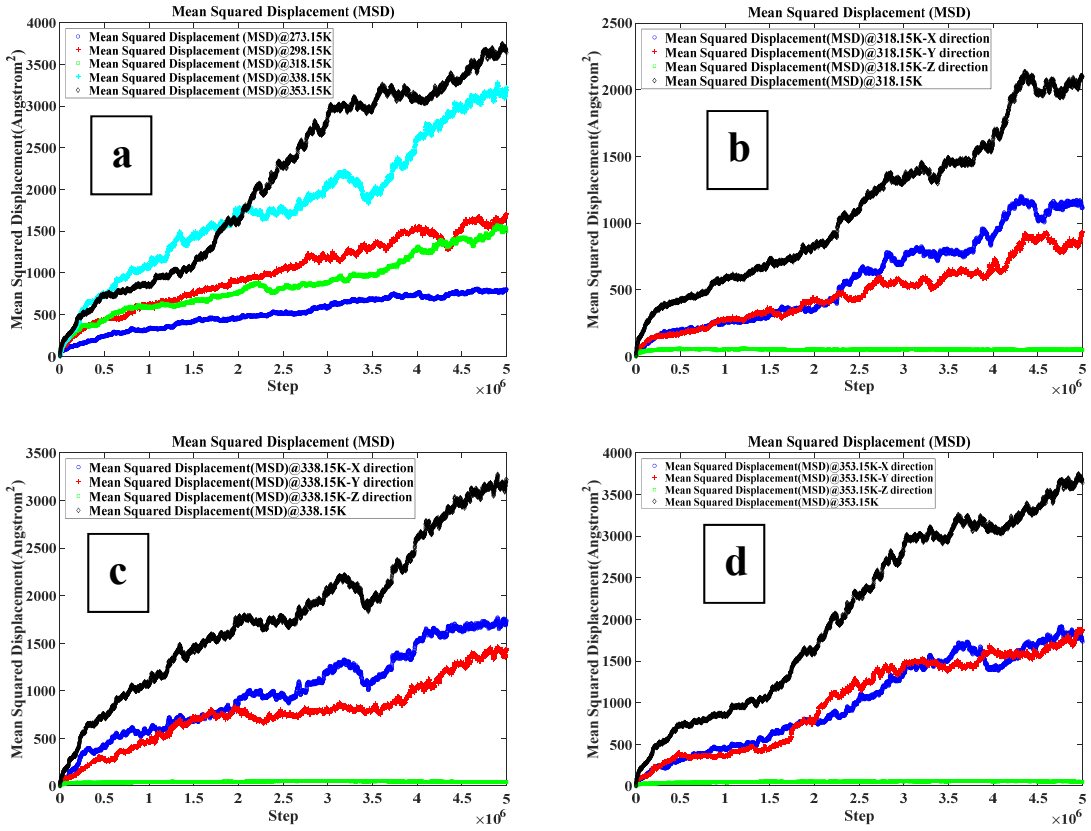

Figure 7.9. Mean Squared Displacement (MSD) of asphalt molecules in interface models under different temperatures: a) mean squared displacements of molecules of asphalt in the interface model at different temperatures; b) squared displacements (dx, dy, and dz) at 318.15 K; c) squared displacements (dx, dy, and dz) at 338.15 K; d) squared displacements (dx, dy, and dz) at 353.15 K

Figure 7.9 shows that squared displacements of molecules of asphalt in interface models along three axial directions at different temperatures. In Figure 7.9a, the MSD of molecules of asphalt at 353.15 K is larger than MSDs at other temperatures. It implies that the high temperature accelerates the movements of molecules and moves further due to more thermal energies input. However, there is a difference or reverse trend between 298.15 K and 318.15 K. This phenomenon is caused by the glass transition of this asphalt model. The glass transition temperature of the asphalt model is around 300 K [182], and the specific energy is required for the glass transition. In Figure 7.9b and Figure 7.9c, the

squared displacement along x direction at the temperature of 318.15 K and 338.15 K is also greater than the squared displacements of molecules of asphalt along y and z directions. The squared displacement along z direction was restricted by the periodic boundary condition (the asphalt model layered by the aggregate model, similar to real asphalt mixture). The squared displacements along x and y directions at the temperature of 353.15 K (Figure 7.9d) are the same, and it infers that the high temperature also is helpful for molecules of asphalt to diffuse at a same speed to different directions. Therefore, the low contact angles of the asphalt-aggregate model at high temperatures were observed in the interface model, and the high MSDs of the molecules of the asphalt model in the interface model were also recorded at high temperatures. The input thermal energy is useful for the diffusion of the asphalt binder.

7.6 Contact Angle Test

The contact angle was computed through the MD simulations in previous section, the contact angle test was also evaluated by the contact angle measuring instrument, KRÜSS G10. The Drop Shape Analysis (DSA) was used to process the image and determine the contact angle. The Young-Laplace equation (equation (7.5)) was used to fit the shape line of the sessile drop. The density of the asphalt droplet is around 1.0 g/cm^3, which is the same as water. The equilibrium of the asphalt droplet is balanced by the surface tension and its weight. In the laboratory, the asphalt droplet was dropped on the aggregate at room temperature, and the samples were heated by oven or infrared light. It is assumed that the surface tension and its weight of asphalt was based on those of water in these tests due to the test limitations. Four samples are selected in the tests, and two samples are shown

in Figure 7.10. The test images of asphalt-aggregate at different temperatures from one sample (sample A) are represented and shown in Figure 7.11.

$$\Delta p = \gamma(\frac{1}{R_1} + \frac{1}{R_2}) \tag{7.5}$$

where, Δp is the pressure difference; γ is the surface tension; R_1 and R_2 are the principle radii of curvature.

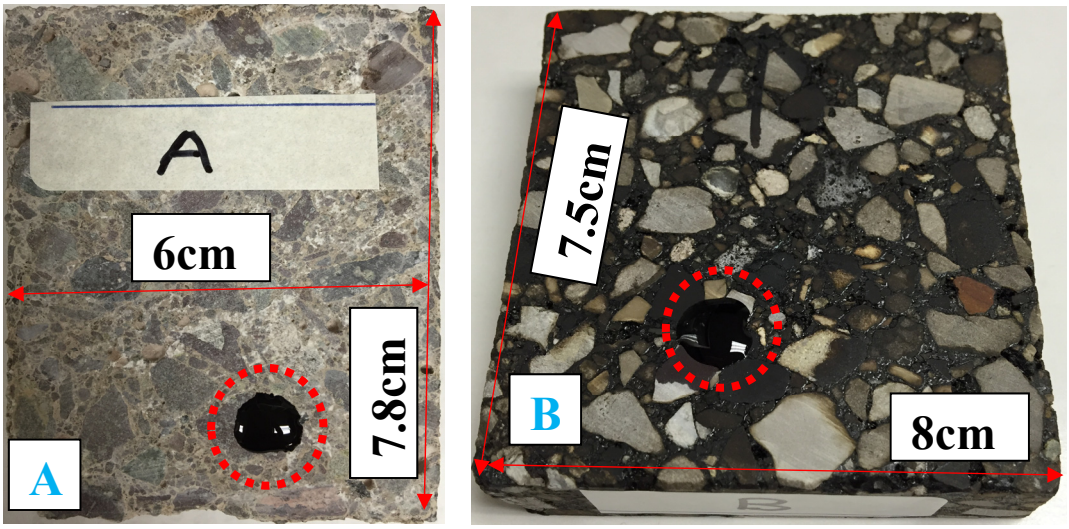

Note: (A: the base is the concrete sample, and the asphalt was dropped on the aggregates. B: the base is the asphalt mixture. The white means aggregates, and the black is the asphalt mastic. The asphalt was dropped on the white part, aggregates. It is easier to cut the concrete and asphalt mixture samples than the small aggregates)

Figure 7.10. The samples after contact angle tests: an asphalt droplet on the aggregates (large aggregates are selected in the asphalt mixture or concrete samples)

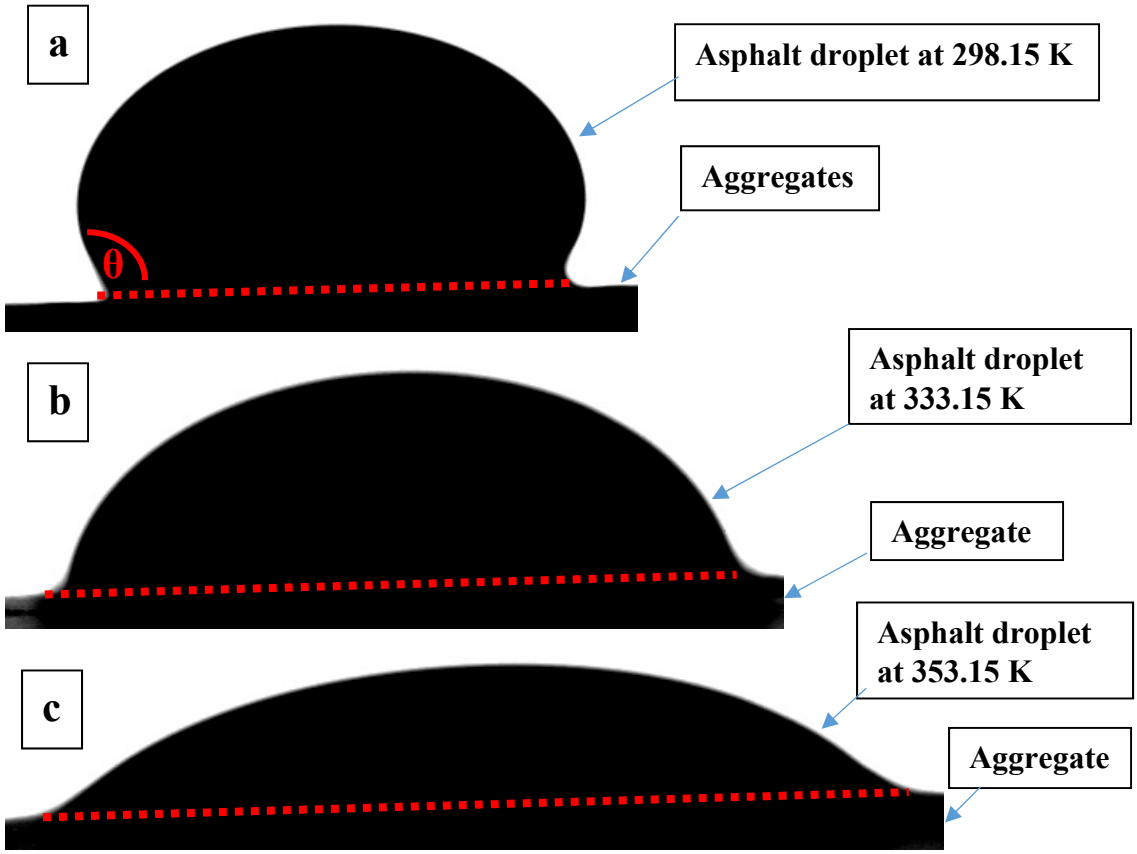

Figure 7.11. The asphalt droplet on the aggregates: a) contact angle at 298.15 K; b) contact angle at 333.15 K; c) contact angle at 353.15 K

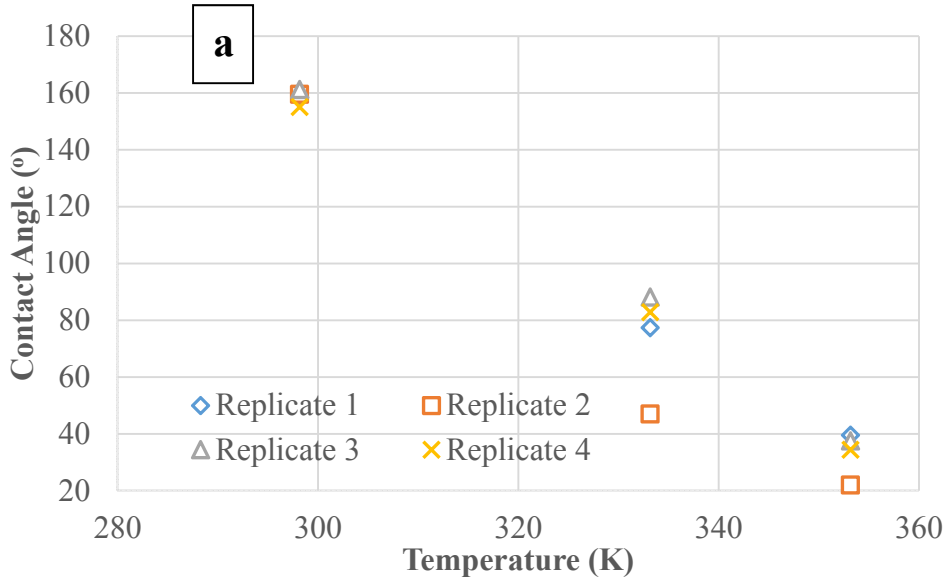

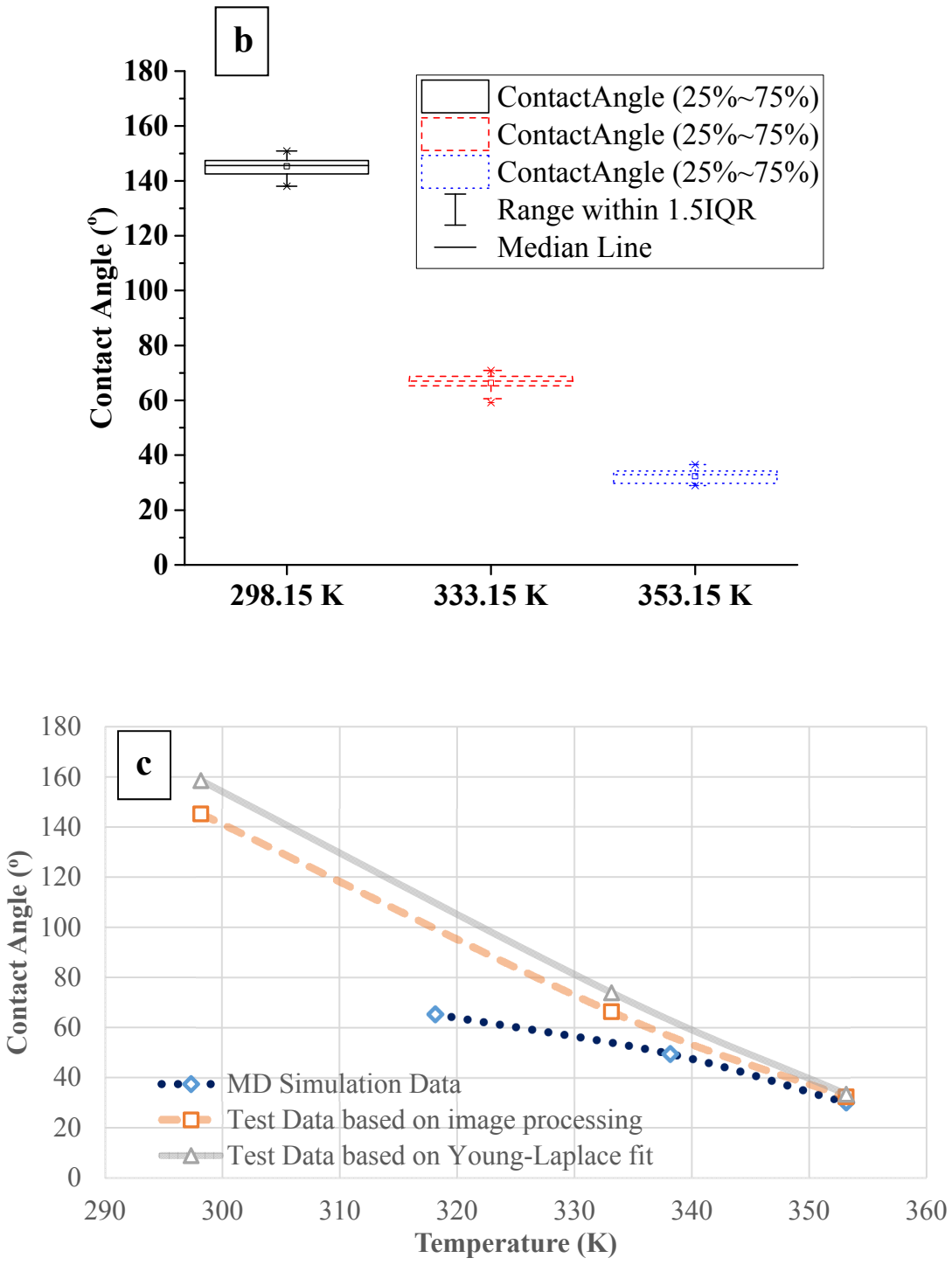

Figure 7.12. Contact angles between the asphalt droplet and aggregates at different temperatures: a) using the Young-Laplace fit to calculate the contact angle; b) to measure the contact angle by image processing (IQR, interquartile range; outlier, more than 1.5 IQRs); c) comparison between MD simulation and test data.

Figure 7.11 displays that the asphalt droplets on the aggregates at different temperatures, (298.15 K (25^{o}C), 333.15 K (60^{o}C), and 353.15 K (80^{o}C)). It is apparent that the contact angle between the asphalt and aggregates changes with different temperatures, the angle decreases with increasing the test temperature. The angle is obviously higher than 90^{o} at 298.15 K, and it infers partial non-wetting between the asphalt and aggregates. However, the angle is lower than 90^{o} from 333.15 K, and it indicates the interface state of asphalt-aggregate is changed from partial non-wetting to partial wetting after heating. After the Young-Laplace fit or simple measurement (ImageJ), the contact angles between the asphalt droplet and aggregates are shown in Figure 7.12. In Figure 7.12a and Figure 7.12b, it is obvious that there is one common point: the angle decreases with increasing the test temperatures. Minor difference between two calculation methods at the temperature of 298.15 K was observed, and no much difference at other temperatures. It is most likely caused by the difference of surface tension between the asphalt and water, but the difference is tiny. Therefore, the assumption is validated that the surface tension and its weight of asphalt was based on those of water in these tests. The diffusion of the asphalt binder on the aggregates was reproduced step by step in the experiments. In addition, based on the data in Figure 12c, there is also minor difference of the contact angle between the test results and MD simulations (298.15 K: around 150^{o}; 333.15 K: around 65^{o}; and 353.15 K: around 30^{o}). Therefore, the temperature definitely affects the contact angle between the asphalt and aggregates, and determines the wetting condition of the interface.

We also performed one-way analysis of variance (ANOVA) to evaluate whether the three levels of temperature produce different contact angles shown in Figure 7.12b.

There was a statistically significant effect of types of temperature (the p-value < 0.0001). The multiple comparisons with the Bonferroni correction at α=0.05 showed that all three pairs of differences among means of temperature are statistically different, indicating that the contact angle is sensitive to different levels of temperatures. In addition, a trend analysis of contact angle at α=0.05 for this design also showed a strong negative linear trend of temperature with the p-value less than 0.0001.

7.7 Discussions and Conclusions

In this chapter, the diffusion of the asphalt binder in the asphalt mastic sample was explored and discussed based on the image data produced by the beam line in Argonne National Laboratory. The molecular dynamics method was employed to simulate and explain the diffusion of the asphalt binder in the mastic. The contact angle between the asphalt and aggregates was also used to validate the diffusion steps of the binder in the mastic. After evaluation of the test and simulation data, the following conclusions are summarized.

(1) The asphalt binder diffused after heating in the asphalt mastic from the images, and the activation energy of the asphalt binder was mentioned and calculated for the PG 58-28 binder. The diffusion steps of the asphalt binder was also proposed by a diagram, and the assumption of diffusion of the asphalt binder on aggregates was made. This assumption was verified and validated by the MD simulations and contact angle tests.

(2) The interface model of the asphalt binder and aggregates was built with the Amber Cornell Extension Force Field. The conjugate gradient method was used to optimize the interface system energy. The NVT ensemble was applied to the interface system to

analyze the contact angle between the asphalt model and aggregate model at different temperatures. The high contact angle was observed in the interface system at low temperatures (around or below room temperature), and low contact angle was monitored at high temperatures (around 318.15 K (45^{o}C)). The wetting state of the interface between the asphalt binder and aggregates transforms from partial non-wetting to partial wetting after heating. The asphalt tends to coat more on aggregates under high temperatures. The mean squared displacements were also employed to analyze the movement of molecules of the asphalt model, and the reference positions or locations were averaged in the interface models. The MSD results indicate that the high temperature provides more kinetic energy for movement of molecules, and causes the molecules move fast in the asphalt model.

(3) The contact angle goniometer was used to evaluate the contact angle between the asphalt droplet and aggregates. The temperature largely influences the contact angle of asphalt-aggregate samples. The wetting condition of the interface between the asphalt and aggregates definitely changes from partial non-wetting to partial wetting. The high temperature provides the energy for the asphalt to spread on the aggregates. The results from MD simulations and assumptions are in agreement with the contact angle tests.

Therefore, the diffusion phenomena and mechanism of the asphalt on the aggregates were explored and analyzed. The diffusion of the asphalt also relates to the self-healing properties. In addition, our group would focus on more quantitative analysis of the diffusion in the future plan.

7.8 Acknowledgements

The authors appreciate the financial support of the U.S. National Science Foundation (NSF) under grant 1300286. The computational studies were performed using computer cluster (Superior research center) at Michigan Technological University. This research used resources of the Advanced Photon Source, a U.S. Department of Energy (DOE) Office of Science User Facility operated for the DOE Office of Science by Argonne National Laboratory under Contract No. DE-AC02-06CH11357. Any opinion, finding, and conclusion expressed in this paper are those of the authors and do not necessarily represent the view of any organization.

Chapter 8 Conclusions and Recommendations

In this dissertation, a comprehensive literature review of Molecular Dynamics (MD) application in the field of civil engineering was completed, and the properties of the base and modified asphalt models were investigated using the MD method, and the properties include density, glass transition temperature, viscosity, thermal conductivity, modulus, etc. The relationships of asphalt-aggregate and asphalt-modifier were explored and discussed, as well as the self-diffusion mechanism of the asphalt binders. The MD simulation data was compared to the experimental results. In addition, the recommendation and future works are also made in this dissertation.

8.1 Summary

8.1.1 The properties of the base asphalt model

The asphalt model with three components was used to mimic the asphalt in this experimental MD simulation, and the Amber Cornell Extension Force Field was employed in the asphalt model. The NWChem analysis was applied to calculate and assign the ESP charge to the asphalt components. The conjugate gradient method, particle mesh Ewald method, and Savitzky-Golay filter were used to optimize the system energy and data smoothing. The physical properties of the asphatl1 model were computed including the density, glass transition temperatures, viscosity, and bulk modulus. The computational results and conclusions in the asphatl1 model are drawn.

(1) During the asphalt model building process, the three components, asphaltenes, aromatics and saturates, were represented by asphaltene, dimethylnaphthalene, and

docosane, respectively, and the ratio of the three components in the asphalt model was 5:27:41. The conjugate gradient and NWChem were applied to the asphatl1 model with the Amber Cornell Extension Force Field for optimizing the energy and geometry.

(2) The densities of the asphalt model at different temperatures using the Amber Cornell Extension Force Field were closer to the laboratory densities and reference data from Zhang and Greenfield [5]. The density property was also used to validate the asphalt model.

(3) The glass transition temperatures of asphalt can be a small temperature range due to the complex composition of the asphalt, and the temperatures can be varied from the sources and components. The glass transition temperatures were computed based on the relationship between the temperatures and specific volumes. The glass transition temperature of the asphalt model with the Amber Cornell Extension Force Field was narrowed down into one small temperature range (around 300 K) compared to the wide reference range (298 K to 353 K) from Zhang and Greenfield [5], based on the laboratory testing data.

(4) There were four methods to calculate the viscosity in material engineering [25], and the Muller-Plathe algorithm was utilized to compute the viscosity of the asphalt model in this experimental MD simulation. The results of the asphalt model using the Muller-Plathe method in the rNEMD simulation are closer to the laboratory testing data compared to the reference data from Zhang and Greenfield [5] using the Green-Kubo and Einstein methods.

(5) The bulk modulus was computed by applying volumetric and small strains to three coordinates of the asphatl1 model. The stress response in the mode was monitored, and

the stress results in three coordinates were averaged for the calculation of the bulk modulus. The bulk modulus of the asphalt model is closer to the laboratory data than the reference data from Zhang and Greenfield [5].

8.1.2 The relationship between asphalt and aggregates

The control and NHL modified asphalt were tested by FTIR ATR to analyze the polar groups with carbonyl in the asphalt at a liquid state. Parts of the control and the NHL modified asphalt mixture samples tested by TSR were also used to be extracted by solutions. These solutions contained the polar functional groups that were detected by the FTIR ATR to analyze the carbonyl groups in the asphalt. The mechanical driving reasons between the asphalt-aggregate and aggregate-water systems were explored and discussed for the water damage of asphalt mixtures using molecular dynamics simulations. Based on the data analysis of extracted control and NHL modified asphalt, the following conclusions can be drawn.

(1) During asphalt oxidation, the resins and maltenes in the asphalt help generate polar group components, including carbonyl groups, sulfoxide groups and nitrogen oxides. The carboxylic acids and ketones are the major products in the oxidized asphalt, which also produces high amounts of anhydrides. The limited amount of amides, esters and aldehydes in the oxidized and extracted asphalt is detected in this study. The carboxylic acids, ketones and anhydrides may be the pivotal components in the asphalt that link to the rutting and moisture resistance in asphalt mixtures, as well as the bonding strength between the asphalt and aggregates. The asphalt aging definitely improves the moisture resistance in wet environments at an early stage. However, the long-term aging of

asphalt causes the degradation of bonding strength between the asphalt and aggregates, as well as the fatigue life and water resistance.

(2) The interface MD models of asphalt-aggregate and aggregate-water systems are generated to simulate the mechanism that produces asphalt-aggregate adhesion energy, and also mimic the interactions between aggregates and asphalt/water. The potential energies of each MD interface system and separated systems (asphalt, water and aggregate) are computed to determine the bonding energy of each system. The difference of adhesion energies between the asphalt-aggregate and aggregate-water systems is the fundamental reason for moisture damage in asphalt mixtures. The water tends to adhere to aggregates rather than asphalt under the same conditions. In addition, from investigating the different adhesive strength between the aggregate and asphalt with/without the carboxylic acid group (aging group), the moderately aged asphalt has improved the adhesion and, thus, helped to resist moisture damage in asphalt mixtures.

8.1.3 The properties of the modified asphalt binder model

The MD model of multi-layer graphite nanoplatelets (xGNP) was created and used for the investigation of the effect of modification on the control asphalt model. The control asphalt model was composed of three components: asphaltenes, aromatics, and saturates. The xGNP modified asphalt model was generated from the addition of the xGNP model in the control asphalt model. The conjugate gradient method and PPPM were used for energy optimization, and the Savitzky-Golay filter was used for smoothing data. The Amber Cornell Extension Force Field was used in these asphalt models, and the physical properties

of the models were calculated including density, the glass transition temperature, viscosity, and thermal conductivity.

(1) The densities of these asphalt models were computed, and the addition of the multi-layer xGNP model increased the density of the xGNP modified asphalt model compared to that of the control asphalt model. The molecular number in MD systems significantly affects the data variation for density calculation. The density of MD asphalt systems decreases with the increase in temperature.

(2) The glass transition temperature of the xGNP modified asphalt model is around 250 K, and it is better than the results of the reference, 298 K to 358 K [13]. This glass transition temperature is better than previous results (around 300 K [182]) for the control asphalt model, because it is the same as the glass transition temperature of SHRP asphalt binders, around 250 K, from laboratory results [115].

(3) The Muller-Plathe method was used to calculate the viscosity of the control and xGNP modified asphalt models. The twenty layers in the MD asphalt models were separated for this calculation. The addition of xGNP particles in the control asphalt matrix improves viscosities of the modified asphalt at different temperatures, and the same effect of multi-layer xGNP models in the control asphalt model was observed. Compared to the experimental viscosities of the xGNP modified asphalt, the viscosities of the MD simulation is close to the experimental results at the temperatures of 403 K, 423 K, and 443 K. The relationship between viscosities and temperatures in the data of the MD simulation is also the same as that of the laboratory results.

(4) The experimental data shows that the xGNP particles in the control asphalt increase the thermal conductivity of the modified asphalt at room temperature. During the calculation of thermal conductivity, the Muller-Plathe method was used in these MD simulations, and the multi-layer xGNP model in the control model also improves the thermal conductivity of the xGNP model at room temperature. The thermal conductivity of the control and xGNP modified asphalt increase with increasing temperatures, and the same trend is observed in the data of MD simulations.

8.1.4 The modulus of the base and modified asphalt binder models

The control and xGNP modified asphalt binders were simulated in this study using the Molecular Dynamics (MD) method, and different properties of these asphalt models were simulated and computed. The multi-layer graphene model was generated to represent the xGNP particles, which were used to modify the control asphalt in the experiments. The components of the control asphalt model were based on the previous study by the authors. The xGNP modified asphalt model was prepared using the same conditions and procedures from the experiments. After calculating different properties, the following summaries can be drawn.

(1) The density of the xGNP modified asphalt model is higher than that of the control asphalt, and it indicates that the addition of the xGNP model increases the density of the asphalt model. The test process of the bulk modulus in the laboratory was simulated using MD algorithm, and the bulk moduli of the control and xGNP modified asphalt were calculated with two methods. There is no difference between the results from the two methods. The bulk moduli of the models linearly decrease with the increase in

temperature. The trends of the bulk modulus in the MD simulations agree with those of the reference and laboratory data. The difference between the simulation and experimental results was observed due to the time scale and limited molecules.

(2) The test process of the Young's modulus in these asphalt models was simulated using the MD method, and the Young's modulus of the models was calculated based on the second regression method. The Young's moduli of these models increase linearly with decreasing test temperature. The trend of Young's modulus in MD simulations is similar to the predicted trend in the experiments. The Young's moduli of the control and xGNP modified asphalt models are larger than laboratory data, and it is caused by several factors: time steps, simulation time, and molecular numbers.

(3) The shear modulus of these asphalt models was calculated by applying a small shear strain in one direction (XY direction) to these models based on the first method mentioned above. The shear moduli of these asphalt models decrease exponentially with increasing test temperature. The trends in the MD simulation data of these asphalt models fit the regressed curves of the experimental results. The Young's moduli of these models are higher than the experimental results. The large modulus of the models is induced by the time scale and limited molecules in MD simulations. However, it can be predicted that if the test temperature is lower than 273 K, the shear modulus of the asphalt models would be close to the experimental data, as well as the Young's modulus and bulk modulus.

(4) Poisson's ratios of these asphalt models are also obtained from different modulus results. The range of Poisson's ratio is the same as that of the experimental data. It

implies that the stress response of asphalt models is reasonable after applying the small strain to these models.

8.1.5 The self-healing mechanism of the asphalt binder

The diffusion of the asphalt binder in the asphalt mastic sample was explored and discussed based on the image data produced by the beam line in Argonne National Laboratory. The molecular dynamics method was employed to simulate and explain the diffusion of the asphalt binder in the mastic. The contact angle between the asphalt and aggregates was also used to validate the diffusion steps of the binder in the mastic. After evaluation of the test and simulation data, the following conclusions are summarized.

(1) The asphalt binder diffused after heating in the asphalt mastic from the images, and the activation energy of the asphalt binder was mentioned and calculated for the PG 58-28 binder. The diffusion steps of the asphalt binder was also proposed by a diagram, and the assumption of diffusion of the asphalt binder on aggregates was made. This assumption was verified and validated by the MD simulations and contact angle tests.

(2) The interface model of the asphalt binder and aggregates was built with the Amber Cornell Extension Force Field. The conjugate gradient method was used to optimize the energy of the interface system. The NVT ensemble was applied to the interface system to analyze the contact angle between the asphalt model and aggregate model at different temperatures. The high contact angle was observed in the interface system at low temperatures (around or below room temperature), and a low contact angle was monitored at high temperatures (around 318.15 K (45^{o}C)). The wetting state of the interface between the asphalt binder and aggregates transforms from partial non-

wetting to partial wetting after heating. The asphalt tends to coat more on aggregates under high temperatures. Mean squared displacements were also employed to analyze the movement of molecules of the asphalt model, and the reference positions or locations were averaged in the interface models. The MSD results indicate that the high temperature provides more kinetic energy for movement of molecules, and causes the molecules to move fast in the asphalt model.

(3) The contact angle goniometer was used to evaluate the contact angle between the asphalt droplet and aggregates. The temperature largely influences the contact angle of asphalt-aggregate samples. The wetting condition of the interface between the asphalt and aggregates definitely changes from partial non-wetting to partial wetting. The high temperature provides the energy for the asphalt to spread on the aggregates. The results from MD simulations and assumptions are in agreement with the contact angle tests.

8.2 Conclusions

Based on the summary and findings from these chapters, the conclusions can be drawn as follows:

(1) Three components (asphaltenes, aromatics and saturates) were selected and mixed to represent the asphalt model. The physical properties of the asphalt model computed in the experimental MD simulation include density, glass transition temperature, viscosity, and the bulk modulus. The computational results of the physical properties of the asphalt model are generally better than the reference data from Zhang and Greenfield [5]. Therefore, the asphalt model in this study has a relatively good prediction for the properties compared to the reference model [5] due to the use of the Amber Cornell

Extension Force Field and the ESP charge, as well as new calculation method for viscosity. Furthermore, the calculation and optimization methods used in this manuscript are promising ways to simulate the materials, such as the numerical procedures to generate the asphalt model and optimize the system energy, and to calculate the physical properties and process the data of the simulation. The contributions of this chapter are as follows: 1) The modified force field, Amber Cornell Extension Force Field, was applied to the components of the asphalt model, as well as the ESP charge and the optimization method, conjugate gradient method. This force field and ESP charge can also be applied to other materials; and 2) The Muller-Plathe method (a kind of NEMD method) was used to calculate the viscosity of the asphalt model.

(2) With chemical extraction, the polar and non-polar components in the asphalt were separated and analyzed to link the moisture susceptibility of asphalt mixtures with FTIR characterization. Ketones, carboxylic acids and anhydrides are the main compounds during asphalt oxidation in this study, and these also relate to the pavement performance. The MD simulations discovered the difference in adhesive strength between asphalt-aggregate and aggregate-water systems. The analysis results explained the chemo-physical properties of asphalt related to the moisture damage in asphalt mixtures. The contributions of this chapter are as follows: 1) The six functional groups with the carbonyl group in the aged asphalt were found using the FTIR images; 2) ketones, carboxylic acids and anhydrides are main compounds; 3) mild aging is good for resistance to moisture damage in the asphalt mixture from MD results; 4) the

adhesion energy of the interface was calculated through MD methods; and 5) the aged components of the asphalt model were proposed.

(3) The multi-layer xGNP graphite particles in asphalt can improve the viscosity and thermal conductivity of the modified asphalt, and the xGNP graphite model in the control asphalt model can also enhance the density, glass transition temperature, viscosity and thermal conductivity. It is obvious that the same trend of experimental data and MD results is observed during the testing and MD calculation of different properties of asphalt. It is likely that the xGNP particles can be utilized and generalized for pavement construction and heat sink. The contributions of this chapter include 1) the use of the xGNP graphite particles to enhance the performance of the asphalt binder, 2) the generation of the xGNP model for the modification of the asphalt model, 3) the application of the Muller-Plathe method to compute the thermal conductivity of the asphalt models, and 4) the use of the correlation analysis to reveal the linear relationship in MD simulation data.

(4) The modulus properties of the control and xGNP modified asphalt models were analyzed and compared. The trends in different moduli of the asphalt models were the same as those of the experimental results. The contributions of this chapter include 1) the use of the NPH ensemble to obtain the Young's modulus of the asphalt models with the Amber Cornell Extension Force Field, 2) a method using NVT and SLLOD algorithm to calculate the bulk and shear moduli of the asphalt models with the Lee-Edwards boundary conditions, and 3) the rules for producing data in MD simulation by applying a correlation analysis. Even though a large difference between the simulation and experimental data was observed, which is likely due to time frame and complexity

as well as the elastic response of the model materials, the research method is useful for the simulation of other materials.

(5) The diffusion and its mechanism of the asphalt binder on the aggregates were explored and analyzed. The diffusion of the asphalt also relates to the self-healing properties. The contact angle between asphalt and aggregates decreased with the increase in temperatures. The contributions of this chapter include 1) the detected diffusion of the asphalt binder on aggregates using the X-ray test; 2) the introduction of the contact angle method for self-diffusion analysis between the asphalt binder and aggregates from both sides, MD simulation and tests; 3) analyzed movements of the components in the asphalt model; and 4) nanoscale movement simulated using the MD method.

8.3 Recommendations and future works

MD method is a new analysis and simulation tool for the researchers. Many advantages of the MD method were mentioned in the dissertation, and it is beneficial to use the MD method to explore mechanisms and applications for material developments. Based on the experience and results of the MD method obtained in this dissertation, the following recommendations are made.

(1) The new asphalt model could be generated to better represent the real asphalt, which will contain more related components. The new model will be validated and the properties of the model are computed using different MD methods. New asphalt models or methods will be developed to narrow the differences between the simulation and the laboratory data.

(2) The diffusion coefficients of the asphalt model and its components will be calculated and linked to the self-healing properties under different temperatures. The Radial Distribution Function (RDF) of each component in the asphalt binder model will be calculated to determine the molecular/atomic movements.

(3) The issue of aging of the asphalt binder model is always a hot topic for researchers. The aging effect and mechanism of the asphalt or asphalt model is needed to be explored and discussed thoroughly. The different components in the asphalt may have a different aging process with the ReaxFF (reactive force field), and the extent of the aging of components is also an important issue to be understood using MD simulations.

(4) More quantitative analysis on the diffusion and reactions between asphalt and modifiers will be explored and discussed using MD simulations. The solubility parameters of the components and asphalt will be analyzed under different solutions.

(5) The molecular orientation and relaxation time under different loadings of the asphalt models can be deeply studied for the modification, as well as the loading rate. The moisture susceptibility and movements of asphalt-aggregate are significant subjects for the improvement of performance in the asphalt mixtures, and it is helpful to use the MD method to understand more comprehensively. The details of these topics would be discussed in future research.

References

[1] Y. Zhanping, G.S. Wei, R.C. Williams, Development of Specification for the Superpave Simple Performance Tests (SPT): Final Report, in, Michigan Department of Transportation, Lansing, 2009, pp. 220.

[2] L.N. Mohammad, W.H. Daly, I.I. Negulescu, Z. Wu, C. Daranga, Investigation of the Use of Recycled Polymer-Modified Asphalt in Asphaltic Concrete Pavements, in, Louisiana State University, Baton Rouge, Louisiana Transportation Research Center, Federal Highway Administration, 2004, pp. 94p.

[3] K.K. M. W. Witczak, T. Pellinen, M. El-basyouny and H. Von Quintus, Simple Performance Test for Superpave Mix Design (NCHRP Report 465), in, Arizona State University, Tempe, AZ, 2002, pp. 114.

[4] Y. Yildirim, M. Solaimanian, T.W. Kennedy, Mixing and compaction temperatures for hot mix asphalt concrete, in, The University of Texas at Austin, Center for Transportation Research, 2000, pp. 1-99.

[5] M.L. Greenfield, Molecular modelling and simulation of asphaltenes and bituminous materials, International Journal of Pavement Engineering, 12 (2011) 325-341.

[6] Asphalt Institute, Superpave Performance Graded Asphalt Binder Specification and Testing. Superpave Series No 1(SP-1), Lexington KY, USA, 2003.

[7] H. Yao, Z. You, L. Li, C.H. Lee, D. Wingard, Y.K. Yap, X. Shi, S.W. Goh, Rheological Properties and Chemical Bonding of Asphalt Modified with Nanosilica, Journal of Materials in Civil Engineering, 25 (2013c) 1619-1630.

[8] H. Yao, Z. You, L. Li, X. Shi, S.W. Goh, J. Mills-Beale, D. Wingard, Performance of asphalt binder blended with non-modified and polymer-modified nanoclay, Construction and Building Materials, 35 (2012) 159-170.

[9] G.W. Tillson, Street Pavements and Paving Materials. a Manual of City Pavements: The Methods and Materials of Their Construction. 1st Ed, 1900.

[10] H.J.H.C.A. Collins, Principles of road engineering, Arnold, London, 1947.

[11] A.P. Karvonen, T.U.o.T.a.A. Community, R. Planning, Botanizing the Asphalt: Politics of Urban Drainage, University of Texas at Austin, 2008.

[12] A. Bandyopadhyay, G.M. Odegard, Molecular modeling of crosslink distribution in epoxy polymers, Modelling and Simulation in Materials Science and Engineering, 20 (2012) 045018.

[13] L. Zhang, M.L. Greenfield, Analyzing Properties of Model Asphalts Using Molecular Simulation, Energy & Fuels, 21 (2007) 1712-1716.

[14] H. Yao, Z. You, L. Li, S.W. Goh, C.H. Lee, Y.K. Yap, X. Shi, Rheological properties and chemical analysis of nanoclay and carbon microfiber modified asphalt with Fourier transform infrared spectroscopy, Construction and Building Materials, 38 (2013b) 327-337.

[15] Z. You, J. Mills-Beale, J.M. Foley, S. Roy, G.M. Odegard, Q. Dai, S.W. Goh, Nanoclay-modified asphalt materials: Preparation and characterization, Construction and Building Materials, 25 (2011) 1072-1078.

[16] Y. Yildirim, Polymer modified asphalt binders, Construction and Building Materials, 21 (2007) 66-72.

[17] A.I. Al-Hadidy, Y.-q. Tan, Mechanistic analysis of ST and SBS-modified flexible pavements, Construction and Building Materials, 23 (2009) 2941-2950.

[18] H. Zhang, Y. Wang, Y. Wu, L. Zhang, J. Yang, Study on flammability of montmorillonite/styrene-butadiene rubber (SBR) nanocomposites, Journal of Applied Polymer Science, 97 (2005) 844-849.

[19] M. Witczak, I. Hafez, X. Qi, Laboratory characterization of Elvaloy® modified asphalt mixtures: vol, in, I–Technical report.‖ College Park, Maryland: University of Maryland. Dupont< http://www. dupont. com/asphalt/link5. html>(November, 2010), 1995.

[20] J.W. Oliver, Modification of paving asphalts by digestion with scrap rubber, Transportation Research Record, 821 (1981) 37.

[21] X. Shu, B. Huang, Recycling of waste tire rubber in asphalt and portland cement concrete: An overview, Construction and Building Materials, 67 (2014) 217-224.

[22] Q. Dai, Z. Wang, M.R. Mohd Hasan, Investigation of induction healing effects on electrically conductive asphalt mastic and asphalt concrete beams through fracture-healing tests, Construction and Building Materials, 49 (2013) 729-737.

[23] H. Chen, Q. Xu, Experimental study of fibers in stabilizing and reinforcing asphalt binder, Fuel, 89 (2010) 1616-1622.

[24] B.J. Putman, S.N. Amirkhanian, Utilization of waste fibers in stone matrix asphalt mixtures, Resources, Conservation and Recycling, 42 (2004) 265-274.

[25] E. Ahmadinia, M. Zargar, M.R. Karim, M. Abdelaziz, P. Shafigh, Using waste plastic bottles as additive for stone mastic asphalt, Materials & Design, 32 (2011) 4844-4849.

[26] H.K. Lindberg, V. Väänänen, H. Järventaus, S. Suhonen, J. Nygren, M. Hämeilä, J. Valtonen, P. Heikkilä, H. Norppa, Genotoxic effects of fumes from asphalt modified with

waste plastic and tall oil pitch, Mutation Research/Genetic Toxicology and Environmental Mutagenesis, 653 (2008) 82-90.

[27] M.S. Cortizo, D.O. Larsen, H. Bianchetto, J.L. Alessandrini, Effect of the thermal degradation of SBS copolymers during the ageing of modified asphalts, Polymer Degradation and Stability, 86 (2004) 275-282.

[28] A.S. Karakas, N. Kuloglu, B.V. Kok, M. Yilmaz, The evaluation of the field performance of the neat and SBS modified hot mixture asphalt, Construction and Building Materials, 98 (2015) 678-684.

[29] G. King, H. King, R. Pavlovich, A.L. Epps, P. Kandhal, Additives in asphalt, Journal of the Associatino of Asphalt Paving Technologists, 68 (1999) 32-69.

[30] H. Wang, Z. You, J. Mills-Beale, P. Hao, Laboratory evaluation on high temperature viscosity and low temperature stiffness of asphalt binder with high percent scrap tire rubber, Construction and Building Materials, 26 (2012) 583-590.

[31] H. Yao, Z. You, L. Li, S.W. Goh, J. Mills-Beale, X. Shi, D. Wingard, Evaluation of Asphalt Blended With Low Percentage of Carbon Micro-Fiber and Nanoclay, Journal of testing and evaluation, 41 (2013a) 278-288.

[32] M. Jamal Khattak, A. Khattab, H. R. Rizvi, Characterization of carbon nano-fiber modified hot mix asphalt mixtures, Construction and Building Materials, 40 (2013) 738-745.

[33] M.J. Khattak, A. Khattab, H.R. Rizvi, Mechanistic Characteristics of Asphalt Binder and Asphalt Matrix Modified with Nano-Fibers, in, ASCE, Dallas, TX, 2011, pp. 492-492.

[34] K. Anurag, F. Xiao, S.N. Amirkhanian, Laboratory investigation of indirect tensile strength using roofing polyester waste fibers in hot mix asphalt, Construction and Building Materials, 23 (2009) 2035-2040.

[35] H. Jin, G. Gao, Y. Zhang, Y. Zhang, K. Sun, Y. Fan, Improved properties of polystyrene-modified asphalt through dynamic vulcanization, Polymer Testing, 21 (2002) 633-640.

[36] G. Polacco, S. Berlincioni, D. Biondi, J. Stastna, L. Zanzotto, Asphalt modification with different polyethylene-based polymers, European Polymer Journal, 41 (2005) 2831-2844.

[37] M. Khattak, A. Khattab, P. Zhang, H. Rizvi, T. Pesacreta, Microstructure and fracture morphology of carbon nano-fiber modified asphalt and hot mix asphalt mixtures, Mater Struct, 46 (2013) 2045-2057.

[38] J. Cheng, J. Shen, F. Xiao, Moisture Susceptibility of Warm-Mix Asphalt Mixtures Containing Nanosized Hydrated Lime, Journal of Materials in Civil Engineering, 23 (2011) 1552-1559.

[39] H. Yao, Q. Dai, Z. You, Chemo-physical analysis and molecular dynamics (MD) simulation of moisture susceptibility of nano hydrated lime modified asphalt mixtures, Construction and Building Materials, 101, Part 1 (2015) 536-547.

[40] E. Santagata, O. Baglieri, L. Tsantilis, D. Dalmazzo, Rheological characterization of bituminous binders modified with carbon nanotubes, Procedia-Social and Behavioral Sciences, 53 (2012) 546-555.

[41] H. Yao, Q. Dai, Z. You, Fourier Transform Infrared Spectroscopy characterization of aging-related properties of original and nano-modified asphalt binders, Construction and Building Materials, 101, Part 1 (2015) 1078-1087.

[42] H. Yao, L. Li, H. Xie, H.-C. Dan, X.-L. Yang, Microstructure and Performance Analysis of Nanomaterials Modified Asphalt, in, American Society of Civil Engineers, Hunan, China, 2011, pp. 220-228.

[43] B. Colbert, Z. You, Properties of Modified Asphalt Binders Blended with Electronic Waste Powders, Journal of Materials in Civil Engineering, 24 (2012) 1261-1267.

[44] M.R. Mohd Hasan, B. Colbert, Z. You, A. Jamshidi, P.A. Heiden, M.O. Hamzah, A simple treatment of electronic-waste plastics to produce asphalt binder additives with improved properties, Construction and Building Materials, 110 (2016) 79-88.

[45] Y. Huang, R.N. Bird, O. Heidrich, A review of the use of recycled solid waste materials in asphalt pavements, Resources, Conservation and Recycling, 52 (2007) 58-73.

[46] A. Villanueva, S. Ho, L. Zanzotto, Asphalt modification with used lubricating oil, Canadian Journal of Civil Engineering, 35 (2008) 148-157.

[47] Z. You, J. Mills-Beale, E. Fini, S. Goh, B. Colbert, Evaluation of Low-Temperature Binder Properties of Warm-Mix Asphalt, Extracted and Recovered RAP and RAS, and Bioasphalt, Journal of Materials in Civil Engineering, 23 (2011) 1569-1574.

[48] M.O. Steinhauser, Computational Multiscale Modeling of Fluids and Solids: Theory and Applications, Springer, 2008.

[49] Q. Dai, Z. You, Prediction of Creep Stiffness of Asphalt Mixture with Micromechanical Finite-Element and Discrete-Element Models, Journal of Engineering Mechanics, 133 (2007) 163-173.

[50] Q. Dai, Two- and three-dimensional micromechanical viscoelastic finite element modeling of stone-based materials with X-ray computed tomography images, Construction and Building Materials, 25 (2011) 1102-1114.

[51] Y. Liu, Q. Dai, Z. You, Viscoelastic Model for Discrete Element Simulation of Asphalt Mixtures, Journal of Engineering Mechanics, 135 (2009) 324-333.

[52] Y. Liu, Z. You, Q. Dai, Stiffness of Sand Mastic versus Stiffness of Asphalt Binder Using Three-Dimensional Discrete Element Method, in, ASCE, Los Angeles, CA, 2011, pp. 5-5.

[53] Y. Liu, Z. You, Q. Dai, J. Mills-Beale, Review of advances in understanding impacts of mix composition characteristics on asphalt concrete (AC) mechanics, International Journal of Pavement Engineering, 12 (2011) 385-405.

[54] A.R. Abbas, Simulation of the micromechanical behavior of asphalt mixtures using the discrete element method, in: Department of Civil and Environmental Engineering, Washington State University, 2004, pp. 180.

[55] Y. Liu, Discrete element methods for asphalt concrete: development and application of user-defined microstructural models and a viscoelastic micromechanical model, in: Department of Civil and Environmental Engineering, Michigan Technological University, Houghton, 2011, pp. 407.

[56] W. Buttlar, Z. You, Discrete Element Modeling of Asphalt Concrete: Microfabric Approach, Transportation Research Record: Journal of the Transportation Research Board, 1757 (2001) 111-118.

[57] Z. You, Y. Liu, Q. Dai, Three-Dimensional Microstructural-Based Discrete Element Viscoelastic Modeling of Creep Compliance Tests for Asphalt Mixtures, Journal of Materials in Civil Engineering, 23 (2011) 79-87.

[58] B.J. Alder, T.E. Wainwright, Studies in Molecular Dynamics. I. General Method, The Journal of Chemical Physics, 31 (1959) 459-466.

[59] A. Rahman, Correlations in the Motion of Atoms in Liquid Argon, Physical Review, 136 (1964) A405-A411.

[60] L. Boltzmann, Vorlesungen über Gastheorie: Th. Theorie van der Waals'; Gase mit zusammengesetzten Molekülen; Gasdissociation; Schlussbemerkungen, J. A. Barth, 1898.

[61] T. Schlick, Pursuing Laplace's Vision on Modern Computers, in: J. Mesirov, K. Schulten, D. Sumners (Eds.) Mathematical Approaches to Biomolecular Structure and Dynamics, Springer New York, 1996, pp. 219-247.

[62] A. Bandyopadhyay, Molecular Modeling of EPON 862-DETDA Polymer, Michigan Technological University, 2012.

[63] S.L. Mayo, B.D. Olafson, W.A. Goddard, DREIDING: a generic force field for molecular simulations, The Journal of Physical Chemistry, 94 (1990) 8897-8909.

[64] J. Wang, R.M. Wolf, J.W. Caldwell, P.A. Kollman, D.A. Case, Development and testing of a general amber force field, Journal of Computational Chemistry, 25 (2004) 1157-1174.

[65] W.D. Cornell, P. Cieplak, C.I. Bayly, I.R. Gould, K.M. Merz, D.M. Ferguson, D.C. Spellmeyer, T. Fox, J.W. Caldwell, P.A. Kollman, A Second Generation Force Field for the Simulation of Proteins, Nucleic Acids, and Organic Molecules, Journal of the American Chemical Society, 117 (1995) 5179-5197.

[66] Z. Li, H. Yu, W. Zhuang, S. Mukamel, Geometry and excitation energy fluctuations of NMA in aqueous solution with CHARMM, AMBER, OPLS, and GROMOS force fields: Implications for protein ultraviolet spectra simulation, Chemical Physics Letters, 452 (2008) 78-83.

[67] M.G. Martin, Comparison of the AMBER, CHARMM, COMPASS, GROMOS, OPLS, TraPPE and UFF force fields for prediction of vapor–liquid coexistence curves and liquid densities, Fluid Phase Equilibria, 248 (2006) 50-55.

[68] J.B. Klauda, R.M. Venable, J.A. Freites, J.W. O'Connor, D.J. Tobias, C. Mondragon-Ramirez, I. Vorobyov, A.D. MacKerell, R.W. Pastor, Update of the CHARMM All-Atom Additive Force Field for Lipids: Validation on Six Lipid Types, The Journal of Physical Chemistry B, 114 (2010) 7830-7843.

[69] H. Sun, COMPASS: An ab Initio Force-Field Optimized for Condensed-Phase ApplicationsOverview with Details on Alkane and Benzene Compounds, The Journal of Physical Chemistry B, 102 (1998) 7338-7364.

[70] W.L. Jorgensen, D.S. Maxwell, J. Tirado-Rives, Development and Testing of the OPLS All-Atom Force Field on Conformational Energetics and Properties of Organic Liquids, Journal of the American Chemical Society, 118 (1996) 11225-11236.

[71] P.J.W. Debye, The collected papers of Peter J.W. Debye, Interscience Publishers, New York, 1954.

[72] M.R. Hestenes, E. Stiefel, Methods of conjugate gradients for solving linear systems, NBS, 1952.

[73] D. Sheppard, R. Terrell, G. Henkelman, Optimization methods for finding minimum energy paths, The Journal of Chemical Physics, 128 (2008) 134106.

[74] E. Bitzek, P. Koskinen, F. Gähler, M. Moseler, P. Gumbsch, Structural Relaxation Made Simple, Physical Review Letters, 97 (2006) 170201.

[75] A. Savitzky, A Historic Collaboration, Analytical Chemistry, 61 (1989) 921A-923A.

[76] A. Savitzky, M.J.E. Golay, Smoothing and Differentiation of Data by Simplified Least Squares Procedures, Analytical Chemistry, 36 (1964) 1627-1639.

[77] P.G. Guest, P.G. Guest, Numerical Methods of Curve Fitting, Cambridge University Press, 2012.

[78] E.T. Whittaker, G. Robinson, The Calculus of Observations: An Introduction to Numerical Analysis, Dover Publications, 1924.

[79] R.W. Hockney, J.W. Eastwood, Computer Simulation Using Particles, CRC Press, 1988.

[80] L. Artok, Y. Su, Y. Hirose, M. Hosokawa, S. Murata, M. Nomura, Structure and Reactivity of Petroleum-Derived Asphaltene†, Energy & Fuels, 13 (1999) 287-296.

[81] H. Groenzin, O.C. Mullins, Molecular Size and Structure of Asphaltenes from Various Sources, Energy & Fuels, 14 (2000) 677-684.

[82] Y. Ding, B. Huang, X. Shu, Y. Zhang, M.E. Woods, Use of molecular dynamics to investigate diffusion between virgin and aged asphalt binders, Fuel, 174 (2016) 267-273.

[83] L. Zhang, M.L. Greenfield, Molecular Orientation in Model Asphalts Using Molecular Simulation, Energy & Fuels, 21 (2007) 1102-1111.

[84] L. Zhang, M.L. Greenfield, Effects of Polymer Modification on Properties and Microstructure of Model Asphalt Systems, Energy & Fuels, 22 (2008) 3363-3375.

[85] L. Zhang, M.L. Greenfield, Relaxation time, diffusion, and viscosity analysis of model asphalt systems using molecular simulation, The Journal of Chemical Physics, 127 (2007) 1-13.

[86] L. Zhang, M.L. Greenfield, Rotational relaxation times of individual compounds within simulations of molecular asphalt models, The Journal of Chemical Physics, 132 (2010) 1-11.

[87] C.A. Lemarchand, T.B. Schrøder, J.C. Dyre, J.S. Hansen, Cooee bitumen: Chemical aging, The Journal of Chemical Physics, 139 (2013) 1-13.

[88] O.C. Mullins, The Modified Yen Model†, Energy & Fuels, 24 (2010) 2179-2207.

[89] D.D. Li, M.L. Greenfield, Chemical compositions of improved model asphalt systems for molecular simulations, Fuel, 115 (2014) 347-356.

[90] D.D. Li, M.L. Greenfield, Viscosity, relaxation time, and dynamics within a model asphalt of larger molecules, The Journal of Chemical Physics, 140 (2014) 1-11.

[91] A. Bhasin, R. Bommavaram, M. Greenfield, D. Little, Use of Molecular Dynamics to Investigate Self-Healing Mechanisms in Asphalt Binders, Journal of Materials in Civil Engineering, 23 (2011) 485-492.

[92] T. Pan, A first-principles based chemophysical environment for studying lignins as an asphalt antioxidant, Construction and Building Materials, 36 (2012) 654-664.

[93] A. Bhasin, D. Bommavaram, M. Greenfiled, Intrinsic healing in asphalt binders–Measurement and impact of molecular morphology, in: Proc. 6th Int. Symp. on Maintenance and Rehabilitation of Pavements and Technological Control, Politecnico di Torino, Torino, Italy, 2009.

[94] D.A. Netzel, Apparent Activation Energies for Molecular Motions in Solid Asphalt, Energy & Fuels, 20 (2006) 2181-2188.

[95] T. Kuznicki, J.H. Masliyah, S. Bhattacharjee, Aggregation and Partitioning of Model Asphaltenes at Toluene−Water Interfaces: Molecular Dynamics Simulations, Energy & Fuels, 23 (2009) 5027-5035.

[96] Y. Mikami, Y. Liang, T. Matsuoka, E.S. Boek, Molecular dynamics simulations of asphaltenes at the oil–water interface: from nanoaggregation to thin-film formation, Energy & Fuels, 27 (2013) 1838-1845.

[97] T. Kuznicki, J.H. Masliyah, S. Bhattacharjee, Molecular dynamics study of model molecules resembling asphaltene-like structures in aqueous organic solvent systems, Energy & Fuels, 22 (2008) 2379-2389.

[98] C. Jian, T. Tang, S. Bhattacharjee, Molecular dynamics investigation on the aggregation of Violanthrone78-based model asphaltenes in toluene, Energy & Fuels, 28 (2014) 3604-3613.

[99] T. Takanohashi, S. Sato, I. Saito, R. Tanaka, Molecular dynamics simulation of the heat-induced relaxation of asphaltene aggregates, Energy & fuels, 17 (2003) 135-139.

[100] A. Ortega-Rodríguez, S.A. Cruz, A. Gil-Villegas, F. Guevara-Rodríguez, C. Lira-Galeana, Molecular View of the Asphaltene Aggregation Behavior in Asphaltene−Resin Mixtures, Energy & Fuels, 17 (2003) 1100-1108.

[101] C. Jian, T. Tang, S. Bhattacharjee, Probing the Effect of Side-Chain Length on the Aggregation of a Model Asphaltene Using Molecular Dynamics Simulations, Energy & Fuels, 27 (2013) 2057-2067.

[102] E. Rogel, Theoretical Estimation of the Solubility Parameter Distributions of Asphaltenes, Resins, and Oils from Crude Oils and Related Materials, Energy & Fuels, 11 (1997) 920-925.

[103] E. Rogel, L. Carbognani, Density Estimation of Asphaltenes Using Molecular Dynamics Simulations, Energy & Fuels, 17 (2003) 378-386.

[104] R.A. Tarefder, I. Arisa, Molecular Dynamic Simulations for Determining Change in Thermodynamic Properties of Asphaltene and Resin Because of Aging, Energy & Fuels, 25 (2011) 2211-2222.

[105] Y. Lu, L. Wang, Nanoscale modelling of mechanical properties of asphalt–aggregate interface under tensile loading, International Journal of Pavement Engineering, 11 (2010) 393-401.

[106] H. Wang, E. Lin, G. Xu, Molecular dynamics simulation of asphalt-aggregate interface adhesion strength with moisture effect, International Journal of Pavement Engineering, (2015) 1-10.

[107] Y. Ding, B. Tang, Y. Zhang, J. Wei, X. Cao, Molecular Dynamics Simulation to Investigate the Influence of SBS on Molecular Agglomeration Behavior of Asphalt, Journal of Materials in Civil Engineering, 27 (2013) C4014004.

[108] D. Sun, T. Lin, X. Zhu, Y. Tian, F. Liu, Indices for self-healing performance assessments based on molecular dynamics simulation of asphalt binders, Computational Materials Science, 114 (2016) 86-93.

[109] F. Khabaz, R. Khare, Glass Transition and Molecular Mobility in Styrene–Butadiene Rubber Modified Asphalt, The Journal of Physical Chemistry B, 119 (2015) 14261-14269.

[110] W.H. Press, Numerical Recipes in C: The Art of Scientific Computing, Cambridge University Press, 1992.

[111] M. Hazewinkel, Encyclopaedia of Mathematics (set), Springer Netherlands, 1994.

[112] J. Kolafa, J.W. Perram, Cutoff Errors in the Ewald Summation Formulae for Point Charge Systems, Molecular Simulation, 9 (1992) 351-368.

[113] T. Darden, L. Perera, L. Li, L. Pedersen, New tricks for modelers from the crystallography toolkit: the particle mesh Ewald algorithm and its use in nucleic acid simulations, Structure, 7 (1999) R55-R60.

[114] T. Darden, D. York, L. Pedersen, Particle mesh Ewald: An N·log(N) method for Ewald sums in large systems, The Journal of Chemical Physics, 98 (1993) 10089-10092.

[115] A. Usmani, Asphalt Science and Technology, Taylor & Francis, 1997.

[116] D.A. Storm, J.C. Edwards, S.J. DeCanio, E.Y. Sheu, Molecular Representations of Ratawi and Alaska North Slope Asphaltenes Based on Liquid- and Solid-State NMR, Energy & Fuels, 8 (1994) 561-566.

[117] I. Kowalewski, M. Vandenbroucke, A.Y. Huc, M.J. Taylor, J.L. Faulon, Preliminary Results on Molecular Modeling of Asphaltenes Using Structure Elucidation Programs in Conjunction with Molecular Simulation Programs, Energy & Fuels, 10 (1996) 97-107.

[118] S. Plimpton, Fast Parallel Algorithms for Short-Range Molecular Dynamics, Journal of Computational Physics, 117 (1995) 1-19.

[119] F. Frigerio, D. Molinari, A multiscale approach to the simulation of asphaltenes, Computational and Theoretical Chemistry, 975 (2011) 76-82.

[120] M. Valiev, E.J. Bylaska, N. Govind, K. Kowalski, T.P. Straatsma, H.J.J. Van Dam, D. Wang, J. Nieplocha, E. Apra, T.L. Windus, W.A. de Jong, NWChem: A comprehensive and scalable open-source solution for large scale molecular simulations, Computer Physics Communications, 181 (2010) 1477-1489.

[121] T.E. Cheatham, III, J.L. Miller, T. Fox, T.A. Darden, P.A. Kollman, Molecular Dynamics Simulations on Solvated Biomolecular Systems: The Particle Mesh Ewald Method Leads to Stable Trajectories of DNA, RNA, and Proteins, Journal of the American Chemical Society, 117 (1995) 4193-4194.

[122] M.L. Greenfield, L. Zhang, Final Report-Developing Model Asphalt Systems Using Molecular Simulation, in: URITC Project No. 000216, University of Rhode Island Transportation Center, Department of Chemical Engineering, University of Rhode Island, Kingston, RI 02881, 2009, pp. 1-109.

[123] P. de Bievre, H.S. Peiser, 'Atomic weight': The name, its history, definition, and units, in: Pure and Applied Chemistry, 1992, pp. 1535.

[124] H.A. Tabatabaee, R. Velasquez, H.U. Bahia, Predicting low temperature physical hardening in asphalt binders, Construction and Building Materials, 34 (2012) 162-169.

[125] P.G. Debenedetti, F.H. Stillinger, Supercooled liquids and the glass transition, Nature, 410 (2001) 259-267.

[126] J. Zarzycki, Glasses and the Vitreous State, Cambridge University Press, 1991.

[127] A.D. McNaught, A. Wilkinson, IUPAC Compendium of Chemical Terminology (Gold Book), 2 ed., Blackwell Scientific Publications, Oxford 1997.

[128] D.J. Evans, G.P. Morriss, Nonlinear-response theory for steady planar Couette flow, Physical Review A, 30 (1984) 1528-1530.

[129] F. Müller-Plathe, Reversing the perturbation in nonequilibrium molecular dynamics: An easy way to calculate the shear viscosity of fluids, Physical Review E, 59 (1999) 4894-4898.

[130] G.V. Chilingarian, T.F. Yen, Asphaltenes and Asphalts, 1, Elsevier Science, 1994.

[131] G.R. K., G.S. L., Engineering Physics, PHI Learning Pvt. Ltd. DHANPAT RAI, 1998.

[132] A. Motamed, A. Bhasin, K. Liechti, Using the poker-chip test for determining the bulk modulus of asphalt binders, Mech Time-Depend Mater, 18 (2014) 197-215.

[133] J.C. Petersen, P.M. Harnsberger, R.E. Robertson, Factors affecting the kinetics and mechanisms of asphalt oxidation and the relative effects of oxidation products on age hardening, Preprints of Papers, American Chemical Society, Division of Fuel Chemistry 41 (1996) 1232-1244.

[134] P.G. Campbell, J.R. Wright, Infrared spectra of asphalts: Some aspects of the changes caused by photooxidation, Journal of Research of the National Bureau of Standards. Section C: Engineering and Instrumentation, 68C (1964) 115-123.

[135] W.D. Fernandez-Gomez, H.R. Quintana, F.R. Lizcano, A review of asphalt and asphalt mixture aging, INGENIERÍA E INVESTIGACIÓN, 33 (2013) 5-12.

[136] S. Caro, A. Diaz, D. Rojas, H. Nuñez, A micromechanical model to evaluate the impact of air void content and connectivity in the oxidation of asphalt mixtures, Construction and Building Materials, 61 (2014) 181-190.

[137] P.E. Yuhong Wang, K. Zhao, C. Glover, L. Chen, Y. Wen, D. Chong, C. Hu, Effects of aging on the properties of asphalt at the nanoscale, Construction and Building Materials, 80 (2015) 244-254.

[138] L. Xiang, J. Cheng, S. Kang, Thermal oxidative aging mechanism of crumb rubber/SBS composite modified asphalt, Construction and Building Materials, 75 (2015) 169-175.

[139] S.W. Goh, M. Akin, Z. You, X. Shi, Effect of deicing solutions on the tensile strength of micro- or nano-modified asphalt mixture, Construction and Building Materials, 25 (2011) 195-200.

[140] S. Zhao, B. Huang, X. Shu, M. Woods, Comparative evaluation of warm mix asphalt containing high percentages of reclaimed asphalt pavement, Construction and Building Materials, 44 (2013) 92-100.

[141] S. Zhao, B. Huang, X. Shu, X. Jia, M. Woods, Laboratory performance evaluation of warm-mix asphalt containing high percentages of reclaimed asphalt pavement, Transportation Research Record: Journal of the Transportation Research Board, (2012) 98-105.

[142] X. Shu, B. Huang, E.D. Shrum, X. Jia, Laboratory evaluation of moisture susceptibility of foamed warm mix asphalt containing high percentages of RAP, Construction and Building Materials, 35 (2012) 125-130.

[143] S. Huang, R. Robertson, J. Branthaver, J. Claine Petersen, Impact of Lime Modification of Asphalt and Freeze–Thaw Cycling on the Asphalt–Aggregate Interaction and Moisture Resistance to Moisture Damage, Journal of Materials in Civil Engineering, 17 (2005) 711-718.

[144] S.-C. Huang, F.P. Miknis, W. Schuster, S. Salmans, R. Boysen, Rheological and Chemical Properties of Hydrated Lime and Polyphosphoric Acid Modified Asphalts with

Long Term Aging, Journal of Materials in Civil Engineering, American Society of Civil Engineering (ASCE), 23 (2011) 628-637.

[145] D. Lesueur, J. Petit, H.-J. Ritter, The mechanisms of hydrated lime modification of asphalt mixtures: a state-of-the-art review, Road Materials and Pavement Design, 14 (2012) 1-16.

[146] B. Huang, X. Shu, Q. Dong, J. Shen, Laboratory evaluation of moisture susceptibility of hot-mix asphalt containing cementitious fillers, Journal Of Materials in Civil Engineering, 22 (2010) 667-673.

[147] I. Ishai, J. Craus, Effect of the filler on aggregate-bitumen adhesion properties in bituminous mixtures, in: Association of Asphalt Paving Technologists Proc, From the Technical Session, San Antonio, Texas, 21-23 February 1977, 1977, pp. 228-258.

[148] J. Blazek, G. Sebor, D. Maxa, M. Ajib, H. Paniagua, Effect of hydrated lime addition on properties of asphalt, Petroleum and Coal, 42(1), pp.41-45, (2000).

[149] I.U.o.P.a.A. Chemistry, Compendium of Chemical Terminology, Version 2.3 ed., International Union of Pure and Applied Chemistry, 2011.

[150] R.T.B.R.N. Morrison, Organic chemistry, 6 ed., Prentice-Hall, Englewood Cliffs,N.J., 1993.

[151] J. McMurry, Organic Chemistry, 8 ed., Cengage Learning, 2011.

[152] H. Held, A. Rengstl, D. Mayer, Acetic Anhydride and Mixed Fatty Acid Anhydrides, in: Ullmann's Encyclopedia of Industrial Chemistry, Wiley-VCH Verlag GmbH & Co. KGaA, 2000.

[153] F.A. Carey, R.J. Sundberg, Advanced Organic Chemistry: Part B: Reaction and Synthesis, Springer, 2007.

[154] M. Jerry, Advanced organic chemistry : reactions, mechanisms and structure (A Wiley-Interscience Publication), 3 ed., Wiley, the University of Michigan, 1985.

[155] C.R. Kemnitz, M.J. Loewen, "Amide Resonance" Correlates with a Breadth of C−N Rotation Barriers, Journal of the American Chemical Society, 129 (2007) 2521-2528.

[156] W. Riemenschneider, H.M. Bolt, Esters, Organic, in: Ullmann's Encyclopedia of Industrial Chemistry, Wiley-VCH Verlag GmbH & Co. KGaA, 2000.

[157] R.J. Williams, A. Gabriel, R.C. Andrews, THE RELATION BETWEEN THE HYDROLYSIS EQUILIBRIUM CONSTANT OF ESTERS AND THE STRENGTHS OF THE CORRESPONDING ACIDS, Journal of the American Chemical Society, 50 (1928) 1267-1271.

[158] B. Neises, W. Steglich, Esterification of Carboxylic Acids with Dicyclohexylcarbodiimide/4-Dimethylaminopyridine: tert-Butyl Ethyl Fumarate, in: Organic Syntheses, John Wiley & Sons, Inc., 2003.

[159] P. Griffiths, J.A. De Haseth, Fourier Transform Infrared Spectrometry, John Wiley & Sons, 2007.

[160] P. Atkins, J. de Paula, Elements of Physical Chemistry, OUP Oxford, 2013.

[161] S.E.S. NIST Mass Spec Data Center, director, "Infrared Spectra" in NIST Chemistry WebBook, NIST Standard Reference Database Number 69, National Institute of Standards and Technology, Gaithersburg MD, 20899, United States, 2014.

[162] R.A. Tomasi, A Spectrum of Spectra, Sunbelt R & T, Incorporated, 1992.

[163] R.A. Tomasi, A Spectrum of Spectral Problems: Supplement, Sunbelt R & T, Incorporated, 1994.

[164] R.M. Silverstein, G.C. Bassler, Spectrometric identification of organic compounds, Journal of Chemical Education, 39 (1962) 546.

[165] R.M. Silverstein, G.C. Bassler, T.C. Morrill, Spectrometric identification of organic compounds, Wiley, New York, 1981.

[166] D.N. Little, J.A. Epps, P.E. Sebaaly, The benefits of hydrated lime in hot mix asphalt, in, National Lime Association, 2006, pp. 80.

[167] J.C. Petersen, C. National Research, B. Transportation Research, M. Committee on Characteristics of Bituminous, A review of the fundamentals of asphalt oxidation chemical, physicochemical, physical property, and durability relationships, (2009).

[168] H. Yao, L. Li, X.-l. Yang, H.-c. Dan, S. Luo, Mechanics Performance Research and Microstructure Analysis of Nanomaterials Modified Asphalt, Journal of Building Materials, 14 (2011) 712-717.

[169] S. Caro, E. Masad, A. Bhasin, D. Little, Coupled Micromechanical Model of Moisture-Induced Damage in Asphalt Mixtures, Journal of Materials in Civil Engineering, 22 (2010) 380-388.

[170] H. Yao, Y. Liu, Z. You, L. Li, S.W. Goh, Discrete Element Simulation of Bending Beam Rheometer Tests for Asphalt Binder, International Journal of Pavement Research and Technology, 5 (2012) 161-168.

[171] S. Adhikari, Z. You, Investigating the Sensitivity of Aggregate Size within Sand Mastic by Modeling the Microstructure of an Asphalt Mixture, Journal of Materials in Civil Engineering, 23 (2011) 580-586.

[172] L. Xiang, J. Cheng, G. Que, Microstructure and performance of crumb rubber modified asphalt, Construction and Building Materials, 23 (2009) 3586-3590.

[173] H. Wang, Z. Dang, Z. You, D. Cao, Effect of warm mixture asphalt (WMA) additives on high failure temperature properties for crumb rubber modified (CRM) binders, Construction and Building Materials, 35 (2012) 281-288.

[174] S. Lee, S. Mun, Y. Richard Kim, Fatigue and rutting performance of lime-modified hot-mix asphalt mixtures, Construction and Building Materials, 25 (2011) 4202-4209.

[175] X. Liu, S. Wu, Study on the graphite and carbon fiber modified asphalt concrete, Construction and Building Materials, 25 (2011) 1807-1811.

[176] F. Bonaccorso, L. Colombo, G. Yu, M. Stoller, V. Tozzini, A.C. Ferrari, R.S. Ruoff, V. Pellegrini, Graphene, related two-dimensional crystals, and hybrid systems for energy conversion and storage, Science, 347 (2015).

[177] Ç.Ö. Girit, J.C. Meyer, R. Erni, M.D. Rossell, C. Kisielowski, L. Yang, C.-H. Park, M.F. Crommie, M.L. Cohen, S.G. Louie, A. Zettl, Graphene at the Edge: Stability and Dynamics, Science, 323 (2009) 1705-1708.

[178] A.K. Geim, Graphene: Status and Prospects, Science, 324 (2009) 1530-1534.

[179] S. Ghosh, I. Calizo, D. Teweldebrhan, E.P. Pokatilov, D.L. Nika, A.A. Balandin, W. Bao, F. Miao, C.N. Lau, Extremely high thermal conductivity of graphene: Prospects for thermal management applications in nanoelectronic circuits, Applied Physics Letters, 92 (2008) 151911.

[180] M.G. Martin, MCCCS Towhee: a tool for Monte Carlo molecular simulation, Molecular Simulation, 39 (2013) 1212-1222.

[181] S. Schweizer, A. Bick, L. Subramanian, X. Krokidis, Influences on the stability of collagen triple-helix, Fluid Phase Equilibria, 362 (2014) 113-117.

[182] H. Yao, Q. Dai, Z. You, Molecular dynamics simulation of physicochemical properties of the asphalt model, Fuel, 164 (2016) 83-93.

[183] V. Vacquier, The measurement of thermal conductivity of solids with a transient linear heat source on the plane surface of a poorly conducting body, Earth and Planetary Science Letters, 74 (1985) 275-279.

[184] F. Müller-Plathe, A simple nonequilibrium molecular dynamics method for calculating the thermal conductivity, The Journal of Chemical Physics, 106 (1997) 6082-6085.

[185] P. Pan, S. Wu, Y. Xiao, P. Wang, X. Liu, Influence of graphite on the thermal characteristics and anti-ageing properties of asphalt binder, Construction and Building Materials, 68 (2014) 220-226.

[186] P.W.S.H.R.P.N.R.C. Jennings, Binder characterization and evaluation by nuclear magnetic resonance spectroscopy, Strategic Highway Research Program, National Research Council, Washington, DC, 1993.

[187] D. Lo Presti, Recycled Tyre Rubber Modified Bitumens for road asphalt mixtures: A literature review, Construction and Building Materials, 49 (2013) 863-881.

[188] C. Thodesen, K. Shatanawi, S. Amirkhanian, Effect of crumb rubber characteristics on crumb rubber modified (CRM) binder viscosity, Construction and Building Materials, 23 (2009) 295-303.

[189] J. Shen, S. Amirkhanian, F. Xiao, B. Tang, Influence of surface area and size of crumb rubber on high temperature properties of crumb rubber modified binders, Construction and Building Materials, 23 (2009) 304-310.

[190] G.D. Airey, T.M. Singleton, A.C. Collop, Properties of polymer modified bitumen after rubber-bitumen interaction, Journal of Materials in Civil Engineering, 14 (2002) 344-354.

[191] S. Kim, S.W. Loh, H. Zhai, H.U. Bahia, Advanced Characterization of Crumb Rubber-Modified Asphalts, using Protocols Developed for Complex Binders, in: Transportation Research Record, Transportation Research Board, 2001, pp. p. 15-24.

[192] Z. Ge, H. Wang, Q. Zhang, C. Xiong, Glass fiber reinforced asphalt membrane for interlayer bonding between asphalt overlay and concrete pavement, Construction and Building Materials, 101, Part 1 (2015) 918-925.

[193] I. Al-Qadi, H. Wang, Impact of Wide-Base Tires on Pavements, Transportation Research Record: Journal of the Transportation Research Board, 2304 (2012) 169-176.

[194] H. Li, J. Harvey, D. Jones, Multi-dimensional transient temperature simulation and back-calculation for thermal properties of building materials, Building and Environment, 59 (2013) 501-516.

[195] M. Karplus, J.A. McCammon, Molecular dynamics simulations of biomolecules, Nat Struct Mol Biol, 9 (2002) 646-652.

[196] R.A. Tarefder, A.M. Zaman, W. Uddin, Determining Hardness and Elastic Modulus of Asphalt by Nanoindentation, International Journal of Geomechanics, 10 (2010) 106-116.

[197] S.G. Silverman, K. Tuncali, D.F. Adams, R.D. Nawfel, K.H. Zou, P.F. Judy, CT fluoroscopy-guided abdominal interventions: techniques, results, and radiation exposure, Radiology, 212 (1999) 673-681.

[198] H.I. Ling, A. Smyth, R. Betti, Poromechanics IV, DEStech Publications, Incorporated, 2009.

[199] S.R. White, N.R. Sottos, P.H. Geubelle, J.S. Moore, M.R. Kessler, S.R. Sriram, E.N. Brown, S. Viswanathan, Autonomic healing of polymer composites, Nature, 409 (2001) 794-797.

[200] J. Qiu, M. van de Ven, S. Wu, J. Yu, A. Molenaar, Evaluating Self Healing Capability of Bituminous Mastics, Exp Mech, 52 (2012) 1163-1171.

[201] Y. Tan, L. Shan, Y. Richard Kim, B.S. Underwood, Healing characteristics of asphalt binder, Construction and Building Materials, 27 (2012) 570-577.

[202] Á. García, E. Schlangen, M. van de Ven, Q. Liu, A simple model to define induction heating in asphalt mastic, Construction and Building Materials, 31 (2012) 38-46.

[203] Q. Liu, E. Schlangen, M. van de Ven, G. van Bochove, J. van Montfort, Evaluation of the induction healing effect of porous asphalt concrete through four point bending fatigue test, Construction and Building Materials, 29 (2012) 403-409.

[204] G. Kumar, K.N. Prabhu, Review of non-reactive and reactive wetting of liquids on surfaces, Advances in Colloid and Interface Science, 133 (2007) 61-89.

[205] Q. Liu, Á. García, E. Schlangen, M.v.d. Ven, Induction healing of asphalt mastic and porous asphalt concrete, Construction and Building Materials, 25 (2011) 3746-3752.

[206] Á. García, Self-healing of open cracks in asphalt mastic, Fuel, 93 (2012) 264-272.

[207] D. Salomon, H. Zhai, Asphalt binder flow activation energy and its significance for compaction effort, in: Proceedings of 3rd Euroasphalt & Eurobitume Congress, 2004, pp. 1754-1762.

[208] S. Alexander, Visualization and analysis of atomistic simulation data with OVITO–the Open Visualization Tool, Modelling and Simulation in Materials Science and Engineering, 18 (2010) 015012.

Appendix A: Copyright Clearance

ARTICLE 1: Copyright Clearance of Published Journal paper "Molecular dynamics simulation of physicochemical properties of the asphalt model", Fuel, Vol. 164, 15 January 2016, Pages 83–93. Elsevier.

The full articles has been used in Chapter 3 of this dissertation, as well as part of Chapter 1 and 8. The permission to reuse in this dissertation is shown as follows.

License Details

Thank you very much for your order.

This is a License Agreement between Hui Yao ("You") and Elsevier ("Elsevier"). The license consists of your order details, the terms and conditions provided by Elsevier, and the payment terms and conditions.

Get the printable license.

License Number	3851700743284
License date	Apr 17, 2016
Licensed Content Publisher	Elsevier
Licensed Content Publication	Fuel
Licensed Content Title	Molecular dynamics simulation of physicochemical properties of the asphalt model
Licensed Content Author	Hui Yao,Qingli Dai,Zhanping You
Licensed Content Date	15 January 2016
Licensed content volume number	164
Licensed content issue number	n/a
Number of pages	11
Type of Use	reuse in a thesis/dissertation
Portion	full article
Format	both print and electronic
Are you the author of this Elsevier article?	Yes
Will you be translating?	No
Title of your thesis/dissertation	PROPERTY ANALYSIS OF THE ASPHALT MATERIALS USING MOLECULAR DYNAMICS (MD) METHOD
Expected completion date	May 2016
Estimated size (number of pages)	230
Elsevier VAT number	GB 494 6272 12
Price	0.00 USD
VAT/Local Sales Tax	0.00 USD / 0.00 GBP
Total	**0.00 USD**

BACK

ARTICLE 2: Copyright Clearance of Published Journal paper "Chemo-physical analysis and molecular dynamics (MD) simulation of moisture susceptibility of nano hydrated lime modified asphalt mixtures", Construction and Building Materials, Vol. 101, 30 December 2015, Pages 536–547. Elsevier.

The full articles has been used in Chapter 4 of this dissertation, as well as part of Chapter 1 and 8. The permission to reuse in this dissertation is shown as follows.

License Details

Thank you very much for your order.

This is a License Agreement between Hui Yao ("You") and Elsevier ("Elsevier"). The license consists of your order details, the terms and conditions provided by Elsevier, and the payment terms and conditions.

Get the printable license.

License Number	3852121113684
License date	Apr 18, 2016
Licensed Content Publisher	Elsevier
Licensed Content Publication	Construction and Building Materials
Licensed Content Title	Chemo-physical analysis and molecular dynamics (MD) simulation of moisture susceptibility of nano hydrated lime modified asphalt mixtures
Licensed Content Author	Hui Yao,Qingli Dai,Zhanping You
Licensed Content Date	30 December 2015
Licensed content volume number	101
Licensed content issue number	n/a
Number of pages	12
Type of Use	reuse in a thesis/dissertation
Portion	full article
Format	both print and electronic
Are you the author of this Elsevier article?	Yes
Will you be translating?	No
Title of your thesis/dissertation	PROPERTY ANALYSIS OF THE ASPHALT MATERIALS USING MOLECULAR DYNAMICS (MD) METHOD
Expected completion date	May 2016
Estimated size (number of pages)	230
Elsevier VAT number	GB 494 6272 12
Price	0.00 USD
VAT/Local Sales Tax	0.00 USD / 0.00 GBP
Total	**0.00 USD**

BACK

Hui Yao's Vitae

My primary research interests focus on Molecular Dynamics (MD), Discrete Element Method (DEM), construction materials, asphalt concrete, and mechanics. I have published more than 34 publications in the field of civil engineering, with most papers being published in high-impact journals. One of my publications is in the *Top 25 Hottest Articles* in Elsevier. Simultaneously, I am serving as a reviewer for several academic journals. I have published 16 papers at Michigan Technological University, including 11 papers as first author, and papers are listed as follows:

[1] **Hui Yao**, Qingli Dai, Zhanping You, Rheological properties, low-temperature cracking resistance, and optical performance of exfoliated graphite nanoplatelets modified asphalt, Construction and Building Materials, June, 2016.
http://www.sciencedirect.com/science/article/pii/S0950061816304561

[2] **Hui Yao**, and Zhanping You, Effectiveness of Micro- and Nano-materials in Asphalt Mixtures through Dynamic Modulus and Rutting Tests. Journal of Nanomaterials, 2016.
http://www.hindawi.com/journals/jnm/2016/2645250/

[3] **Hui Yao**, Qingli Dai, and Zhanping You, Molecular Dynamics Simulation of Physicochemical Properties of Asphalt Model, Fuel, 2016, Jan.
http://www.sciencedirect.com/science/article/pii/S0016236115009424

[4] **Hui Yao**, Qingli Dai, and Zhanping You, Chemo-physical Analysis and Molecular Dynamics (MD) Simulation of Moisture Susceptibility of Nano Hydrated Lime Modified Asphalt Mixtures. Construction and Building Materials. 2015.
http://www.sciencedirect.com/science/article/pii/S0950061815305080

[5] **Hui Yao**, Qingli Dai, and Zhanping You, Fourier Transform Infrared Spectroscopy Characterization of Aging-related Properties of Original and Nano-modified Asphalt Binders, Construction and Building Materials. 2015. http://www.sciencedirect.com/science/article/pii/S0950061815305067

[6] **Hui Yao**, Zhanping You, Liang Li, et al. Rheological Properties and Chemical Analysis of Nanoclay and Carbon Microfiber modified Asphalt with Fourier Transform Infrared Spectroscopy, Construction and Building Materials, 2013, 38:327-337. http://www.sciencedirect.com/science/article/pii/S0950061812005673

TOP25 hottest articles: http://top25.sciencedirect.com/subject/engineering/12/journal/construction-and-building-materials/09500618/archive/41/

[7] **Hui Yao**, Zhanping You, Liang Li, et al. Performance of Asphalt Binder Blended with Non-Modified and Polymer-Modified Nanoclay, Construction and Building Materials, 2012, 35:159-170. http://www.sciencedirect.com/science/article/pii/S095006181200133X

[8] **Hui Yao**, Zhanping You, Liang Li, et al. Properties and Chemical Bonding of Asphalt and Asphalt Mixtures Modified with Nanosilica, ASCE Journal of Materials in Civil Engineering, 2013, 25(11):1619-1630. http://ascelibrary.org/doi/abs/10.1061/(ASCE)MT.1943-5533.0000690

[9] **Hui Yao**, Zhanping You, Liang Li, et al. Evaluation of Asphalt Blended with Low Percentage of Carbon Micro-fiber and Nanoclay, ASTM Journal of Testing and Evaluation, 2013, 41(2):278-288.

http://www.astm.org/DIGITAL_LIBRARY/JOURNALS/TESTEVAL/PAGES/JTE20120068.htm

[10] **Hui Yao**, Zhanping You, Liang Li, et al. Discrete Element Simulation of Bending Beam Rheometer Test for Nanomaterials modified asphalt, International Journal of Pavement and Research Technology, 2012, 5(3):161-168. http://144.171.11.39/view/2012/C/1141971

[11] Ali Jamshidi, Mohd Rosli Mohd Hasan, **Hui Yao**, Zhanping You, Meor Othman Hamzah, Characterization of the rate of change of rheological properties of nano-modified asphalt, Construction and Building Materials, 2015, 98: 437-446. http://www.sciencedirect.com/science/article/pii/S0950061815303019

[12] Yu Liu, Zhanping You, **Hui Yao**, An idealized discrete element model for pavement-wheel interaction, Journal of Marine Science and Technology-Taiwan, 23(3): 339-343. http://jmst.ntou.edu.tw/marine/23-3/339-343.pdf

[13] Jie Ji, **Hui Yao**, Xu Yang, Ying Xu, Zhi Suo, Zhanping You. Performance Analysis of Direct Coal Liquefaction Residue (DCLR) and Trinidad Lake Asphalt (TLA) for the Purpose of Modifying Traditional Asphalt, Arabian Journal for Science and Engineering. Feb. 2016. http://link.springer.com/article/10.1007/s13369-016-2034-5

[14] **Hui Yao**, Zhanping You, Liang Li, et al. Evaluation of the Master Curves for Complex Shear Modulus for Nano-modified Asphalt Binders[C]. Proceeding of COTA International of Conference of Transportation Professional, American Society of Civil Engineers, Beijing, China, 2012:3399-3414. http://ascelibrary.org/doi/abs/10.1061/9780784412442.345

[15] Zhanping You, Xu Yang, **Hui Yao**, Shu Wei Goh. Preliminary Study of Materials Effect of Cold In-Place and Full-Depth Reclamation Asphalt Concrete in Mechanistic-Empirical Pavement Design, 2012, CICTP 2012@ sMultimodal Transportation Systems—Convenient, Safe, Cost-Effective, Efficient. ASCE, 3475-3485. http://ascelibrary.org/doi/abs/10.1061/9780784412442.352

[16] Jie Ji, Yuefeng Shi, Zhi Suo, **Hui Yao**, Shifa Xu, Influence of direct coal liquefaction residue on viscoelastic properties of asphalt mortar, Journal of Traffic and Transportation Engineering, 15(4), 2015, 1-8. https://www.researchgate.net/publication/283780434_Influence_of_direct_coal_liquefaction_residue_on_viscoelastic_properties_of_asphalt_mortar

[17] Jia-qi Chen, Liang Li, Lian-heng Zhao, Han-cheng Dan, **Hui Yao**. Solution of pavement temperature field in "Environment-Surface" system through Green's function, Journal of Central South University, 2014, 21(5):2108-2116. http://link.springer.com/article/10.1007/s11771-014-2160-8

[18] **Hui Yao**, Liang Li, Hua Xie, et al. Mechanics Analysis of Vehicle Bumping at Approach Slabs with Superelevation [J]. Journal of Southeast University (English Edition), 2012, 28 (2): 221-228. https://www.researchgate.net/publication/288533429_Mechanics_analysis_of_vehicle_bumping_at_approach_slabs_with_superelevation

[19] **Hui Yao**, Liang Li, Hua Xie, et al. Microstructure and Performance Analysis of Nanomaterials Modified asphalt [C]. Proceeding of the 2011 GeoHunan International Conference, Road Materials and New Innovations in Pavement Engineering, American Society of Civil Engineers, GSP 223, Changsha, China, 2011:220-228.

http://ascelibrary.org/doi/pdf/10.1061/47634(413)28

[20] **Hui Yao**, Liang Li, Hua Xie, et al. Gradation and Performance Research of Cold Recycled Mixture [C]. Proceeding of the 2011 GeoHunan International Conference, Road Pavement and Material Characterization, Modeling, and Maintenance, American Society of Civil Engineers, GSP 213, Changsha, China, 2011:1-9.

http://ascelibrary.org/doi/pdf/10.1061/47624(403)1

[21] **Hui Yao**, Liang Li, Xiaoli Yang, et al. Mechanics Performance Research and Microstructure Analysis of Nanomaterials Modified asphalt, Journal of Building Materials, 2011, 14 (5): 712-718. (In Chinese)

http://www.cnki.com.cn/Article/CJFDTOTAL-JZCX201105035.htm

[22] **Hui Yao**, Liang Li, Ronghua Ying, et al. Research of Gradation Design of Cold Recycled Mixture Based on Bailey Method, Journal of Highway and Transportation Research and Development, 2011, 28 (1): 7-12. (In Chinese)

http://www.cnki.com.cn/Article/CJFDTOTAL-GLJK201101003.htm

[23] Zhifang Huang and **Hui Yao**. Mechanical Analysis of Cement Concrete at the Pavement Bends, The Electronic Journal of Geotechnical Engineering, 2013, 18(S): 4017-4026.

http://www.ejge.com/2013/Abs2013.365.htm

[24] Bangyan Tang, **Hui Yao**, Yu Feng, et al. Performance of Nanomodified Asphalt Binder and Mixture, Advanced Materials Research, 2013, 721(0):219-223.

http://www.scientific.net/AMR.721.219.pdf

[25] Dongli Peng, **Hui Yao** and Xudong Hu. Mechanics Analysis of Vehicle Vibration at Approach Slabs, The Electronic Journal of Geotechnical Engineering, 2013, 18(K): 2157-2164.
http://www.ejge.com/2013/Abs2013.203.htm

[26] Yingbin Zhang, Liang Li, Lianheng Zhao, **Hui Yao**, Dongya Ren, Limit analysis of slope stability based on nonlinear failure criterion, Rock and Soil Mechanics, 2011, 32(11): 3312-3318.

[27] Hancheng Dan, Liang Li, **Hui Yao**, et al. Experimental Analysis of Rainfall Simulation at Median of Highway, Journal of Highway and Transportation Research and Development, 2010, 27(11): 20-26. (In Chinese)

[28] Hancheng Dan, Liang Li, **Hui Yao**, et al. Regression calculation and analysis for the thermal stress of cement concrete pavement [J]. Journal of Railway Science and Engineering, 2010, 7(4):15-19. (In Chinese)

[29] Hancheng Dan, Liang Li, **Hui Yao**, et al. Effect of Unsaturated Flow on the Groundwater Table in Drainage Layer and Saturated Model Modification, Proceeding of the 2011 GeoHunan International Conference, American Society of Civil Engineers, GSP 213, Changsha, China, 2011:140-148.

[30] Hancheng Dan, Liang Li, **Hui Yao**, et al. Study on Transfer Behavior of Negative Friction of Single Pile in Two-Layer Soil, Proceeding of the 2010 GeoShanghai International Conference, American Society of Civil Engineers, GSP 205, Shanghai, China, 2010:177-183.

[31] Hancheng Dan, Liang Li, **Hui Yao**, et al. Method of Design for Improving the Drainage Layer of Asphalt Pavement, Proceeding of the 2010 GeoShanghai

International Conference, American Society of Civil Engineers, GSP 203, Shanghai, China, 2010:460-467.

[32] Ronghua Ying and **Hui Yao**. Cold-In Place Research and Design of Foamed Bitumen Mixture, Journal of China & Foreign Highway, 2007, 27(2):141-144. (In Chinese)

[33] Ronghua Ying, Zhiyong Zhang and **Hui Yao**. Performance analysis of water proof bonding layer of asphalt pavement, Journal of Changsha University of Science and Technology (Natural Science), 2007, (4): 1-3. (In Chinese)

[34] Ronghua Ying, Hao Feng and **Hui Yao**. Research on Scour Resistance of Lime-fly ash and Gravel Base Using Grey Method, Journal of China & Foreign Highway, 2008, 28(4):1-4. (In Chinese)